Preface

This report has been written within the framework of my master thesis with an assignment from TNO Defence, Security and Safety, Rijswijk, The Netherlands at the Faculty of Aerospace Engineering of the Delft University of Technology in the Netherlands. The assignment was to investigate several different ramjet concepts for flight in the hypersonic regime, and to compare them through their overall performance and discuss their gasdynamic phenomena within the engine flow path. This was done in order to determine a pre-design test setup for a proof-of-concept of that ramjet concept which outperforms the other concepts to test its feasibility.

During my thesis work I have had the privilege of working with many people from all over the university, and at TNO. Overall, I would like to thank my supervisors, P.G. Bakker, R.G. Veraar and W.J. Bannink, for their advice and comments to my work and their patience. I have enjoyed the discussions and debates with my teachers, fellow students, roommates, friends and family about all the issues I faced during my work on my thesis and appreciated all their support. I could not have done this without them.

Bert Tayara.

Delft, December 2008

Summary

Recently, supersonic combustion ramjets are more and more realised to become the next-generation steady airbreathing propulsion systems operating in the hypersonic flow regime. Due to this renewed interest, this thesis investigates several hypersonic ramjet engine concepts using supersonic combustion to determine which concept is more viable of becoming the next-generation propulsion system. The investigation of hypersonic ramjets is done by identifying two kinds of supersonic combustion methods for ramjet engine concepts, which are diffusion combustion and pre-mixed combustion. From these two combustion types four different ramjet concepts are investigated: the scramjet, the dual-mode combustor, the shock-induced combustion ramjet (shcramjet), and the oblique detonation wave engine (ODWE). To analyse their overall performance, diffusion combustion is modelled as a constant-pressure heat addition process (Brayton model), and pre-mixed combustion (associated with shock-induced combustion) is modelled as a constant-volume heat addition process (Humphrey model). Detonations, however, are modelled as a discontinuity wave where across heat addition occurs (Fickett-Jacob model). The analysis comprises of an ideal thermodynamic effciency determination and an one-, or quasi-one-dimensional analytic performance analysis with freestream Mach numbers up to 20. The analysis investigates three combustion performance charachteristics; the total pressure loss, the entropy increase, and the specific impulse. The results show that detonation waves have the highest ideal thermodynamic efficiency, followed by constant-volume heat addition and then constant-pressure heat addition. The analytical performance analysis however shows that detonation waves have the lowest overall performance and constant-volume heat addition the highest overall performance. This contradiction is explained due to the fact of irreversible entropy generation, coinciding with total pressure losses, being higher for detonation waves than for the other two heat addition models. The detonation wave thus remains a theoretical limit of the shock-induced combustion wave. A proof-of-concept test setup pre-design is then suggested to demonstrate the feasibility of shock-induced combustion as a next-generation propulsion system.

Contents

List of Figures

Nomenclature

Roman

a	=	velocity of sound	[m/s]
c_p	=	specific heat at constant pressure	[J/mol·K]
c_v	=	specific heat at constant volume	[J/mol·K]
d	=	downstream limit of adverse axial pressure gradient	[Pa]
f	=	fuel to air ratio	[-]
f_{stoich}	=	stoichiometric fuel to air ratio	[-]
f	=	degree of detonation wave overdrive	[-]
g	=	acceleration due to gravity	[m/s^2]
h	=	specific enthalpy	[J/kg]
h	=	isolator radius	[m]
h_t	=	specific total enthalpy	[J/kg]
$\dot{m}$	=	mass flow rate	[kg/s]
p	=	static pressure	[Pa]
$\bar{p}$	=	average static pressure	[Pa]
p_t	=	total or stagnation pressure	[Pa]
q	=	heat input rate per unit of air mass flow rate	[J/kg]
r	=	distance between shock and reaction	[m]
s	=	specific entropy	[J/kg/K]
s	=	limit of negative axial pressure gradient	[Pa]
s_s	=	shock stand-off distance	[m]
t	=	time	[s]
t_i	=	induction time	[s]
u	=	flow velocity	[m/s]
u	=	upstream limit of adverse axial pressure gradient	[Pa]
w	=	flow velocity	[m/s]
A	=	area	[m^2]
A	=	constant of proportionality	[-]
D	=	cavity depth	[m]
D	=	detonation wave velocity	[m/s]
E	=	specific internal energy	[J/kg]
F	=	thrust	[N]
F_n	=	net thrust	[N]
G	=	constant	[-]
H	=	non-dimensional heat of combustion	[-]
H_c	=	combustion energy value	[J/kg]
H_{cowl}	=	cowl height	[m]
H_i	=	isolator diameter	[m]
H_n	=	nozzle height	[m]

H	=	Hugoniot curve	[-]
I_{sp}	=	specific impulse	[s]
L	=	cavity length	[m]
L_b	=	boundary layer length	[m]
L_{cowl}	=	cowl length	[m]
L_n	=	nozzle length	[m]
M	=	Mach number	[-]
M_k	=	onset Mach number	[-]
M_{CJ}	=	Chapman-Jouguet Mach number	[-]
Q	=	heat added to a system	[J]
R	=	gas constant	[J/Kmol]
R	=	Rayleigh line	[-]
Re	=	Reynolds number	[-]
S	=	entropy	[J/K]
S_i	=	isolator length	[m]
T	=	static temperature	[K]
T_t	=	total or stagnation temperature	[K]
U	=	internal energy of a system	[J]
U_{CJ}	=	Chapman-Jouguet velocity	[m/s]
U	=	stream velocity behind a bow shock	[m/s]
V	=	volume	$[m^3]$
W	=	work done by a system	[J]

Greek

α_n	=	nozzle initial expansion ramp angle	[^{0}]
β	=	shock angle	[^{0}]
β_c	=	nozzle initial expansion cowl angle	[^{0}]
γ	=	ratio of specific heats	[-]
δ	=	shock deflection angle	[^{0}]
ϵ	=	cavity back wall angle	[^{0}]
ζ	=		[ ]
$\eta_{Brayton}$	=	Brayton cycle efficiency	[-]
$\eta_{Humphrey}$	=	Humphrey cycle efficiency	[-]
η_j	=	propulsion efficiency	[-]
η_k	=	kinetic efficiency	[-]
η_n	=	nozzle efficiency	[-]
η_R	=	inlet efficiency	[-]
η_{th}	=	thermodynamic efficiency	[-]
η_{tot}	=	total efficiency	[-]
θ	=	undisturbed boundary layer thickness	[m]
θ	=	shock turning angle	[^{0}]
λ	=	degree of chemical reaction or reaction rate	[-]
λ	=	detonation cell width	[m]
μ	=	dynamic fluid viscosity	[N$\cdot s/m^2$]
ρ	=	density	[kg/m^3]
ρ_t	=	total or stagnation density	[kg/m^3]
τ_c	=	stagnation temperature ratio	[-]
ϕ	=	equivalence ratio	[-]
ψ	=	specific thrust	[N/kg/s]
Δ	=	induction zone length	[m]

Acronyms

CFD	=	Computational Fluid Dynamics
CJ	=	Chapman-Jouguet
CV	=	Constant Volume
CP	=	Constant Pressure
DDT	=	Deflagration-to-Detonation Transition
DMC	=	Dual-Mode Combustor
DRDC	=	Defence Research and Development Canada
DWE	=	Detonation Wave Engine
NASA	=	National Aeronautics and Space Administration
ODWE	=	Oblique Detonation Wave Engine
PDE	=	Pulse Detonation Engine
RMJ	=	Ramjet
SCRM	=	Scramjet
TNO	=	Netherlands Organization for Applied Scientific Research
ZND	=	Zeldovich Neumann Döring

Chapter 1

Introduction

At TNO Defence, Security and Safety Rijswijk, the Netherlands, theoretical and experimental research has been done on ramjet engines. Primarily, this research was meant to answer certain questions raised by the Dutch military concerning the current capacities and threat of ramjet propelled weapon systems as well as in the near future. The knowledge that is acquired, could also be used for design projects for ramjet propelled vehicles for space and defence purposes. Recent succesfull tests include Mach 4+ tests with solid fuel ramjet propelled gun launched projectiles.

For the last decade, renewed interest has been expressed towards supersonic combustion ramjet engines as the next generation steady airbreathing engines, making it possible to shorten flight time, say for space planes to reach their destinations or for a missile to reach its target. Thus shortening the time to anticipate an attack. The succesfull flight tests of the X-43 from NASA, which flew at Mach 7 and Mach 10, show that supersonic combustion ramjet propulsion can now also be used for space and defence purposes. At this moment of writing, TNO has started a cooperation project with DRDC (Defence Research and Development Canada) on the subject High Speed Weapon Systems. Within this project several aspects of different vehicle system levels will be investigated, including propulsion and aerodynamics of high speed vehicles.

This master thesis will be placed in this field of international cooperation and will focus on an investigation of the internal aerodynamic flow path of different ramjet engine concepts using supersonic combustion and will give ideal performance analyses to determine a viable simple proof-of-concept pre-design test setup. A proof-of-concept here has the purpose to investigate if that particular ramjet engine design is feasible and competitive with other high speed vehicle propulsion system designs through simple testing.

1.1 Thesis Structure

This chapter will give a short introduction to the subsonic combustion ramjet engine and why supersonic combustion instead of subsonic combustion is necessary for ramjets when operating in the hypersonic regime. Chapter two will discuss two ramjet engine concepts operating with supersonic combustion, the classic or conventional scramjet and the dual-mode combustor. Chapter three will discuss shock-induced combustion and detonations with two ramjet engine concepts operating with this (supersonic) combustion phenomenon. Chapter four will give a theoretical performance analysis of three combustion processes modeling the ramjet engine concepts discussed in chapters two and three and will conclude with a suggestion for a proof-of-concept and a test setup predesign. Chapter five will conclude this thesis by summarizing the results found for the ramjet engine concepts and by giving recommendations for future research.

Though this thesis will give an understanding of the aerodynamic phenomena within the ramjet engine flow path, it does not have the purpose to go into a detailed discussion of each flow phenomena. Where needed a detailed discussion will be given, but otherwise references to other literature will be given to avoid venturing beyond the scope of this thesis. The focus will be placed on the performance analysis of each ramjet engine concept and its feasibility.

1.2 Steady Airbreathing Engines

Airbreathing engines use atmospheric air captured by their inlets to oxidize the fuel, added in the combustor, to generate thrust. By doing this, they have a big advantage over other non-airbreathing engines which must carry the oxidizer, thus decreasing their maximum payload or increasing their mass and size. For the next generation propulsion systems for high speed vehicles, an airbreathing engine is favored because of this. Airbreathing propulsion systems can be divided into steady (quasisteady) and unsteady (or pulsating) cycle systems. Pulsating propulsion systems, like the pulse detonation engine, have the main disadvantage of oscillating combustion waves, resulting in heavy vibrations and noise. Since the interest of this thesis is placed in the field of steady propulsion cycles, cyclic propulsion systems will not be investigated. In this thesis steady airbreathing propulsion systems can also be divided into airbreathing systems with either subsonic or supersonic combustion. First, airbreathing engines with subsonic combustion will be considered and it will become clear later on in this chapter why supersonic combustion is the preferred choice of combustion, when the engine has to operate in the hypersonic region. Allthough there are several types of steady airbreathing engines working today, another distinction can be made between them. Those that have moving or rotating parts and those that do not. The first airbreathing engine that will be discussed is the turboprop, shown in figure 1.1.

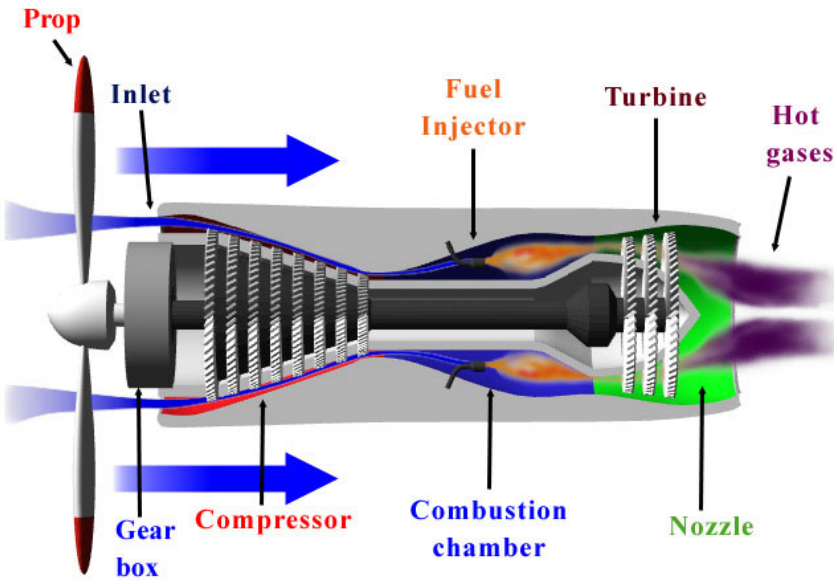

Figure 1.1: The turboprop, [Source: Cislunar Aerospace Inc.]

The turboprop has an outside propellor and consists of five components: an inlet, a compressor, a combustor, a turbine and a nozzle. The maximum velocity of the turboprop is around $M \approx 0.5$.

The turbofan produces more thrust than the turboprop because of an internal propellor or fan, shown in figure 1.2. It is because of this also regarded as a ducted turboprop, since it places a duct around the internal propellor to increase its aerodynamic performance. This allows the turbofan to have a velocity range up to $M = 0.9$. Both engines produce two thrusts, one from the fan and one from the jet exhaust.

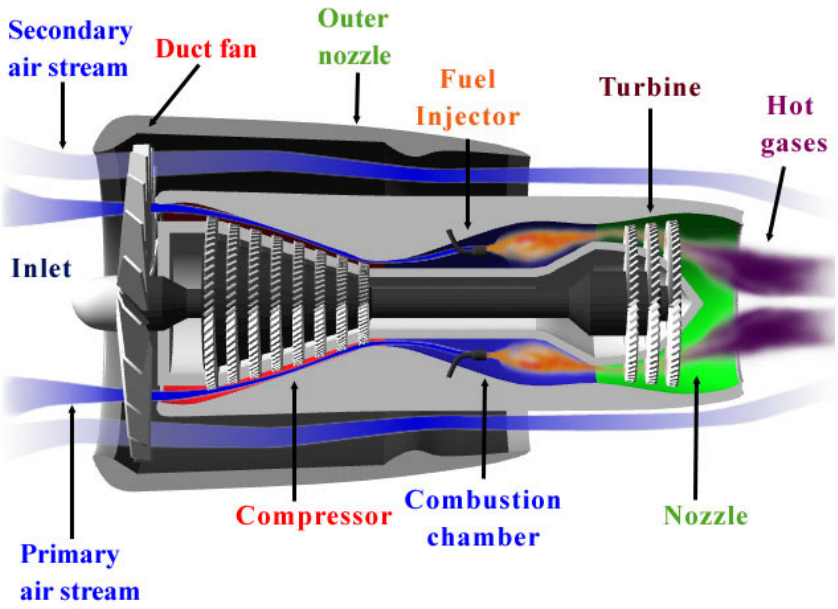

Figure 1.2: The turbofan, [Source: Cislunar Aerospace Inc.]

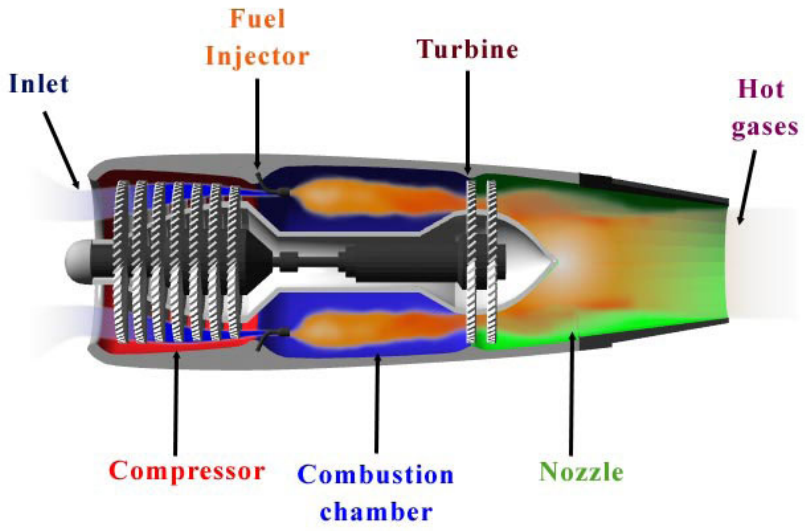

Figure 1.3: The turbojet, [Source: Cislunar Aerospace Inc.]

The turbojet is the first airbreathing engine with a velocity faster than Mach 1, shown in figure 1.3, and was used for the Concorde. The velocity range is dependent on the internal temperature of the engine, more specific the melting point of the turbine blades, and has a maximum just above Mach 2.

When the engine has to operate with freestream Mach numbers higher than one, the previous three engines are not able to fulfill that demand because their internal rotating parts are vulnerable due to the high flow temperatures. An airbreathing engine capable of operating above Mach 1 and without those temperature limitations, thus without moving or rotating parts, is the ramjet.

1.3 The Ramjet

The ramjet is a simple engine concept consisting of a diffuser (consisting of an inlet and an isolator), a burner (or combustion chamber) and a nozzle, shown in figure 1.4. Because it differs from other airbreathing engines by having no moving or rotating parts, like a compressor in the turbojet, or a turbine, the ramjet is lighter and simpler than the turbojet.

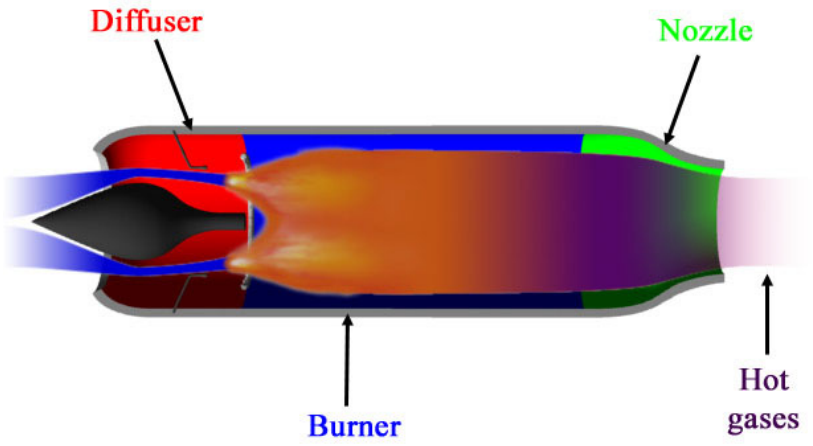

Figure 1.4: The ramjet, [source: Cislunar Aerospace Inc.]

The name *ramjet* comes from the way of air compression done by the inlet, which collects and compresses, or rams, the incoming air flow to the isolator and from there on to the combustor. By doing this, the air flow velocity decreases dramatically from supersonic to subsonic speeds by means of a normal shock system inside the isolator, and produces ram pressure and an increase in temperature of the air flow. In the fixed area combustor (consisting of a fuel injector and a flame holder), heat and mass is added, through injection, mixing and burning of fuel with the incoming air flow. And finally the nozzle converts a portion of the energy of the outgoing combustion flow to kinetic energy to produce thrust. This is done by accelerating the flow and the reaction to this acceleration produces the thrust, as is explained by Newton's Third Law. The thrust F can be seen as a mechanical force, which is defined as the change in momentum, which is the mass flow

rate $\dot{m}$ times the velocity u (the velocity will be termed u in this thesis to avoid confusion with V, which will be used further for the volume), plus the pressure difference Δp times the exit area A_e:

$$F = \dot{m}_e u_e - \dot{m}_0 u_0 + (p_e - p_0) A_e \tag{1.1}$$

The thrust equation, given above, contains three terms. The first term, referred as the *gross thrust*, is the exit mass flow rate times the exit velocity, and is associated with the conditions in the nozzle of the ramjet. The second term, called the *ram drag*, is the free stream mass flow rate times the free stream velocity. The last term, is the *pressure correction term*, and is needed because the exit pressure is not equal to the free stream static pressure. It is usually small compared to the first term of the thrust equation.

One of the characteristics of the ramjet is that the engine has two sections where the air flow has a velocity in the vicinity of Mach 1, which is also known as *choked flow*. When the flow is choked, it means that the mass flow rate has become independent of the pressure downstream, and only dependent on the pressure and temperature upstream. Before choking occurs, the flow is dependent on the downstream conditions. The flow is choked in the throat section, between the exit of the combustor and the nozzle, and generates a back pressure towards the entrance of the combustor. And for a ramjet to have subsonic combustion, it is therefore required to have a strong or normal shock system between the inlet and the combustor, reducing the flow velocity to below $M = 1$. The section where this shock system (further refferred to as *shock train*)is located is called the *isolator*. The isolator and choked flow are further discussed in chapter two.

One major drawback of the ramjet is the lack of producing static thrust. A ramjet only produces thrust when the vehicle is moving and cannot produce thrust when the engine is stationary or static. Because of this, ramjets need other propulsion systems to accelerate the vehicle to a speed where the ramjet is able to produce thrust. Rockets for example could be used to accelerate ramjets to supersonic velocities.

1.3.1 The TurboRamjet

One example of practical use of a ramjet engine in an airplane (other examples include use of ramjets in missiles), is the combination of a ramjet with a turbojet. This combination or hybrid is called the *turboramjet* and is used in the SR-71, also known as the *BlackBird*, shown in figure 1.5. The figure shows the SR-71 and a schematic of the engine. The engine is a ramjet mounted with a turbojet inside. The turbojet core is located inside a duct, which contains a combustion chamber downstream of the turbojet nozzle. The entire engine can run in turbojet mode at takeoff and speeds upto Mach 2.2, which is the upper limit for the turbine blades of the turbojet. Accelerating above this velocity limit it has to switch to the ramjet mode. The switching occurs by closing or opening bypass flaps inside the engine, located just downstream of the diffuser. When closed, the air is forced directly into the compressor section of the turbojet. And when opened, the air is blocked from the turbojet and forced to the aft combustion chamber, by which the engine then produces thrust as a ramjet engine.

During a SR-71 flight, the engine would start as a turbojet during takeoff and climbing to a high altitude with high subsonic speeds. The portion of the engine downstream of the turbojet would then be used as an afterburner to accelerate the plane above Mach 1. After reaching a high enough Mach number the bypass flaps close and the engine switches to ramjet mode to accelerate to cruise speed. The SR-71 flight speeds were typically around Mach 3 and 3.5 during cruise flight. By using this engine, the SR-71 could operate from zero to Mach 3^+ using the features of both turbojet and ramjet into one engine.

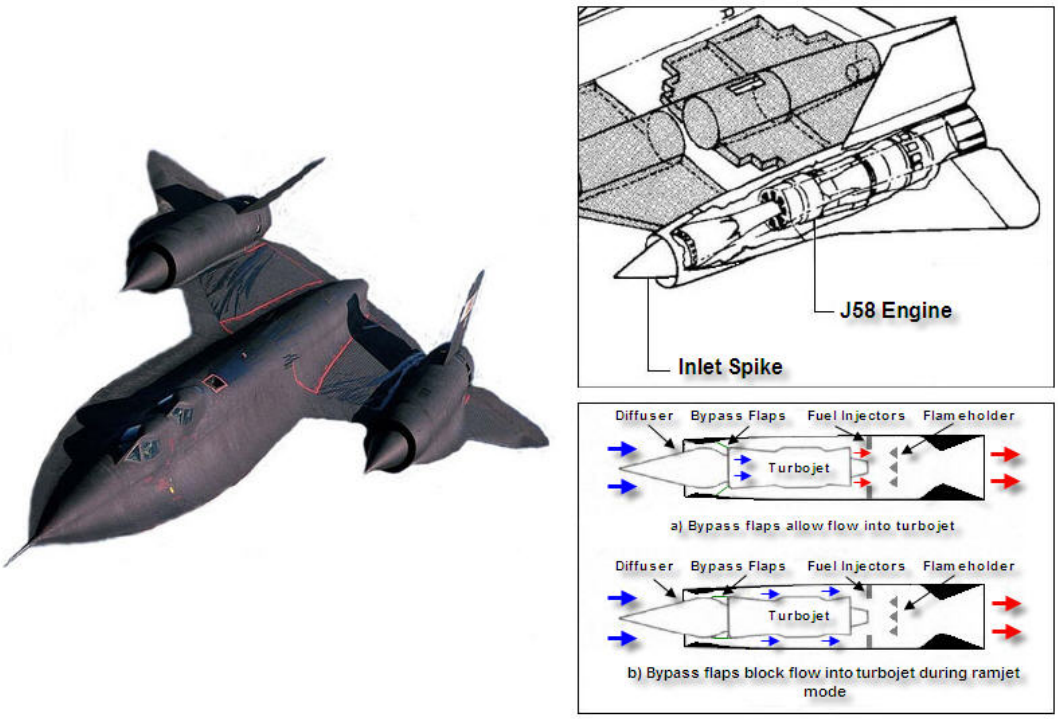

Figure 1.5: The Blackbird

1.3.2 Ideal Ramjet Performance

The ideal theoretical performance of the subsonic ramjet can be shown by considering several ideal conditions and by using a control volume analysis schematically shown in figure 1.6. The performance itself is indicated throughout the whole thesis by three characteristics: the total pressure loss, the entropy increase and the specific impulse. For the subsonic ramjet the thrust and specific impulse are sufficient here to indicate the performance, since the interest in this thesis is placed with the supersonic combustion ramjet.

Between stations 0 and 2 isentropic (reversible and adiabatic) diffusion and compression with a decrease in Mach number ($M_2 << 1$). In this thesis station 1 is taken as the entrance of the internal inlet, station 0 is in fact the entrance of the external inlet. Between stations 2 and 3 there is constant pressure combustion, according to the ideal Brayton cycle. And between stations 3 and 4 ideal expansion through the nozzle ($p_4 = p_0$). There are no moving or rotating parts, so there are no mechanical losses to take into account. The working fluid inside the engine is air, which is assumed to behave as a perfect gas with constant specific heats.

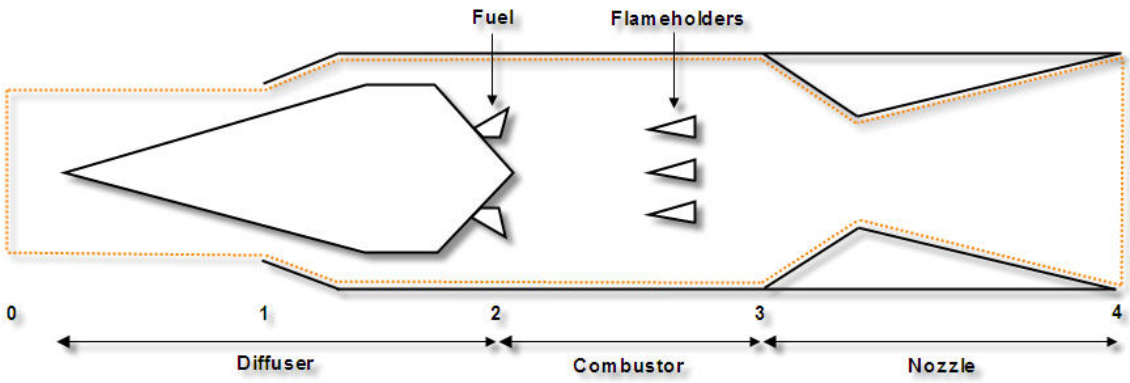

Figure 1.6: Ramjet schematic

Using equation (1.1) to calculate the thrust F, with ideal expansion:

$$F = \dot{m}(u_4 - u_0) \tag{1.2}$$

where u_4 and u_0 are the exit and inlet flow velocities. The thrust equation given in terms of non-dimensional parameters is:

$$\frac{F}{\dot{m}a_0} = \frac{u_4}{a_4}\frac{a_4}{a_0} - \frac{u_0}{a_0} \tag{1.3}$$

where $a = \sqrt{\gamma RT}$ the speed of sound. This results in:

$$\frac{F}{\dot{m}a_0} = M_4\frac{a_4}{a_0} - M_0 = M_4\sqrt{\frac{T_4}{T_0}} - M_0 \tag{1.4}$$

Subsonic combustion ramjets have combustor flow velocities M_2 usually taken between 0.3 and 0.35, and for ideal performance analysis the pressure remains constant (Brayton cycle). The low velocity flow is necessary to keep the flameholders from blowing out, meaning the flames deattach from the flameholders. The conservation of momentum equation now becomes:

$$p_2A_2 + \rho_2u_2^2A_2 = p_3A_3 + \rho_3u_3^2A_3$$

$$A_2(1 + \gamma M_2^2) = A_3(1 + \gamma M_3^2)$$

where it can be seen that the flow velocity after combustion is larger then before combustion, but still smaller than unity $M_2 < M_3 << 1$. The ratio of the temperature at the inlet and the temperature at the exit is needed to find the thrust. Since both sections are isentropic and adiabactic compressed or expanded, the temperature ratio can be given by:

$$\frac{T_{t_4}}{T_{t0}} = \frac{T_{t_3}}{T_{t2}} = \tau_c \tag{1.5}$$

with τ_c the stagnation temperature ratio across the combustor. The thrust can now be written as:

$$\frac{F}{\dot{m}a_0} = M_0\left(\sqrt{\frac{T_{t_3}}{T_{t_2}}} - 1\right) = M_0(\sqrt{\tau_c} - 1) \tag{1.6}$$

It can be seen that a ramjet needs to move forward to develop thrust and is dependent on the *ram compression* of the incoming air flow. Efficient compression of the incoming flow requires high enough velocities. And equation (1.8) shows that the thrust performance of the ramjet depends on the stagnation temperature ratio between stations 2 and 3, the higher the ratio, the better the thrust performance (T_{t_2} increases with increasing flight Mach number). This also shows the second

disadvantage of the ramjet for using subsonic combustion, the static temperature at station 3 (the combustor) increases to very high values at higher mach numbers, which could be catastrofic to the material used inside the engine. For this reason, at higher Mach numbers, the high specific impulse through subsonic combustion loses its advantage due to the increasing static combustor temperature and supersonic combustion would then be more favorable.

A characteristic to determine the performance of the ramjet is the specific impulse I_{sp} and is used to measure the efficiency. It is defined as the change in momentum per unit mass of propellant and is given by:

$$I_{sp} = \frac{F}{f\dot{m}g} = \frac{1}{g}\frac{(\sqrt{\tau_c}-1)(c_0\Delta h_{fuel}/c_pT_0)}{\theta_0(\tau_c-1)} \tag{1.7}$$

For an ideal ramjet performance calculation, an ideal condition is stoichiometric or ideal combustion. Stoichiometric fuel consumption means that all the fuel is burned and the fuel/air ratio is denoted as f_{stoich}.

A simple calculation of the performance of the stoichiometric ramjet with inlet losses is given next (de Wolf, 1994). The losses are not because of friction or spillage, but due to shock waves inside the engine. The inlet efficiency η_R is assumed to be according to the American militairy specification MIL-E-5008B used for engine designs with supersonic velocities up to Mach 5:

$$\eta_R = \frac{p_{t_2}}{p_{t_0}} = 1 - 0.075(M_0-1)^{1.35} \tag{1.8}$$

At very high velocities the inlet efficiency η_R is usually replaced by a kinetic energy efficiency η_{KE}, defined as:

$$\eta_{KE} = \left(\frac{u_{2,is}}{u_0}\right)^2 \tag{1.9}$$

Here $u_{2,is}$ is the velocity after isentropic compression. Rewriting eq.(1.2) with the kinetic energy efficiency:

$$\frac{F}{\dot{m}u_0} = \eta_{KE}^{\frac{1}{2}}\left(\frac{u_e}{u_{2,is}}\right) - 1 \tag{1.10}$$

Or, in tems of the *specific thrust* Ψ

$$\Psi = \frac{F}{\dot{m}} = u_0\left[\eta_{KE}^{\frac{1}{2}}\left(\frac{T_{t_4}}{T_{t_0}}^{\frac{1}{2}}\right) - 1\right] \tag{1.11}$$

Also needed is the thrust specific fuel consumption *TSFC* and the specific impulse I_{sp}. The TSFC is defined as the ratio between the fuel to air ratio f and the specific thrust Ψ:

$$TSFC = \frac{\dot{m}_f}{\dot{m}}\frac{1}{\Psi} \tag{1.12}$$

A low TSFC means a high efficiency and vice versa a high TSFC a low efficiency. The specific impulse is given as the specific thrust devided by the fuel to air ratio and the gravitational constant g:

$$I_{sp} = \frac{\Psi}{g\left(\frac{\dot{m}_f}{\dot{m}}\right)} \tag{1.13}$$

Using certain values for the flight Mach number M_0, the temperature and the velocity of sound in the stratosphere ($T_0 = 216.7$K and $a_0 = 295$m/s), and stoichiometric combustion of hydrogen (ER=1 and $\dot{m}_f/\dot{m} = 0.0292$), with a combustion heating value H_c=120 MJ/kg for hydrogen the temperature rise in the combustor can be determined and is found to be $T_{t_4} - T_{t_2}$=3490 K (de Wolf, 1993). In reality, because of real-gas effects, these temperatures will not be reached (de Wolf, 1995). The specific impulse and the specific thrust with stoichiometric combustion can be determined using the above mentioned values and are both shown in figures 1.7 and 1.8.

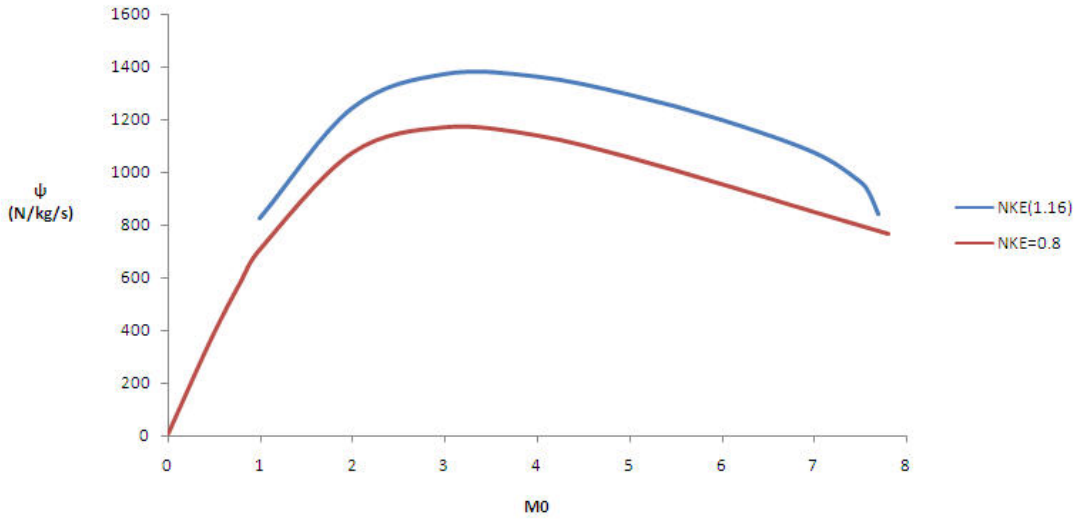

Figure 1.7: Ramjet specific thrust (de Wolf)

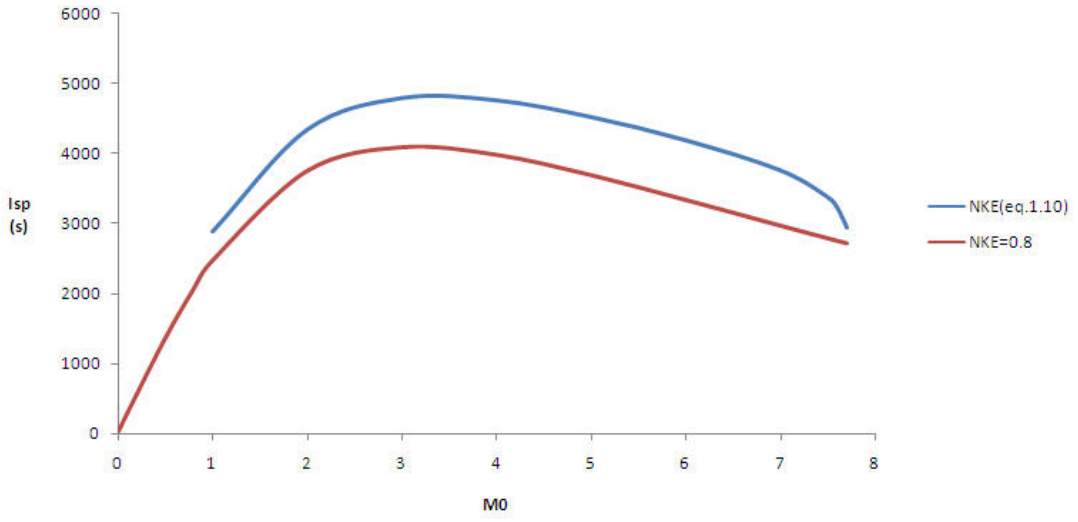

Figure 1.8: Ramjet specific thrust (de Wolf)

In figures 1.7 and 1.8 the dark blue line has a pressure recovery according to eq.(1.9) and the light blue line has a constant pressure recovery of 0.80 (de Wolf, 1994). It can be seen in both graphs that the maximum performance of a ramjet with hydrogen as fuel is around Mach 3 and continues to decrease with increasing flight Mach number. The graphs indicate an upper practical limit for the ramjet when flying faster than Mach 7 when using a pressure recovery according to eq.(1.10).

Another approach to determine the performance of the ramjet is by looking at the structural limits of a ramjet (Mattingly, 2006). Structural limits are for instance the melting temperature or maximum internal pressure of a material or construction. A structural limit of the ramjet, in

particular the ramjet combustor, is the combustor stagnation temperature T_{t_3} for a chosen material, which is increased by the addition of fuel and the conversion of chemical energy into thermal energy during combustion. From literature several maximum temperatures are given, depending on the choice of material, ranging from 1600K to 2200K. With this we can determine the specific thrust of an ideal ramjet, assuming no losses in the inlet. Using eq.(1.8) and rewriting it we find for the specific thrust:

$$\frac{F}{\dot{m}_0} = a_0 M_0 \left(\sqrt{\frac{T_{t_3}}{T_{t_2}}} - 1 \right) = a_0 M_0 \left(\sqrt{\frac{T_{t_4}}{T_{t_0}}} - 1 \right) \tag{1.14}$$

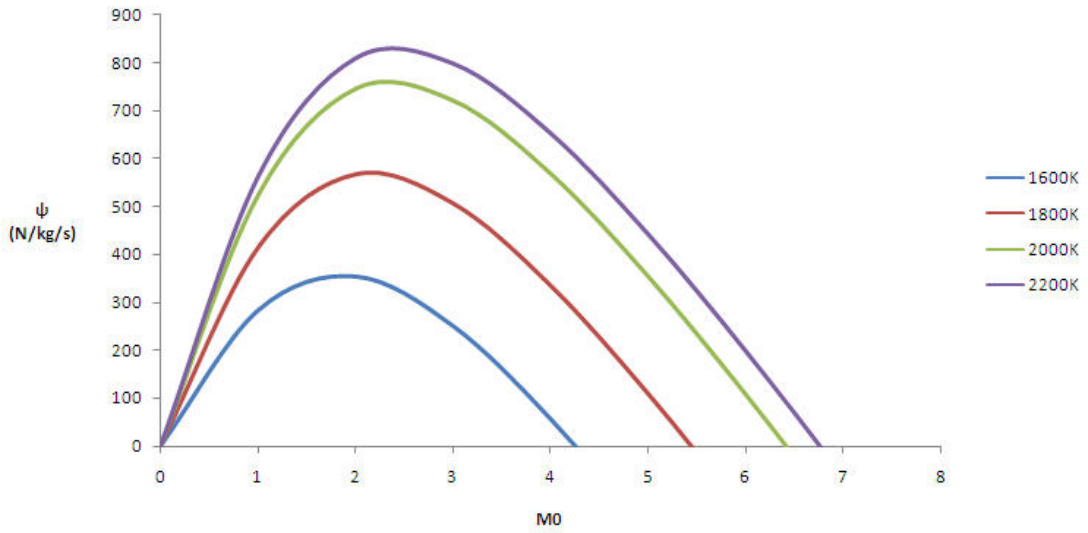

Figure 1.9: Ramjet specific thrust (Mattingly)

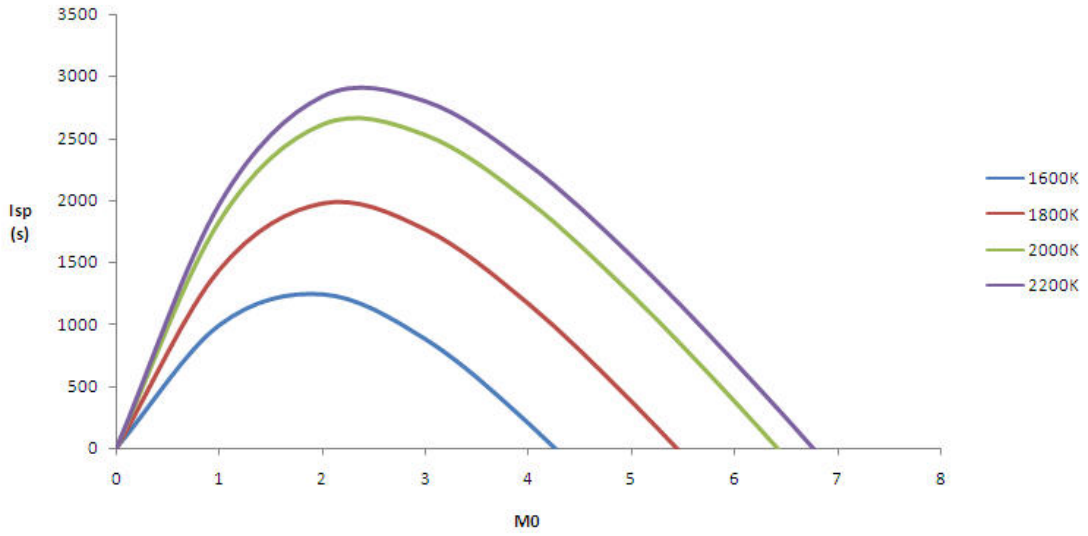

Figure 1.10: Ramjet specific impulse (Mattingly)

The specific thrust and specific impulse are plotted in figures 1.9 and 1.10, in which it can be seen that with a combustor temperature limit the maximum are obtained at a Mach number between 2 and 3. And that the maximum Mach number is between 5.5 and 7.

1.4 Supersonic Combustion

The velocity of the oncoming airflow to the engine inlet can be represented as relative kinetic energy. When the airflow is decelerated within the inlet, the velocity and thus the kinetic energy decrease. Since the conservation of energy in a flow must hold, the missing kinetic energy will reappear as *internal energy*. This means that the more the airflow is decelerated to subsonic flow, the more internal energy appears inside the engine, resulting in a higher pressure, temperature and density of the airflow entering the combustor.

When the temperature is increased too much through combustion, dissociation of combustion products will occur. Dissociation is the separation of molecules into less complicated molecules, with accompanying absorption of energy. This means that much of the chemical energy of the fuel in dissociation products will not be usable but is *lost*, resulting in a decrease in generation of thrust. Because of this, the static temperature at the entrance of the combustion chamber has an upper limit. From literature, this limit for subsonic combustion is around 2000K, corresponding with an inlet Mach number of 6 to 7, depending on material choice, cooling, and the altitude of the engine. The stagnation temperature is given by:

$$\frac{T_t}{T} = 1 + \frac{\gamma - 1}{2} M^2 \tag{1.15}$$

and with $T_{t_2} = T_{t_0}$ the static entrance temperature T_2 can be found with:

$$T_2 = \frac{T_{t_0}}{1 + \frac{\gamma - 1}{2} M_2^2} \tag{1.16}$$

For subsonic combustion ramjets, an upper limit can be set for the velocity inside the combustion chamber, called the *blow-off limit*, which is the maximum velocity at which the flame remains attached to the flame holders. A higher Mach number will cause the flame to deattach from the flame holders. From literature (de Wolf, 1994) this limit is a Mach number of $M = 0.35$. With this the static temperature T_2 at the entrance of the combustion chamber can be determined. But, when the airflow is not slowed down to a Mach number of below one, the flow at the entrance of the combustor remains supersonic and combustion changes from subsonic combustion to supersonic combustion. One of the important changes is the static temperature difference at the entrance of the combustor. Figure 1.11 shows combustor entrance static temperature levels (for different inlet entrance Mach numbers) versus the freestream flow Mach number and it can be seen that when the inlet entrance Mach number increases the slope of the combustor static entrance temperature decreases. Thus when the ramjet operates in the hypersonic regime it must operate with supersonic combustion and without normal shock waves to avoid reaching unnecesary high heat transfer and structural loads.

Supersonic combustion is dependent on two rates, the mixing rate (the rate at which the fuel mixes with the incoming flow) and the chemical kinetic rate (the rate at which the mixed fuel will oxidize), and can thus be divided in four types of methods for obtaining combustion (Curran, 2000):

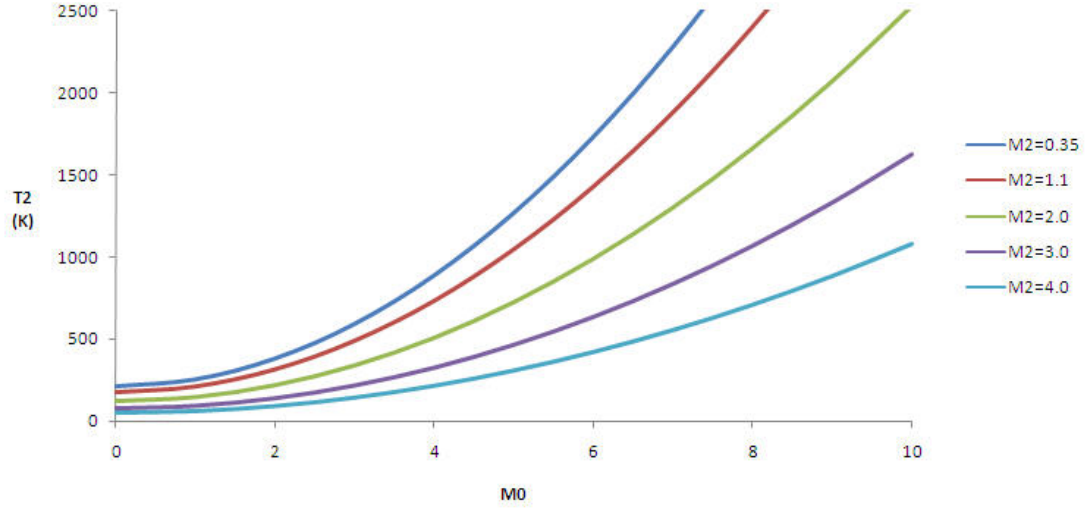

Figure 1.11: Ramjet combustor entrance temperature

- mixing controlled combustion
- kinetically controlled combustion
- shock-induced ignition
- shock-induced mixing

Mixing controlled combustion causes an almost linear pressure rise with distance from the ignition point but the associated mixing process is slower than the time to complete oxidation, thus the energy release from the fuel is limited by the mixing rate. *Kinetically controlled combustion* however has an almost step-like sharp rise in pressure produced by the combustion process and is limited only by the kinetic rate and not by mixing rate.

When the fuel is not injected inside the combustion chamber, but in the inlet section where the air has a lower pressure and temperature, the fuel has more time to mix before entering the combustor. Through shock waves inside the inlet/combustor an increase in pressure and temperature will occur in the mixture, inducing combustion. This is known as *shock-induced ignition* and can be compared with kinetically controlled combustion. This form of combustion could reduce the combustor length.

Another aspect of shock waves inducing combustion is that shock waves also generate vorticity, while crossing the fuel-air mixing region. Vorticity has been shown to enhance mixing and is thus favorable in a combustion process (Curran, 2000). This mixing process is known as *shock-induced mixing* and is closely coupled to shock-induced ignition.

The following two chapters will distinguish ramjet engine concepts by consepts using pre-mixed combustion where fuel and oxidizer flow together before ignition, and by diffusion combustion where fuel and oxidizer flow separately and has to be mixed before combustion can take place. The second chapter will investigate two ramjet engine concepts using diffusion combustion. The third chapter will investigate two ramjet engine concepts using pre-mixed combustion, where combustion is ignited through the use of a shock wave (refferred to as *shock-induced combustion*).

The modelling of combustion throughout this thesis will be done by assuming one-dimensional or quasi-one-dimensional steady homogeneous flow and by using the following conservation equations:

- conservation of mass (continuity equation)
- conservation of momentum
- conservation of energy

They are used together with the equations of state and the assumption that the molecular mass does not change after combustion in order to determine the post-combustion flow properties. Two other important conditions also are the assumption of *frictionless* flow by which Bernoulli's equation can be used. And the other is the assumption that the total mass of the flow remains constant after injection of fuel. Combustion can than be modelled as a heat addition process.

1.5 Hypersonic Flow

To determine the performance of the ramjet concepts in the next chapters calculations will be done with freestream Mach numbers increasing from 1 to 20. It is known that when the Mach number exceeds 5 the flow is commonly termed as *hypersonic flow*. In this thesis there will be no distinction made between the main characteristics of supersonic and hypersonic flow. It is however important to realise that these characteristics play a very important role when operating in the hypersonic region.

The flow is considered hypersonic in textbooks when the Mach number increases above 5 as a rule of thumb, but there is a much more important reason to choose this number. First, the hypersonic regime can not clearly be defined as going from one velocity region to another, accompanied with different reactions occurring in the flow, but it is defined as a region between Mach numbers 3 and 7. In this region certain characteristics become increasingly more important. When the freestream Mach number increases the shockwave will become steeper and the flowfield between the shockwave and the body reduces, with increasing density. This is known as the *shock layer*. The amount of kinetic energy also increases with increasing Mach numbers causing the boundary layer to grow in thickness, since viscous effects within the boundary layer convert kinetic energy to internal energy. The increase in temperature also increases the viscosity coefficient thus thickening the boundary layer. And when the temperature is high enough dissociation and ionisation of the flow occurs making an analysis of the flow field even more complex. Because of this, the hypersonic flow effects are negelected during the calculations. More information on hypersonic flow however can be found in literature (Anderson, 1989).

Chapter 2

Supersonic Combustion Ramjets

In chapter one it was determined that when ramjets are used for flight in the hypersonic region ($M_0 \geq 7$) supersonic combustion is necessary to avoid high structural loads and heat transfer. Supersonic combustion can be dependent on mixing rates, chemical kinetic rates, and shock waves. This chapter will investigate two known ramjet engine concepts using supersonic combustion depending on both mixing and chemical rates inside the combustion chambers. The first is a supersonic combustion ramjet engine, referred to as the *scramjet*, and the second is a ramjet engine with two combustion modes, changing from subsonic combustion to supersonic combustion when the flight Mach number increases, called the *dual-mode combustor*.

2.1 The Scramjet

A basic design of the scramjet engine consists of a supersonic inlet, a combustion chamber (or combustor) and a nozzle. An example of such a design can be seen in figure 2.1 showing NASA's first operational hydrogen-fueled integrated scramjet vehicle the X-43, which flew succesfull at Mach 7 and Mach 10 in 2004.

Figure 2.1: The X-43

Because of the difference in core flow velocity, the geometry changes with respect to the ramjet. Figure 2.2 shows the geometric differences between a scramjet and a ramjet. The figure shows that the ramjet geometry has two throat sections, one at the inlet exit and one at the combustor exit. The first throat choking the supersonic flow to subsonic flow and the second throat causes sthe subsonic flow to choke only to become supersonic again through expansion within the nozzle section. The scramjet, however, does not need these throats since the engine does not require subsonic flow anywhere. The scramjet does have a narrow section in the inlet section, but from thereon it diverges to the nozzle. The second throat in the ramjet geometry is also needed to stabilize the normal shock system between the inlet and the combustor through a back pressure generated by the throat. This section with a near-constant cross-section is called the isolator and is a critical component for the subsonic ramjet, but less for the supersonic ramjet when the

freestream Mach number is high enough. The function of the isolator and the phenomena occurring within this component will be discussed in section 2.2.1.

For a ramjet a relatively large contraction ratio is needed compared to a scramjet at high velocities ($M > 5$). A higher contraction ratio results in higher internal pressures for the ramjet, which is different from the scramjet inlet needing a smaller contraction ratio, and thus having lower internal pressures. However, the ramjet does have one significant advantage over the scramjet during the combustion process, being smaller Rayleigh losses or total pressure losses due to the presence of subsonic velocities.

Figure 2.2: Ramjet and scramjet geometry

The performance of a scramjet engine depends on an efficient balance between a supersonic inlet compression process, the combustion process in a supersonic combustor, and the expansion process in the nozzle. When this balance is not optimized at design conditions and possibly a wider range of conditions, the engine performance is seriously degraded. These three components will be investigated in the first part of this chapter. The second part will investigate the dual-mode combustor and the isolator, which is a necessary component for containing a pre-combustion shock system between the combustor and the inlet, as a result of the large difference in pressure between the combustor and the inlet.

2.1.1 Supersonic Inlets

The inlet for a ramjet engine design is required to capture and compress the incoming air flow, which is then mixed with fuel inside their combustor. An optimal inlet is considered to be a minimum weight geometry that provides efficient compression, generates minimum drag, and still being able to produce an uniform flow entering the combustor over a wide range of flight conditions (van Wie, 1996(a)).

There are two operating modes in which the inlet of a supersonic ramjet engine design can operate, depending on the air flow characteristics. The supersonic inlet can either be in a *started* mode, or an *unstarted* mode. The started mode basically defines the inlet to be working, when a supersonic core flow is present at the exit of the inlet and when the flow phenomena in the internal part of the inlet does not affect the air capture performance of the inlet. The air capture characteristics are defined as the free stream conditions (M_0, p_0, T_0), which affect the Reynolds number R_e defining the condition of the boundary layer, which can be either laminar, transitional, or turbulent (Van Wie, 1996(b)). The supersonic inlet is said to be unstarted when the flow at the exit of the inlet is choked, either due to over-contracting by the inlet itself or by an unsustainable level of back pressure caused by combustion in the combustor. Compared to the started inlet the unstarted inlet is less efficient in capuring airflow and has higher aerodynamic and thermal loads.

The maximum permissible internal contraction ratio just before unstart of the supersonic inlet is found by using the classical Kantrowitz limit on a control volume containing a supersonic inlet

design (Van Wie, 1996(a), Mölder, 2004). The supersonic inlet stations are defined in figure 2.3

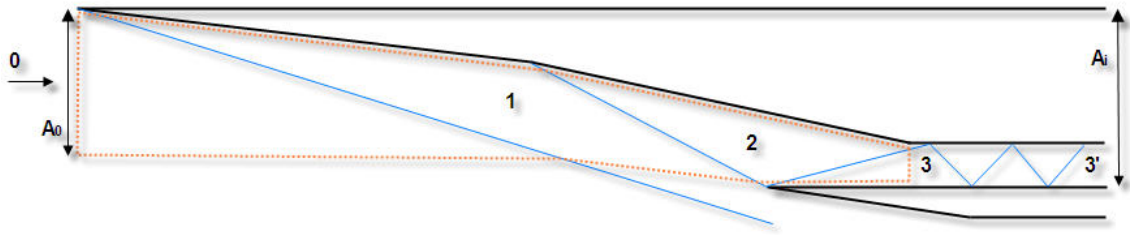

Figure 2.3: Scramjet inlet station definitions

where station 0 refers to the freestream conditions, station 1 the conditions downstream of the bow shock, station 2 the conditions at the cowl lip plane, station 3 the conditions at the inlet throat, and station 3' the conditions downstream of the pre-combustion shock system. The Kantrowitz criterion states that, when a normal shock stands in front of internal inlet part (station 2), thus choking the flow, the inlet will not start. The criterion thus assumes a normal shock and uses a one-dimensional, isentropic calculation of the internal area ratio and is given as:

$$\left(\frac{A_2}{A_3}\right)_{Kantrowitz} = \frac{1}{M_2}\left[\frac{(\gamma+1)M_2^2}{(\gamma-1)M_2^2+2}\right]^{\frac{\gamma}{\gamma-1}}\left[\frac{\gamma+1}{2\gamma M_2^2-(\gamma-1)}\right]^{\frac{1}{\gamma-1}}\left[\frac{1+\frac{\gamma-1}{2}}{M_2^2}\frac{\gamma+1}{2}\right]^{\frac{\gamma+1}{2(\gamma-1)}} \tag{2.1}$$

or rewritten

$$\left(\frac{A_3}{A_2}\right)_{Kantrowitz} = \left[\frac{\gamma-1}{\gamma+1}+\frac{2}{(\gamma+1)M_2^2}\right]^{\frac{1}{2}}\left[\frac{2\gamma}{\gamma+1}-\frac{\gamma-1}{(\gamma+1)M_2^2}\right]^{\frac{1}{\gamma-1}} \tag{2.2}$$

The Kantrowitz limit is the theoretical starting limit for an inlet start and the isentropic limit is the theoretical maximum contraction ratio and is given as

$$\left(\frac{A_3}{A_2}\right)_{isentropic} = M_2\left(\frac{\gamma+1}{2}\right)^{\frac{\gamma+1}{2(\gamma-1)}}\left(1+\frac{\gamma-1}{2}M_2^2\right)^{-\frac{\gamma+1}{2(\gamma+1)}} \tag{2.3}$$

Both limits are shown in figure 2.4. The limits both become conservative at higher Mach numbers as a result of the assumption of one normal shock.

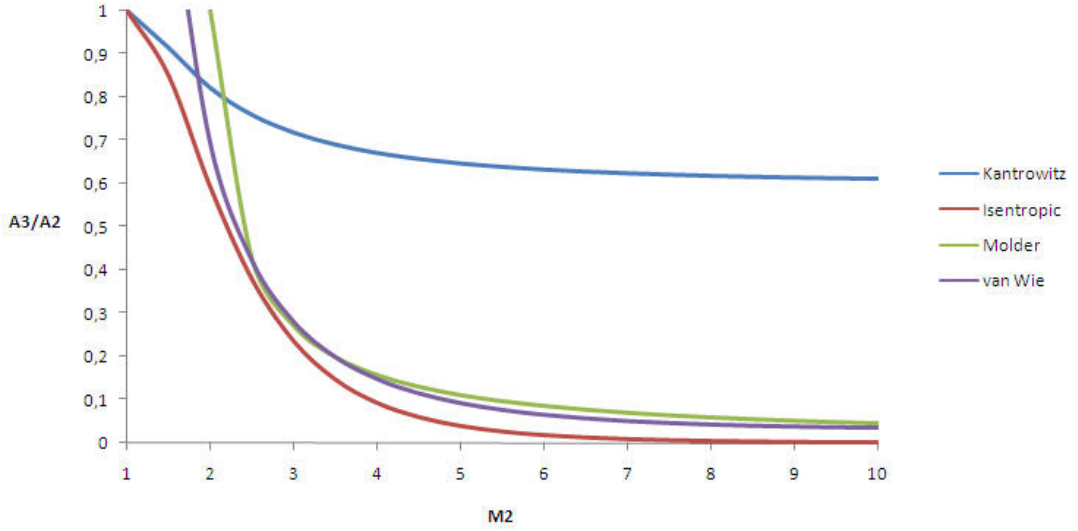

Figure 2.4: Starting and maximum contraction ratios

Also shown in figure 2.4 are two empirical relations, the first implying a practical limit on the maximum contraction ratio (Van Wie, 2000)

$$\frac{A_3}{A_2} = 0.05 - \frac{0.52}{M_2} + \frac{3.65}{M_2^2} \tag{2.4}$$

and the second relation(Mölder)

$$\frac{A_3}{A_2} = \frac{1}{2.7M_2 - 4.4} \tag{2.5}$$

is a limit of stable operation of experimental supersonic and hypersonic inlets, just above the isentropic relation due to shock losses and boundary layer growth. It represents a reasonable minimum design goal for design contraction ratios before inlet unstart. The region between the Kantrowitz limit and either the empirical relations or the isentropic limit is where a *safe* design contraction ratio can be chosen for starting the inlet. When a contraction ratio is chosen outside this region (unstarted region) at the designated Mach number, inlet unstart will most likely occur.

Next to being either started or unstarted, the scramjet inlet can also operate in three different operating modes dependening on the flight Mach number, shown in figure 2.5 (Bormotova, 2003). The first mode (a) is the design mode, also known in literature as the *shock-on-lip* mode, where the shock waves induced by the forebody inpinge on the cowl lip at design conditions. When the Mach number is varied from the design Mach number, the oblique shock waves also vary from inpinging on the cowl or not. The second mode (b) is when the Mach number is higher than the design Mach number and the oblique shock waves enter the internal part of the inlet and form an intense shock wave reflected from the cowl. This can result in a separation of flow, a stagnation zone, higher local thermal zones, and a decrease in flow uniformity entering the combustor. The third mode is when the Mach number is lower than the design Mach number, causing the oblique shock waves to propagate in front of the cowl decreasing the air mass capture and a reduction of the total pressure recovery factor.

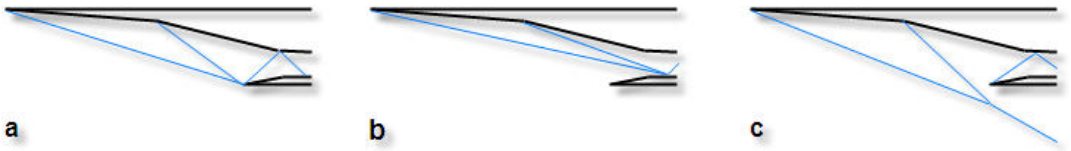

Figure 2.5: Operating modes of a scramjet inlet: (a) design mode, (b) flight Mach number higher than the design value, (c) flight Mach number lower than the design value.

Many different supersonic inlet designs have been developed to provide scramjet engines with high performances without violating design constraints. The design itself is a carefull tradeoff between inlet performance, structural weight, thermal survivability, and geometrical integration possibility in the overal vehicle design. The following two sections will give more details about the design of the inlet.

Supersonic Inlet Design

A scramjet inlet design can be divided into three different geometrical designs, being:

- two-dimensional planar
- two dimensional axisymmetric
- three dimensional

Planar flow analysis can be used for both two-dimensional and axisymmetric inlet designs. The use of planar flow assumptions simplifies the geometry and flow analysis, which can serve as a design base for more complex inlet shapes. The analysis uses a series of oblique shock waves and isentropic compression regions (where the entropy remains constant, or a reversible process) to acquire a certain level of compression in a viscid or inviscid flow, as shown in figure 2.6. The level of compression must be high enough to sustain combustion, but also low enough to ensure non-occurance of nonequilibrium chemical losses within the combustor and nozzle.

The design must also ensure a maximum total pressure recovery, since the loss in total pressure diminishes the thrust performance. In literature it is stated that for every 1% increase of total pressure loss, 1% of thrust is lost (Ran, 2005). A general two-dimensional inlet design has two parts, an external compression part and an internal compression part.

To optimize the inlet for maximum total pressure recovery, it has been stated that the inlet-generated shock waves are of (almost) equal strength (Smart, 1999). To show an example of inlet optimization design analysis using planar flow analysis, Oswatitsch determined an optimal inviscid compression system analysis for supersonic inlets, consisting of $n-1$ oblique shock waves and one terminating normal shock wave, resulting in a subsonic flow with maximum pressure recovery (Oswatitsch, 1947). The analysis showed that total pressure recovery is maximum when all the oblique shock waves are of equal strength. This analysis however is only applicable for supersonic inlets with subsonic combustors. Supersonic combustion ramjets, however, have supersonic inlets and supersonic flow combustors.

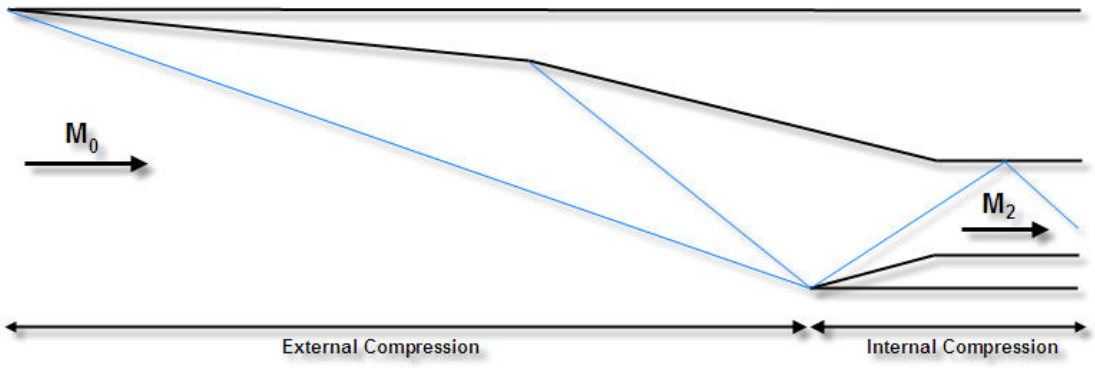

Figure 2.6: 2D-planar scramjet inlet design

The analysis was therefore adjusted with replacing the final normal shock wave with an oblique shock wave in the internal compression part of the inlet, as seen in figure 2.7 (Smart 1999, Ran 2005).

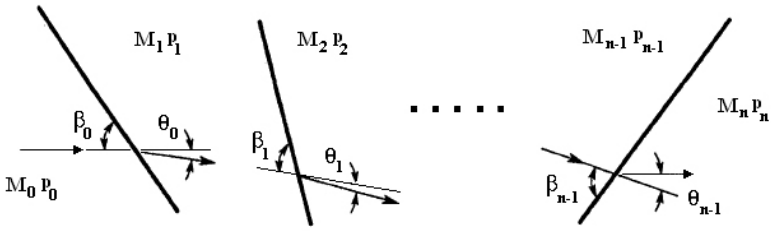

Figure 2.7: Shock wave system used for the analysis, source [Smart, 1999]

An optimization criterion was used for this analysis, which states that in a system of $n-1$ oblique shocks in two dimensions, the maximum pressure recovery is obtained when the shock waves are of equal strenght. This results in the Mach numbers perpendicular to the individual shock waves are equal:

$$M_1 sin\theta_1 = M_2 sin\theta_2 = ... = M_{n-1} sin\theta_{n-1} \tag{2.6}$$

The following notation will be used for the oblique shock wave in this thesis, with the shock angle θ and δ the shock deflection angle, shown in figure 2.8.

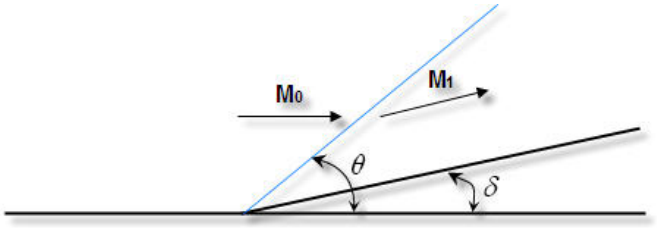

Figure 2.8: Oblique shock wave definitions

The Mach number behind an oblique shock wave can be found with (Bakker, 1997):

$$M_1^2 sin^2(\theta - \delta) = \frac{2 + (\gamma - 1)M_0^2 sin^2\theta}{2\gamma M_0^2 sin^2\theta - (\gamma - 1)} \tag{2.7}$$

Or rewritten to M_1 only being a function of θ and M_0 according to Naca 1135 (AMES, 1953):

$$M_1^2 = \frac{(\gamma + 1)^2 M_0^4 sin^2\theta - 4(M_0^2 sin^2\theta - 1)(^2_0 sin^2\theta + 1)}{[2\gamma M_0^2 sin^2\theta - (\gamma - 1)][(\gamma - 1)M_0^2 sin^2\theta + 2]} \tag{2.8}$$

The total pressure ratio across an oblique shock wave with shock angle θ can be found with (Bakker, 1997):

$$\frac{p_{t_1}}{p_{t_0}} = \left[\frac{(\gamma + 1)M_0^2 sin^2\theta}{2 + (\gamma - 1)M_0^2 sin^2\theta}\right]^{\frac{\gamma}{\gamma - 1}} \left[1 + \frac{2\gamma}{\gamma + 1}(M_0^2 sin^2\theta - 1)\right]^{-\frac{1}{\gamma - 1}} \tag{2.9}$$

The analysis concludes that to increase the maximum pressure recovery with increasing flight Mach number, the number of oblique shock waves must also increase, as shown in figure 2.9.

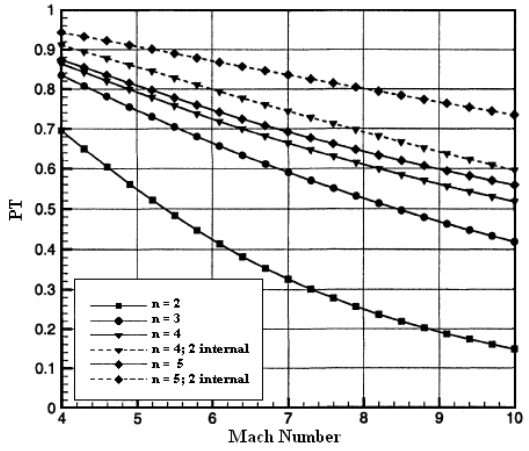

Figure 2.9: Maximum total pressure recovery for two-dimensional scramjet inlets with up to five shocks, source [Smart, 1999]

And it is concluded that the optimised shock turning angle (in the analysis termed θ_n, with $n = 0, 1, 2, 3...$ and β the shock angle) for $n + 1$ shock waves, shown in figure 2.10, with increasing Mach number remain nearly constant, which is very convenient for fixed inlet geometries used for a wide flight Mach range.

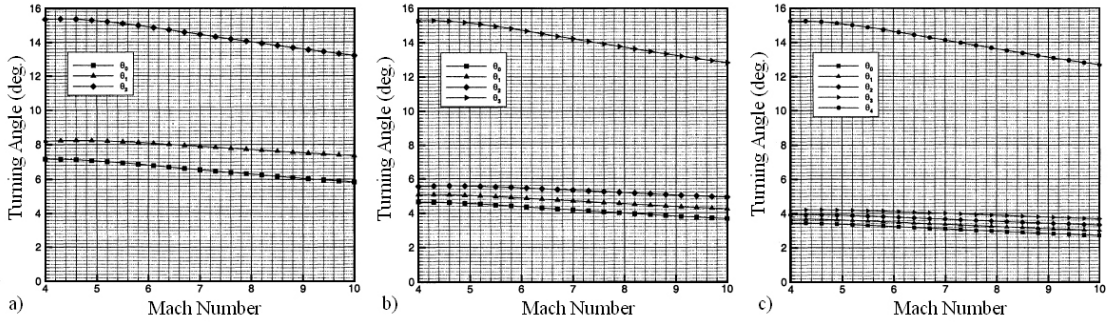

Figure 2.10: Optimal turning angles for two-dimensional scramjet inlets with one internal shock wave: a) n = 3, b) n = 4, c) n = 5 shock waves, source [Smart, 1999]

Two-dimensional inlets can be axisymmetric, which in turn can divided in outward-turning and inward-turning designs. The outward-turning designs are similarly developed with the same approach as two-dimensional planar inlet designs. However they require slightly more turning to acquire the same amount of compression. An outward-turning axisymmetric inlet is the *Oswatitsch inlet*, shown in figure 2.11.

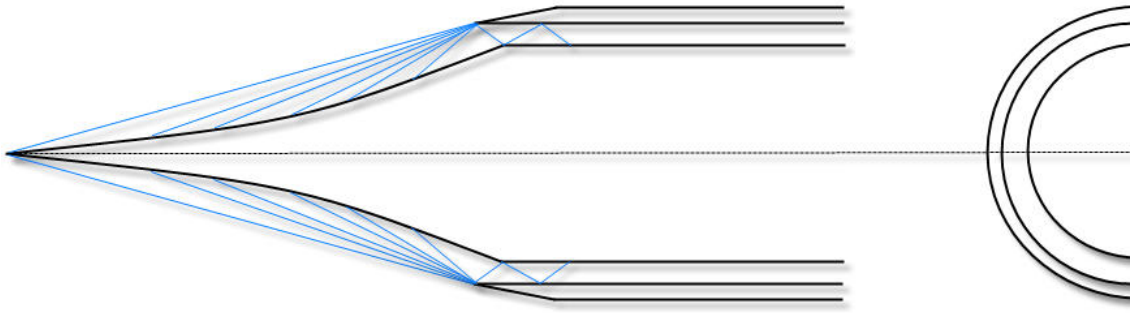

Figure 2.11: Oswatitsch inlet design, source [Curran, 2000]

The Oswatitsch inlet consists of a conical shock wave, an isentropic compression field, and a single shock wave reflected from the cowl, which is cancelled when impinging on the *shoulder*. The shoulder is the section of the center body, where the compression of the flow field changes from external compression to internal compression. The design is based on the Oswatitsch inviscid design analysis, shown in the beginning of this section. The inviscid design can be modified to account for the viscid flow, or boundary-layer growth. The main disadvantages for this design, and also for the outward-turning axisymmetric inlet in general, are small internal throat heights leading to large viscous losses, high cowl-lip drag, and sensitivity to the angle of attack influencing the air capture performance of the design.

An inward-turning axisymmetric inlet design is the *Busemann inlet*, as shown in figure 2.12. The design provides an uniform parallel inviscid flow to the combustor. The inlet consists of an inward-turning isentropic compression leading to a free-standing conical shock wave, which is cancelled when impinging on the shoulder. The main advantage of these kind of axisymmetric inlets is a high performance because of a large region of isentropic compression. Also the boundary layer in the forward region of the inlet is more likely to be laminar resulting in less drag, compared to a turbulent boundary layer which results in higher drag.

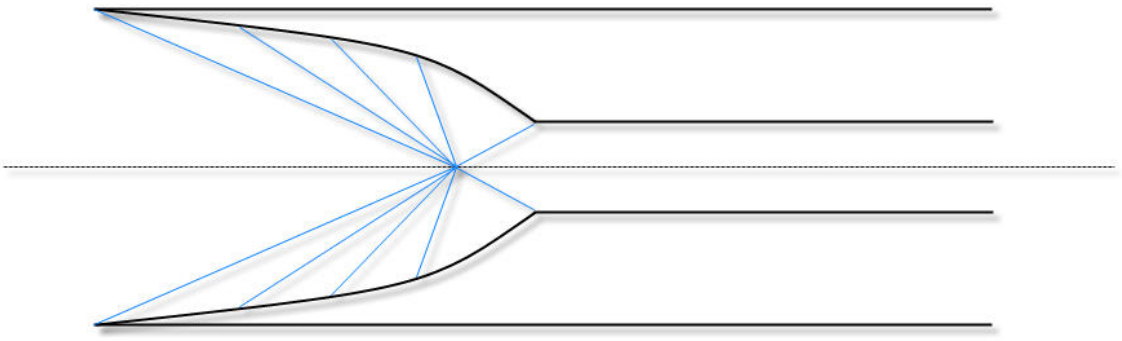

Figure 2.12: Busemann inlet design, source [Curran, 2000]

Next to two-dimensional design, three-dimensional inlet designs have also been developed for scramjets. In three-dimensional inlet designs, the sidewalls of the inlet become important, which introduce lateral compression. Sidewalls are usually designed with an aft sweep, instead of a forward sweep, see figure 2.13.

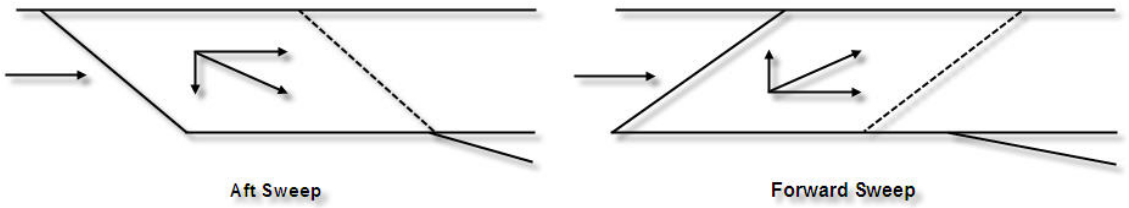

Figure 2.13: Aft sweep and forward sweep inlets, source:[Curran, 2000]

Compared to an forward sweep inlet, the aft sweep inlet is easier to start because of the flow component generated in the direction of the sweep. On the other hand, the forward sweep inlet, with an upward flow component, has an increased mass capture and reduced throat flow distortion compared to the aft sweep inlet, which has an increase in spillage due to the downward flow component, which also causes the increase in throat flow distortion. The increase in spillage however is desired at low flight speeds, because this avoids a normal shock wave at the entrance of the inlet, providing supersonic flow to enable the engine with a fixed configuration to operate over a wide range of Mach numbers (Chen, 2003). When the flight Mach number increases, the sidewall shock angles become smaller and the spillage is reduced, increasing the mass capture.

Figure 2.14 shows an aft sweep sidewall-compression inlet for a scramjet. The sidewalls thus offer further compression of the incoming flow in horizontal direction, reducing the total inplane turning of the flow to obtain the desired compression at the exit of the inlet. The sidewall leading edges are swep to reduce the aerothermal loads on the leading edges during high flight Mach numbers.

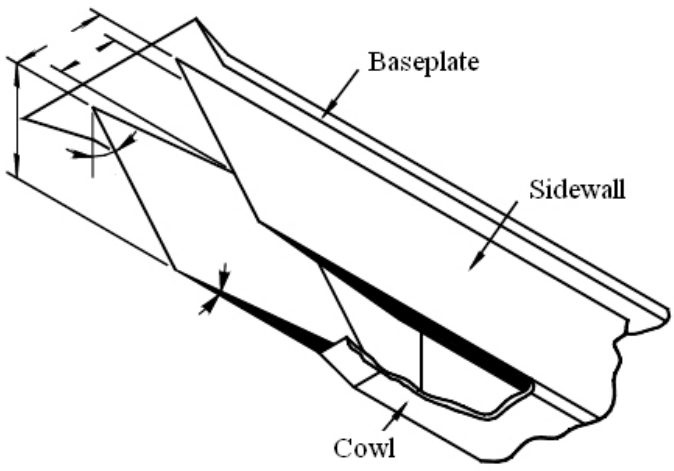

Figure 2.14: Three-dimensional inlet design, source:[Curran, 2000]

Shock-Boundary Layer Interaction

Within the aerodynamic flowpath of the inlet and combustor, boundary layers are present. Boundary layers are layers in that part of the flow near a surface where the viscosity is dominant. Within this layer molecules are slowed down near the surface because of collisions with other molecules. These collisions thus cause a velocity gradient, with a zero velocity at the surface (no-slip condition). Hypersonic velocity flows are also known as high enthalpy flows and with the enthalpy of a flow remaining constant, the decrease of velocity in a boundary layer towards the surface will result in a increase of static temperature towards the surface. The static pressure increases through friction in the flow direction along the surface, with the pressure remaining constant perpendicular from the surface. Figure 2.15 shows the main characteristics of a boundary layer and the impingment of an oblique shock wave.

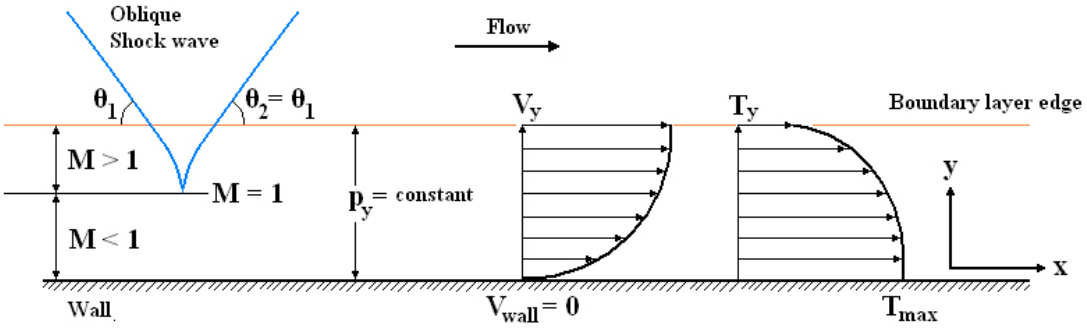

Figure 2.15: Main characteristics of a boundary layer

The thickness of the layer depends on the Reynolds number and running length of the boundary layer $L_b(x)$, which is the ratio of inertial forces (resistant to change or motion) to viscous forces and defined as:

$$Re = \frac{\rho c x}{\mu}$$

An increase of the Reynolds number means an increase in boundary layer thickness and an increase in possible boundary layer separation or turbulence. Boundary layer separation can also occur when a discontinuity, say combustion, downstream causes an increase in pressure. When this happens, acoustic pressure waves will move upstream with velocity of sound a in that part of the boundary layer which is subsonic, since acoustic waves can only propagate upstream within subsonic flow regions. These acoustic waves can *push* the boundary layer outwards, increasing the thickness and deattaching or separating them from the surface. This results in a boundary layer momentum loss, which reduces the internal performance of the engine and increases the distortion of the boundary layer velocity profile, blocking more of the incoming flow.

When the boundary layer separates, a so-called *separation region* is created, which is unstable and is capable of moving downstream depending on the disturbance and negative pressure gradient downstream. Separation regions increase wall heat transfer from the high enthalpy flow to the surface, higher than within attached or laminar boundary layers. The separation region is than also known as a *hot spot* and complicates the thermal design of the vehicle since these hot spots can move within the boundary layer. When the separation region causes the boundary layer to change from laminar to turbulent heat transfer is also increased for the region downstream. Figures 2.16 and 2.17 show two different situation for oblique shock waves in a flow with and without viscosity.

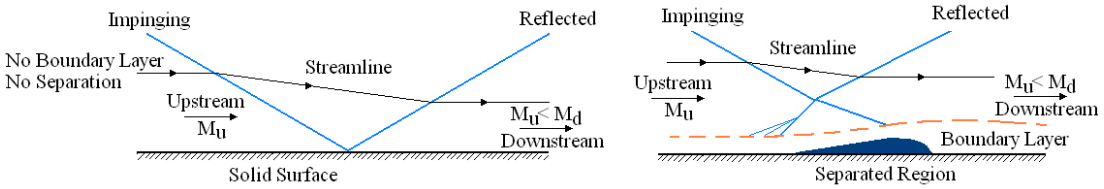

Figure 2.16: Impinging oblique shock wave with and without a boundary layer

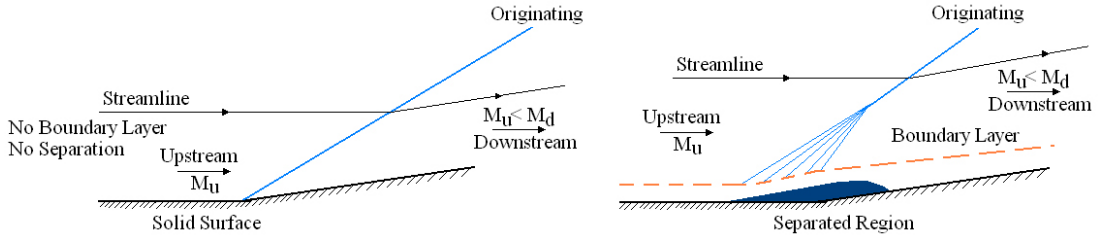

Figure 2.17: Originating oblique shock wave with and without a boundary layer

Shock-boundary layer separation must be avoided to ensure steady and uniform flow propagation downstream of the flowpath.

Heat Transfer

A very important aerodynamic phenomenon is the transfer from heat from one system to another, changing the internal energy of both systems, also known as *heat transfer*. Heat or thermal energy is normally transferred from *hot* systems to *colder* systems, by means of either convection, radiation, evaporation, or conduction, as a result of the Second Thermodynamic Law. It states that two systems with different temperatures will reach an equilibrium, thus one region has a decrease in temperature, while the other encounters an increase in temperature.

Heat transfer is very important characteristic for supersonic ramjet concepts, having very hot boundary layers engulfing the vehicle body and engine and a high temperature combustion zone inside the combustor. Boundary layers have temperature gradients resulting in an increase in static temperature towards the wall as the result of friction, while the combustor holds a high temperature flame front. The two main methods of heat transfer for hypersonic vehicles are by convection and by conduction. Convection occurs through fluids moving through or near hot zones, which is seen in cooling systems. Conduction is the transfer of thermal energy from a region of high temperature to a region of lower temperature through direct molecular contact within a medium, for instance the boundary layer. The walls of the hypersonic vehicle or the walls of the engine show heat transfer through conduction and are usually cooled through convection by cooling systems pumping cryogenic fluids near the hot regions.

The increase in temperature, through heat transfer, of the body and/or engine can lead to higher structural loads, in the form of thermal loads, which can result in structural failure. This implicates the importance of dealing with heat transfer, but the goal of this thesis is to investigate the flowpath characteristics and not the entire engine/vehicle concept. Though heat transfer also influences aerodynamic phenomena and is highly recommended to take into account when designing vehicle concepts, it will not be considered in this thesis.

Inlet Performance

There are several ways to measure the performance of an inlet. It is well known that the inlet efficiency, or compression efficiency is of the utmost importance to the overall engine performance. The inlet efficiency can be described through many parameters. Three standard inlet performance measurements used in the literature are the total pressure ratio, the kinetic energy efficiency, and the entropy increase (Curran 2000, Heiser 1994, Wittenberg 2000, de Wolf 1995). Other measurements include the air mass capture ratio, boundary layer properties (thickness, laminar or turbulent), or flow uniformity at the entrance of the combustor.

The total pressure ratio in the inlet section is defined as the ratio of the total pressure at the entrance of the combustor p_{t_3} divided by the total pressure of the freestream flow p_{t_0} at the beginning of the inlet. For simplicity, the section between stations 3 and 3' in figure 2.3 is disregarded and no pre-combustion shock system is assumed.

$$\frac{p_{t_3}}{p_{t_0}} = \frac{p_3}{p_0}\left[\frac{1+\frac{\gamma-1}{2}M_3^2}{1+\frac{\gamma-1}{2}M_0^2}\right]^{\frac{\gamma}{\gamma-1}} \tag{2.10}$$

This ratio is also known as the pressure recovery and the higher this ratio the better the inlet efficiency. The pressure recovery is directly related to the thrust performance of the engine, when the pressure recovery decreases the thrust also decreases. The pressure recovery is always smaller than one, due to the losses through shock waves.

The inlet kinetic energy efficiency η_{KE} is the ratio of the square of the velocity at the entrance of the combustor u_3, when the flow is isentropically expanded to the freestream static pressure p_0, and the square of the freestream velocity u_0 expressed as

$$\eta_{KE} = \frac{u_{is,3}^2}{u_0^2} \tag{2.11}$$

The kinetic energy efficiency is a measurement of the kinetic energy or velocity momentum, which is needed to produce thrust. The kinetic energy can be calculated using the relation for the stagnation enthalpy h_t of the flow. The relation is also known as the energy equation and is defined as

$$h_t = h_0 + \frac{u_0^2}{2} \tag{2.12}$$

which shows that the total enthalpy remains constant in an energy flow and when can be expressed for the inlet as

$$h_{t_0} = c_p T_0 + \frac{u_0^2}{2} = h_{t_3} = c_p T_3 + \frac{u_3^2}{2} \tag{2.13}$$

Combining equations (2.11) and (2.12) the kinetic energy efficiency can be expressed as

$$\eta_{KE} = \frac{u_{is,3}^2}{u_0^2} = \frac{2c_p T_{t_3}}{u_0^2}\left(1-\left(\frac{p_0}{p_{t_3}}\right)^{\frac{\gamma-1}{\gamma}}\right) = \left(1+\frac{1}{\frac{\gamma-1}{2}M_0^2}\right)\left(1-\left(\frac{p_0}{p_{t_3}}\right)^{\frac{\gamma-1}{\gamma}}\right) \tag{2.14}$$

From experimental results certain correlations are used for optimized oblique shock waves, which produce the most efficient compression for the approximate range $4 < M_0 < 14$. One correlation, used for inviscid flow is (Heiser 1996, de Wolf 1995)

$$\eta_{KE} = 1 - 0.2\left(1-\frac{M_3}{M_0}\right)^5 \tag{2.15}$$

and a correlation for viscid flow is given (Heiser 1996, de Wolf 1995)

$$\eta_{KE} = 1 - 0.4\left(1-\frac{M_3}{M_0}\right)^4 \tag{2.16}$$

The shock waves and boundary layers present in the inlet make the compression process irreversible and coincide with an increase of entropy. The entropy s is that amount of energy that can not be used for other processes. So when the entropy increases, the amount of energy lost increases and a process that uses that energy will perform less. The expression for the entropy can be found by integrating the Gibbs equation

$$Tds = dh - \frac{dp}{\rho} \tag{2.17}$$

where the enthalpy h is defined as $c_p dT$ and thus the entropy increase

$$s_3 - s_0 = c_p ln\frac{T_3}{T_0} - Rln\frac{p_3}{p_0} \tag{2.18}$$

It can be seen that this relationship is independent of the freestream Mach number, in contrast to the previous two inlet performance measurements. All three of the measurements can be used to indicate the inlet performance.

2.1.2 Supersonic Combustors

It is not the purpose of this thesis to investigate the fundamentals of combustion concerning supersonic combustion for ramjets, because these are beyond the scope of the investigation. Therefore the effects of viscid flow resulting in different combustor losses will not be investigated, allthough these play an important part in combustor efficiency and design. This section will give short definitions to shape a clear view of combustion. Next to this, the design of the combustor which can influence the aerodynamic flow path and performance of the engine will be discussed. A good resource for further details on combustion physics is Kuo's book *Principles of Combustion* (Kuo, 2005).

Combustion is said to be the act or process of burning, and occurs when fuel, oxygen (air) and heat are together. Per definition combustion is the chemical reaction of a particular substance or fuel with oxygen, where that process is heating that substance above its ignition temperature with the presence of oxygen, causing the chemical bonds of the fuel to split. This will release chemical energy from the fuel in the form of thermal energy which can be used. In this thesis combustion is assumed to be *complete combustion*, where 100% of the energy in the fuel is extracted, and combustion is to be assumed to *stoichiometric combustion*, with stoichiometric being the theoretical point at which the fuel to air ratio is ideal ensuring optimal combustion efficiency, unless otherwise mentioned.

Knowing the definition of combustion, it is important to also know the fundamental apects of, in this case, supersonic combustion in combustors for scramjets (Ben-Yakar, 1998), which are:

- flameholding
- flame stabilization
- mixing enhancement

Flameholding consists of two processes: ignition, where the flame is established, and flame holding by which combustion is maintained after flame establishing. *Flame stabilization* can be achieved by the following techniques:

1. by creating a recirculation area where the fuel and air can be mixed partially at low velocities

2. by interaction of a shock wave with partially or mixed fuel and oxidizer

3. by creating coherent structures containing unmixed fuel and air, where a diffusion flame occurs as they are convected downstream of the combustor

Combustion can be defined in several ways, depending on strenght or intensity, velocity, or where inside the combustor it occurs. When looking at intensity, two sorts of combustion can occur, *weak combustion* or *strong combustion*. Weak combustion occurs when the fuel flow rate is small and when there is no to little thrust generated. But, when the fuel flow rate increases, the engine jumps to an intensive or strong combustion mode, resulting in large thrust generation. The main goal of combustors is to provide scramjets with strong combustion. Research has shown that for weak combustion mode the combustion efficiency is around 5% and for strong combustion around 90%.

In terms of velocity inside the combustor, combustion can be either subsonic, supersonic, or hypersonic. *Subsonic combustion* means that there is a subsonic ($M \leq 1$) flow inside the combustor and that the combustor needs two *throat* sections, either geometrical or by thermal choking the flow, for the supersonic flow inside the inlet to become subsonic and the exit subsonic flow to become supersonic in the nozzle. Subsonic combustion occurs with a velocity around $M = 0.3$-0.35. Because of this low combustor flow velocity, resulting in a low flow kinetic energy, the total energy of the flow or enthalpy consists mainly of the combustion heat release energy.

Supersonic combustion is combustion in a combustor where the bulk flow remains supersonic ($M \geq 1.1$). Characteristics of supersonic combustion in ducted flows are a large rise in temperature and pressure, flow deflection, and separation. This is especially characteristic of supersonic combustion in constant area channels with $M \leq 8$ (Timnat, 1996). In these flows with local separation and a bulk flow Mach number near $M = 1$, the local wall static pressure is representative for the pressure across the entire flow at a given axial station in the combustor channel. Because of this the flow can be approximated with a one-dimensional flow analysis, which is given in section 2.2.1.2. In conrast to subsonic flow, the flow kinetic energy is now an important contribution to the total energy of the flow (Zimont, 1983).

When the combustor entrance Mach number is increased above Mach 5 and the bulk flow remains hypersonic throughout the fuel injection, mixing and burning process, supersonic combustion becomes *hypersonic combustion*. Hypersonic combustion can only occur when the vehicle has a velocity high in the hypersonic regime ($M \geq 15$), and because of this the kinetic energy of the freestream flow entering the inlet is large compared to the energy released by combustion. With increasing Mach number, the heat release percentage of the total enthalpy of the flow inside is decreased to a very low percentage (around 10% for $M \approx 25$). This is lower than for supersonic combustion, where the flow kinetic energy and the combustion heat release are roughly equal. Flow deflections and separation are thus small due to the heat release in hypersonic flow. But, since the Mach number inside remains high, Mach angles are small, and the pressure variation at a given axial station is significant, a full three-dimensional representation of the flow field is required to describe hypersonic combustion.

Combustion or ignition of the fuel/air mixture occurs at some point or distance from the moment of injection in the combustor. This can happen either *downstream* or *upstream* of the flow path (Chun, 2006). This can be controlled by varying the temperature by heat addition in the chamber until the self-ignition point of the fuel/air mixture. Usually combustion occurs upstream, but research has shown that different results are obtained when delaying the combustion to downstream conditions, in the divergent part of the combustion chamber of ramjets (Kato, 2005). The results show differences in combustion efficiency, thrust and thrust performance, summarized:

- the average combustion efficiency was higher for the downstream combustion then for the upstream combustion
- thrust performance was better for the upstream combustion then for the downstream combustion, when the (low) equivalence ratio (φ) was held constant
- a larger thrust was seen for the downstream combustion then the upstream combustion, because of the larger amount of fuel that could be injected (a higher equivalence ratio)
- the maximum wall pressure is lower when combustion occurs downstream and it occurred in the divergent section, which is more favorable for thrust generation

To remark on these results, the first result seems logical because downstream combustion means a longer path inside the combustion chamber, the fuel and air can mix better before the self-ignition point is reached. Upstream combustion has a shorther mixing path or time for the fuel/air mixture before being ignited. The second result can be explained because of the lower equivalence ratio, meaning less fuel was used. In a short path the fuel can be mixed fast and then ignited, but with a longer path the impulse would be lower. A higher equivalence ratio, the third result, showed a better performance for downstream combustion. This is plausible because with upstream combustion not all fuel would properly or mix sufficiently before ignition. Figure 2.18 shows two different combustion modes, 2.18.a shows weak combustion with the flames downstream of the combustor test section and relatively weak illumination as a result of a small equivalence ratio. When the equivalence ratio was increased, in figure 2.18.b, the flames moved more upstream towards the injector with bright illumination which is characteristic for strong combustion.

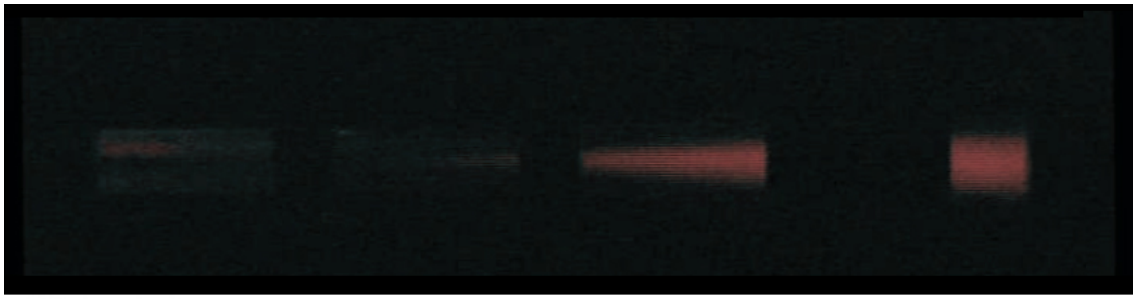

a) Weak combustion

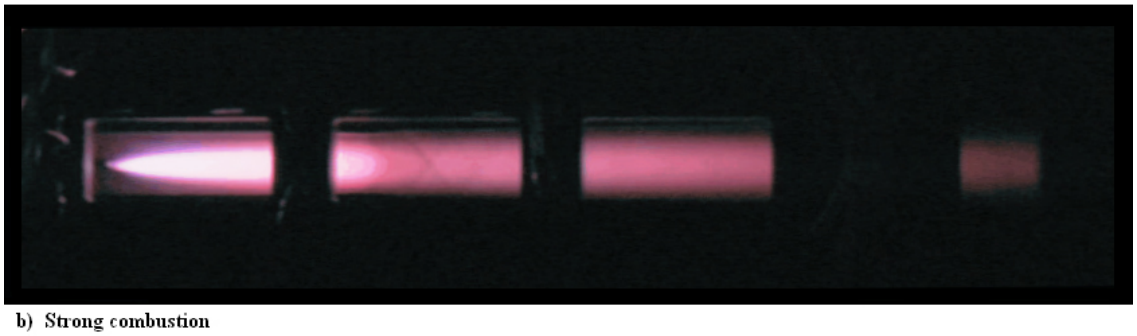

b) Strong combustion

Figure 2.18: a) weak combustion and b) strong combustion

When the fuel amount is increased even more and the equivalence ratio increases to a certain level, the whole supersonic flow will thermally choke, thus also proving that heat addition in a supersonic flow decreases the Mach number to $M = 1$ (Chun, 2006).

Combustor Design

Investigating the design of a supersonic combustor can be done by looking at the shape of the area and if it remains constant in length. The area shapes can be round, elliptical or rectangular. There are three reasons why an elliptical or rounded shape for the area is preferred above a rectangular area:

- rounded structures have the advantage of an inherent better structural efficiency, which can potentially reduce structural weight
- an elliptical area has a smaller wetted area compared to a rectangular shape with the same crosssectional or flow area, a smaller wetted area lowers the viscous drag and cooling requirements in the high dynamic pressure combustor environment
- rectangular areas have potential detrimental fluid dynamic effects of corner flows, which elliptical areas avoid, thus improving the back-pressure limits of the inlet/isolator or reducing isolator length requirements

These three reasons combined can lead to a scramjet engine with a high overall system performance and it can improve the capability of the engine to operate over a large Mach number range with a fixed-geometry. A scramjet engine design with a rectangular capture area to an elliptical throat, including an elliptical combustor, is called Rectangular-to-Elliptical Shape Transition or REST scramjet (Smart, 2006). Figure 2.19 shows a test design for a REST inlet/combustor.

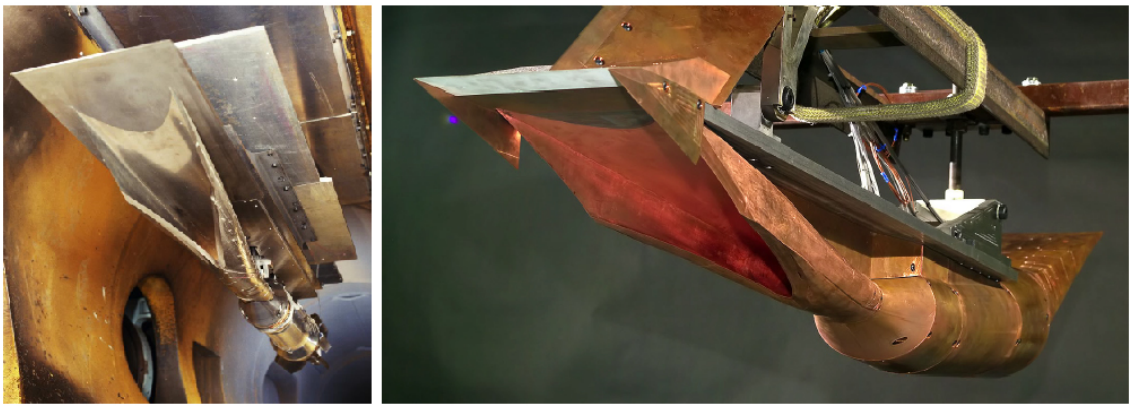

Figure 2.19: REST inlet model (Smart, 2006)

The area can be either constant, divergent or convergent in length. Since it is not desirable to have a throat, a converging area is disregarded. That leaves a constant or a divergent area to investigate. The following section will investigate inviscid flow with heat addition through the two different areas. It is assumed that the combustion process does not change the gas conditions, thus $p = \rho RT$ remains constant and $\gamma = 1.4$.

A chamber with a constant area, with inviscid flow and heat addition is also known as a *Rayleigh flow*, and is shown in figure 2.20 with the stations 3 as the combustor entrance and 4 as the combustor exit.

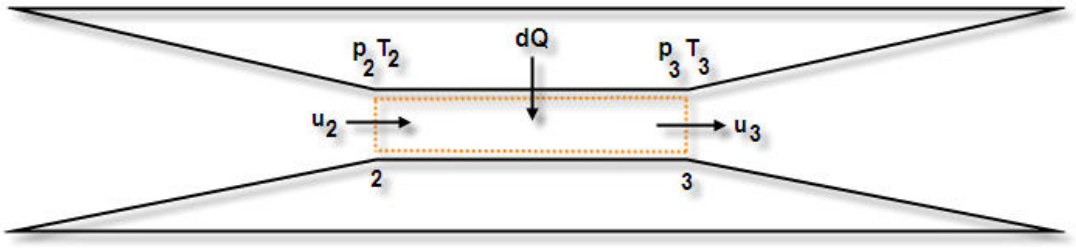

Figure 2.20: Control volume constant area combustor

Using the continuity equation and with ρ constant

$$p_2 M_2 = \sqrt{\frac{T_2}{T_3}} p_3 M_3 \tag{2.19}$$

and the momentum equation

$$p_2(1+\gamma M_2^2) = p_3(1+\gamma M_3^2) \tag{2.20}$$

and by dividing eq.(2.19) by eq.(2.20) the pressure is eliminated and with eq.(1.17)

$$\frac{M_3^2\left(1+\frac{\gamma-1}{2}M_3^2\right)}{\left(1+\gamma M_3^2\right)^2} = \frac{M_2^2\left(1+\frac{\gamma-1}{2}M_2^2\right)}{\left(1+\gamma M_2^2\right)^2}\left(\frac{T_{t_3}}{T_{t_2}}\right) \tag{2.21}$$

or:

$$G_2(M_3) = G_2(M_2)\left(\frac{T_{t_3}}{T_{t_2}}\right) \tag{2.22}$$

This equation shows how to determine M_3 with a given M_2 and T_2 and is plotted in figure 2.21 with M on a logarithmic scale

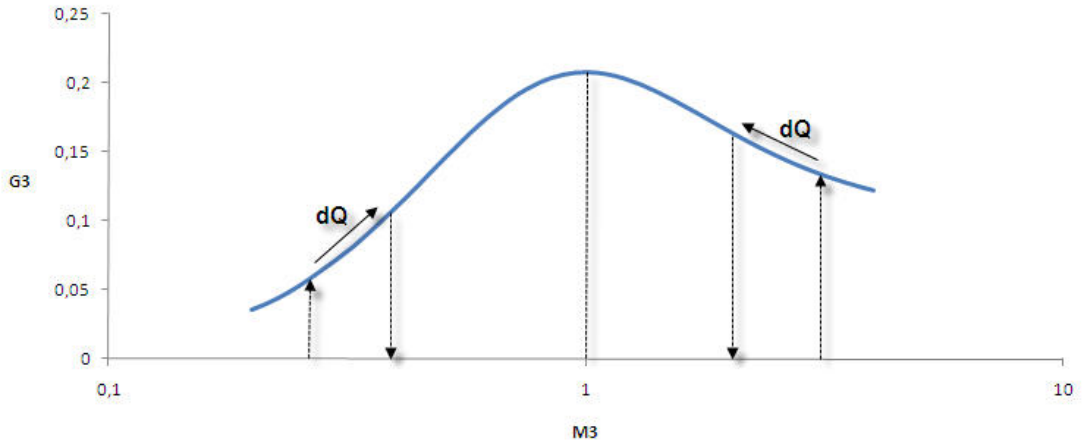

Figure 2.21: Course of G_3

Using figure 2.21 and the energy equation dQ can be found:

$$\frac{dQ}{c_p T_{t_2}} + 1 = \frac{T_{t_3}}{T_{t_2}} \tag{2.23}$$

By showing two examples, one with a subsonic M_2 and one with a supersonic M_2, an important characteristic of a Rayleigh flow is shown. For example take $M_2 = 0.35$, with $T_{t_2} = 500K$ and $T_{t_3} = 1000K$, $M_4 = 0.429$. And for example take $M_2 = 3.5$, with $T_{t_2} = 500K$ and $T_{t_3} = 1000K$, $M_3 = 2.452$. These examples show that with a subsonic flow inside a constant area and heat addition the Mach number is increased towards unity and that with a supersonic flow inside a constant area and heat addition the Mach number is decreased towards unity.

For scramjets supersonic flow is needed, thus $M_2 \geq 1.1$ and $M_3 \geq 1.1$. It is therefore important that the sonic condition is no reached anywhere inside the combustor area. When more heat is added the Mach number is decreased towards unity and when enough heat is added and unity is reached the flow is said to be *thermally choked*. Thermal choking can thus be considered as constraint for the maximum heat addition and can be found by using eq.(2.23) and stating $M_3 = 1$

$$\frac{T_{t_2}}{T_{t_{3,crit}}} = \frac{(1+\gamma)M_2^2}{(1+\gamma M_2^2)^2}(2+(\gamma-1)M_2^2) \tag{2.24}$$

and is one of the *Rayleigh functions*. These equations show the relation between the flow conditions in a constant area channel and the condition reached with heat addition leading to the sonic condition. The Rayleigh function for the pressure is given as

$$\frac{p_2}{p_{3,crit}} = \frac{1+\gamma}{1+\gamma M_2^2} \tag{2.25}$$

For the temperature:

$$\frac{T_2}{T_{3,crit}} = \left(\frac{(1+\gamma)M_2}{1+\gamma M_2^2}\right)^2 \tag{2.26}$$

The Rayleigh function for the density is given as:

$$\frac{\rho_2}{\rho_{3,crit}} = \frac{(1+\gamma)M_2^2}{1+\gamma M_2^2} \tag{2.27}$$

And the Rayleigh function for the total pressure:

$$\frac{p_{t_2}}{p_{t_{3,crit}}} = \frac{1+\gamma}{1+\gamma M_2^2}\left(\frac{2+(\gamma-1)M_2^2}{\gamma+1}\right)^{\frac{\gamma}{\gamma-1}} \tag{2.28}$$

The Rayleigh functions are plotted in figure 2.22

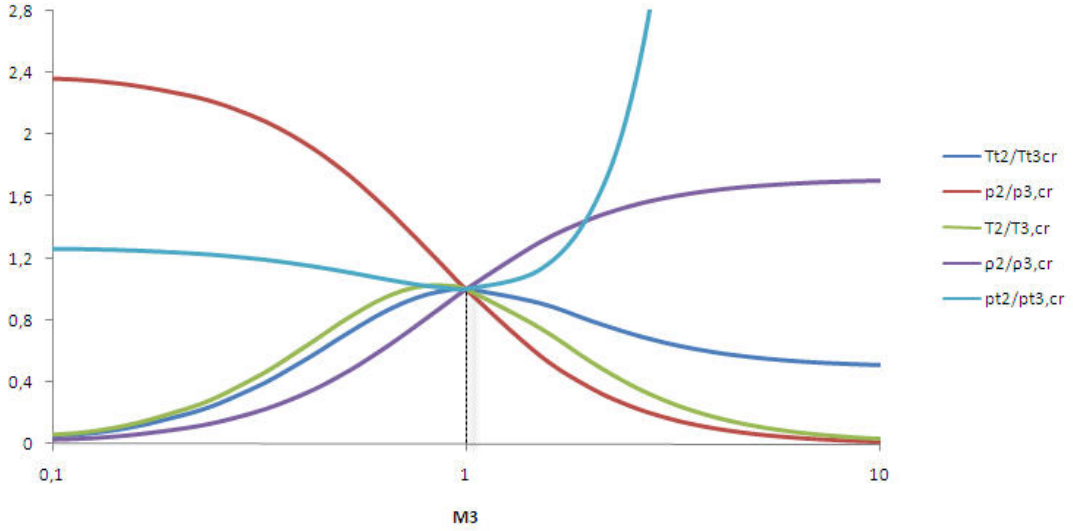

Figure 2.22: Rayleigh functions for a constant area channel with heat addition

In the figure it can be seen that the Rayleigh function for the total pressure shows that the total pressure decreases in both the subsonic flow as the supersonic flow. Thus, in a constant area channel, when heat is added the total pressure always decreases. This is also known as the total pressure loss during the combustion process and is very important for the performance of the engine. It shows that combustion at high Mach numbers decreases the total pressure very fast and should thus be done at lower Mach numbers. For example, when at $M_2 = 2.5$ heat is added, then $p_{t_{3,crit}} = 1/2.2218 p_{t_2}$ thus the total pressure is decreased to 45 percent. And to show the rate of decrease, when $M_2 = 3$ and heat is added, $p_{t_{3,crit}} = 1/3.4244 p_{t_2}$ the total pressure is decreased to 29.2 percent. Because of this, a divergent area is chosen for scramjet combustors with a dA/dx related to the increase of total temperature.

To confirm this characteristic for Rayleigh flow, another analysis is shown expressing the change of the ratio p_3/p_2 as a function of the combustor entrance conditions and the energy addition Δh or the quantity $\Delta h/\hat{h}_2$.

$$\frac{p_3}{p_2} = \frac{1+\gamma M_2^2}{\gamma+1} \pm \left(\left[\frac{\gamma}{\gamma+1}(1-M_2^2) \right]^2 - \frac{2\gamma^2}{\gamma+1} M_2^2 \left(1 + \frac{\gamma-1}{2} M_2^2 \right) \frac{\Delta h}{\hat{h}_2} \right)^{\frac{1}{2}} \tag{2.29}$$

This equation was derived by Barrère when he analysed supersonic flow in a cylindrical chamber (Timnat, 1996). The equation shows two roots which correspond to the subsonic(+) and supersonic(−) solutions. The derivation of this equation can be found in his works and is plotted for supersonic combustion in figure 2.23.

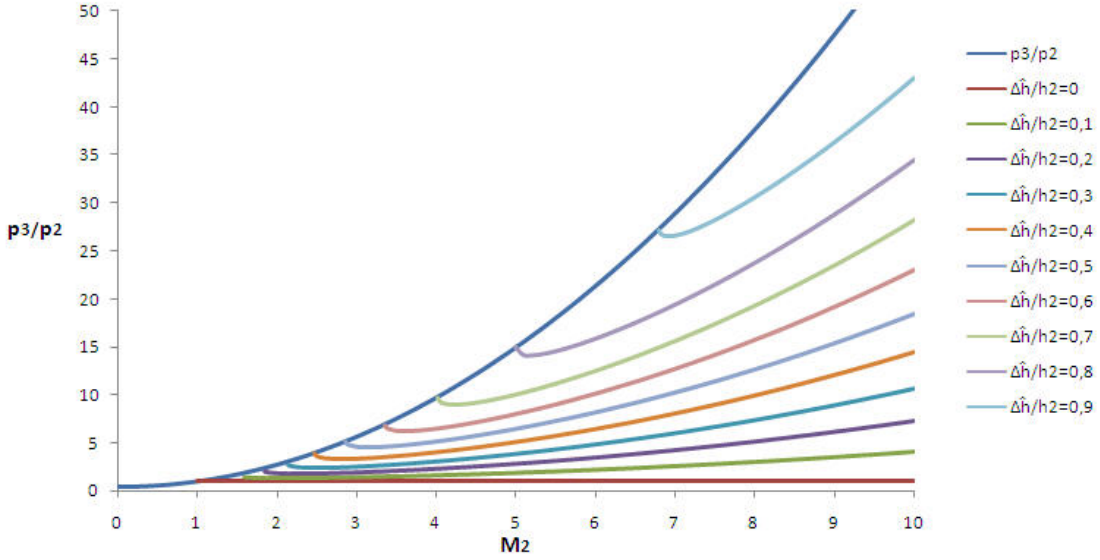

Figure 2.23: The pressure ratio p_3/p_2 as function of entrance conditions and energy addition

The momentum equation is again used here but now for the sonic condition with $M_2 = M_{CR} = 1$ and it can be seen that when too much heat is added the sonic condition is reached. This confirms the main characteristics of supersonic combustion in a constant area: heat addition decreases the velocity and the Mach number, but in turn increases the pressure and temperature.

When the area is divergent and designed in such a way, the static pressure will remain constant. The divergence rate dA/dx is dependent on the total temperature increase. Using the control volume shown in figure 2.24 the performance of a divergent area combustor is given.

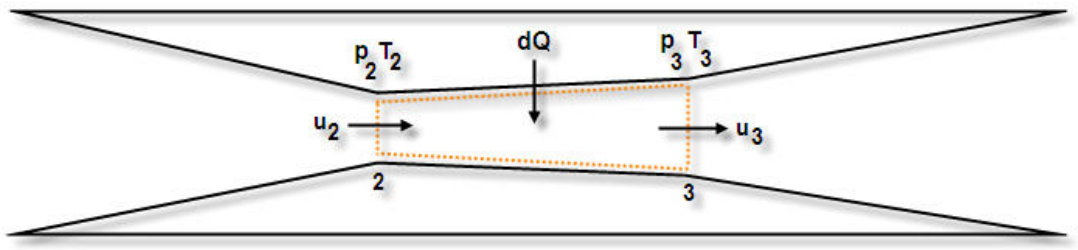

Figure 2.24: Control volume divergent area combustor

The momentum equation, including the average wall pressure term $\int \bar{p} dA$, becomes

$$u_2 = u_3 \tag{2.30}$$

Using the continuity equation $\rho_2 A_2 = \rho_3 A_3$ and $\rho_2 T_2 = \rho_3 T_3$:

$$\frac{A_3}{A_2} = \frac{T_3}{T_2} = \left(\frac{M_2}{M_3}\right)^2 \tag{2.31}$$

The loss in total pressure when $p_3 = p_2$ can be found using eq.(2.29)

$$\frac{p_{t_3}}{p_{t_2}} = \left(\frac{1 + \frac{\gamma-1}{2} M_3^2}{1 + \frac{\gamma-1}{2} M_2^2} \right)^{\frac{\gamma}{\gamma-1}} \tag{2.32}$$

The change in area A can be found by taking $A_3 = A_x$ and using eq.(2.24) and eq.(2.31)

$$\frac{T_{t_3}}{T_{t_2}} = \frac{(2 + (\gamma-1)M_3^2)M_3^{-2}}{(2 + (\gamma-1)M_2^2)M_2^{-2}} = \frac{G_3(M_3)}{G_3(M_2)} \tag{2.33}$$

In eq.(2.31) A_x increases in proportion with T_x and if this is used with eq.(2.33) the result is:

$$\frac{A_x}{A_2} = \frac{T_{t_x}}{T_{t_2}} \left(1 + \frac{\gamma-1}{2} M_2^2 \right) - \frac{(\gamma-1)}{2} M_2^2 \tag{2.34}$$

To prove that a divergent area is more advantageous than a constant area, the total pressure loss and the Mach number in a divergent and constant area are compared. The Mach number is found through eq.(2.34) and plotted in figure 2.25

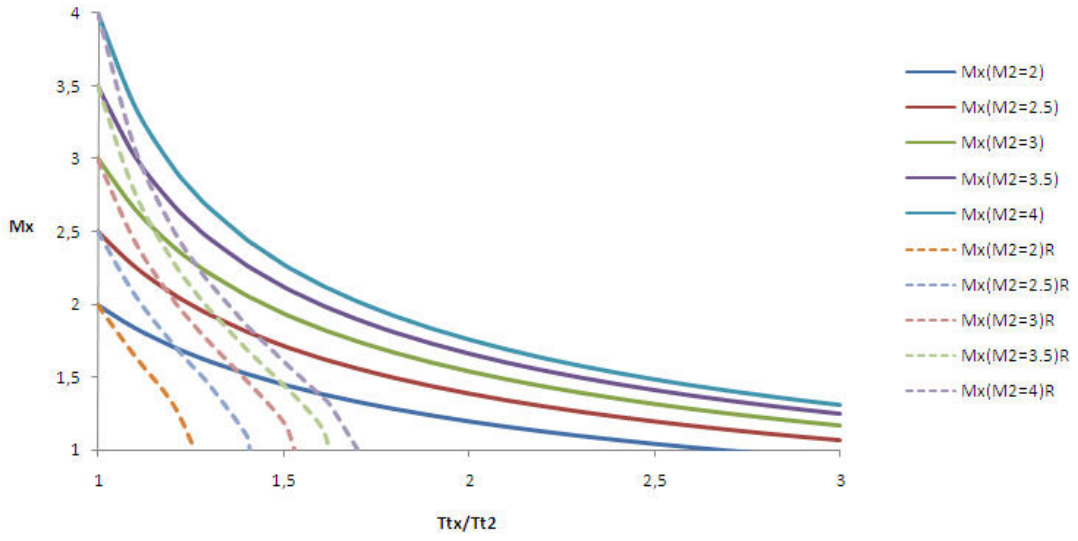

Figure 2.25: The local Mach number M_x in a divergent combustor and in a Rayleigh flow

The total pressure loss is found through eq.(2.32) and is plotted in figure 2.26. Both figures show a better performance with a divergent area. The Mach number rate and the total pressure loss rate for the divergent section decrease less than within a Rayleigh flow, thus proving the advantage of a divergent area.

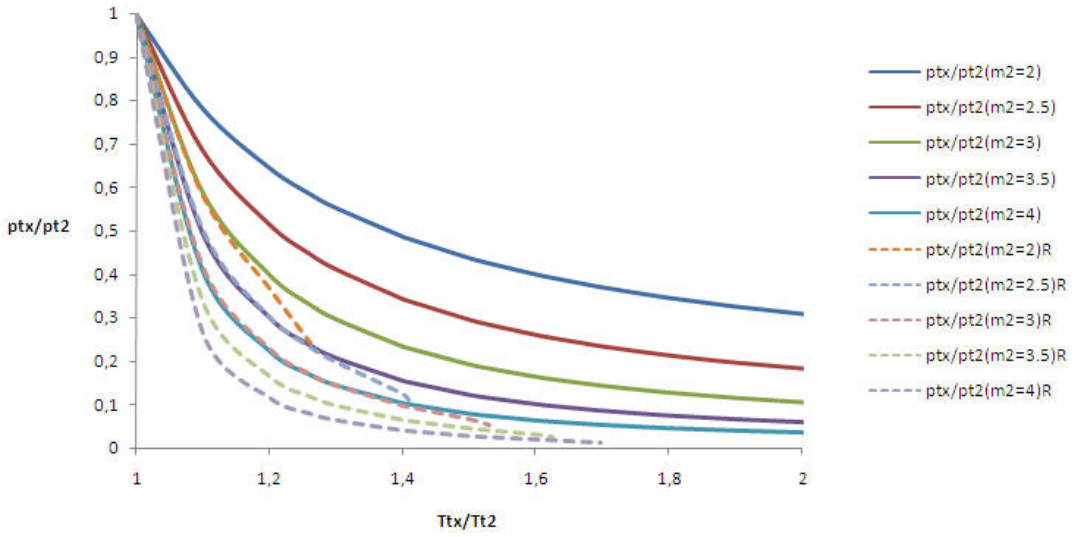

Figure 2.26: The total pressure loss in a divergent combustor and in a Rayleigh flow

Combustion Oscillations

It is known that within the flame zone in the combustor the heat release fluctuates. These fluctuations, or flow disturbances, cause acoustic waves, or *signals*, which can only travel upstream inside subsonic regions. When the waves *hits* something, they reflect and travel downstream again to the flame zone, interacting with it. These interactions result in an oscillatory flowfield in the subsonic region, which can be boundary layers, recirculation zones in flame-holding areas, and/or regions begind precombustion shock waves. Combustion is then said to be *oscillating*, due to the mutual coupling between the unsteady heat release and the local flow fluctuations within the flame zone (Ma 2005, Li 2007). A schematic is given in figure 2.27 showing an acoustic-convective loop region between the combustion zone and a fuel injection zone, with a the acoustic wave velocity (or sound velocity) and u the flow velocity.

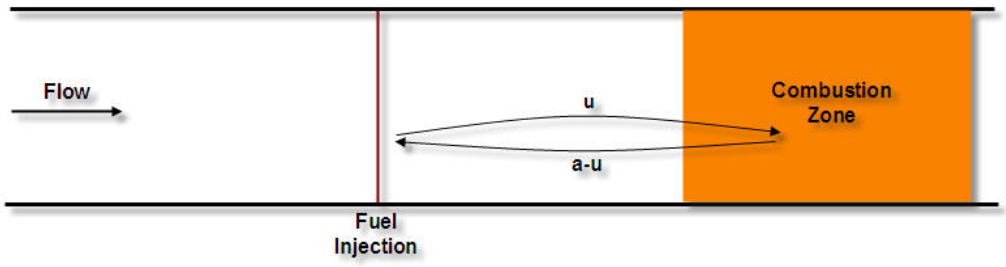

Figure 2.27: Schematic of an acoustic-convective feedback loop in a scramjet combustor, source: [Li, 2007]

The acoustic waves moving upstream from the combustion zone interfere with the fuel injection/mixing system causing oscillations in the fuel distribution and the fuel/air composition. These oscillations in the composition of the reactive mixture travel downstream to the combustion zone

and there they affect the heat release. Which in turn produce acoustic waves moving back upstream, thus creating a feedback loop of oscillating flows inside the combustor.

This problem has only recently been recognized and explored, since the general thought is that since acoustic waves cannot propagate upstream in a supersonic flow, typical for supersonic ramjet concepts, any flow oscillations resulting from an unsteady combustion zone will simply move out of the engine through the nozzle, without interacting with the flame zone. These interactions are required to develop the closed feedback loop, mentioned above, to sustain the combustion oscillations.

Injection Systems

Fuel injection schemes are designed to inject fuel into the flowpath of the scramjet to rapidly mix with air and burn in the combustor since the residence time of the mixture is in the order of milliseconds. The injection schemes will not be discussed in further detail in this thesis, because in the following analytical models injector interferences are neglected or accounted for in a combustor efficiency. They are mentioned here because they do introduce disturbances in the flowpath. These disturbances can result in total pressure losses caused by the injection schemes and are also known as shock related losses. This is because when fuel is injected in the flowstream a bow shock wave is introduced, increasing the total pressure loss within the combustor. The shock wave is the major disturbance in the flow path, followed by separated regions and vortexes, also adding to the total pressure loss.

There are three different injection schemes:

- transverse injection
- parallel injection
- cavity injection

Transverse injection provides rapid mixing and rapid penetration of the fuel into the flowpath. But it also introduces a three-dimensional bow shock wave into the stream in front of the injection hole, making the flowfield very complex. The flowfield includes shock waves and vortexes, which produce conflicting results. Shock waves increase total pressure losses, but vortexes increase the mixing efficiency. Previous studies have shown that the back pressure, the pressure around the injection hole, influences the structure of the shock waves and the vorticity (Lee, 2003). A two-dimensional and three-dimensional of a transverse injection flowfield is given in figure 2.28.

When the fuel is not injected transverse, or *normal*, but by means of *oblique injection* the total pressure loss is decreased. When the injection angle is decreased from 90^0 to 0^0, thus going from normal injection to oblique injection, the total pressure loss is decreased and the mixing efficiency is improved until a certain angle, but when the angle becomes too small the mixing efficiency starts to degrade.

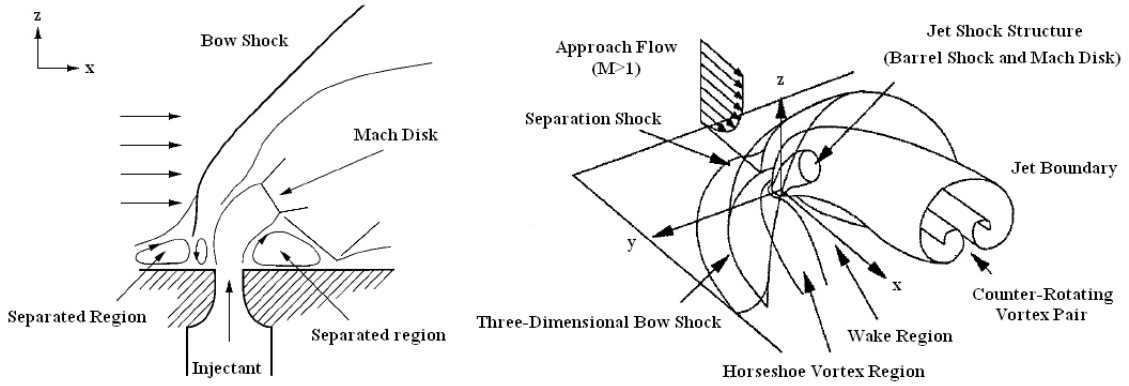

Figure 2.28: Transverse injection flowfield two- and three-dimensional, source: [Gruber 2000, Lee 2003]

Parallel injection is injection of fuel parallel to the flow inside the combustor through struts, ramps or hypermixers. It has the advantage of creating a recirculation zone behind the parallel injection scheme which enhances mixing (Glawe, 1996). The recirculation zone enables back mixing of partially or wholly burned gasses into the fuel-air mixture, and thereby sustaining self-ignition or flame holding. Another advantage is additional thrust generated by injecting the fuel in the downstream direction, without suffering from the undesireable bow shock waves as introduced by transverse injection schemes (Donohue, 1992).A parallel injection scheme is illustrated in figure 2.29.

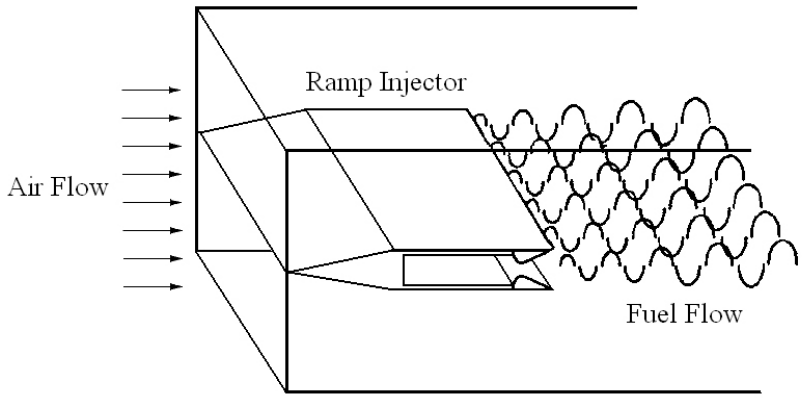

Figure 2.29: Parallel injection scheme

Cavity injection, or cavity flame holders, is an integrated fuel injection/flame holding approach. Inside a cavity a recirculation zone forms while fuel is injected either inside the cavity or just before it. The shape of the cavity can determine the character of the cavity being either *open* or *closed*. In an open cavity, a shear layer spans the entire cavity length, whereas with a closed cavity the shear layer reattaches itself to the bottom wall. Open cavities are preferred due to lower drag penalties, but also experience self-sustained oscillations inducing fluctuating pressures, densities and velocities in and outside the cavity. Though these oscillations need to be stable for having a stable and continuous ignition source for a stable combustion process, the unstability of these oscillations enhance the mixing process and possible improve combustion efficiency. Therefore determining the optimal cavity configuration is of great interest. Figure 2.30.a shows the flow and shear layer of a rectangular cavity with a L/D ratio and figures 2.30.b and 2.30.c the flow

oscillation characteristics of a cavity without and with a slanted back wall, showing that a slanted back wall has no reflected waves and thus reduced cavity oscillations.

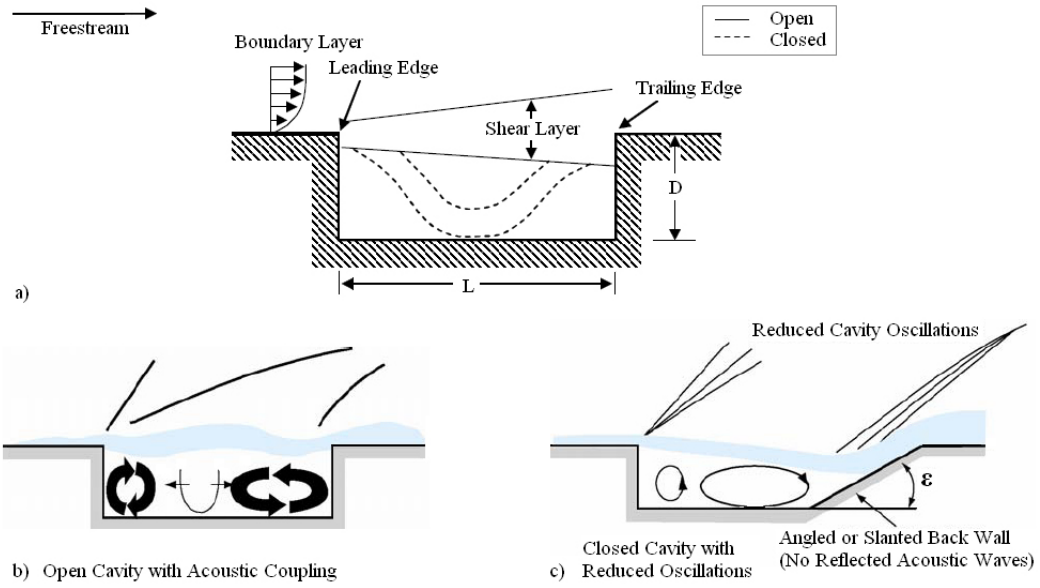

Figure 2.30: Flame holding cavity design

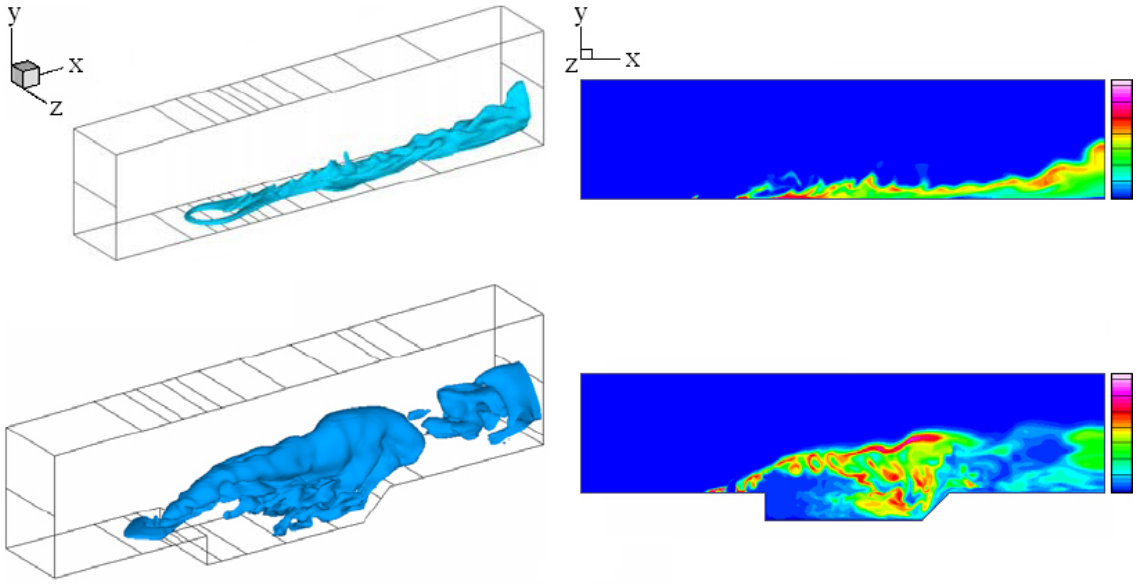

Figure 2.31: Transverse injection without and with cavity, source: [Mingbo, 2007]

Figure 2.31 shows two different transverse injector schemes, one with only an transverse injector mounted in the wall and one with an transverse injector followed by a cavity downstream (Mingbo, 2007). The flow moves from left to right and the substance used in the simulation is hydrogen (H), with the simulation itself showing the distribution of hydrogen after transverse injection in the moving flow. The distribution is characterized with a colour going from blue (low concentration) to red/pink (high concentration) of hydrogen.

2.1.3 The Nozzle

The last component of the scramjet flowpath is the nozzle and can be considered as an expansion system. The function of a scramjet nozzle is therefore to expand the high pressure supersonic flow coming from the combustor to the freestream flow pressure in order to generate thrust. In this flow high pressure combustion products are present and produce high chemistry levels and high total enthalpy levels in the nozzle region. The expansion of these exhaust products over the external nozzle-afterbody surface produces large forces and pitching moments on the scramjet as they are viscously mixed with the external freestream flow. During this expansion potential energy generated by the combustor is converted into kinetic energy, and thus completing the propulsion flowpath.

The design of a nozzle for a scramjet integrated hypersonic vehicle is in general a single expansion ramp nozzle, or *SERN*, and has an internal part and an external part (Xu Xu, 2005). The internal part is within the nozzle expansion ramp and the cowl (not to be confused with the inlet cowl), and the external part is beyond the cowl lip. An example of a SERN nozzle is given in figure 2.32 where L is the length, H the height, for the nozzle (n) and the cowl (c). The angles of the nozzle initial expansion ramp and the cowl are α_n and β_c respectively. Station 4 is the exit of the combustor.

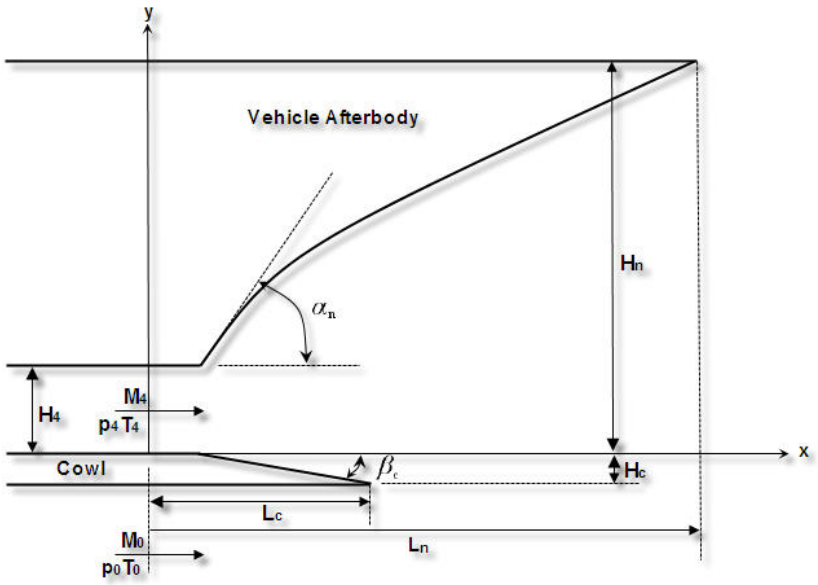

Figure 2.32: Scramjet nozzle design SERN

In literature the nozzle performance is usually not considered to be a problem (Ortwerth, Curran 2000). Within this thesis the nozzle is considered the same way, and therefore this component will be briefly investigated by looking at what influences the performance.

The performance is dependent on the combustion process upstream and the flow process within the nozzle. The combustion process in turn is dependent on the inlet. But for the nozzle in particular the inlet contraction ratio, because the inlet increases pressure and temperature by compression, and temperatures too high will result in dissociation losses. Dissociation is the opposite of recombination and is unwanted, because it decreases engine performance. This shows again the importance of the inlet design and the interaction between the scramjet components. Dissociation losses are those losses resulting from the flow freezing in the rapid expansion process within the

nozzle, so that energy is not generated by the recombination of free radicals produced by the combustion process. At low speeds this is not a significant problem because dissociation within the combustor is a strong function of the static temperature and pressure, and at low speeds the pressure is relatively high and the static temperature relatively low. These losses are considered to be very complex.

For most conventional nozzles, say for rockets, the forces and moments generated, can be determined by analyzing the flow up to the nozzle exit plane only. For a scramjet nozzle, the analysis must be done further downstream because the lower aft part of the scramjet forms the external part of the nozzle. The flow over this afterbody region will have dramatic effects on the thrust vector and pitching moment generated by the engine.

Another design concern for a scramjet nozzle is the location and structure of the shear layer. The external flow, usually hypersonic, and internal flow, usually supersonic, which are initialy separated by the nozzle cowl, are joined and mixed together through a shear layer. Through this layer mass, momentum and energy transfers occur. The shear layer direction is governed by a large pressure gradient present between the two flows. It can either turn inward or it can turn outward depending on the sign of the pressure gradient between the internal and external, or freestream flows.

Another aerodynamic flow phenomenon encountered in the nozzle region is flow separation. Flow separation occurs when the momentum of the flow within a boundary layer region becomes too small to overcome a positive or adverse pressure gradient. When this happens, the flow breaks away from the boundary, causing a backflow or reversed flow region towards the engine. The point where this starts to happen has a velocity gradient near the surface in the direction normal to the boundary becoming zero.

There are in fact several exhaust conditions which may exist at the nozzle exit plane. Two of these are overexpanded flow and underexpanded flow. With *overexpanded flow* the flow reaches the nozzle exit plane with a static pressure lower than that of the external freestream pressure, which will result in a shock wave emanating from the tip of the nozzle cowl. This type of flow is not desirable in actual flight because the shockwave would impinge on the afterbody of the airframe and could cause an adverse effect on the stability and trim of the aircraft. An *underexpanded flow* though results in the internal flow continuing to expand rapidly down the nozzle surface. And when reaching the nozzle exit plane it will not encounter a shock wave but an expansion wave to match the internal flow conditions to the freestream flow conditions. At the tip of the cowl the interaction of these two flows produces a shock and a contact discontinuity.

2.1.4 Scramjet Performance

In the previous chapter the ideal performance was given for the ramjet and it showed a practical limit between Mach 6 and 7 when using subsonic combustion. The practical limit was that of the maximum temperature at the entrance of the combustion chamber, which is around 2000K. When this temperature limit is exceeded a large part of the chemical energy of the fuel will be lost due to dissociation. The performance given was concluded with the recommendation of supersonic combustion when flying faster than Mach 6. The ideal performance will now be given of a ramjet using supersonic combustion ($M_3 \geq 1.1$) with a flight Mach number range higher than Mach 6.

The air until at the entrance of the combustor will be considered as an ideal gas with $\gamma = 1.4$, $c_p = 1004 J/kg/K$ and $R = 287 J/kg/K$. Stoichiometric (or ideal) combustion of hydrogen (H_2) is assumed ($ER = 1$) and the gas properties from the entrance of the combustor change to $\gamma = 1.25$ and $R = 350 J/kg/K$.

One of the inlet performance characteristics is the total pressure loss, or the pressure recovery, and two empirical relations for the kinetic efficiency η_{KE} were given in section 2.1.1 for an inlet optimized with four oblique shock waves. Using these relations, the inlet efficiency η_R can be calculated with the inlet kinetic energy efficiency η_{KE}:

$$\eta_{KE} = 1 - \frac{2}{(\gamma - 1)M_0^2}\left(\frac{1}{\eta_R^{\frac{\gamma-1}{\gamma}}} - 1\right)$$

and with η_R

$$\eta_R = \frac{p_{t_3}}{p_{t_0}}$$

When friction is disregarded the empirical relations given in section 2.1.1 can be used to determine the total pressure ratio:

$$\eta_{KE} = 1 - 0.2\left(1 - \frac{M_3}{M_0}\right)^5$$

for inviscid flow, and for viscid flow:

$$\eta_{KE} = 1 - 0.4\left(1 - \frac{M_3}{M_0}\right)^4$$

Both correlations show that the inlet kinetic efficiency is dependent on the Mach number M_3 at the entrance of the combustor, which is dependent on the inlet contraction ratio. The calculation of the performance of the scramjet can be done by choosing a certain value for M_3 as long as it is supersonic ($M_3 \geq 1$). Figure 2.33 shows for viscid flow and inviscid flow the inlet kinetic efficiencies for $1.1 \leq M_3 \leq 4$:

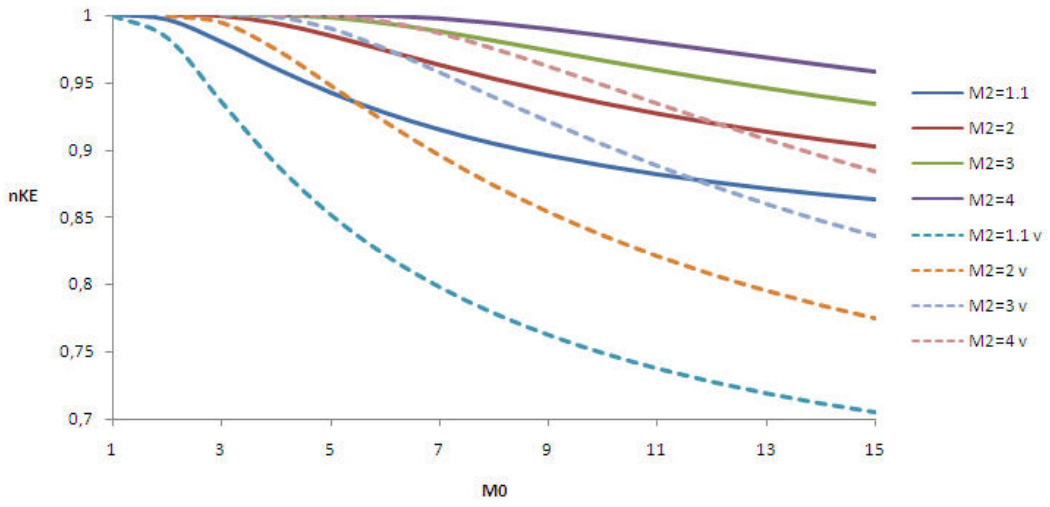

Figure 2.33: Inlet kinetic energy efficiency non-viscous flow and viscous flow for different values of M_3

To determine the temperature T_3 or the Mach number M_3 at the combustor entrance, assuming an adiabatic flow in the inlet section, the total temperature is conserved ($T_{t_3} = T_{t_0}$), thus

$$\frac{T_3}{T_0} = \left[\frac{1 + \frac{\gamma-1}{2}M_0^2}{1 + \frac{\gamma-1}{2}M_3^2}\right] \tag{2.35}$$

For the combustion process an empirical relation is used (de Wolf, 1995), to attain the temperature at the combustor exit T_4, with T in $K/1000$:

$$T_4 = 2.34 + 0.39T_3 - 0.03T_3^2 \tag{2.36}$$

The Mach number at the combustor exit M_4 has to be supersonic for a scramjet, thus at a certain T_3 the velocity at the exit must result in $M_4 \geq 1.1$ for the engine to work. The combustion process itself will be modelled as a constant-pressure combustion process, described earlier in section 2.1.2, thus the pressure remains the same over the combustion process ($p_4 = p_3$).

Combining the continuity equation

$$\rho_3 A_3 = \rho_4 A_4 \tag{2.37}$$

and the equation of state

$$\rho_3 T_3 = \rho_4 T_4 \tag{2.38}$$

gives the following equation to find M_4:

$$\frac{A_4}{A_3} = \frac{T_4}{T_3} = \left(\frac{M_3}{M_4}\right)^2 \tag{2.39}$$

From station 3 on the chemical composition of the flow is changed to $\gamma_c = 1.25$ and $R = 350 J/kg/K$. The total temperature can be found with T_4 and M_4. And the total pressure ratio across the combustor, with $p_4 = p_3$ with

$$\frac{p_{t_4}}{p_{t_3}} = \frac{p_4}{p_3} \frac{\left(1 + \frac{\gamma_c - 1}{2} M_4^2\right)^{\frac{\gamma_c}{\gamma_c - 1}}}{\left(1 + \frac{\gamma - 1}{2} M_3^2\right)^{\frac{\gamma}{\gamma - 1}}} = \frac{\left(1 + \frac{\gamma_c - 1}{2} M_4^2\right)^{\frac{\gamma_c}{\gamma_c - 1}}}{\left(1 + \frac{\gamma - 1}{2} M_3^2\right)^{\frac{\gamma}{\gamma - 1}}} \tag{2.40}$$

and is shown in figure 2.34 where it can be seen that the drop in total pressure during combustion decreases when the static temperature at the entrance increases.

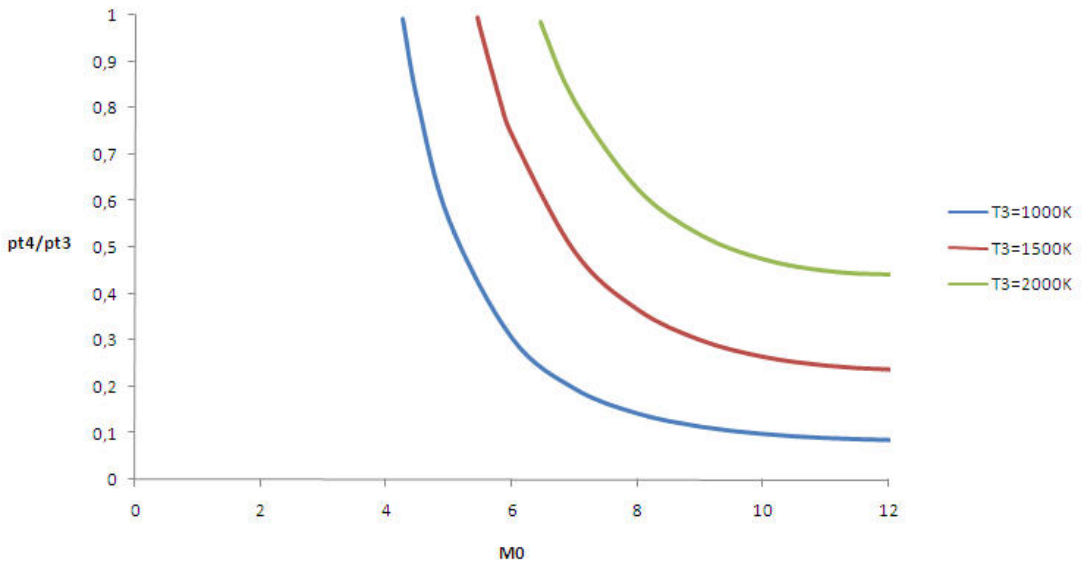

Figure 2.34: Total pressure ratio across the combustor

To finally calculate the specific impulse I_{sp} and the specific thrust Ψ the nozzle pressure ratio and the exit velocity have to be calculated first. The nozzle pressure ratio NPR is the ratio between

the exit total pressure p_{t_e} and the exit freestream pressure p_e. When ideal expansion occurs in the nozzle the pressure p_4 will expand to the freestream pressure $p_e = p_0$ and is $p_{t_e} = p_{t_4}$, and can NPR be found through

$$NPR = \frac{p_{t_4}}{p_0} = \frac{p_{t_e}}{p_0} = \frac{p_{t_4}}{p_{t_3}} \frac{p_{t_3}}{p_0} \tag{2.41}$$

The exit Mach number M_e can be found with the isentropic relation for the total pressure with $p_{t_e} = p_{t_4}$ and with $p_e = p_0$

$$M_e = \sqrt{\frac{\left(\frac{p_{t_4}}{p_0}\right)^{\frac{\gamma_c - 1}{\gamma_c}} - 1}{\frac{\gamma_c - 1}{2}}} \tag{2.42}$$

With M_e the exit velocity u_e can be found and with this the specific thrust Ψ $(N/(kg/s))$ using (de Wolf, 1995):

$$\Psi = u_e - u_0 \tag{2.43}$$

and is shown in figure 2.35

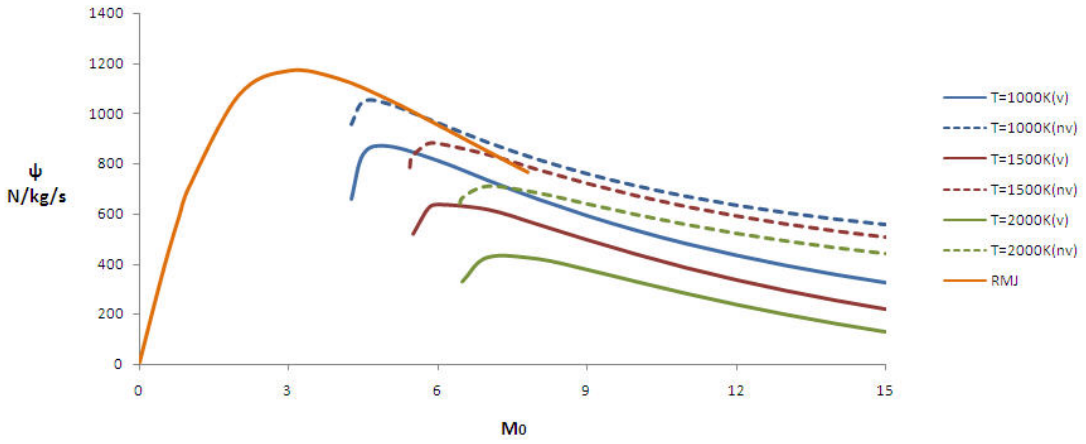

Figure 2.35: Scramjet and ramjet specific thrust

The figure shows the specific thrust for a scramjet using three different combustor entrance temperatures T_3 in inviscid and viscid flow compared to the specific thrust of a ramjet, calculated in the previous chapter. It shows that the performance is lower with viscid flow than for inviscid flow, which is obvious, and it shows better performance at higher Mach numbers than the ramjet.

The specific impulse I_{sp} (sec) is calculated with the relation:

$$I_{sp} = \frac{\Psi}{g_0 \dot{m}_f} \tag{2.44}$$

and with $g_0 = 9.81$ and $\dot{m}_f = 0.0292$ eq.(2.44) becomes

$$I_{sp} = 3.5\Psi \tag{2.45}$$

and is shown in figure 2.36 for three different combustor entrance temperatures and in either viscid or inviscid flow with the specific impulse calculated for the ramjet in the previous chapter.

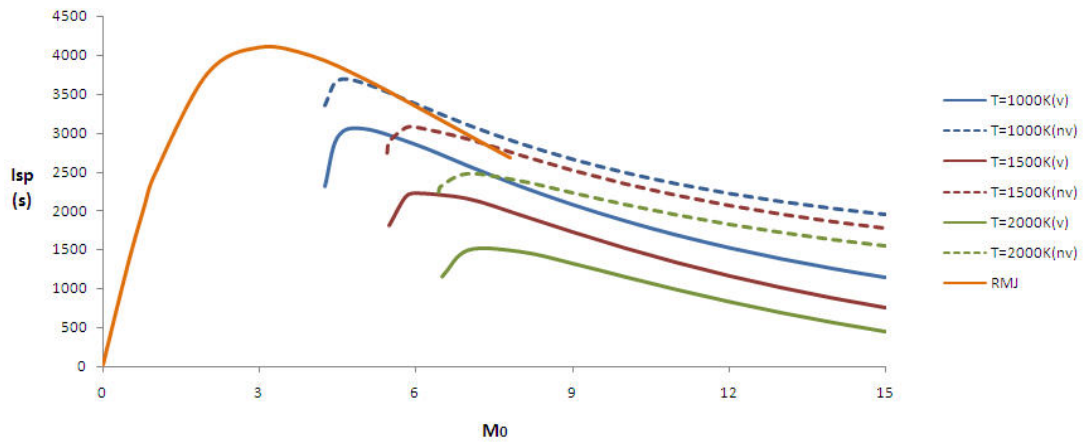

Figure 2.36: Scramjet and ramjet specific impulse

It can be seen that the scramjet has better specific impulse performances than the ramjet with higher Mach numbers and that the specific impulse increases with decreasing combustor entrance temperatures.

2.2 The Dual-Mode Combustor

A scramjet has a general operating region between Mach 6 and Mach 12 (Kanda, 2001). A ramjet has a good performance up to Mach 6. So if the scramjet could also operate in that region, it would press its advantage over the ramjet even further. It was therefore suggested to design a ramjet engine concept operating with two combustion modes:

- a ramjet-mode operating with subsonic combustion
- a ramjet-mode operating with supersonic combustion

moving from one mode to the other with increasing flight Mach number. This suggested ramjet engine concept is named the *dual-mode combustor* after its dual-mode operating system.

The dual-mode combustor has a fixed geometry, the same as the scramjet in the previous section, but now with an added constant-area section between the inlet and the combustor, the isolator. When the dual-mode combustor is in ramjet mode it needs to decelerate the incoming air flow to a subsonic velocity, but doing so in a scramjet inlet. This can only happen if somehow a *throat* is created at the combustor entrance. The interactions between the isolator and the combustor can cause the flow to choke before entering the combustor. This is one of the two characteristics of the dual-mode combustor. The second characteristic is the use of thermal choking at the exit of the combustor to create another throat to accelerate the subsonic flow to sonic velocities and from there to supersonic velocities through expansion in the nozzle section. These two characteristics will be investigated in the following two sections, as they are fundamental for the performance of the dual-mode combustor.

The combustion system of the dual-mode combustor in this thesis will be considered as consisting of the isolator and the combustor, which is illustrated in figure 2.37. In figure 2.37.a the stations 2 and 3 are the isolator entrance and isolator exit or combustor entrance, u and d are the upstream and downstream limits of the positive or adverse axial pressure gradient, s is the limit of the favorable negative pressure gradient (pressure decreases, while velocity increases), which extends throughout the combustor into the nozzle, and is the location of the lowest Mach number in the combustion system. Station 3 is also the axial station for the injector(s). The system process is adiabatic until the end op the shock train, station d and diabatic from there on, because of combustion.

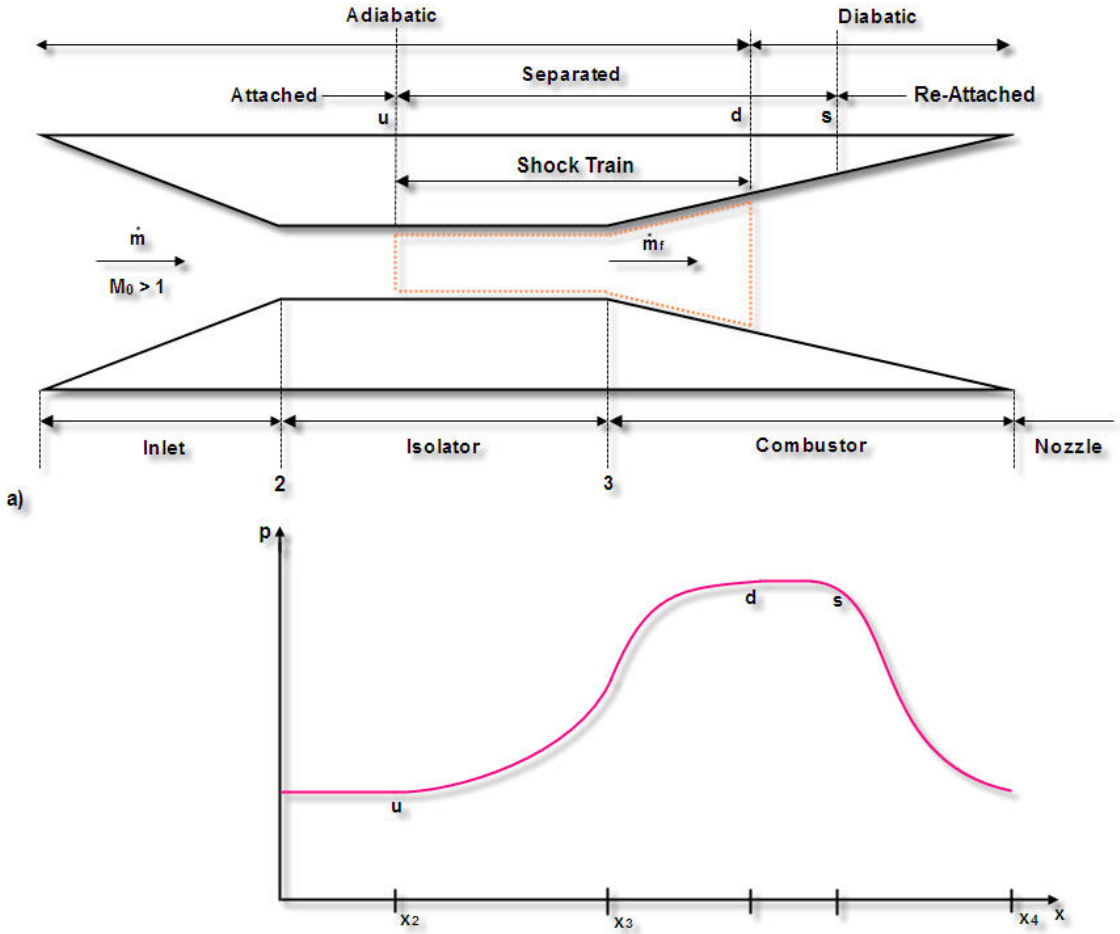

Figure 2.37: a) dual-mode combustor schematic, b) typical axial distribution of wall pressure when operating in scramjet mode

As was mentioned before, a pressure rise can cause an adverse pressure gradient inside a boundary layer causing it to separate. Combining a) and b) in figure 2.37 it shows that separation of the boundary layer occurs inside the isolator when the pressure rise is sufficient (between station u and d). It will re-attach itself when the pressure rise is decreased (station s), the expansion process also starts from that station.

2.2.1 The Isolator

The isolator is a constant (or nearly constant) area duct between the inlet and the combustor with the primary function to contain the pressure rise generated by the heat release within the combustor. When a scramjet is operating at high flight Mach numbers, the engine flow field has a higher enthalpy, causing the heat release within the combustor to be insufficient to choke the incoming flow (Tam, 2005). This results in no upstream interaction, and no occurence of a pre-combustion shock system. Because of this, a *pure* scramjet engine as investigated in the first part of this chapter has no need of an isolator. But when the flight Mach number decreases and thus also the flow field enthalpy, upstream interactions will occur and must be contained in the form of a pre-combustion shock train.

The pre-combustion shock train has several advantages for flame stabilization:

- it increases the static temperature and pressure of the incoming air flow, reducing thus the ignition delay
- it decelerates the flow, and thus increasing the residence time of the air/fuel mixture inside the combustor

The disadvantage of the pre-combustion shock train is that it will interact with the inlet flow field, when the pressure rise is too large and the isolator is not able contain it. The interaction will decrease the effective isolator entrance area resulting in an increase of flow spillage leading to an inlet unstart.

The Pseudo-Shock and Shock Train

The term *shock train* is used to define a repeated series of shock waves, either oblique or normal in nature. The *shock train region* represents a region where the series of shock waves in line are visible by optical observations, shown in figure 2.38 (Matsuo, 1999).

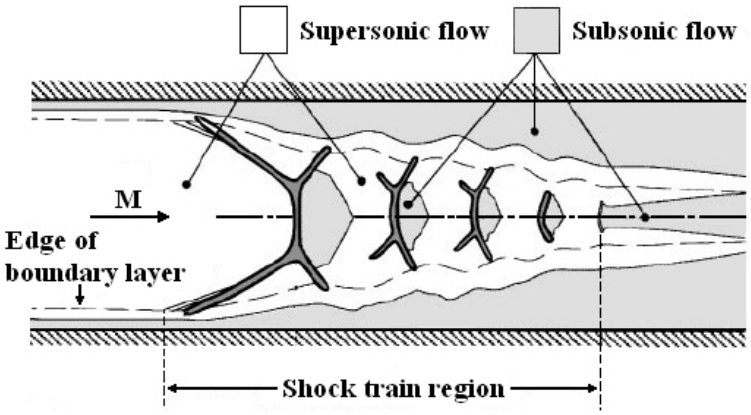

Figure 2.38: Structure of the flow in a shock train region, source: [Matsuo, 1999]

The shock train region is followed by a *mixing region*, where no shock waves exists, but where the pressure increases to some extent and the pressures at the wall surface and at the center line are

the same. If the flow behind the final shock wave is fully subsonic and uniform the static pressure will decrease due to frictional effects. The mixing region is thus a region where static pressure recovery is achieved, but appears only when the isolator is long enough. The region containing both the shock train region and the mixing region is called the *pseudo shock region*, shown in figure 2.39.

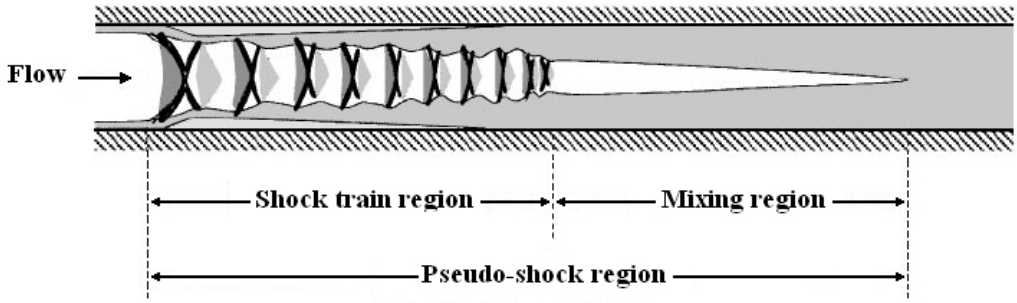

Figure 2.39: Structure of the flow in a pseudo shock region, source: [Matsuo, 1999]

The pseudo-shock inside the isolator has a similar role to a normal shock wave, since it decelerates the flow from supersonic to subsonic velocity. To design an isolator to contain the pseudo-shock, the pressure distribution is required along the flow direction, the pressure rise, and the length necessary to achieve that pressure rise. Figure 2.40 shows a typical schlieren photograph of a shock train where the flow with a Mach number of 1.75 is moving from left to right (Matsuo, 1999).

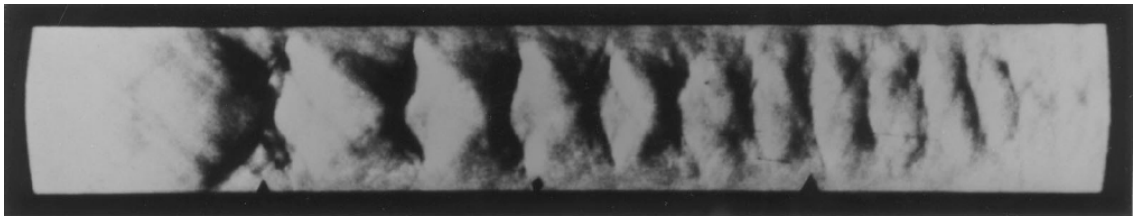

Figure 2.40: Schlieren photograph of a shock train, moving from left to right with $M = 1.75$

The interaction of the shock waves was generated with a fully developed turbulent boundary layer and there are ten normal shock waves in the shock train region.

Taking a closer look at the shock train pattern, it has a resemblance of the so-called *shock diamonds* or *Mach disks* formed behind nozzles, shown in figure 2.41. This phenomenon occurs when a supersonic flow exits the nozzle with a different pressure than the freestream pressure.

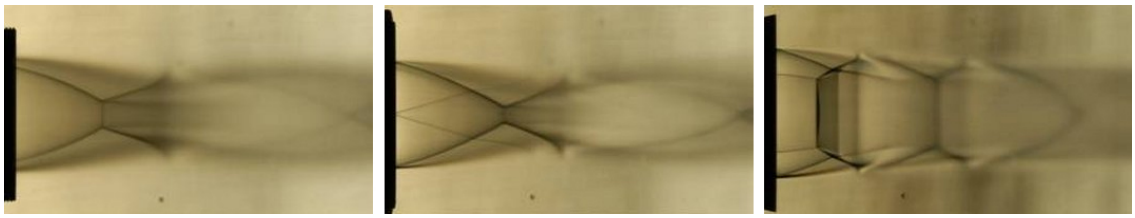

Figure 2.41: Experimental photos of shock diamond patterns in an overexpanded flow, source: www.aerospaceweb.org

The shape of the shock waves is mainly determined by the Mach number and the boundary layer upstream of the shock train, the effect of the latter is also known as the flow confinement effect, characterized by the ratio of the undisturbed boundary layer thickness (θ) to the isolator radius (h). When there are normal shock wave/boundary layer interactions and with the leading shock wave being a normal shock wave, the shock train is called a *normal shock train*. But when the Mach number increases and the point of bifurcation of the leading shock waves moves away from the wall towards the centerline, the shock wave becomes an oblique shock wave and the shock train is then called an *oblique shock train*. Figure 2.42 shows the development of a normal shock wave to a normal shock train and eventually an oblique shock train when the Mach number of the flow enetering the isolator increases. First a normal shock wave is formed, which curves near the walls. Then, when the Mach number increases, the boundary layer starts separating and the shock wave develops bifurcation patterns near the wall.

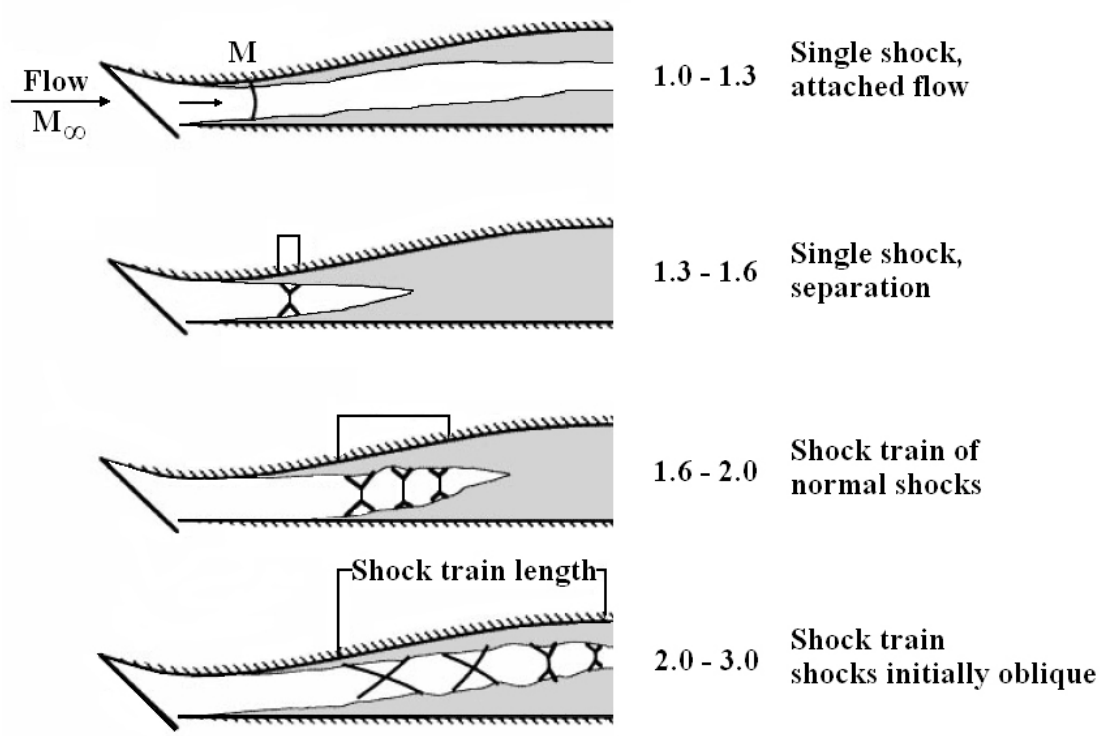

Figure 2.42: Typical shock train patterns with increasing Mach number M, source: [Matsuo, 1999]

Isolator Performance

The performance of the isolator is of critical importance to the overal performance of the dual-mode combustor (Heiser 1994, Curran 2000). It must contain the precombustion shock system by containing the pressure rise. Figure 2.43 shows a control volume for an isolator. The control volume contains a shock train which reduces the area at station 3 from A_3 to A_{3c} which is the core flow where the velocity is still supersonic, but smaller than the isolator entrance velocity ($1.1 \leq c_3 \leq c_2$). The separation of the boundary layer starts at station u.

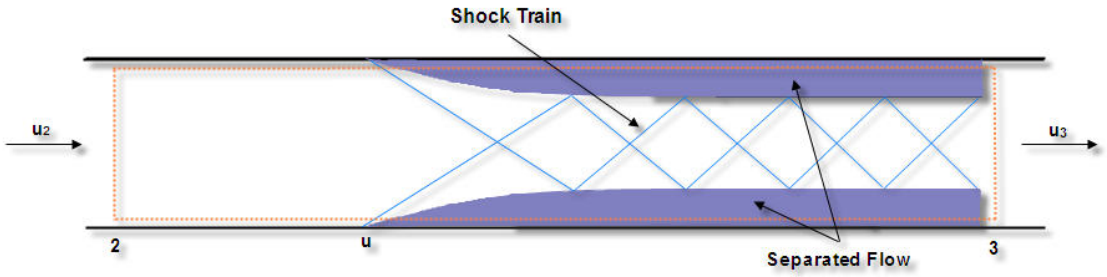

Figure 2.43: Control volume for the isolator containing a shock train

It is important to understand what the limits of the pressure rise are. During subsonic combustion, a normal shock is necessary to reduce the velocity to $M_3 < 1$ and that shock must be contained inside the isolator. When the pressure rise is increased the shock wave will move upstream towards the inlet, and once it reaches the isolator entrance, it will *block* the isolator and the inlet will unstart. Therefore the maximum pressure increase p_{3max} must be smaller than the pressure increase p_{2n} corresponding to a normal shock at the entrance of the isolator ($p_{3max} = p_{2n}$). The minimum pressure p_{3min} is the pressure at the entrance of the isolator p_2 with supersonic flow ($p_{3min} = p_2$).

Three important performance parameters for the isolator are the exit Mach number, the area ratio, and the length of the isolator. The exit Mach number can be found using (Curran, 2000):

$$M_3 = \left[\frac{\gamma^2 M_2^2 \left(1 + \frac{\gamma-1}{2} M_2^2\right)}{\left(1 + \gamma M_2^2 - \left(\frac{p_3}{p_2}\right)\right)^2} - \left(\frac{\gamma - 1}{2}\right) \right]^{-\frac{1}{2}} \tag{2.46}$$

And is plotted in figure 2.44.

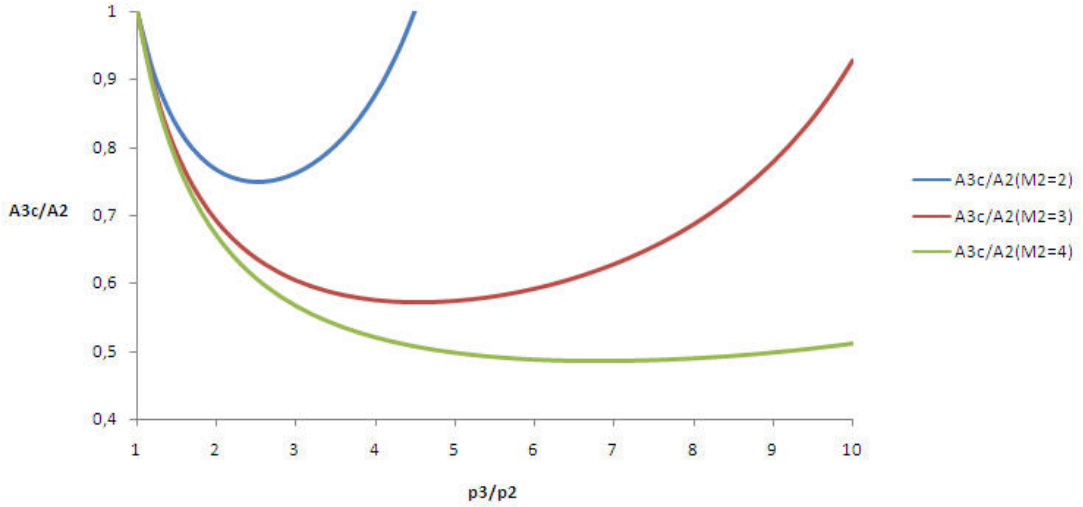

Figure 2.44: Variation of M_3 with increasing p_3/p_2 and constant M_2

It can be seen that the Mach number decreases with increasing pressure ratio, corresponding with an increasing heat addition. When the pressure rise is large enough the Mach number will go sonic, and the flow will choke.

Using the momentum equation on the control volume, but now with $A_{3c} \neq A_2$, the isolator area ratio becomes:

$$\frac{A_{3c}}{A_2} = \frac{1}{\gamma M_3^2}\left[\frac{p_2}{p_3}(1+\gamma M_2^2) - 1\right] \tag{2.47}$$

and is plotted in figure 2.45.

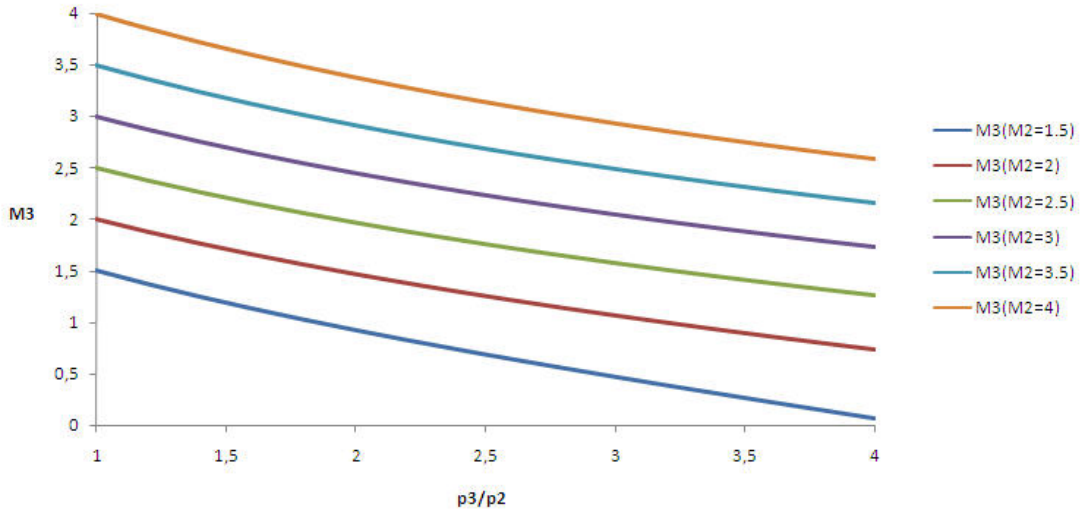

Figure 2.45: Variation of A_{3c}/A_2 with increasing p_3/p_2 and constant M_2

The area ratios are given as parabolas and the left side of the parabola corresponds with a supersonic Mach number, the right side with a subsonic Mach number. A supersonic Mach number corresponds with an oblique shock train and a subsonic Mach number with a normal shock train. The area ratio region around the minimum corresponds to a transient shock train changing from normal to oblique or vice versa.

The last performance parameter of the isolator mentioned in this section, is the isolator length. The length of the isolator can determine the performance throughout a specified operating Mach range in three ways:

- the length is optimal and contains the shock train
- the length is insufficient to contain the shock train
- the length is too long

Through statistically analyzing experimental results, the following empirical relation between the pressure distribution in the shock train region and several duct flow parameters was formulated:

$$\frac{x(M_2^2-1)Re_\theta^{0.25}}{H_i^{0.5}\theta_2^{0.5}} = 50\left(\frac{p_x}{p_2}-1\right)+170\left(\frac{p_x}{p_2}-1\right)^2 \tag{2.48}$$

where x is the distance downstream from the start of the pressure rise, M_2 is the Mach number at the entrance of the isolator, θ_2 is the boundary layer thickness at the entrance of the isolator, H is the diameter of the isolator, Re_θ the Reynolds number based on the boundary layer momentum thickness, and p_x/p_2 the ratio of the local axial station wall pressure to the static pressure at the start of the pressure rise. The *normalized length* S/H of the isolator can be found by taking the pressure ratio at the end of the isolator:

$$\frac{S_i}{H_i} = \frac{\sqrt{\theta}}{(M_2^2-1)Re_\theta^{0.25}\sqrt{H_i}}\left[50\left(\frac{p_3}{p_2}-1\right)+170\left(\frac{p_3}{p_2}-1\right)^2\right] \tag{2.49}$$

with S the isolator length. CFD research shows that this correlation is suitable for designing the isolator length (Wang, 2005).

2.2.2 Thermal Choking

Section 2.1.2 showed that heat addition in a constant-area or a divergent section can cause choking of the flow when the amount of heat release reaches a certain critical level. The mass flow rate in the flow is then at a maximum or at its limit. Choking of the flow can be done through:

1. area choking
2. friction choking
3. thermal choking

Area choking is done by inserting a throat section in the geometry of a channel where a flow passes through. Choking of the flow by adding heat is called *thermal choking* and it is then commonly assumed that the flow Mach number reaches unity. It was shown that heat addition has the effect of increasing a subsonic Mach number and decreasing a supersonic Mach number. When the flow

Mach number reaches unity, it is then visualized by the existence of a (almost) normal shock wave caused by the compressive effects from the amount of heat addition and the flow is then termed *supercritical* (Delale, 1993). After this shock wave the subsonic flow is accelerated to supersonic conditions. The position of this shock wave is dependent on the amount of heat addition, it will be driven further upstream when the heat addition is increased after establishment (Zierep, 1974).

A physical example is seen in figure 2.46 which shows schlieren photographs of a Laval-nozzle where heat addition causes the presence of a normal shock wave. The flow is from left to right and the onset Mach number M_k is decreased to one. Here different flows are defined:

subcritical when the amount of heat addition is lower than the critical amount of heat addition

supercritical when the amount of heat addition exceeds the critical amount of heat addition

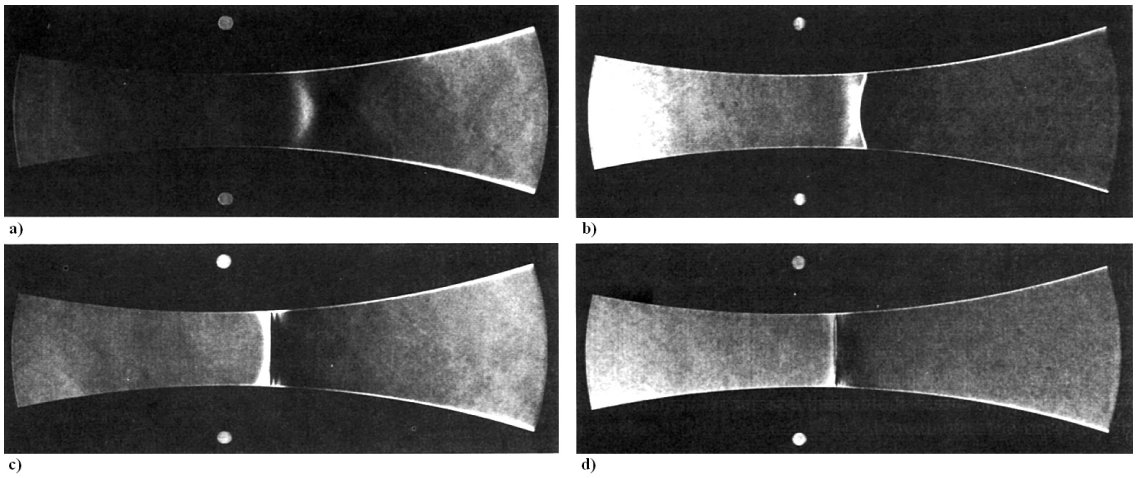

Figure 2.46: Flow visualization by schlieren photographs of runs conducted by Schnerr; a) subcritical flow with $M_k \approx 1.27$, b) supercritical flow with $M_k \approx 1.16$, c) supercritical flow with $M_k \approx 1.13$, and d) supercritical flow with $M_k \approx 1.1$

Since it was determined that for a scramjet a divergent combustor geometry is needed, a one-dimensional analysis of heat addition in a channel of variable cross-section $A(x)$ is given. This analysis shows the effect of heat addition q(x) at position x. Since the cross-section now is variable, and not constant, the continuity equation, the momentum theorem, and the energy theorem are adjusted:

$$\frac{1}{\rho}\frac{d\rho}{dx} + \frac{1}{w}\frac{dw}{dx} = -\frac{1}{A}\frac{dA}{dx} \tag{2.50}$$

$$\frac{1}{\gamma M^2}\frac{1}{p}\frac{dp}{dx} + \frac{1}{w}\frac{dw}{dx} = 0 \tag{2.51}$$

$$-\frac{1}{\rho}\frac{d\rho}{dx} + \frac{1}{\gamma p}\frac{dp}{dx} = \frac{1}{c_p T}\frac{dq}{dx} \tag{2.52}$$

In this analysis the flow velocity is now denoted as w and not as c as in the previous chapter, to prevent confusion with the inlet flow velocity. To determine the unknowns at location x the velocity is rewritten to let the unknowns be function of the temperature and the Mach number. The velocity term

$$\frac{1}{w}\frac{dw}{dx}$$

can be rewritten as

$$\frac{1}{w}\frac{dw}{dx} = -\frac{1}{M^2}\left[\frac{1}{\rho}\frac{d\rho}{dx} + \frac{1}{c_pT}\frac{dq}{dx}\right] = -\frac{1}{1-M^2}\left[\frac{1}{A}\frac{dA}{dx} + \frac{1}{c_pT}\frac{dq}{dx}\right]$$

and used to find the temperature and Mach number at station x:

$$\frac{1}{T}\frac{dT}{dx} = \frac{1}{p}\frac{dp}{dx} - \frac{1}{\rho}\frac{d\rho}{dx} = \frac{1}{1-M^2}\left[\frac{(\gamma-1)M^2}{A}\frac{dA}{dx} + \frac{(1-\gamma M^2)}{c_pT}\frac{dq}{dx}\right] \tag{2.53}$$

and

$$\frac{1}{M}\frac{dM}{dx} = \frac{1}{w}\frac{dw}{dx} - \frac{1}{2T}\frac{dT}{dx} = \frac{1}{1-M^2}\left[-\frac{\left(1+\frac{\gamma-1}{2}M^2\right)}{A}\frac{dA}{dx} + \frac{(1+\gamma M^2)}{2c_pT}\frac{dq}{dx}\right] \tag{2.54}$$

This equation shows a simple way to determine the possible location of thermal choking depending only on the temperature and the velocity within the combustor. It however does not say if thermal choking *occurs*.

Dual-Mode Combustor Oscillations

In section 2.1.2 combustion oscillations were introduced, and it was said that these are the result of acoustic waves bouncing in a subsonic region interfering with fual/air compositions and the heat release front. When the dual-mode combustor is in ramjet mode, the isolator has subsonic regions and a final normal shock wave at the exit and the combustor region is completely subsonic. This region is than very susceptable for acoustic waves travelling freely throughout the whole combustor region making the whole region intrinsic unstable. The bouncing of acoustic waves and influencing both fronts where they reflect can be seen as closed feedback loops, shown earlier in figure 2.27, but now with an added normal shock wave to the unsteady region, characteristic for the combustor to be in ramjet mode, is shown in figure 2.47.

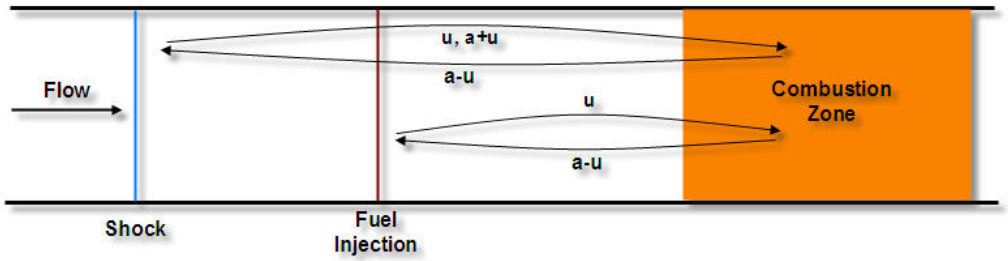

Figure 2.47: Schematic of acoustic-convective feedback loops in a dual-mode combustor

The mechanism responsible for driving these flow oscillations, to become acoustic-convective feedback loops, are identified to be the acoustic-convective wave interactions between the fuel injector(s) and the flame zone, which are results of interactions between the unsteady heat release and local flow fluctuations (Ma 2005, Li 2007). Local flow fluctuations are considered to be local differences in flow velocity, local differences in air/fuel composition, or local pressure or density differences. To reduce the frequency of the oscillations, the flow has to approach an uniform flow before interacting with the flame zone. Since this is almost impossible due to the mixing of the fuel inside the combustor, creating mixing layers and flow fluctuations, the main characteristic of the dual-mode combustor remains having unsteady combustion.

Chapter 3

Shock-Induced Combustion Ramjets

The second type of ramjet engine concept investigated in this thesis is a ramjet depending on shock waves for mixing and combustion. This chapter will investigate shock-induced combustion and detonation waves, which occur when the combustion wave and the shock wave responsible for ignition are closely coupled. The main focus of this chapter will be to give an understanding of the two combustion waves, to explore the experimental and numerical results on shock-induced combustion and detonations, and give two examples of engine concept designs operating with these combustion waves. A shock-induced combustion performance analysis will be given at the end compared with the ramjet engine concept of the previous two chapters.

3.1 Shock-Induced Combustion

Shock-induced combustion, as the name implies, is combustion of a mixture (fuel and oxidizer) instigated when it encounters a shock wave. The shock wave must increase the static temperature of the passing mixture high enough above the self-ignition temperature of the mixture. To model shock-induced combustion, it can be seen as a discontinuity, saying that at some point the mixture passes through the standing (oblique or normal) shockwave and inmediately ignites, if the temperature and pressure are high enough depending on the strenght of the shock wave and the velocity of the mixture before encountering the shock wave. In reality this is not the case, because at some point behind the shock wave combustion will occur, but not inmediately after passing through. The mixture notices the sudden increase in temperature and pressure and starts to chemically react to it and after some time or length it will ignite. This distance between the point of ignition and passing of the shock wave is called the *induction zone* or *induction length* and the time from passing the shock wave until combustion is called the *induction time*. The induction zone is characterized by an almost constant value of flow quantities, such as temperature, density and pressure after the shockwave. In fact with experiments, there are two discontinuities that model shock-induced combustions, the (bow) shock wave and the reaction front.

3.1.1 Experimental Results with Shock-Induced Combustion

One of the first experiments on shock-induced combustion was done by Lehr, where he used spherical and conical projectiles to induce combustion by shooting them in explosive stoichiometric mixtures of hydrogen/air and hydrogen/oxygen (Lehr, 1972). The chemical reaction, which results in combustion, was caused by the bow shock of the projectile. What Lehr discovered was that the reaction wave was pulsating, but only as long as the projectile was moving slower then the *detonation velocity* of the explosive mixture used in the experiment. This velocity causes combustion to occur as a detonation, which is considered an extreme of shock-induced combustion where

the induction zone length is at a minimum and the combustion waves couples with the bow shock wave (explained further in section 3.2). This pulsating caused the combustion to be unstable, or unsteady. Lehr's work was chosen here because it showed then for the first time very clear images (shadowgraphs) and results of shock-induced combustion. The following images show the pulsating reaction waves in a two and three-dimensional way with the projectile moving from left to right. The first two pictures show a two-dimensional view on the left and a three-dimensional view on the right and with a lower velocity than the two pictures beneath them, resulting in different frequencies for the oscillations.

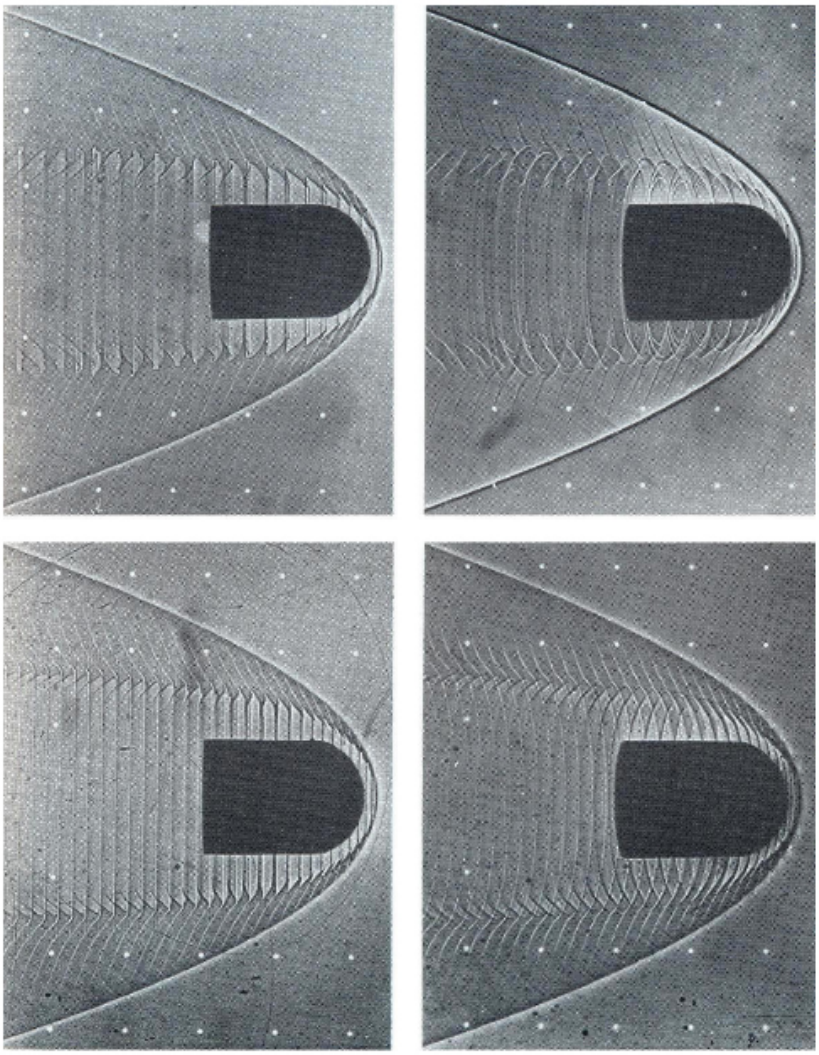

Figure 3.1: Pulsating reaction waves in 2D (left) and 3D (right) with different velocities, source: (Lehr, 1972)

From the experiments Lehr conducted, he concluded that if the model was moving with velocities above the detonation velocity of the gas mixture, the reaction showed a coupled shock-deflagration system near the centerline of the body. When the velocity component normal to the bow shock wave was equal to the detonation velocity, the two fronts started separating from each other. And when the velocity was below the detonation velocity the shock wave and the reaction front separated even more. Besides seeing these two discontinuities, the reaction front also showed a

pulsation of constant frequency, which was seen as an instability. In the experiments it was concluded that the oscillation was coupled with the models velocity. If the velocity increased, so did also the oscillation.

Lehr also proved that the instabilities were caused by the ignition delay, or the length of the induction zone. The experiments showed that with higher Mach numbers the temperature behind the bow wave also increased and thus the induction zone became shorter and the frequencies of the oscillations increased. What could not be explained was that the oscillations seemed to vanish when the projectiles velocity became higher then the detonation velocity. But is was supposed that the oscillations where of high frequency and low amplitude, and therefore not detectable. This assumption was supported afterwards through research which also concluded that instabilities of gaseous detonations showed higher frequency and lower amplitude, when the heat release or energy output was increased, or when the velocity was increased (McVey 1971, Wagner 1963, Soloukhin 1966). Combustion with periodic oscillations was termed a *regular regime* and combustion with large, irregular oscillations was termed a *large-disturbance regime*. Another conclusion was that the projectile diameter had influence on the stability of the reaction zone. The next images in figure 3.2 show that, as the velocity of the projectile increases from left to right, the frequency and the amplitude of the oscillations also increase.

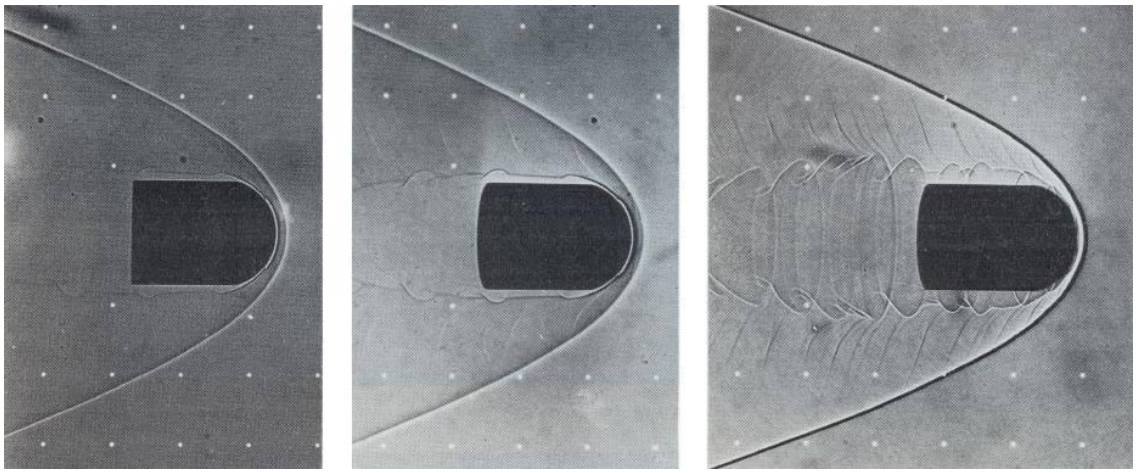

Figure 3.2: Change in oscillation frequency with changing velocity, source: (Lehr, 1972)

The length of the ignition zone, or also termed the ignition delay, was determined by the ignition time at the post-shock conditions and the velocity of the mixture downstream of the shock. The pressure across the energy release front was nearly constant, the temperature increased, and the density decreased. After the energy release front, pressure increased, but the temperature and density relatively remained constant. The distance between the two discontinuities was used to determine the induction time t_i

$$t_i = -\frac{s_s}{U} ln\left(1 - \frac{r}{s_s}\right) \tag{3.1}$$

where s_s is the shock stand-off distance (distance between projectile and bow shock), r is the distance between the shock and the reaction, and U the stream velocity inmediately behind the bow shock wave (Lehr, 1972). Lehr assumed for this calculation a linear velocity decay to zero at the body of the projectile and also constant temperature (the temperature behind the shock wave) in the stagnation region. The clear pictures of the experiments were also used to calculate the distance directly and with other induction time measurements they agreed very well (Rueg 1962, Nicholls 1963).

To explain the instabilities seen in Lehr's experiments, McVey and Toong proposed a one-dimensional wave interaction model (McVey 1971, Yungster 1996, Yungster 2002). This model represents the flow along the stagnation streamline of the blunt projectile Lehr used in his experiments. Two fundamental processes form the basis of this model:

- when a new reaction front is created, compression waves or reaction shocks are generated that travel upstream and downstream from the new reaction front

- when an old reaction front is extinguished, it must be accompanied by the generation of upstream and downstream rarefaction waves, which have a strength comparable to the reaction shocks.

Figure 3.3 shows McVey and Toong's one-dimensional model.

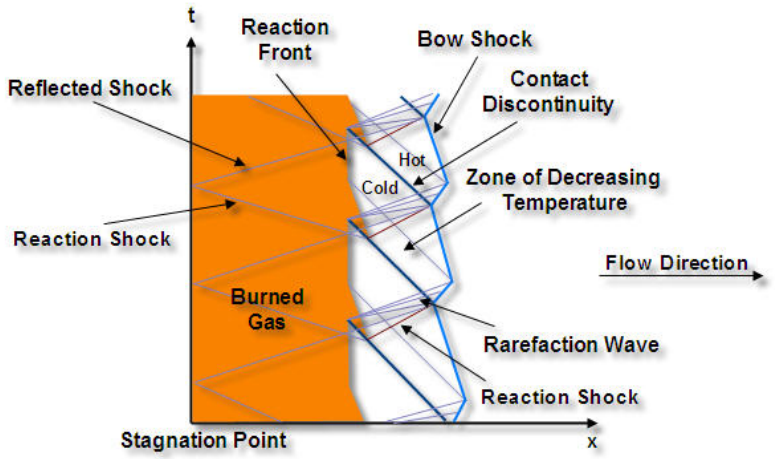

Figure 3.3: McVey and Toong's x-t diagram along the stagnation streamline, source: (McVey, 1971)

The interaction between these waves and the shock front produce the oscillations. To describe the model more in detail, three processes are distinguished and shown through a schematic of a shock tube, where one-dimensionally a shockwave causes a gas mixture to burn inside the tube:

- a) A new reaction front generates compression waves, which are named here reaction shocks. They travel upstream towards the bow shock and downstream towards the body stagnation point. The upstream facing reaction shock will eventually overtake the bow shock, and so strengthening it and producing a reflected rarefaction wave and a contact discontinuity, see figure 3.4

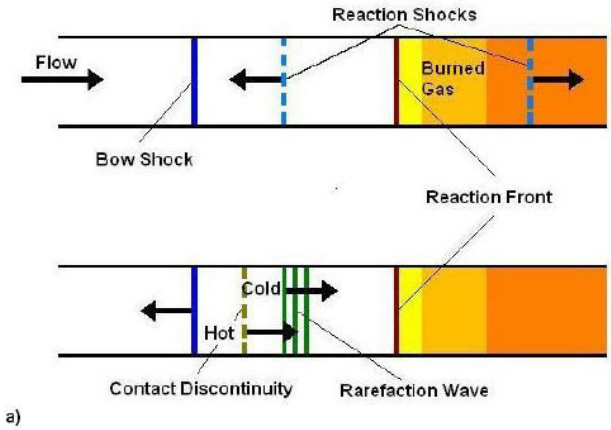

Figure 3.4: Schematic diagram of the one-dimensional wave interactions: a generation of reaction shocks and interaction with bow shock, source: (McVey, 1971)

- b) Across the contact discontinuity, which marks the boundary of the gas which has passed through the reinforced bow shock, a sharp increase in temperature takes place. The induction time in the hot gas is shortened and as a result, a new reaction front is created between the bow shock and the original reaction front. This new reaction front generates a pair of reaction shocks mentioned before in a). The reacted gas behind the new reaction front eventually reaches the location of the original reaction front. The first one is extinguished because there is no more unreacted gas present. When a reaction front is extinguished, it must be accompanied by the generation of upstream and downstream rarefaction waves, which have a strength comparable to the reaction shocks, see figure 3.5

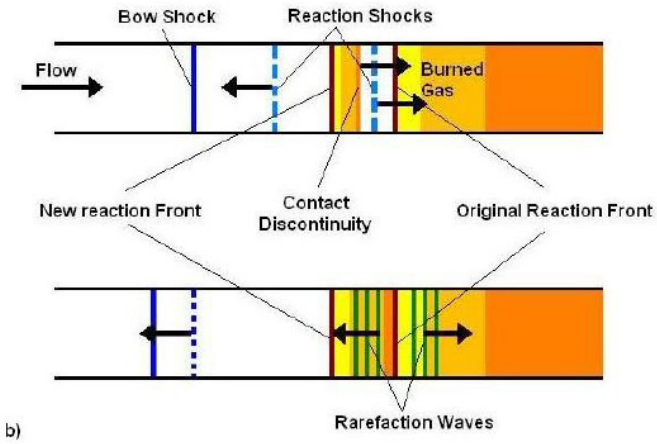

Figure 3.5: Schematic diagram of the one-dimensional wave interactions: b initiation of a new reaction front and extinguishment of the original reaction front, source: (McVey, 1971)

- c) The rarefaction wave generated by the extinguishing of the original reaction front eventually overtakes the bow shock, a fan of weak pressure waves are reflected and a zone of decreasing temperature is created. Because of this the ignition delay time progressively increases and the reaction front recedes towards the body, see figure 3.6.

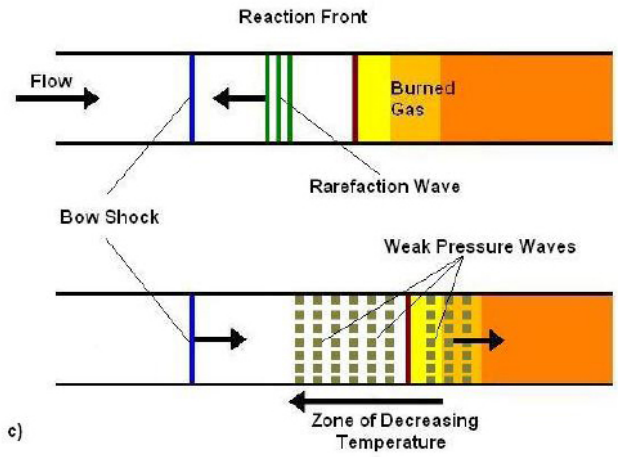

Figure 3.6: Schematic diagram of the one-dimensional wave interactions: c interaction of the rarefaction wave with the bow shock, source: (McVey, 1971)

The x-t diagram from McVey and Toong shows a particular case for which the reflected shock from the projectile overtakes the bow shock at exactly the same time as the reaction shock does, which means that it is a resonant mode. In general, this will not be the case and the diagram becomes more complex. The model also shows that the period of one oscillation is the time required for a reaction shock to overtake the bow shock plus the time required for the contact discontinuity to convect from the bow shock to the new reaction front, which in total is the induction time. When the velocity of the projectile increases, so will also the temperature behind the bow shock and thus shortening the induction time.

3.1.2 Numerical results with Shock-Induced Combustion

After Lehr's experiments, and there have been other experiments aswell, researchers tried to numerically obtain shock-induced combustion data similar to the experimental results. Doing research numerically reduces cost and risk, therefore it is useful to preceed experimental research with numerical research. This proved to be very difficult, since complex reaction kinetic programms were needed. One of the experiments that was numerically done to simulate Lehr's findings, was that of a projectile shot with a velocity of $M = 4.48$ in a stoichiometric hydrogen-air mixture. The following images in figures 3.7 and 3.8 show the shadowgrapgh from Lehr's experiment (projectile now moving from right to left), the computational results for the corresponding instantaneous density, pressure and water mass fraction contours.

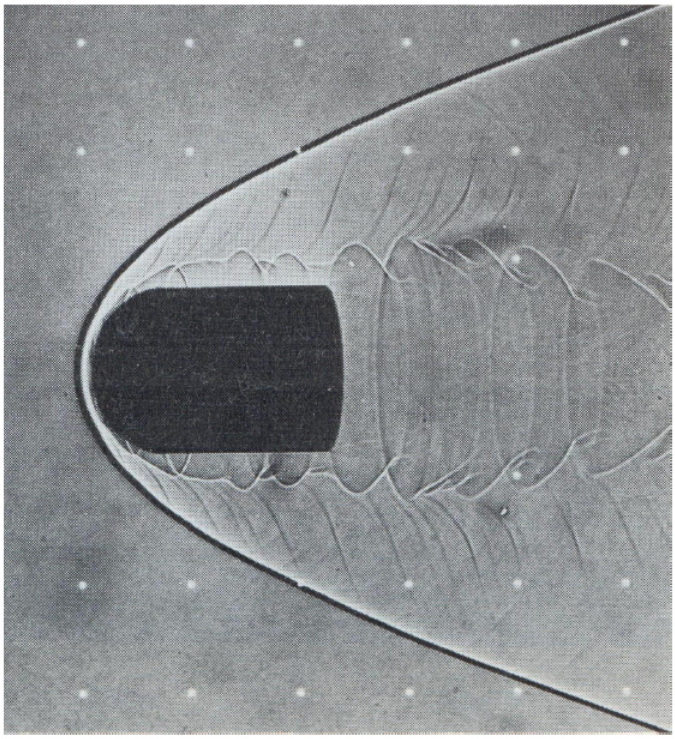

Figure 3.7: Experimental shadowgraph image taken at 12^0 angle from perpendicular direction for $M = 4.48$ projectile in stoichiometric hydrogen-air mixture, source: (Lehr, 1971)

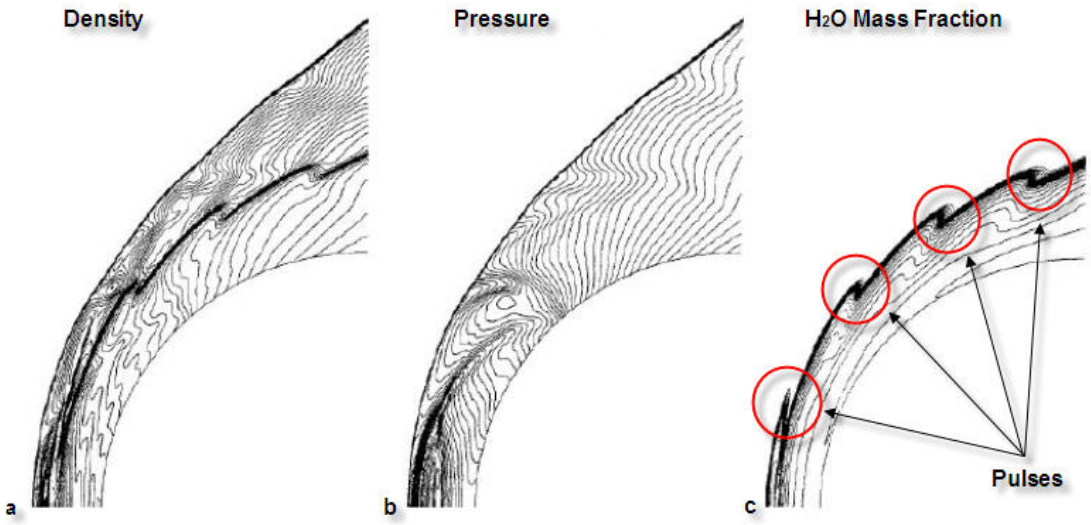

Figure 3.8: Computational results for projectile moving at $M = 4.48$ in stoichiometric hydrogen-air mixture: a density, b pressure, c H_20 mass fraction, source: (Yungster, 1996)

From these images four pulses can be seen, four in the shadowgraph (emanating from the projectile's body) and four in the contour images. A contact discontinuity emanating from each of these pulses can also be seen in the shadowgraph and in contour plot *a* (density). The pressure

contour plot shows a pair of reaction shocks, one moving towards the bow shock and one moving towards the projectile's surface. What is not shown are reaction shocks downstream, which indicates that the instabilities are driven primarily by the interactions occurring in a small region near the stagnation point. The mass fraction contour confirms the formation of the new reaction fronts.

To see if the one-dimensional model of McVey and Toong is accurate, the history of the density and the pressure along the stagnation streamline of the numerical results can be plotted and placed next to each other, seen in figure 3.9. The results were made with the condition that the wave interaction is almost synchronized or in resonant mode, that is, that the reflected shock from the projectile overtakes the bow shock at almost the same time as the reaction shock.

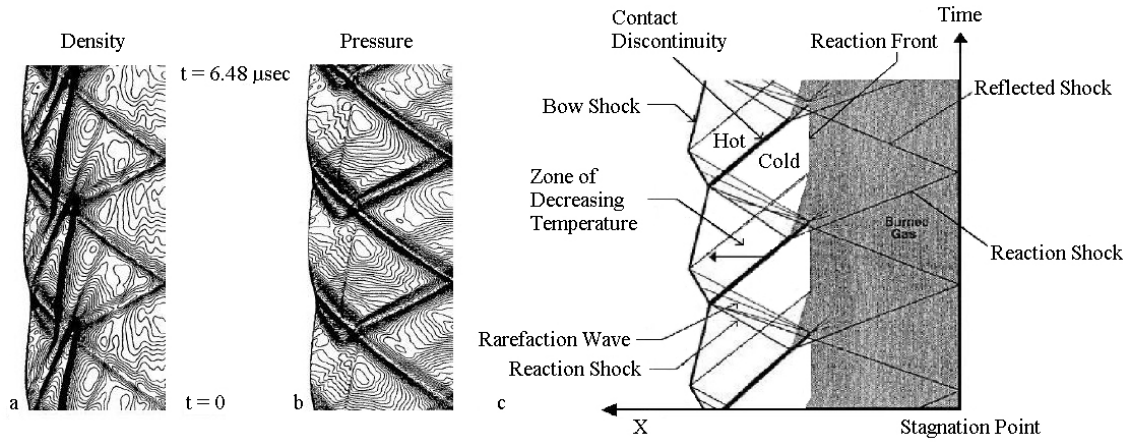

Figure 3.9: History of density and pressure along stagnation streamline; $M = 4.48$: a density, b pressure, c McVey and Toong's one-dimensional model, source: (Yungster 1996, McVey 1971)

As we compare the figures of the numerical results and the experimental result, we find that they correspond almost exactly. The flow is exactly periodic and the frequency is in good agreement with the experimental frequency reported by Lehr. With this we see that numerical simulations can be used to simulate periodic combustion instabilities, which are complex, unsteady, chemically reacting flows. Even the frequencies of oscillation and features of the flow can be numerically simulated. So now we have seen that steady and unsteady shock-induced combustion can be shown both experimentally and numerically, if having the correct reaction mechanism. The reaction mechanism describes the chemical reacting of the flow in the induction zone. Several different mechanisms exist, which have different results. Describing these reaction mechanisms in more detail is beyond the scope of this thesis (Yungster 1996, Yungster 2002, Clutter 1997).

The projectile's diameter also has an effect on the stability of combustion. It became clear that, with lower velocities a smaller diameter increased stability. But with increasing velocity stability will increase if the diameter is too large. Other parameters that have an effect on stability are the induction time, the reaction rate constant, activation energy and heat release (Ahuja 1994, Ahuja 1996). These parameters determine the length of the induction zone, which for stability has to decrease.

3.2 Detonations

Lehr's work described unsteady and steady shock-induced combustion, with the stability depending on the velocity of the projectile. Combustion became more stable when the velocity increased and when the velocity reached a certain value, combustion was said to occur as a *detonation*. Shock-induced combustion occurs at subdetonative velocities and this minimum velocity, where the mixture in fact detonates, is called the Chapman-Jouguet velocity. This is the minimal velocity needed to sustain a detonation. Detonations are considered to be shock-induced reaction fronts moving with supersonic velocities. The flow velocity relative to the front is sufficiently large to neglect diffusion mechanisms, such as viscosity and heat conduction. The hydrodynamic theory of detonation explains that the fundamental property of a detonation wave is that for a given initial state of the gas mixture the velocity of the wave is constant (Zeldovich, 1960).

Detonations have been the subject of research for many years now and it has proved to be very complex. Going back, the phenomenon of detonation was first recognized by Bertholet and Vieille (1881, 1882), and by Mallard and Le Chatelier (1881), during studies of flame propagation, when they observed supersonic combustion waves. The detonation wave is quite different from all other types of flame propagation, because it propagates with a constant supersonic velocity particular to each gas mixture. Another flame propagation similar to the detonation wave, is the deflagration wave, which is also a combustion wave but moving at subsonic speeds. Detonation waves can become end results from deflagration waves, called deflagration-to-detonation transition waves, or DDT waves. When a detonation wave is travelling faster than a Chapman-Jouguet wave, it is said to be an overdriven detonation wave. These waves are dependent on the pressure, temperature and gas composition of the system the wave travels in, and usually have a short life and decay to a stable detonation. Another form of detonation is the spinning detonation, which is still not very well understood. Spinning detonation is basically a self-excited vibratory phenomenon and it is said to occur with uneven combustion, and is sustained by the heating and cooling effects of the vibratory pressure waves generated by the uneven combustion. The last interesting form of detonation to be mentioned, is galloping detonation. This type of detonation is sometimes observed in pipes having not a constant CJ value wave velocity, but a fluctuating velocity between 1.5 and 0.5 M_{CJ} and the occurance can be explained by the transition from a DDT to a detonation leading to an overdriven detonation, which then decays to a steady detonation, which then subsequently fails and then reinitiated, forming a periodical cycle. The phenomena is thus observed as to be galloping.

3.2.1 The Chapman-Jouguet Model

The first simplest one-dimensional theory for detonation was formulated by Chapman (1899) and by Jouguet (1905, 1917). The theory assumed that the entire flow to be one-dimensional and the front to be a discontinuity plane across which the conservation laws for shock waves apply, and the equation of state depending on the degree of chemical reaction. The chemical reaction was regarded as instantaneous or at an infinite reaction rate, meaning that the theory did not take into account an induction zone. The final state of the products behind the front could be specified using the laws of conservation of mass, momentum and energy. They give a unique solution for the detonation velocity, or CJ-velocity and the state of combustion products inmediately behind the detonation wave. The Chapman-Jouguet theory is considered to be simple, because it does not require any information about the chemical reaction rate and it considers the flow to be inviscid. Nor does it consider any other diffusion effects such as heat conduction, diffusion of species and any external force such as gravity. The Chapman-Jouguet condition states that the Mach number normal to the preceding shock wave is unity. The Mach number within the reaction zone, normal to the preceding shock, is subsonic and is increased to unity (choking) due to the maximum heat

release. Other detonation waves (strong detonation waves) have at the end of the reaction zone still subsonic Mach numbers normal to the preceding shock wave.

To describe the different kinds of detonations and deflagrations processes (combustion waves) a pressure-volume diagram, or Hugoniot analysis, can be used. It describes the initial and final state of a gas using the equations of Hugoniot and Rayleigh. These equations are derived from the conservation laws (Strehlow 1968, Fickett 1979, Zeldovich 1960):

Conservation of Mass

$$\rho_0 D = \rho(D - u) \tag{3.2}$$

Conservation of Momentum

$$p - p_0 = \rho_0 u D \tag{3.3}$$

Conservation of Energy

$$E_1 + p_1 v_1 + \frac{1}{2}(D - u)^2 = E_0 + p_0 v_0 + \frac{1}{2}D^2 \tag{3.4}$$

Here the initial state is indicated with 0 and the final state with 1. The detonation wave velocity is D, u is the velocity of the flow, and E the specific internal energy and λ specifies the degree of chemical reaction. When u is eliminated from equations (3.2) and (3.3), we find a line in the p-v plane, called the Rayleigh line, which is expressed by:

$$R = \rho_0^2 D^2 - (p - p_0)/(v_0 - v) = 0 \tag{3.5}$$

where $v = \rho^{-1}$ is the specific volume. A Rayleigh line passes through point (p_0, v_0) and has a slope of $-\rho_0 D^2$. Rayleigh lines have extremes, being horizontally at $D = 0$ and vertically $D = \infty$. The vertical Rayleigh line, corresponding to an infinite propagation velocity, represents the extreme where the process can be considered as a constant-volume detonation in which all of the gas reacts at the same instant of time. The equation for the Hugoniot curve in the p-v plane is found by eliminating u and D from the energy equation and using previous equations (3.2) and (3.3):

$$H = E_1 - E_0 - \frac{1}{2}(p_1 + p_0)(v_0 - v_1) = 0 \tag{3.6}$$

In short the Hugoniot curves, or sometimes also called the shock adiabats, can be expressed with two equivalent forms:

$$H_1 - H_0 = \frac{1}{2}(v_1 - v_0)(p_1 - p_0) \qquad E_1 - E_0 = \frac{1}{2}(p_1 + p_0)(v_{[}1 - v_0) \tag{3.7}$$

The Hugoniot equation gives all possible solutions for the final state, given an initial state and a given energy release. The Hugoniot equation is plotted on a pressure-specific volume diagram, figure 3.10 displays a schematic of this Hugoniot curve with an energy release. Also shown is the Hugoniot curve with no energy release, or the *shock Hugoniot*.

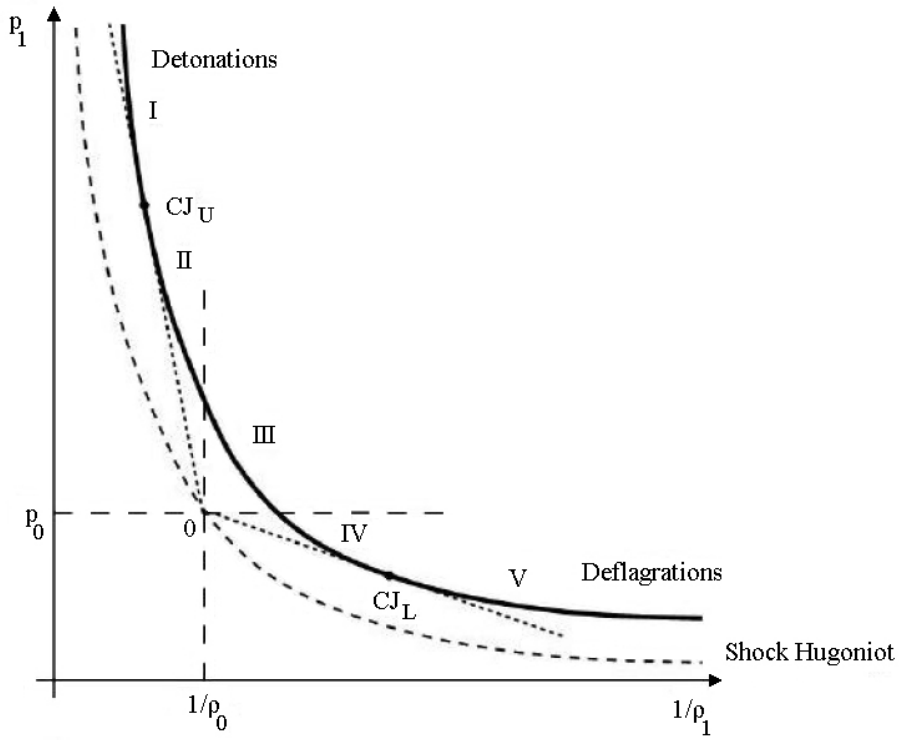

Figure 3.10: The Hugoniot curve

The Rayleigh line relates the initial state to the final state, and it shows that region III of figure 3.10 does not represent real solutions and can therefore be disregarded. The solutions related to regions I and II correspond to supersonic waves or detonations, whereas the solutions located in regions IV and V correspond to subsonic waves or deflagrations. To determine a unique solution to the conservation equations, Chapman and Jouguet independently proposed that detonations travel at one particular velocity, which is the minimum velocity for all the solutions on the detonation branch. This minimum velocity was determined to be the point where the Hugoniot and the Rayleigh line were tangent. Chapman also proposed that these curves were tangent to the isentrope, which makes it possible to show that the flow behind the wave is sonic relative to the wave. This is called the *Chapman-Jouguet rule*, which states that the velocity behind the standing CJ-detonation wave is sonic ($M = 1$), as mentioned earlier. The point where the Hugoniot, the Rayleigh line and the isentrope are all tangent is called the Chapman-Jouguet point. In figure 3.10 two CJ points on the Hugoniot exist, the upper and the lower CJ point. The upper CJ point located on the detonation branch of the Hugoniot and the lower CJ point located on the deflagration branch of the Hugoniot. These points divide the Hugoniot curve in four regions, which indicate what kind of combustion wave occurs as final state. Region I corresponds to strong detonations, which are detonations with a velocity slowing down from supersonic to subsonic. These kind of detonations are very unstable and are seldom observed. Region II corresponds to weak detonations which are detonations which have a supersonic to supersonic flow, which are not possible for this idealized single irreversible reaction. However, they are possible when the dissipative effects are taken into account and the heat of reaction is not zero. Region III was said to have non real solutions. Region IV corrsponds to weak deflagrations, which have a subsonic to subsonic flow and encompasses the laminar flame solutions. Region V corresponds to strong deflagrations, which have a subsonic to supersonic flow. Research has shown that region V has no physically possible region of steady solutions and can therefore be disregarded.

The calculation of the velocity u_{CJ} of the propagating detonation at the CJ point, the main result of the CJ theory, in a perfect gas can be obtained as follows (Thompson, 1988). Assuming different ratios of heat before and after the detonation wave ($\gamma_1 \neq \gamma_2$), and introducing the heat of combustion q_c and using the CJ rule, which states that $M_2 = 1$, in the momentum equations, the CJ Mach number can be found:

$$M_{CJ} = \sqrt{H + \frac{(\gamma_1 = \gamma_2)(\gamma_2 - 1)}{2\gamma_1(\gamma_1 - 1)}} + \sqrt{H + \frac{(\gamma_2 - \gamma_1)(\gamma_2 + 1)}{2\gamma_1(\gamma_1 - 1)}} \tag{3.8}$$

Here H is the non-dimensional heat of ombustion, and is given by

$$H = \frac{(\gamma_2 - 1)(\gamma_2 + 1)q_c}{2\gamma_1 RT_1} \tag{3.9}$$

The CJ velocity can now be found using the velocity of sound c_1

$$u_{CJ} = M_{CJ}c_1 \tag{3.10}$$

Simplifying the model and using only one specific heat of ratio (Fickett, 1979), the CJ velocity becomes:

$$M_{CJ} = \sqrt{H + 1} + \sqrt{H} \tag{3.11}$$

with

$$H = \frac{(\gamma^2 - 1)q_c}{2\gamma RT_1} \tag{3.12}$$

This equation shows that the CJ velocity is dependent only on the static temperature just before the shock wave and the heat addition. These derivations will be more elaborated on in the next chapter.

3.2.2 The ZND Model

The first model to include the reaction rate, thus improving the Chapman-Jouguet model, was that of Zeldovich (1940), Dö̈ring (1942) and von Neumann (1943), during World War II. The model describes a one-dimensional detonation wave structure as a shockwave or a nonreactive shock discontinuity, inmediately followed by a reaction zone or a region of heat addition (due to the chemical reaction). The flow in the reaction zone, the reacting flow, moves with constant subsonic velocity. The reaction rate gives the thickness of this induction zone, which in turn gives the thickness of the detonation wave. The thickness is measured by the length of the heat addition region, which continuous until the flow becomes sonic at $\lambda = 1$ for a CJ detonation or until it reaches a value of $\lambda_{max} < 1$ which stands for an overdriven detonation wave.

The ZND-model gives the same detonation velocities and pressures as the CJ-theory, but with the addition that it also gives the thickness of the wave. It is based on the Euler equations of hydrodynamics, which are inviscid flow equations in which transport effects and dissipative processes, besided the chemical reactions, are neglected. The flow is treated as one-dimensional and the shockwave as a discontinuity, but as one in which no chemical reaction occurs. The reaction is triggered by passing this discontinuity in a mixture and propagates at a finite rate thereafter. So the reaction rate is zero before the discontinuity and fintite, irreversible behind the discontinuity. Also, the conditions in gas detonations (pressure under 100bar and temperature under 7000K) are such that they can be described by the ideal gas equation of state. In fact, the CJ-theory can be considered to be a limit of the ZND model, because with the CJ-theory the reaction rate goes to infinity, or the reaction zone to infinitely small.

Also the same as the Chapman-Jouguet model is that the ZND model uses the assumption that the flow is steady, so the conservation equations also hold for the ZND model. But the energy equation and so also the Hugoniot equation now depends on the extent of the chemical reaction rate λ, which varies now between the intial state (0) and the final state (1). The Hugoniot equation now becomes

$$H = E(p, v, \lambda) - E(p_0, v_0, \lambda = 0) - \frac{1}{2}(p + p_0)(v_0 - v) = 0 \tag{3.13}$$

where λ defines the state completely. The ZND model solution to describe the reaction zone is based on simple and reasonable assumptions on how to model the real physical phenomenon.

The ZND model has two important properties, the first being that the model predicts a pressure maximum at the shock transition. This maximum is called the *von Neumann spike*. The second property is that the ZND model is a simple one-dimensional model and therefore it cannot be used to predict stability. If stability is to needed to be predicted, the equations used have to be changed to include time-dependent terms. Detonation structures are in fact three-dimensional nonsteady structures and say something about the nature or stability of a detonation wave.

3.2.3 Detonation Wave Structure and Stability

From research it is known that all self-sustaining detonation waves have three-dimensional structures from the leading shock front through the reaction zone of the detonation. The actual structure of a detonation wave or the detonation front can almost entirely be found with observation of experiments, and than be interpreted with the help of after-the-fact calculations based on standard shock matching and the blast wave theory. The structure is needed to determine the nature of the detonation wave, being either stable or instable.

One of the main features of the structure is the transverse wave, which is an interior shock joined to the leading shock in a three shock configuration. The ZND theory concludes that the region between the lead shock front and the Chapman-Jouguet plane in a one-dimensional detonation is a region where the flow is subsonic and that because of this pressure waves are able to propagate across the front as the front itself propagates. In research it has been observed that all self-sustaining detonations contain propagating transverse pressure waves, or *transverse waves*, of finite amplitude, which propagate in directions normal to the leading shock front (Strehlow 1968, Fickett 1979). These waves also interact with the leading shock front to produce *Mach stems* (also called Mach front), which themselfes propagate across the detonation front. The Mach stem and the incident shock are part of the leading shock, and the transverse wave is the reflected shock, which moves back and forth across the detonation front. Transverse waves are not steady waves, but decay continuously, and are only kept alive by periodic rejuvenation, caused by collision with other transverse waves moving in the opposite direction. Detonations typically have a cellular structure, which is self-sustaining, with the chemical reaction providing the driving energy. The transverse waves are the cell boundaries and propagate in the reaction zone at approximately accoustic velocity, meaning the pattern changes with time. The three shock configuration, or the point where the transverse wave intersects, or reflects from the leading shock front, is called the *triple point* and is the key feature of the structure of the detonation wave. From these triple points shear layers separate different strength premixed gas streams, which have passed the leading shock front. Figure 3.11 shows the structure of a detonation wave with these triple points, with the shock front moving from left to right.

Looking more closely at the structure, the triple point shear layers are also seen and they separate the gas into a part that has passed through the incident and transverse waves and in a part has passed the Mach stem. Figure 3.12 shows the regions around the triple point in more detail. The triple point trajectories form regular *fish-scale* patterns, or cells, with a characteristic length L

and width λ. The right figure shows the periodic detonation wave configuration around a triple point in more detail, where different shock waves can be seen. The undisturbed detonation front is known as the *incident wave*, and the reflected shock is the transverse wave. The triple point itself is driven forward by a shock wave stronger than the incident wave, being the Mach stem. The contact discontinuity, or the slip line is enclosed by the Mach stem and the reflected shock. The slip line is needed for a stable triple point configuration between the Mach stem and the incident wave. The stronger Mach stem results in a reduction of the induction length, but when the incident wave increases in strenght, the induction length increases. To describe the left figure, the shock front inside the detonation cell travels as two Mach stems from point A to the line BC, where in the points B and C the triple point is inverted almost instantaneously and the front of the cell becomes an incident wave. The shock strength is smooth and decreases continuously along the symmetry line AD. In point D the two triple points merge exactly in one single point. The incident wave vanishes and the slip line is torn off and remains behind. Inmediately after D two new triple points with two new slip lines are developed.

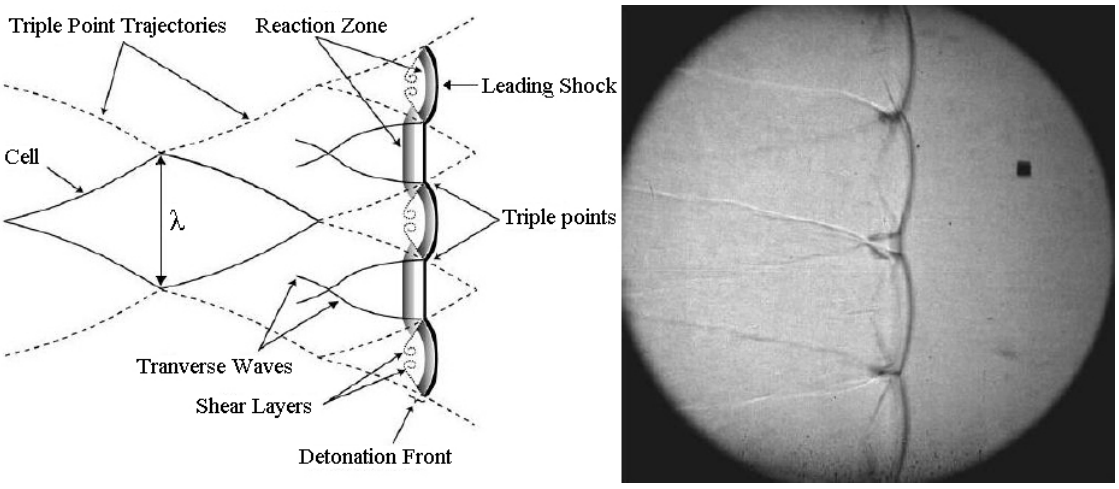

Figure 3.11: Detonation front, source: (Wintenberger, 2004)

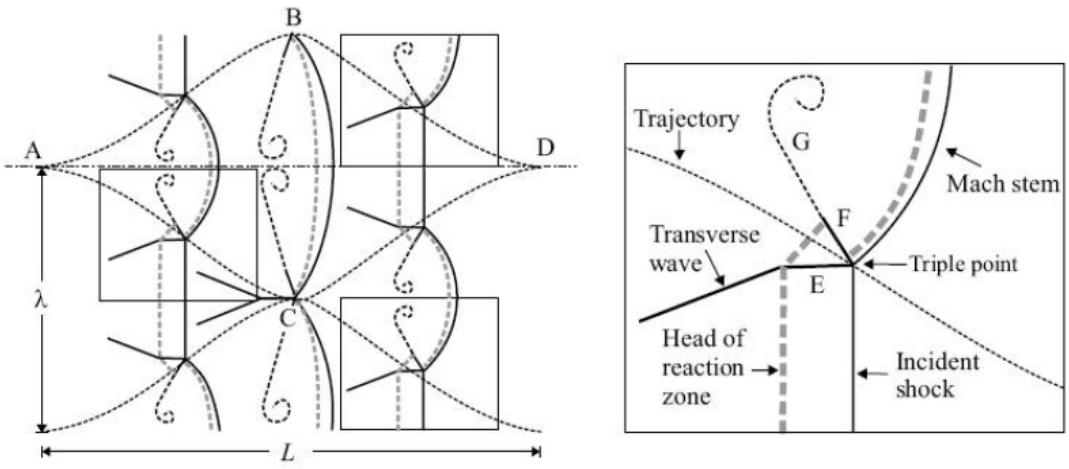

Figure 3.12: Left: regular detonation structure at three different timesteps on triple point trajectories, right: enlargement of a periodic triple point configuration, where E is a reflected shock, F a slip line, G a diffusive extension of the slip line with the flow vortex, source: (Deiterding, 2003)

The properties of a detonation that depend explicitly on the finite reaction rate are also known as the dynamic parameters of a detonation and determine if a detonation fails or not (Lee, 1984). These parameters are:

- The reaction length: the length of th einduction zone or recombination zone between the leading shock and a pre-defined identifier in the reaction zone.
- The cell size λ: the width or length of the characteristic cells seen in soot foil experiments of real multi-dimensional detonations. The cells are the tracks of shock triple points formed by intersection of the leading shock front with transverse waves that exist behind the front. The cell width is also the spacing of the transverse waves.
- Critical energy: the minimum energy of a point blast in a detonable mixture that will succesfully initiate a spherical detonation. Similar definitions apply to energy per unit length or area of a line or plane blast to initiate a cylindrical or planar detonation (Eckett, 2000).

The cell width λ has been proposed to be the most fundamental parameter characterizing the dynamic properties of detonations.

Detonations have a natural cell size one or two orders of magnitude larger than the reaction zone length of the hypothetical steady one-dimensional CJ detonation. But if the detonation is unconfined, random patterns will occur, as are seen in Lehr's experiments with projectiles with a CJ velocity or greater. The cell width λ represents the sensitivity of the mixture to detonation, meaning a mixture with a small cell width is more sensitive to detonation than a mixture with a larger cell width. Although there is no theory for cell width prediction, it is suggested that the cell width is proportional to the other detonation characteristic length scale, being the induction zone length Δ with a constant of proportionality A (Shchelkin 1965, Westbrook 1982)

$$\lambda = A\Delta \tag{3.14}$$

Research has shown that the constant A is dependent on the equivalence ratio of the mixture and if the mixture is stoichiometric or off-stoichiometric (Sheperd, 1986).

In terms of stability of a detonation wave, four fundamental parameters play a critical role for the structure of a steady wave. These parameters are:

- the ratio of specific heats
- the heat release of reaction
- the activation energy of the reaction
- the detonation overdrive

Because of the transverse waves interacting with the front leading shock, or also called transverse perturbations, the detonation wave appears to be unstable. The interaction with the transverse waves causes the front to pulsate. The oscillations are also seen with shock-induced combustion, but seem to disappear when the velocity is increased. Research has shown that a detonation front appears to be stable at velocities greater than the CJ velocity. Detonations are then called *overdriven detonations*. The degree of overdriven detonation determines the oscillatory region the detonation wave is in, being either in the regular regime or the large disturbance regime. So in terms of stability, the degree of overdrive determines if the detonation wave is stable. The degree

of overdrive f is the detonation wave velocity D related to the CJ velocity of the mixture D_{CJ} and is given as

$$f = \left(\frac{D}{D_{CJ}} \right)^2 \tag{3.15}$$

Other non-dimensional parameters that can influence stability are the activation energy, the heat release, and the ratio of specific heats. If detonations are used for practical reasons, say for combustion in an engine, stability must be obtained to a high degree for safety. The amplitude of the oscillation determines the degree of stability, the lower the amplitude, the higher the degree of stability (Lee, 1995).

Numerical studies have revealed that when the activation energy increases beyond a certain stability limit, or when the degree of overdrive decreases towards the CJ velocity, the pulsating nature of the detonation front changes (He, 1995). The pulsating nature can change into three modes, going from harmonic, to nonlinear pulsating and eventually towards a multimode chaotic behavior. Whenever the nature changes, so does the amplitude of oscillations. It increases when the degree of overdrive decreases. The periodic behavior of the oscillations increases aswell. And when the degree of overdrive decreases even further no periodic behavior is found and the oscillations become chaotic. When this happens, the pressure and the temperature in the mixture behind the shock drops to a point where rapid autoignition may not take place. The reaction zone length is then increased, which causes decoupling of the induction zone and the front shock, leading to detonation failure.

The chemical heat release, behind the leading shock front, generates disturbances that interact with the leading shock front and cause the propagation of the detonation wave to be unsteady and nonplanar (Sanchez, 2001). But when a detonation wave is strongly overdriven, the chemical heat release is sufficiently small compared to the thermal enthalpy behind the leading shock, the ZND concludes the detonation in ideal gases to be stable, because the corresponding shock is stable. This has not been usually encountered experimentally. Still the degree of stability can be increased when the chemical heat release is decreased.

3.3 Propulsion System Designs

The following two sections discuss ramjet propulsion system designs operating with either shock-induced combustion or detonations. These designs are still in development and have not been tested experimentally to the knowledge of the author. They have been investigated numerically for the past decade and show great promise.

3.3.1 The Shcramjet

Consider again the flow inside a scramjet from section 2.1, in particular inside the combustion chamber. Here the flow has to be compressed by shock waves in the inlet, then mix and burn with injected fuel sufficiently within the combustor and then expelled through the nozzle section. The velocity of the flow inside the chamber is supersonic so in the order of higher then Mach 1, which means that the residence time inside the chamber is in the order of milliseconds. For the engine to operate with good efficiency, this would result in having either a long combustion chamber or having extremely good mixing qualities in the chamber with the fuel and air. The first option is not a favorable choice because of the increase in structure weight and drag of the

vehicle. The second option is more favorable but very difficult to produce and is still very much in the early stages of research. But a way to reduce the length of the combustion chamber would be to mix the fuel with the air and compressing it before it enters the combustion chamber. This is termed *decoupling* and separates the combustion chamber from the mixing process, which will be done now in the inlet. The inlet being the long slender forebody of the vehicle. Before the flow enters the combustion chamber, it is first mixed with fuel and compressed by series of weak shock waves. By doing this, the mixture of air and fuel will combust or self-ignite after passing the last shock wave, which has a sufficient compression ratio to increase the pressure and temperature of the mixture to the point of combustion or self-ignition. Because of this, this type of concept differs from the concepts investigated in chapter two by not needing recirculation zones or flameholders. When the combustion wave is far enough downstream and does not influence the preceding shock wave, it is called shock-induced combustion. The combustion wave is captured within the combustion chamber and the combustion products are expelled through the nozzle of the vehicle. This propulsion system design is named the shock-induced combustion ramjet, or *shcramjet*, and a concept design is shown in figure 3.13.

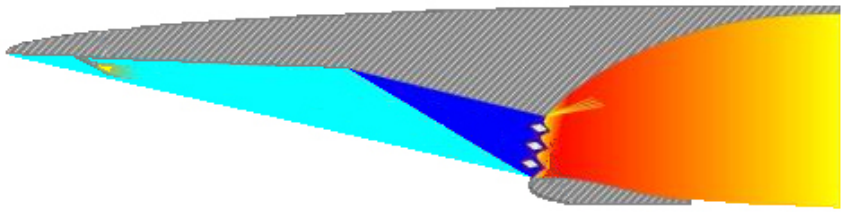

Figure 3.13: The shcramjet, source: (Sislian)

The concept shows three diamond shaped combustion wave instigators just at the exit of the inlet. This is one way of ensuring final shock waves which could ignite the mixture spontaneously.

Research has been done on two types of engine geometries that use shock-induced combustion, with different configurations. Configuration 1 uses three equal-strength weak shock waves and is called a multi-shock *external compression* configuration. Configuration 2 uses two equal-strength weak shock waves (to minimize entropy increase), as a so-called *mixed compression*. Both are shown in figure 3.14. Research has shown that the mixed-compression configuration outperforms the external compression configuration by over 20% in fuel specific impulse for flight Mach numbers between 10 and 23 (Sislian, 2001). The series of shock waves must be tailored in such a way that the last shock wave, which induces the combustion of the mixture, is held constant at the entrance of the combustion chamber, instigated by the cowl. By doing this the shock-induced combustion is held inside the chamber and not before in the inlet or after in the nozzle. It is necessary to have the shock waves intersect at the cowl lip to prevent losses in engine efficiency. The necessity for doing this is clear, outside ignition of the mixture decreases engine efficiency dramatically and creates risks for the vehicle's structural integrity. This must be prevented at all times. But the strenght and the location of the shock waves is not the only concern this engine design faces. The following problems can occur:

- insufficient mixing before combustion
- premature ignition

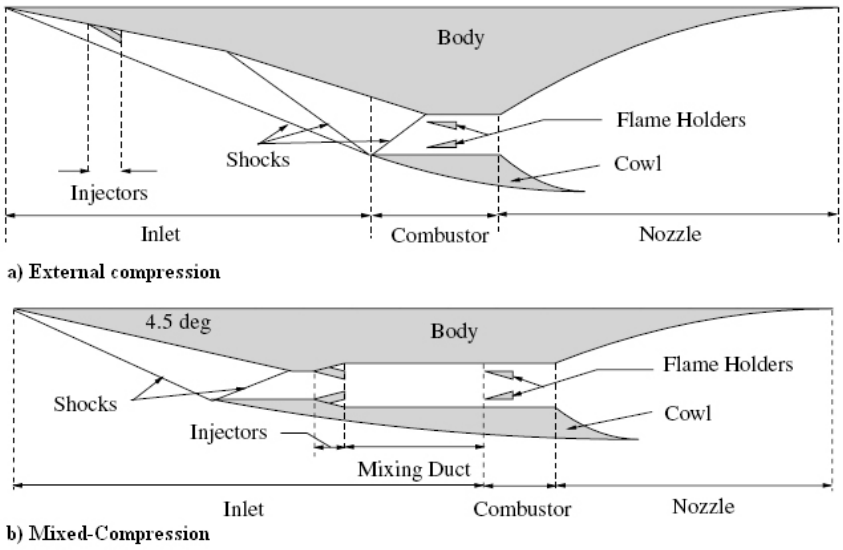

Figure 3.14: Shcramjet geometries, source: (Sislian)

One of the major problems within ramjet combustors discussed in chapter two is efficient mixing of the fuel with the incoming supersonic moving air. This is also the case with shcramjet engines, as they depend heavily on sufficient mixing of fuel and air, before entering the combustion chamber. Incomplete mixing can cause a decrease in specific impulse, and increased ignition delays. A delay in ignition time will increase the need for a longer combustion chamber. For a shcramjet the mixing is done outside the combustion chamber and occurs in the relative long inlet/forebody of the vehicle. The fuel is injected through a type of injector mounted on the lower body of the vehicle. The goal is to have a quasi to homogenous fuel/air mixture through sufficient mixing, before the flow enters the combustion chamber. Figure 3.15 shows a simplistic concept of the forebody of the vehicle and injector (Sislian, 2000).

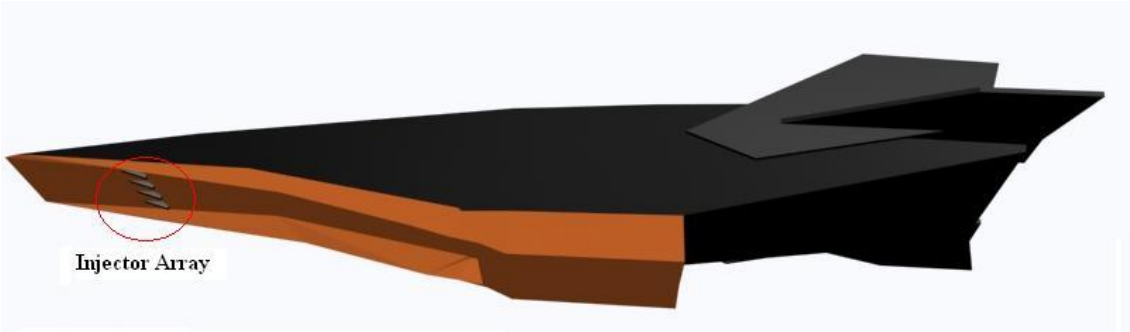

Figure 3.15: Shcramjet forebody with injector array

Extensive research has allready been done for fuel injector concepts, which provide the mixing inside supersonic combustion chambers for ramjets (Seiner, 2001). There are several concepts for doing this, with one being at some point more efficient then the other. But one of the popular choices is the *ramp fuel injector*(a) and most recently the *cantilevered ramp injector*(b), both displayed in the figure 3.16 (Sislian, 1999).

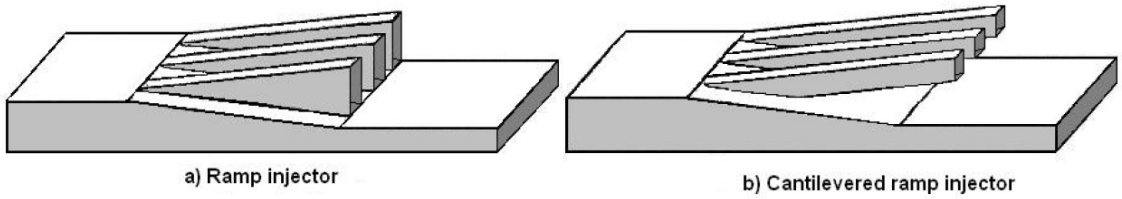

Figure 3.16: Shcramjet injector designs, source: (Sislian)

The ramp injector has a low injection angle, which ensures that most of the fuel momentum is recovered in the thrust balance and it increases the mixing performance by creating axial vortices (Naughton, 1989). These vortices increase the fuel penetration and the fuel/air contact surface. The cantilevered ramp injector for the shcramjet, creates the same axial vortices, with similar strength. The increase in mixing is brought by an addition of a swirl, which can increase the efficiency as much as over 30% in free-stream flows with a Mach number of 3.5. Research indicated that the cantilevered ramp injector, except for fuel penetration, has superioir mixing characteristics, being a higher mixing efficiency than the conventional ramp injector.

Decoupling of the mixing and burning inside the combustor has the result that mixing efficiency can be improved, but decoupling also increases the chance of premature combustion of the mixture. Premature ignition occurs when the fuel enters the hot hypersonic boundary layers. This can be seen in figure 3.17 where shock-induced combustion occurs with premature ignition in the hot boundary layer. The red zones, one at the wall of the inlet and one in the combustor section, indicate a high enough static temperature to induce self-ignition of the fuel/air mixture.

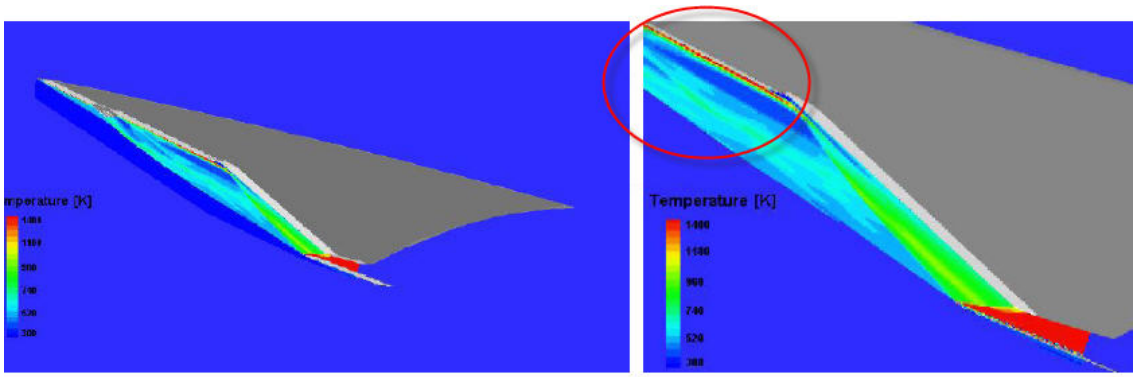

Figure 3.17: Premature combustion in the boundary layer of a shcramjet, source: (Sislian)

A way of suppressing premature ignition is to cool down the boundary layer. This can be done by injecting either nitrogen N_2 or hydrogen gas H_2 via a backward facing step, and thus cooling the boundary layer downstream of the injector array. Research has shown that the addition of hydrogen gas in the backward step cooled the boundary layer enough, thus preventing ignition and did not alter the mixing characteristics.

3.3.2 The Detonation Wave Engine

At some point when the velocity keeps increasing the reaction zone reaches a minimum length and shock-induced combustion becomes a detonation wave with a different structure. When this happens the shock-induced combustion ramjet, or shcramjet, is called a detonation wave engine. A detonation wave engine, or DWE, can be either using normal standing waves or oblique standing waves. Research has shown that it is more advantageous to have oblique shock waves to induce the detonation, because the flow remains supersonic after the shock wave, which in turn has lower static pressures behind it and a lower total pressure loss. There is a difference between continuous and discontinuous, or *pulsed*, detonation waves. This thesis only investigates continuous, steady flow, although detonations are usually considered as unsteady combustion waves, due to transverse waves in the reaction zone causing oscillations. But the combustion wave itself is continuous. When the wave is pulsed, the engine is called a pulse detonation engine, or PDE. This kind of engine uses pulsed cycles of detonations, which is not the same as for instance how the flow inside a shcramjet is considered, being continuous and not cyclical. The thesis will only consider continuous flow and therefore will not further investigate the pulsed variation of the DWE.

It is important for every engine that the combustion process is in some way continuous and steady. But, one key issue in both the shcramjet and the DWE is that the combustion wave must be stable and standing, because a detonation wave can also propagate, which means it could move outside the combustion chamber or even into the nozzle. For equillibrium flows with heat addition, classic gasdynamic theory predicts the existence of a detonation wave for which entropy production and hence stagnation pressure losses, are at a minimum. Such a detonation wave is known as a CJ detonation wave, discussed earlier in section 3.2.1. The combustor angle is chosen to achieve a minimum of entropy production while maintaining stability. This angle is also called the CJ angle and an angle larger than this is called the *overdriven* angle, for an overdriven detonation wave with a velocity greater than the CJ velocity.

The detonation wave engine must be designed to have steady standing oblique detonation waves in either a CJ state or near the CJ-state, because this would mean a minimum of pressure loss and a minimum increase of entropy.

When looking at an actual or typical structure of an oblique detonation wave, there are differences with the ideal oblique detonation wave mentioned above. The first difference is that the oblique shock, instigated by the wedge with angle δ increases the temperature of the oncoming fuel/air mixture above its ignition point. This shock is not termed an oblique detonation wave but a combustion-inducing shock. In the induction region, which follows until the first deflagration wave, concentration of radicals increase with temperature and pressure almost remaining constant, until exothermic reactions begin and deflagration waves are formed. The deflagration waves propagate at the local Mach angle and have each a steeper angle due to the temperature rise across each wave. They merge and intersect with the combustion-inducing shock and form a single structure, which is an oblique detonation wave. The angle of the oblique detonation wave ϵ is steeper than the combustion-inducing angle. From the intersection point a slip line is formed which divides the flow into two velocity regions, one behind the detonation wave and one behind the last deflagration wave, which is termed a shock-induced combustion zone. The Chapman-Jouguet condition corresponds to a wedge angle δ_{CJ} which gives rise to a Chapman-Jouguet oblique detonation wave with angle ϵ_{CJ}, shown in figure 3.18.

For standing stable oblique detonation waves it is important that they are resiliant to inhomogeneities present in the oncoming fuel/air mixture. Research has shown numerically and experimentally that the formation of a standing oblique detonation wave is possible, but the resiliance to inhomogeneities has only been proven numerically, in both viscous and non-viscous flow. The experimental proof is still lacking.

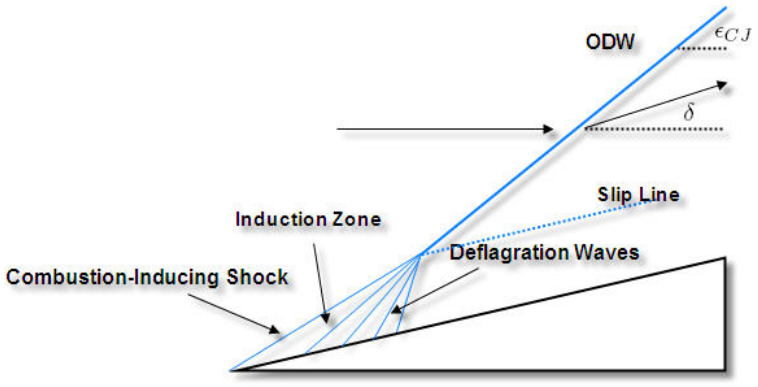

Figure 3.18: Schematic of an oblique detonation wave, source: (Fusina, 2005)

For standing stable oblique detonation waves it is important that they are resiliant to inhomogeneities present in the oncoming fuel/air mixture. Research has shown numerically and experimentally that the formation of a standing oblique detonation wave is possible, but the resiliance to inhomogeneities has only been proven numerically, in both viscous and non-viscous flow. The experimental proof is still lacking.

A classic, ideal, thermodynamic, closed-cycle analysis shows that the performance of a detonation wave is promising. The detonation wave propagates with a supersonic velocity, with several thousand meters per second, and because of the high velocity of the flame the detonation wave can be modelled as a constant-volume process, differing from the deflagration combustion modelled as a constant-pressure process (see also section 3.2.1). This constant-volume process is also known as the Humphrey cycle, and the constant-pressure process is known as the Brayton cycle. The Brayton cycle consists of two constant-pressure processes and two insentropic processes, while the Humphrey cycle differs by having the constant-pressure combustion process replaced with a constant-volume combustion process, see figure 3.19.

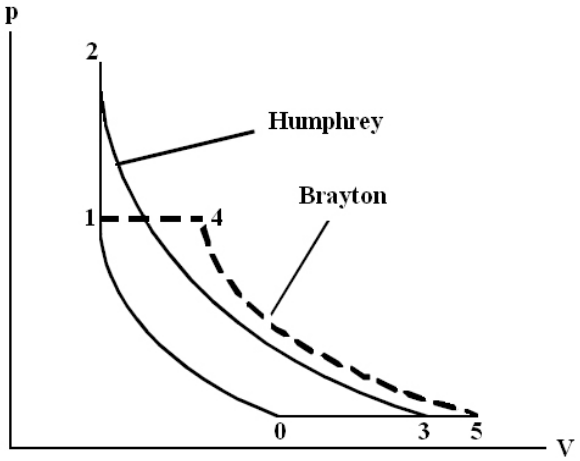

Figure 3.19: Brayton and Humphrey Cycles

The Brayton cycle consists of an isentropic compression (0-1), a constant-pressure heat addition (1-4), an isentropic expansion (4-5) and constant-pressure heat rejection (5-0), the Humphrey cycle

thus only replaces step 1-4 with constant-volume heat addition (1-2) followed then by isentropic compression (2-3). The efficiency of both cycles can be determined by assuming a thermodynamic equillibrium (thermodynamic system with no outside disturbances), perfect gas of constant properties, heat addition with no mass addition, and ideal processes (isentropic compression and expansion). The ideal Brayton efficiency is given as:

$$\eta_{Brayton} = \frac{q_{in} - q_{out}}{q_{in}} = 1 - \frac{q_{out}}{q_{in}} = 1 - \frac{c_p(T_5 - T_0)}{c_p(T_4 - T_1)} = 1 - \frac{T_0}{T_1}\left(\frac{\frac{T_5}{T_0} - 1}{\frac{T_4}{T_1} - 1}\right) \tag{3.16}$$

and with the isentropic processes and constant pressure resulting in:

$$\frac{T_4}{T_1} = \frac{T_5}{T_0}$$

The Brayton efficiency now depends only on the temperature change during either the isentropic compression or expansion process:

$$\eta_{Brayton} = 1 - \frac{T_0}{T_1} = 1 - \frac{T_4}{T_5} \tag{3.17}$$

The same can be done for the efficiency of the Humphrey cycle:

$$\eta_{Humphrey} = \frac{q_{in} - q_{out}}{q_{in}} = 1 - \frac{q_{out}}{q_{in}} = 1 - \frac{c_p}{c_v}\frac{(T_3 - T_0)}{(T_2 - T_1)} \tag{3.18}$$

Rewriting this equation using $p_3 = p_0$:

$$\frac{T_3}{T_0} =$$

$$\frac{T_1}{T_0}\frac{T_3}{T_2}\frac{T_2}{T_1} = \left(\frac{p_1}{p_0}\right)^{\frac{\gamma-1}{\gamma}}\left(\frac{p_3}{p_2}\right)^{\frac{\gamma-1}{\gamma}}\frac{T_2}{T_1} = \left(\frac{p_1}{p_0}\frac{p_3}{p_2}\right)^{\frac{\gamma-1}{\gamma}}\frac{T_2}{T_1} = \left(\frac{p_1}{p_2}\right)^{\frac{\gamma-1}{\gamma}}\frac{T_2}{T_1} = \left(\frac{T_2}{T_1}\right)^{-\left(\frac{\gamma-1}{\gamma}\right)}\frac{T_2}{T_1} =$$

$$= \left(\frac{T_2}{T_1}\right)^{\frac{1}{\gamma}}$$

The Humphrey efficiency now becomes:

$$\eta_{Humphrey} = 1 - \gamma\frac{T_0}{T_1}\left(\frac{\left(\frac{T_2}{T_1}\right)^{\frac{1}{\gamma}} - 1}{\frac{T_2}{T_1} - 1}\right) \tag{3.19}$$

Both efficiencies are plotted in figure 3.20 using a representative detonative combustion process, where γ is held constant and using a stoichiometric hydrogen/air equillibrium chemistry calculation with a detonation temperature ratio T_2/T_1 of 10.2 and a γ of 1.4 for unburned gas and γ=1.16 for burned gas (Bussing, 1996).

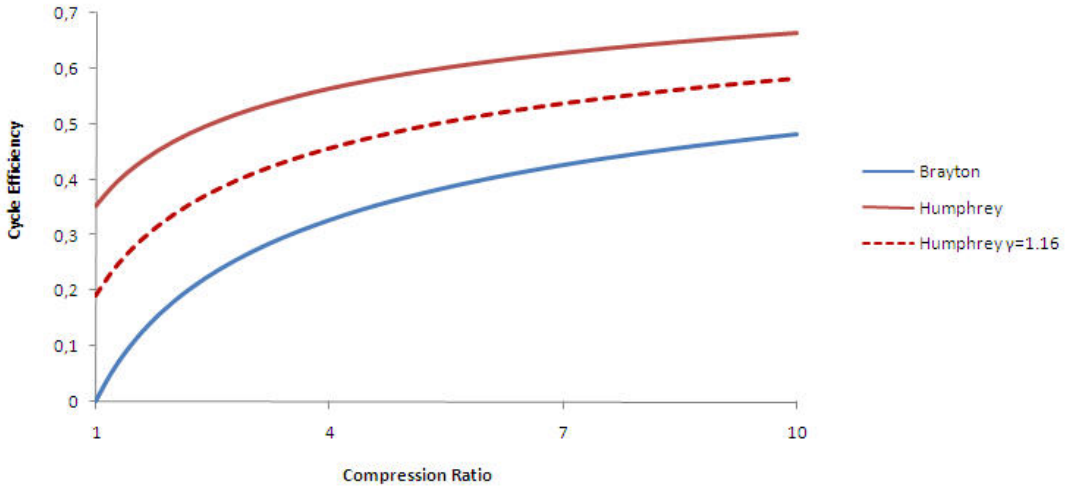

Figure 3.20: Thermal efficiency of the isobaric Brayton cycle and the detonation Humphrey cycle

The actual detonation cycle lies between the two γ limit curves, but still shows a higher efficiency than the Brayton cycle. This ideal cycle analysis shows that the detonation wave as a combustion cycle (modelled as a constant-volume combustion cycle) shows a significant advantage over the Brayton cycle. This has motivated a lot of research into using detonation waves as a combustion process.

Chapter 4

Performance Analysis

Going back to the original question what kind of ramjet engine concept is best suited for the hypersonic regime, the previous three chapters have therefore discussed several ramjet engine concepts using different kinds of combustion methods. It became apparent in chapter one that for an air-breathing engine operating in the hypersonic flight region ($M_0 \geq 5$), supersonic combustion is necessary to avoid very high thermal loads, internal temperatures and pressures within the combustor. Because of this, ramjet engine concepts using supersonic combustion propulsion systems were investigated more thoroughly in chapters two and three. The ramjet engine concepts discussed in the two chapters were distinguished by using either diffusion combustion or by using pre-mixed combustion.

Chapter 2 concluded analytical that diffusion combustion was optimal when using a divergent combustion chamber area, and modelled in such a way that the static pressure before combustion was the same as after combustion. This was then termed a constant-pressure combustion process (CP). In chapter 3 it was indicated that pre-mixed combustion, or shock-induced combustion occurred at such high velocities that it could be modelled as a constant-volume process (CV). When the flow velocity increases and the distance between the preceding shock wave and the combustion front reaches a minimal length (induction zone minimum), the two discontinuities will start to interact with each other. The combustion process can then be modelled as a hydrodynamic discontinuity, across which energy release occurs (DET).

To estimate the performance of a combustion process, a thermodynamic cycle analysis can give more insight into the efficiency of the combustion cycle. It is then practical for performance calculations of preliminary ramjet designs to begin with an one-dimensional steady flow calculation. As seen before, these calculations are based on the use of the continuity, momentum and energy equation. Usually a fourth additional equation is used to solve the system of equations. The performance will be indicated using three characteristics: the total pressure loss, the entropy increase, and the specific impulse. The total pressure loss indicates how much useful work can be done by a flow. When the total pressure loss increases, the efficiency of the engine decreases. The increase of entropy indicates the loss of or irretrievable usable energy of a flow. The increase ds is given by eq.(2.18):

$$ds = c_p ln\frac{T_3}{T_2} - Rln\frac{p_3}{p_2}$$

or

$$ds = c_v ln\frac{T_3}{T_2} + Rln\frac{\rho_3}{\rho_2}$$

The specific impulse indicates the efficiency of the combustion process. The higher the specific impulse, the more momentum or impulse is generated with a specific amount of fuel. The equation

for the specific impulse I_{sp} is given by eq.(1.7) and rewritten here as:

$$I_{sp} = \frac{1}{\varphi \left(\frac{m_f}{m_a}\right)_{stoch}} \frac{1}{g} \left(\frac{u_e}{u_0} - 1\right) u_0 \sqrt{\gamma R T_0} \tag{4.1}$$

with an equivalence ratio φ of 0.485, and a stochiometric fuel/air ratio $(m_f/m_a)_{stoch}$ of 0.029 taken for hydrogen.

So far, the assumption of an ideal gas and a constant value of gamma (the ratio of specific heats) has been made with previous analyses. The fact is that it is a very ideal assumption, because a real gas possesses internal degrees of freedom such as vibration and that the chemical composition is variable. This makes in fact the constant-gamma formulation inaccurate. One way of correcting this would be to use variable specific heat ratios to improve the use of this method and to provide better estimates. However, in literature it is repeatedly noted that one needs to know the upstream state of the product gases just before the detonation or combustion front, which is extremely difficult. Because of this, and within the scope of this thesis, the use of the assumption of a constant gamma is justified.

To determine the flow properties just after heat addition, the conservation equations are used. They are formulated as follows:

$$\rho_2 V_2 A_2 = \rho_3 V_3 A_3 \tag{4.2}$$

$$p_2 A_2 + \rho_2 V_2^2 A_2 - \rho_3 V_3^2 A_3 = p_3 A_3 - \int \bar{p} dA \tag{4.3}$$

$$dq = dU + pd\left(\frac{1}{\rho}\right) \tag{4.4}$$

Another equation added to complete the set is the equation of state for an ideal gas. Since the molecular weight after heat addition is assumed to remain constant, it can be formulated as follows:

$$\frac{p_2}{\rho_2 T_2} = \frac{p_3}{\rho_3 T_3} \tag{4.5}$$

After analytical and numerical investigations, experimental tests can be done, especially to test the feasibility of a concept. This is also known as a proof-of-concept, and a proof-of-concept test setup pre-design is given at the end of this chapter to indicate how a particular concept can thus be tested.

4.1 Thermodynamic Efficiency

Since a ramjet engine can be considered as a chemical propulsion engine, which converts the heating value of combustion of fuel with air into exhaust flow kinetic energy, it can be seen as a thermodynamic device. Therefore an useful method to estimate the ramjet engine's performance, before starting with an one-dimensional analysis, is a thermodynamic cycle analysis. In this analysis the processes are represented on a thermodynamic state diagram. It is important for this to assume a steady flow between the thermodynamic state points and the flow locations within the ramjet engine concept and that the cycle hass no losses. The thermodynamic processes in the ramjet engine design cycle are isentropic compression ($0 \rightarrow 2$), adiabatic combustion ($2 \rightarrow 3$), and isentropic expansion ($3 \rightarrow 4$). When ideal expansion is assumed, the pressure at the end of the expansion is the same as at the beginning of compression, the cycle is considered to be an ideal closed cycle. When combustion occurs adiabatically, the thermal efficiency can be defined as the ratio of the work done by the system to the heat of combustion of the mixture.

$$\eta_{th} = \frac{w}{q_c} = \frac{q_{in} - q_{out}}{q_{in}} \tag{4.6}$$

At the end of the previous chapter a similar thermodynamic cycle analysis was given and for both shock-induced combustion and detonations the Humphrey cycle was chosen to represent those combustion processes. This cycle analysis expands on the previous cycle analysis by not using the surrogate constant-volume cycle for detonations, but another cycle. This cycle assumes that the detonation wave occurs as a Chapman-Jouguet detonation wave, a detonation limit, and is known as the Fickett-Jacob cycle. The Chapman-Jouguet condition is a sonic condition in normal direction behind the discontinuity ($M_{n_3} = 1$) and using this in the conservation equations they become (A is taken constant):

$$\frac{\gamma_3 p_3}{\rho_3} M_{n_3}^2 = \frac{\gamma_2 p_2}{\rho_2} M_{n_2}^2 \tag{4.7}$$

$$p_3(1 + \gamma_3 M_{n_3}^2) = p_2(1 + \gamma_2 M_{n_2}^2) \tag{4.8}$$

$$\frac{\gamma_3}{\gamma_3 - 1} p_3 \rho_3 \left(1 + \frac{\gamma_3 - 1}{2} M_{n_3}^2\right) = \frac{\gamma_2}{\gamma_2 - 1} p_2 \rho_2 \left(1 + \frac{\gamma_2 - 1}{2} M_{n_2}^2\right) + q \tag{4.9}$$

Using the Chapman-Jouguet condition, the (normal) Chapman-Jouguet Mach number is given as

$$M_{n_{CJ}} = M_{n_2} = \sqrt{H + \frac{(\gamma_2 + \gamma_3)(\gamma_3 - 1)}{2\gamma_2(\gamma_2 - 1)}} \pm \sqrt{H + \frac{(\gamma_3 - \gamma_2)(\gamma_3 + 1)}{2\gamma_2(\gamma_2 - 1)}} \tag{4.10}$$

with H the non-dimensional heat of reaction

$$H = \frac{(\gamma_3 - 1)(\gamma_3 + 1)q}{2\gamma_2 R_2 T_2} \tag{4.11}$$

This model is also known as the two-γ model, or Thompson model for Chapman-Jouguet detonations in a perfect gas (Thompson, 1973). The jump relations are derived as follows, the pressure ratio directly from the momentum equation

$$\frac{p_3}{p_2} = \frac{\gamma_2 M_{n_2}^2 + 1}{\gamma_3 + 1} \tag{4.12}$$

The density ratio can be found using the condition that the outflow is sonic $u_3 = \sqrt{\gamma_3 p_3/\rho_3}$, and combining with momentum equation, gives

$$\frac{\rho_3}{\rho_2} = \frac{(\gamma_3 + 1)p_3/p_2 - 1}{\gamma_3 p_3/p_2} = \frac{\gamma_2(\gamma_3 + 1)M_{n_2}^2}{\gamma_3(1 + \gamma_2 M_{n_2}^2)} \tag{4.13}$$

And the temperature ratio can be found using the equation of state

$$\frac{T_3}{T_2} = \frac{p_3}{p_2}\frac{\rho_2}{\rho_3} = \frac{\gamma_3(\gamma_2 M_{n_2}^2 + 1)^2}{\gamma_2(\gamma_3 + 1)^2 M_{n_2}^2} \tag{4.14}$$

When the model is simplified by taking γ constant ($\gamma_3 = \gamma_2$), the one-γ model of Fickett-Jacob (FJ) is found (Fickett and Davis, 2001). The non-dimensional heat of combustion H now becomes:

$$H = \frac{(\gamma_3 - 1)(\gamma_2 + 1)q}{2\gamma_2 R T_2} = \frac{(\gamma^2 - 1)q}{2\gamma R T_2}$$

And the one-γ model is given as ($M_{n_2} = M_{CJ}$):

$$M_{CJ} = \sqrt{H + 1} + \sqrt{H} \tag{4.15}$$

$$\frac{p_3}{p_2} = \frac{\gamma M_{CJ}^2 + 1}{\gamma + 1} \tag{4.16}$$

$$\frac{\rho_3}{\rho_2} = \frac{(\gamma + 1)M_{CJ}^2}{1 + \gamma M_{CJ}^2} \tag{4.17}$$

$$\frac{T_3}{T_2} = \frac{(1+\gamma M_{CJ}^2)^2}{(\gamma+1)^2 M_{CJ}^2} \tag{4.18}$$

Now that an explicit model for detonation waves is derived, the thermal efficiency can be determined. The enthalpy for states 2 and 3 can be expressed as

$$h_2 = c_p T_2$$

$$h_3 = c_p T_3 - q_{in}$$

The thermal efficiency is found by using an arbitrary thermodynamic cycle and looking at the system from initial state 0 to state 4, shown in figure 4.1. When the cycle is considered closed, states 0 and 4 coincide with each other. The heat interaction between steps 2 and 3 is required to remove an amount of thermal energy $q_{out} > 0$ from the products of combustion, which can be determined from the enthalpy change. The heat interaction between steps 3 and 4 is required to add an amount of thermal energy $q_{in} > 0$ in order to convert the combustion products back to reactants.

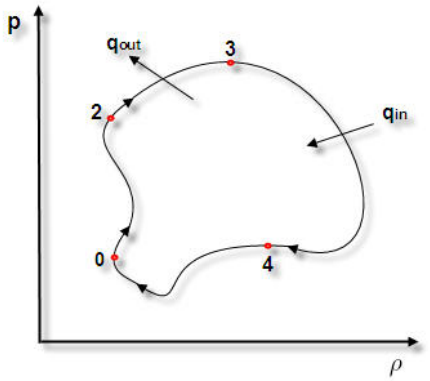

Figure 4.1: Thermodynamic cycle

This defines the quantity $q_c = q_{in}$. The work done by the system can be found with

$$w = q_{in} - q_{out} = 1 - \frac{q_{out}}{q_{in}} = 1 - \frac{c_p(T_3 - T_2)}{q_c} = 1 - \frac{\int_2^3 T ds}{q_c}$$

$$\eta_{th} = 1 - \frac{c_p T_2}{q_c}\left[exp\left(\frac{s_3 - s_2}{c_p}\right) - 1\right]$$

Using the equation for the entropy increase

$$\frac{s_3 - s_2}{R} = \frac{\gamma}{\gamma - 1} ln\left(\frac{T_3}{T_2}\right) - ln\left(\frac{p_3}{p_2}\right)$$

$$\frac{s_3 - s_2}{c_p} = ln\left(\frac{T_3}{T_2}\right) - \frac{\gamma - 1}{\gamma} ln\left(\frac{p_3}{p_2}\right) = ln\left(\frac{T_3}{T_2}\right) - ln\left(\frac{p_3}{p_2}\right)^{\frac{\gamma-1}{\gamma}}$$

$$\frac{s_3 - s_2}{c_p} = ln \frac{\left(\frac{T_3}{T_2}\right)}{\left(\frac{p_3}{p_2}\right)^{\frac{\gamma-1}{\gamma}}}$$

And using the jump relations

$$\frac{s_3 - s_2}{c_p} = ln\left[\frac{\left(\frac{(1+\gamma M_{CJ}^2)^2}{(\gamma+1)^2 M_{CJ}^2}\right)}{\left(\frac{\gamma M_{CJ}^2+1}{\gamma+1}\right)^{\frac{\gamma-1}{\gamma}}}\right] = ln\left[\frac{1}{M_{CJ}^2}\left(\frac{1+\gamma M_{CJ}^2}{\gamma+1}\right)^{\frac{\gamma+1}{\gamma}}\right]$$

The thermal efficiency for a detonation wave can now be written as

$$\eta_{th} = 1 - \frac{c_p T_2}{q_c}\left[\frac{1}{M_{CJ}^2}\left(\frac{1+\gamma M_{CJ}^2}{\gamma+1}\right)^{\frac{\gamma+1}{\gamma}} - 1\right] \tag{4.19}$$

Comparing this result with equations (3.20) and (3.22), and using for $T_0 = 222K$ and $p_0 = 1bar$ as initial conditions, the difference in thermal efficiency for the three combustion processes as function of the inlet compression ratio is given in figure 4.2

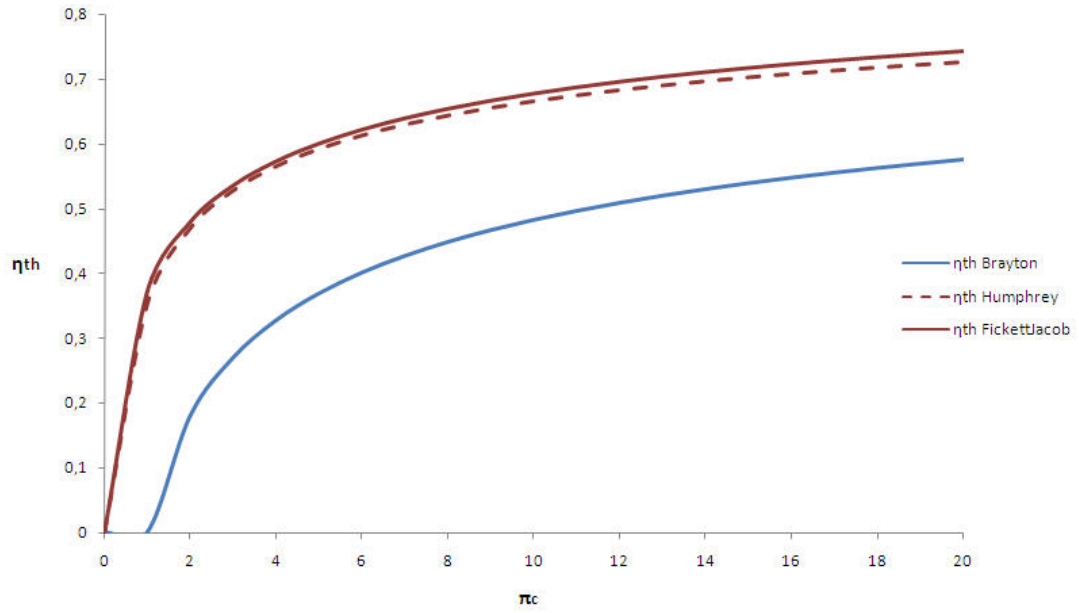

Figure 4.2: Comparison of thermodynamic efficiencies as a function of the inlet compression ratio

It can be seen in figure 4.2 that the Brayton cycle has the lowest efficiency, and the Humphrey and Ficket-Jacob cycles the highest. The Ficket-Jacob cycle has indeed a higher efficiency compared to the Humphrey cycle, but just sligthly. To use the Humphrey cycle analysis as a surrogate for detonation waves can therefore to some extent be justified.

These results show that detonation waves have the potential to generate more mechanical work than the Brayton or Humphrey combustion process and seem to be a more efficient combustion process. This result also thus suggests that detonation waves have a minimal entropy increase. This simple analysis has motivated a lot of research into the field of detonation waves.

4.2 Quasi-One-Dimensional and Two-Dimensional Analysis of Supersonic Flow with Heat Addition

An one-dimensional analysis starts by defining a control volume and the properties of the flow before entering this control volume. The control volume will be the same as used before, with the same cross-sectional stations, depicted in figure 4.3.

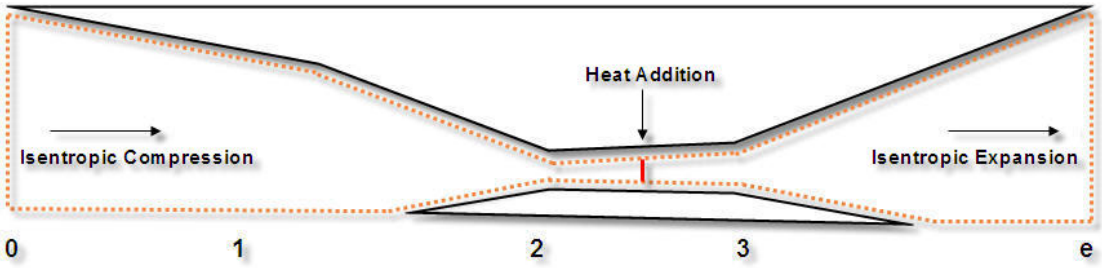

Figure 4.3: Control volume for quasi-one and two-dimensional analysis

Since the analysis is quasi-one-dimensional there are no changes in flow properties in y-direction, the cross-sectional area however varies to indicate the effect of it on the flow properties after heat addition. The velocity in y-direction V is therefore zero ($v = 0$) and the velocity term reduces to just u in normal direction to the heat addition wave. The conservation equations can now be written as:

$$\rho_2 u_2 A_2 = \rho_3 u_3 A_3 \tag{4.20}$$

$$p_2 A_2 + \rho_2 u_2^2 A_2 = p_3 A_3 + \rho_3 u_3^2 A_3 - \int \bar{p} dA \tag{4.21}$$

$$dq = dU + pd\left(\frac{1}{\rho}\right) \tag{4.22}$$

The inlet compression ratio CR is defined as

$$CR = \frac{M_2}{M_0} \tag{4.23}$$

An increase in this ratio corresponds with a decrease of internal compression, meaning a decrease in inlet exit pressure and temperature, but an increase in Mach number. Now the following three heat addition processes can be determined with the following inlet and nozzle conditions. Since the flow within the inlet undergoes an isentropic compression the stagnation temperature and pressure remain constant. The initial flow properties are a temperature $T_0 = 226.25K$, a pressure of $p_0 = 1171.87Pa$, and a density of $\rho_0 = 0.018kg/m^3$. The heating value for liquid hydrogen is taken as $H_f = 1.2 \cdot 10^8 J/kg$, the stochiometric fuel/air ratio is 0.029 with a heat addition $q = 1350240J/kg$. The flow within the nozzle is assumed as an ideal isentropic expansion process, with $p_4 = p_0$. The combustion process is assumed to be adiabatic, so no losses are accounted for during the three processes.

4.2.1 Quasi-One-Dimensional Constant-Pressure Heat Addition

When the pressure remains constant, the one-dimensional conservation equations and the equation of state can be given as:

$$\rho_2 u_2 A_2 = \rho_3 u_3 A_3 \tag{4.24}$$

$$\rho_2 u_2^2 A_2 = \rho_3 u_3^2 A_3 \tag{4.25}$$

$$c_p T_2 + \frac{1}{2}u_2^2 + q = c_p T_3 + \frac{1}{2}u_3^2 \tag{4.26}$$

Another equation added to complete the set is the equation of state for an ideal gas. Since the molecular weight after heat addition is assumed to remain constant, it can be formulated as follows:

$$\frac{\rho_3}{\rho_2} = \frac{T_2}{T_3} \tag{4.27}$$

With these equations the flow properties after CP heat additon can be determined. The temperature jump can be determined, by combining equations (4.24) and (4.25)

$$\rho_2 u_2^2 = \rho_3 u_3^2 = \rho_2 u_2 u_3$$

$$u_2 = u_3$$

Combining this result with eq.(4.26) the temperature jump is found to be:

$$T_3 = T_2 + \frac{q}{c_p} \tag{4.28}$$

Using the equation of state for CP heat addition, the density jump is determined as:

$$\rho_3 = \rho_2 \frac{T_2}{T_3} = \rho_2 \left(1 + \frac{q}{c_p T_2}\right) \tag{4.29}$$

Both jump relations are dependend on the initital temperature and the heat added. It can be concluded, since $T_3 \leq T_2$, that both the Mach number M and density ρ decrease after heat addition at constant pressure heat addition. The Mach number M_3 after heat addition can be determined using:

$$M_3 = \frac{V_3}{a_3} = \frac{u_3}{a_3} = \frac{u_3}{\sqrt{\gamma R T_3}} = \frac{u_3}{\sqrt{\gamma \frac{p_2}{\rho_3}}} \tag{4.30}$$

This result was also concluded in chapter 2. The cross-sectional area ratio is determined by the continuity equation

$$\frac{A_3}{A_2} = \frac{\rho_2}{\rho_3} = \frac{T_3}{T_2} \tag{4.31}$$

and is shown for different inlet compression ratios in figure 4.4

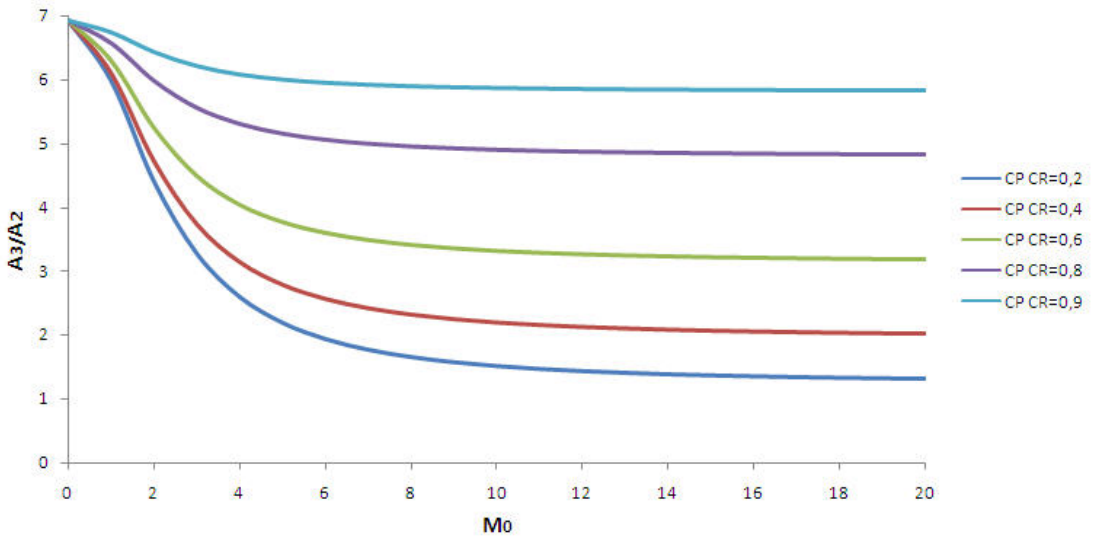

Figure 4.4: Cross-sectional area ratio for quasi-one-dimensional CP Combustion

Figure 4.4 shows that the cross-sectional area ratio increases with an increasing CR and remains nearly constant with Mach numbers above 10. The performance characteristics can now be determined. The total pressure loss, the increase in entropy and the specific impulse for CP heat addition with increasing inlet compression ratio are shown in figures (4.5), (4.6) and (4.7).

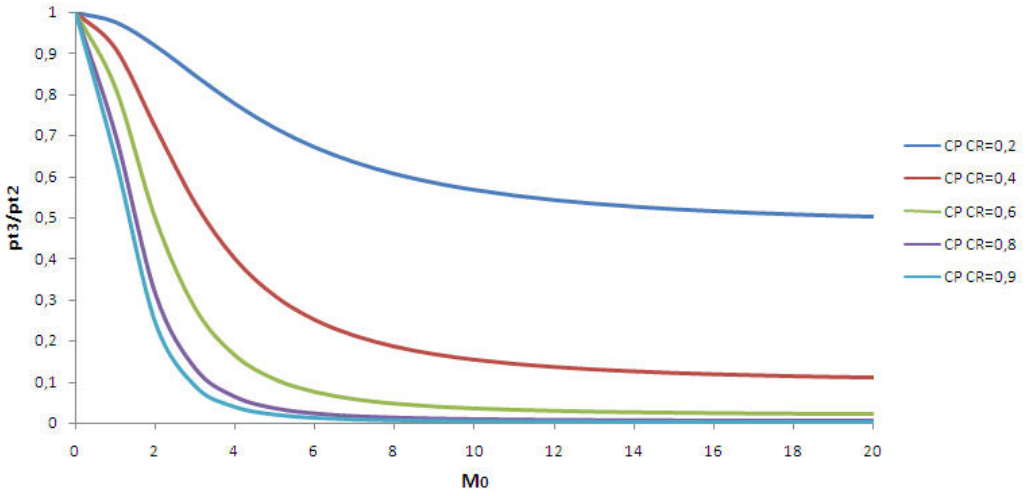

Figure 4.5: Total pressure loss for quasi-one-dimensional CP Combustion

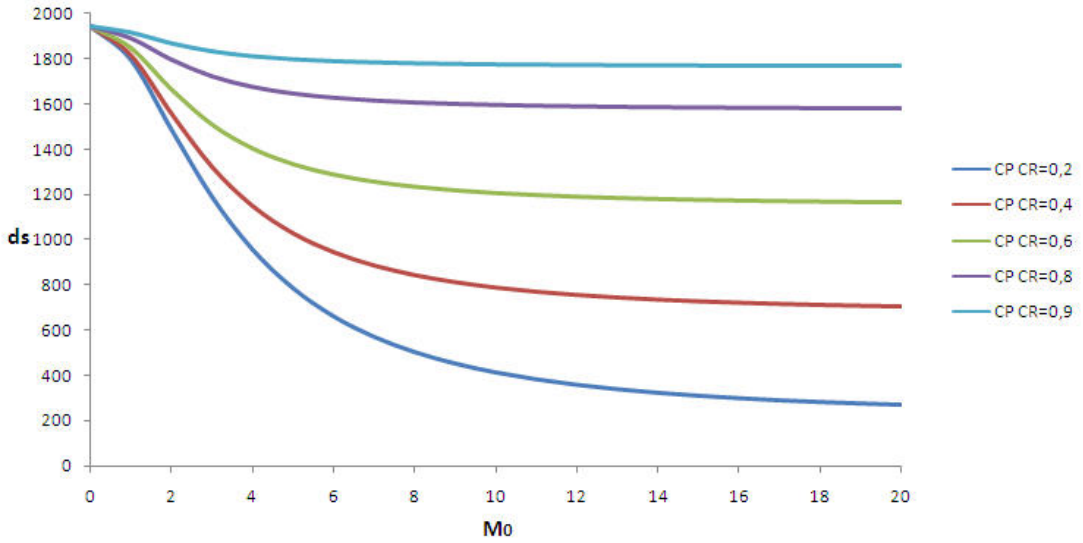

Figure 4.6: Entropy increase for quasi-one-dimensional CP Combustion

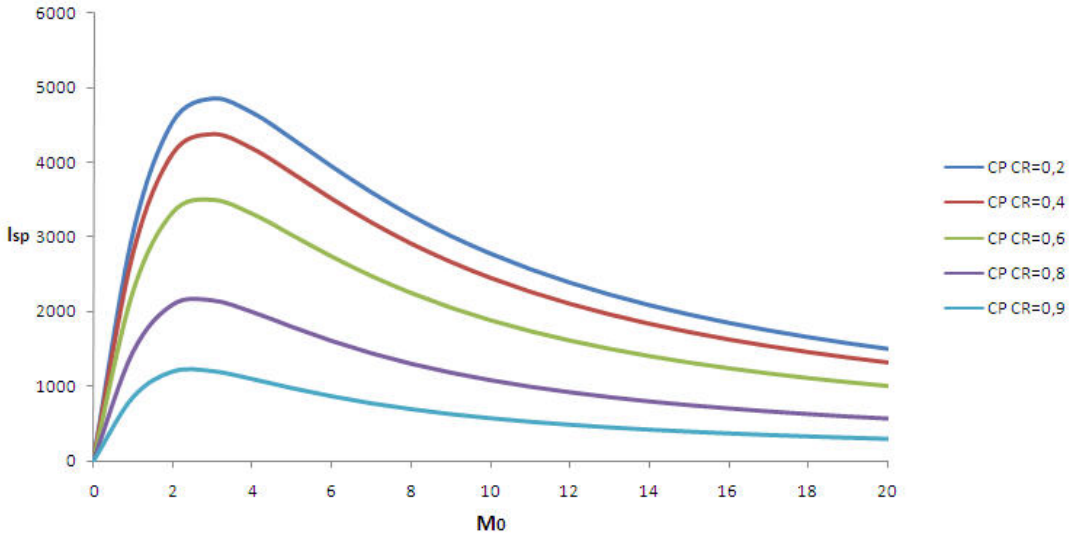

Figure 4.7: Specific impulse for quasi-one-dimensional CP Combustion

Figure 4.5 shows that when CR increases (less compression), with increasing freestream Mach number, the total pressure loss increases, a high inlet compression is thus favorable to reduce the total pressure loss within the inlet. Figure 4.6 shows that the entropy increases with an increasing CR, thus also encouraging a high inlet compression just before heat addition. Figure 4.7 shows that the specific impulse decreases with an increasing CR. Thus, all three results indicate that a higher inlet compression before CP heat addition would result in a higher performance.

4.2.2 Quasi-One-Dimensional Constant-Volume Heat Addition

Now the specific volume is taken constant when heat is added in an quasi-one-dimensional flow. This changes the conservation equations, with the use of eq.(3.26), and the equation of state into:

$$u_2 A_2 = u_3 A_3 \tag{4.32}$$

$$u_2^2 A_2 = u_3^2 A_3 \tag{4.33}$$

$$c_v T_2 + \frac{1}{2}u_2^2 + q = c_v T_3 + \frac{1}{2}u_3^2 \tag{4.34}$$

$$\frac{p_3}{p_2} = \frac{T_3}{T_2} \tag{4.35}$$

It can be seen that the velocity is dependend on the cross-sectional ratio. Since it was stated that shock-induced combustion occurs at very high velocities and therefore the density can be assumed to remain constant, the assumption of a constant cross-sectional area ratio could be justified, but instead is left to be proven here. The pressure jump is equivalent to the temperature jump. And because the velocity remains constant or decreases, with increasing temperature, the Mach number therefore decreases, the same as with the CP heat addition process

$$M_3 = \frac{u_3}{\sqrt{\gamma R T_3}} = \frac{u_2 \frac{A_2}{A_3}}{\sqrt{\gamma R T_3}} \leq M_2 \tag{4.36}$$

The performance characteristics can now be determined. The total pressure loss for CV heat addition for three different CR's and increasing cross-sectional ratio is shown in figures 4.8 to 4.10, the increase in entropy in figures 4.11 to 4.13, and the specific impulse in figures 4.14 to 4.16.

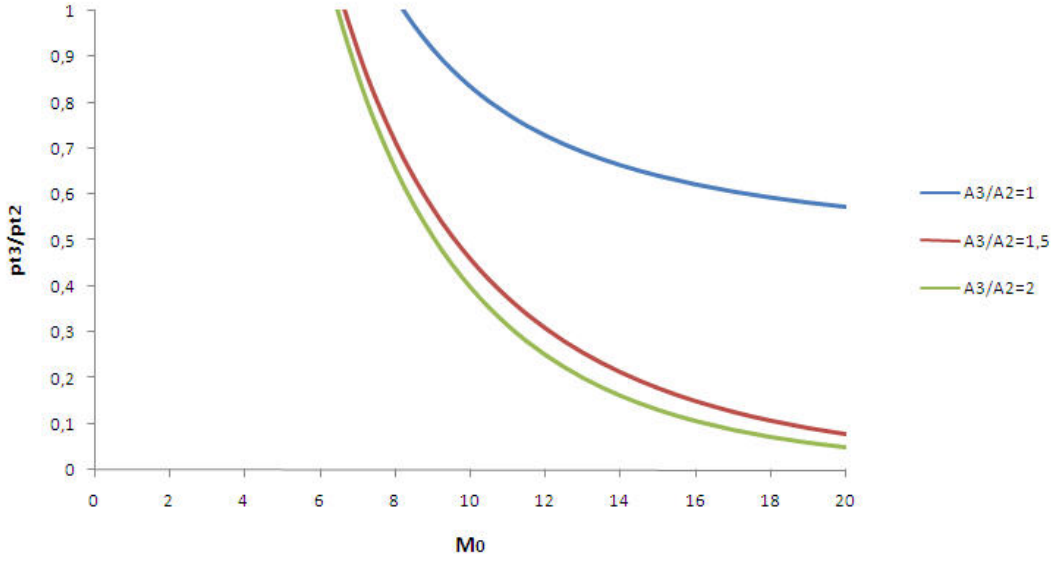

Figure 4.8: Total pressure loss for quasi-one-dimensional CV Combustion with CR=0.2

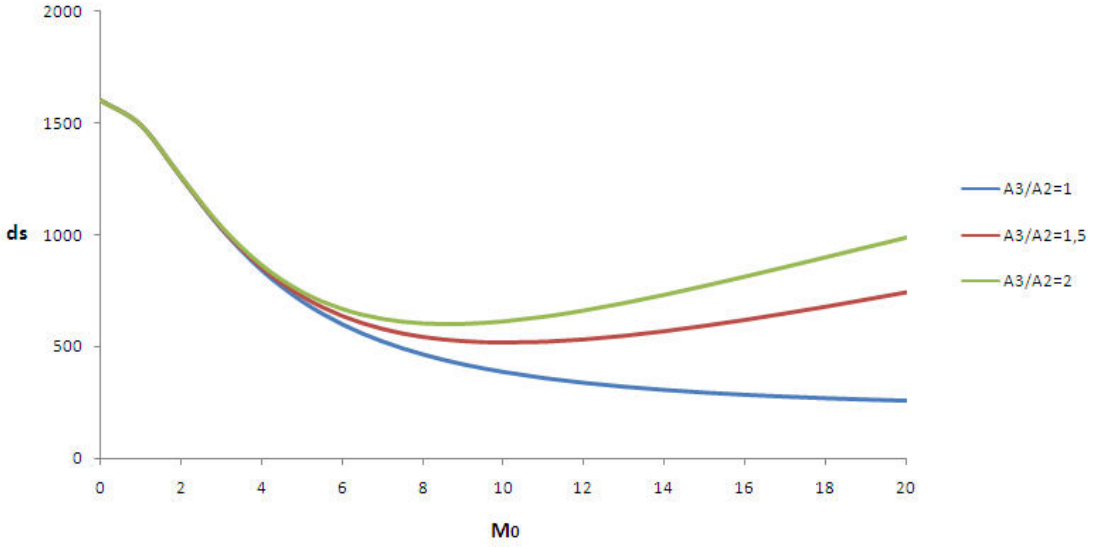

Figure 4.9: Entropy increase for quasi-one-dimensional CV Combustion with CR=0.2

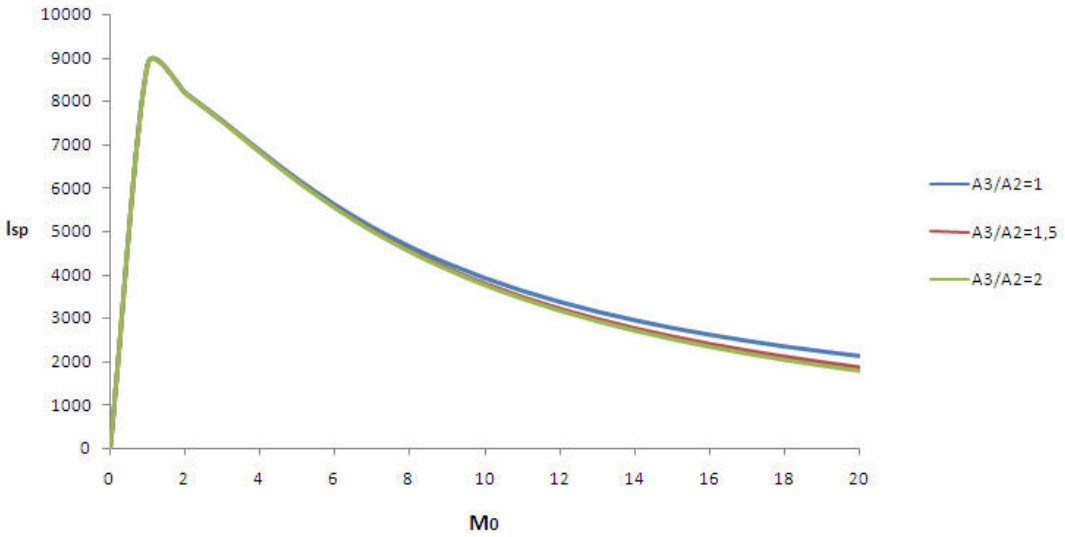

Figure 4.10: Specific impulse for quasi-one-dimensional CV Combustion with CR=0.2

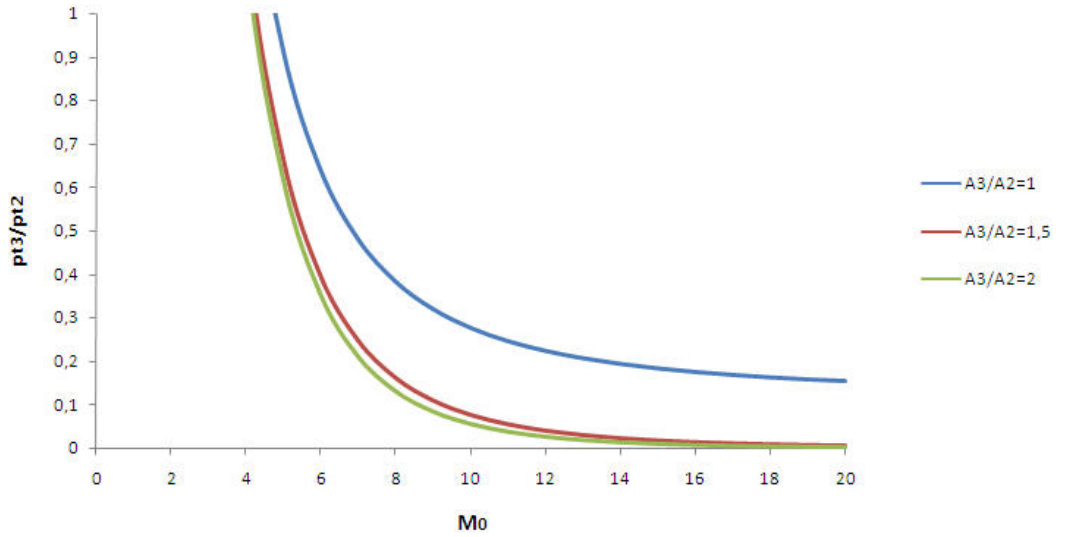

Figure 4.11: Total pressure loss for quasi-one-dimensional CV Combustion with CR=0.4

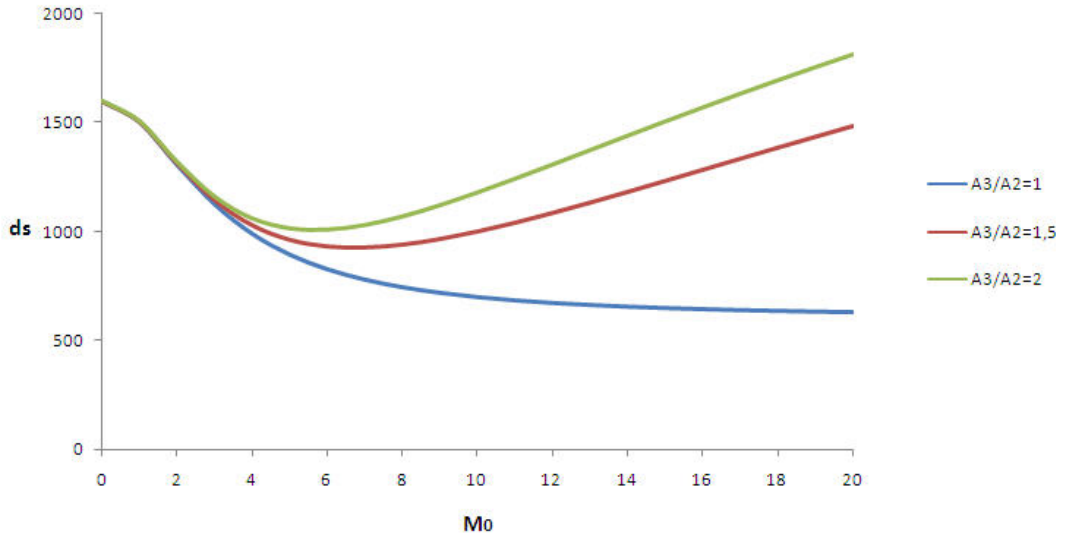

Figure 4.12: Entropy increase for quasi-one-dimensional CV Combustion with CR=0.4

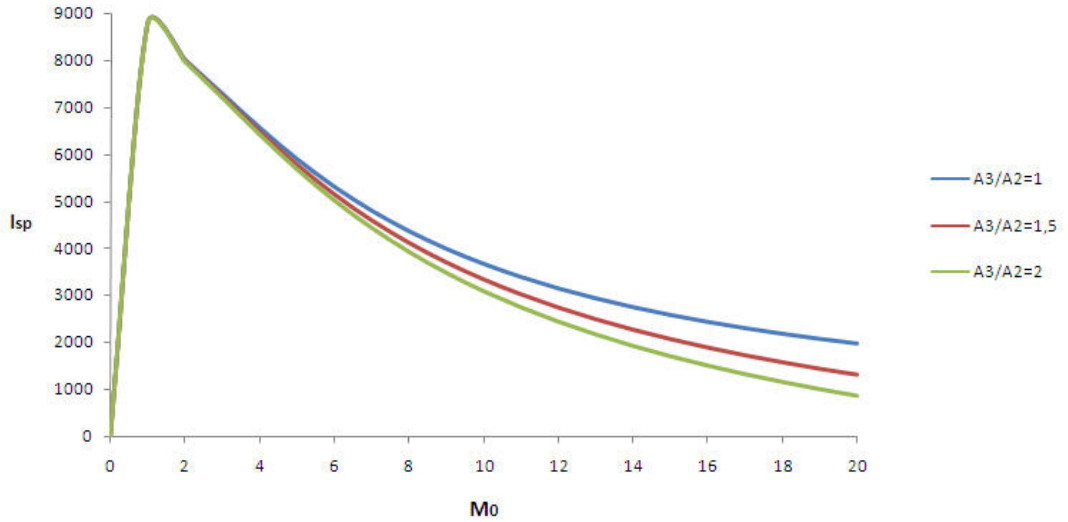

Figure 4.13: Specific impulse for quasi-one-dimensional CV Combustion with CR=0.4

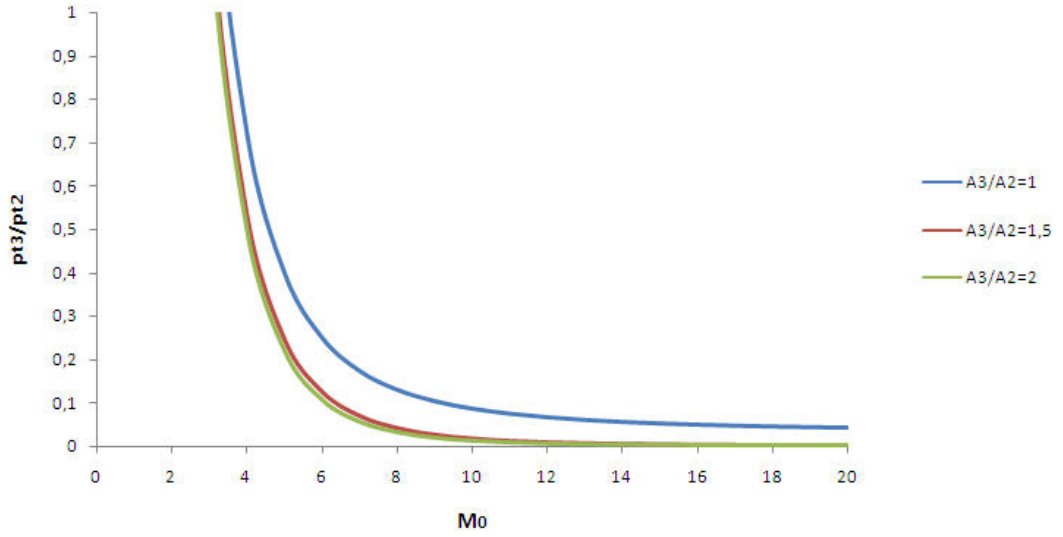

Figure 4.14: Total pressure loss for quasi-one-dimensional CV Combustion with CR=0.6

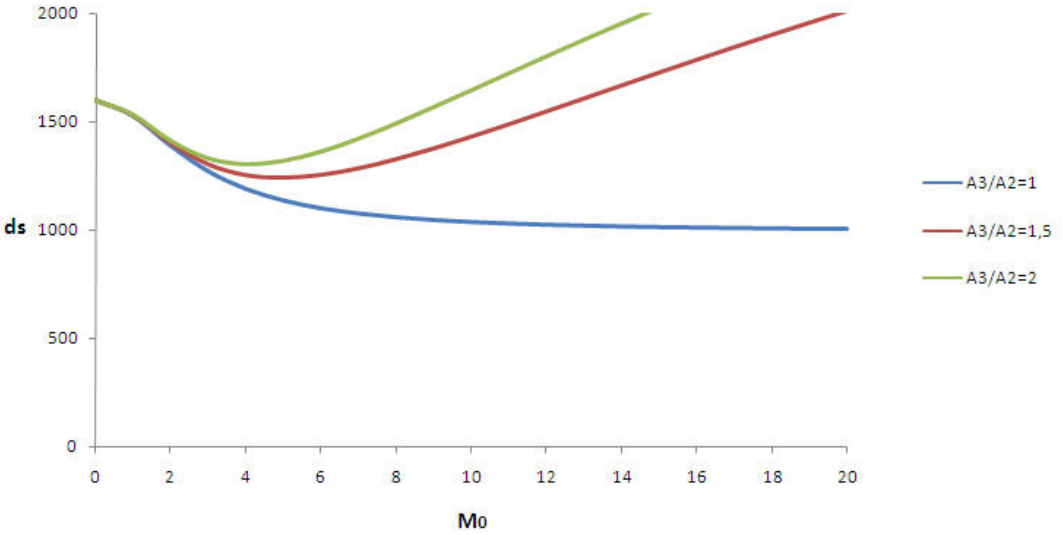

Figure 4.15: Entropy increase for quasi-one-dimensional CV Combustion with CR=0.6

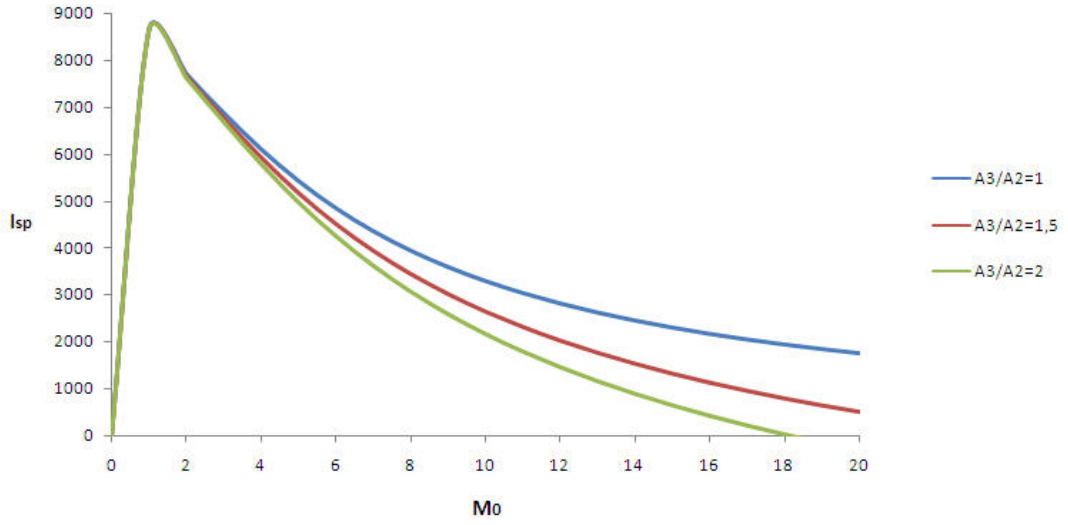

Figure 4.16: Specific impulse for quasi-one-dimensional CV Combustion with CR=0.6

The figures show that when the cross-sectional ratio increases the three performance characteristics all decrease. This result supports that the assumption of a constant cross-sectional area ratio is justified for optimal performance. The following three figures show only the performance characteristics with a constant cross-sectional area and increasing CR.

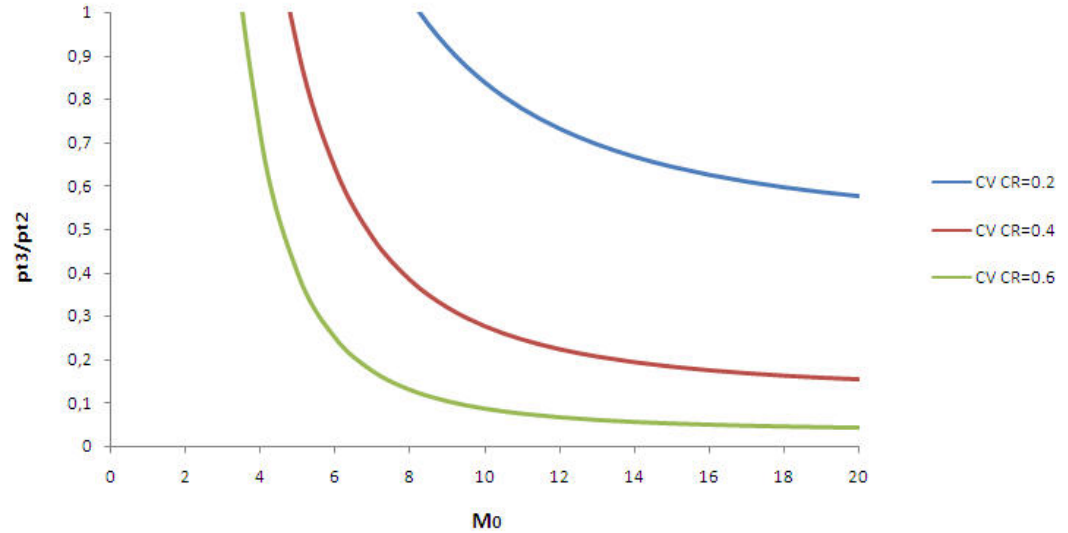

Figure 4.17: Total pressure loss for quasi-one-dimensional CV Combustion

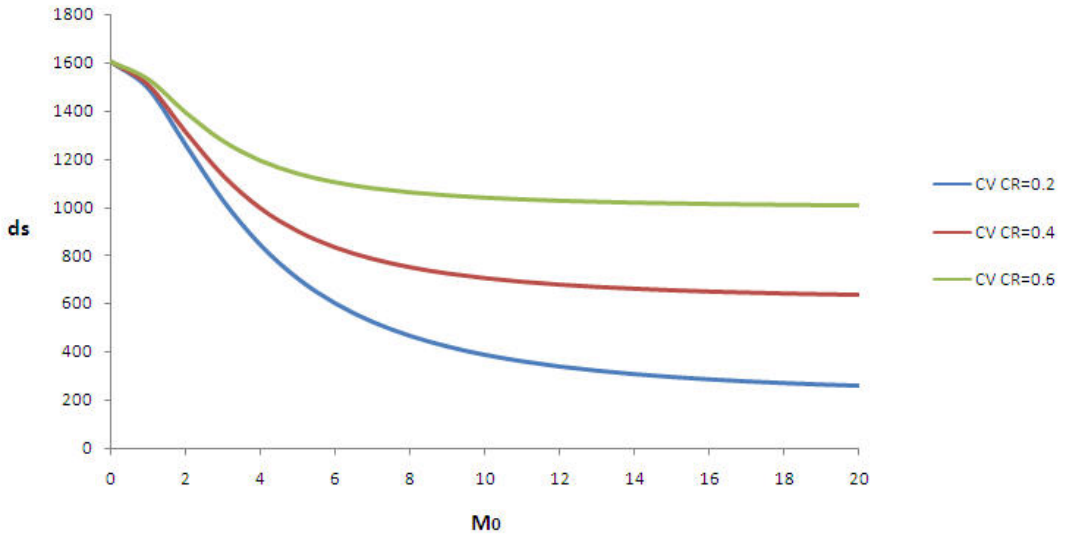

Figure 4.18: Entropy increase for quasi-one-dimensional CV Combustion

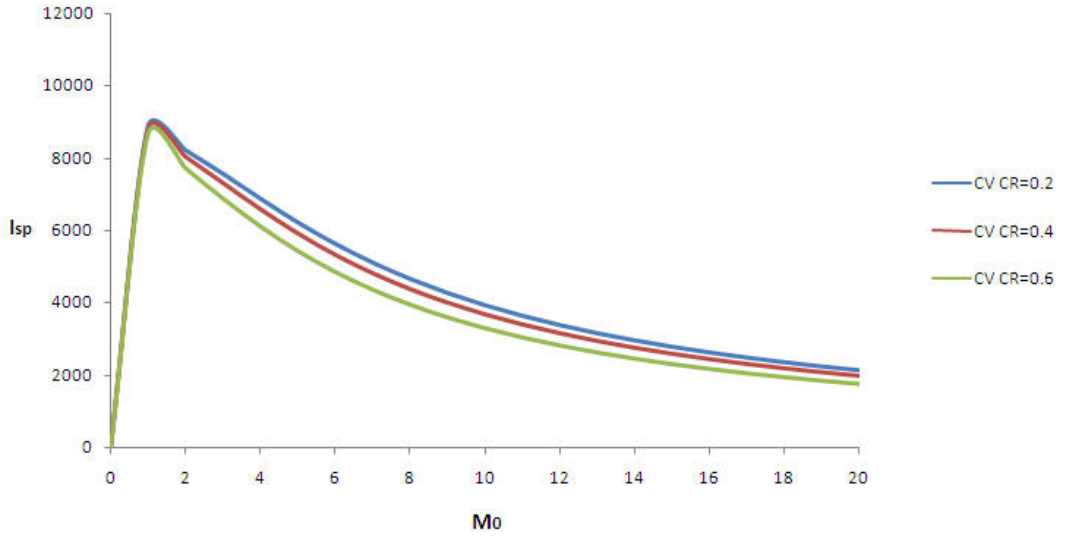

Figure 4.19: Specific impulse for quasi-one-dimensional CV Combustion

Figure 4.17 shows that when the CR increases the total pressure loss increases rapidly with increasing freestream Mach number. The entropy increases also rapidly with an increasing CR and freestream mach number, though reaches constant values at Mach number higher than 10. The specific impulse decreases with increasing freestream Mach number, but does not change much in value with increasing CR. It can thus be seen that the compression ratio has a small effect on the specific impulse. This can be partially explained by the velocity remaining constant and therefore the total temperature ratio also remaining constant with increasing CR.

Figures 4.17, 4.18, and 4.19 show that when CR increases, with increasing freestream Mach number, the performance characteristics decrease. These results also support, as with CP heat addition, that a high inlet compression before CV heat addition results in optimal performance. However, these results do not tell if CV heat addition is qualified to represent normal or oblique shock-induced combustion. One could interpret this method as the flow normal to the preceding shock wave inducing self-ignition of the flow mixture within the reaction zone. A numerical

4.2.3 Normal and Oblique Detonation Waves

In the previous section a model was derived for Chapman-Jouguet detonation waves to determine the thermal efficiency. Since the combustion zone of detonation waves is very thin, the limit of the combustion zone of shock-induced combustion waves, it is safe to assume that the area does not change ($A_2 = A_3$). Chapman-Jouguet detonation waves are considered as limits of detonation waves and are very difficult to analyse and compare with the previous two combustion processes in a similar analysis. They are dependent on the Mach number and initital temperature just before the wave, and must be a specific value. If one or both are not that precise value, the detonation wave will become a strong detonation wave or a deflagration wave with a subsonic normal Mach number ($M_{n_3} < 1$). Because of this, another model for detonation waves is considered, derived by Townend, also known as the Townend-model (Townend, 1970).

$$A_3 = A_2$$

The conservation equations for detonations are given as:

$$\rho_2 u_2 = \rho_3 u_3 \tag{4.37}$$

$$p_2 + \rho_2 u_2^2 = p_3 + \rho_3 u_3^2 \tag{4.38}$$

$$c_p T_2 + \frac{1}{2}(u_2^2 + v_2^2) + q = c_p T_3 + \frac{1}{2}(u_3^2 + v_3^2) \tag{4.39}$$

$$v_2 = v_3 \tag{4.40}$$

$$\frac{p}{\rho} = RT \tag{4.41}$$

And adding the equation to determine the velocity of sound:

$$a^2 = \frac{\gamma p}{\rho} = \gamma RT \tag{4.42}$$

and using

$$a = \frac{u}{M_n}$$

Using these equations, the following two equations can be found where the only the post-velocity u_3 is unknown:

$$\gamma M_{n_2}^2 \left(\frac{u_3}{u_2}\right)^2 - (1 + \gamma M_{n_2}^2)\left(\frac{u_3}{u_2}\right) + \left(\frac{a_3}{a_2}\right) = 0$$

and

$$\left(\frac{u_3}{u_2}\right)^2 = 1 + \frac{2}{(\gamma - 1)M_{n_2}^2}\left(1 + \frac{q}{c_p T_2} - 1\left(\frac{a_3}{a_2}\right)^2\right)$$

Eliminating the term $\left(\frac{a_3}{a_2}\right)$ gives a quadratic equation of $\left(1 + \frac{u_3}{u_2}\right)$. Solving this equation gives the jump relation for the normal velocity component of a detonation wave:

$$1 - \frac{u_3}{u_2} = \frac{M_{n_2}^2 - 1}{M_{n_2}^2(\gamma - 1)}\left(1 \pm \sqrt{1 - \frac{2(\gamma + 1)M_{n_2}^2}{(M_{n_2}^2 - 1)^2}\frac{q}{c_p T_2}}\right)$$

In this relation an important factor is found, namely q/c_pT_2 which is Damköhler's second parameter. This parameter quotes the heat released per unit mass of fluid in terms of the upstream specific enthalpy. And introducing the dimensionless combustion heat release paramater F:

$$F = 1 + \sqrt{1 - \frac{2(\gamma+1)M_{n_2}^2}{(M_{n_2}^2)^2}\frac{q}{c_pT_2}} \tag{4.43}$$

For shock waves, when $q = 0$, $F = 2$ and for Chapman-Jouguet detonation waves $M_{n_3} = 1$ and thus $F = 1$. Every value between $1 < F < 2$ is considered to represent strong detonation waves (Townend, 1970). This parameter can be used for both normal and oblique shock waves. The minus sign represents weak detonations, and as discussed in chapter three, are therefore not considered as physical plausible.

Now the jump relations across detonation waves can be found. Using the mass equation, the velocity and density jump are given as:

$$\frac{u_3}{u_2} = \left(\frac{\rho_3}{\rho_2}\right)^2 = 1 - F\frac{M_{n_2}^2 - 1}{(\gamma+1)M_{n_2}^2} \tag{4.44}$$

The pressure jump using the momentum equation:

$$\frac{p_3}{p_2} = 1 + \frac{p_3 - p_2}{p_2} = 1 + \frac{\rho_2 u_2(u_2 - u_3)}{p_2} = 1 + \gamma M_{n_2}^2\left(1 - \frac{u_3}{u_2}\right)$$

$$\frac{p_3}{p_2} = 1 + \gamma F\frac{M_{n_2}^2 - 1}{\gamma+1} \tag{4.45}$$

The temperature jump can be found using the assumption that the molecular weight of the mixture is constant across the detonation wave:

$$\frac{T_3}{T_2} = \frac{p_3}{p_2}\frac{\rho_2}{\rho_3} = \left(1 + \gamma F\frac{M_{n_2}^2 - 1}{\gamma+1}\right)\left(1 - F\frac{M_{n_2}^2 - 1}{(\gamma+1)M_{n_2}^2}\right) \tag{4.46}$$

The jump in (normal) Mach number can be found using $M_n = u/a$:

$$\frac{M_{n_3}}{M_{n_2}} = \frac{u_3}{u_2}\frac{a_2}{a_3} = \sqrt{\frac{p_2}{p_3}\frac{\rho_2}{\rho_3}} = \sqrt{\left(1 - F\frac{M_{n_2}^2 - 1}{(\gamma+1)M_{n_2}^2}\right) / \left(1 + \gamma F\frac{M_{n_2}^2 - 1}{\gamma+1}\right)} \tag{4.47}$$

The Chapman-Jouguet theory states that the normal Mach number behind a Chapman-Jouguet wave is 1, thus with $F = 1$ the previous found equation should conclude that $M_{n_3} = 1$. Filing in $F = 1$ gives:

$$M_{n_3} = M_{n_2}\sqrt{\frac{p_2}{p_3}\frac{\rho_2}{\rho_3}} = M_{n_2}\sqrt{\left(1 - \frac{M_{n_2}^2 - 1}{(\gamma+1)M_{n_2}^2}\right) / \left(1 + \gamma\frac{M_{n_2}^2 - 1}{\gamma+1}\right)} = \sqrt{\frac{1}{M_{n_2}^2}} = \frac{M_{n_2}}{M_{n_2}} = 1$$

Which is correct.

Normal Detonation Waves

For normal detonation waves the performance characteristics are shown in figures 4.20, 4.21, and 4.22 with different compression ratios.

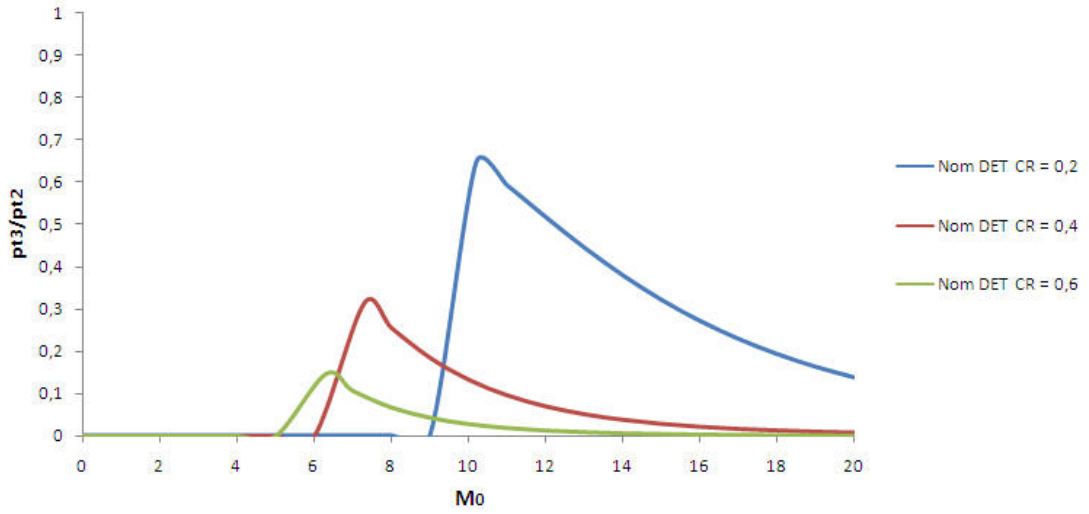

Figure 4.20: Total pressure loss for normal detonation waves

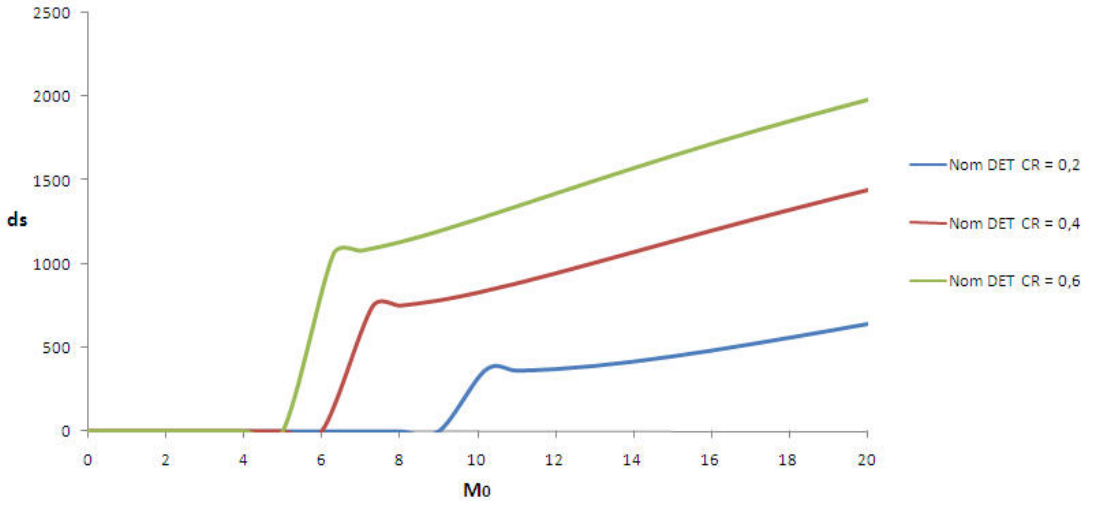

Figure 4.21: Entropy increase for normal detonation waves

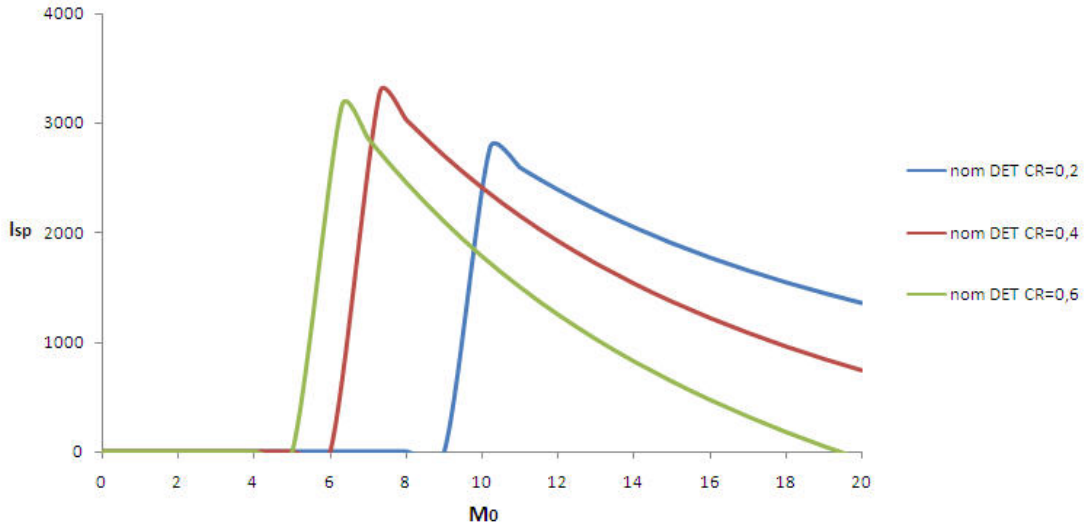

Figure 4.22: Specific impulse for normal detonation waves

The figures show that the performance of normal detonation waves with increasing freestream Mach number decreases strongly when the CR increases. The entropy increases is lowest at the CJ-point, as expected, but for strong detonations it increases with increasing freestream Mach number and increasing CR increases rapidly. This can be explained due to increasing static temperature and pressure ratio for detonation waves and the decreasing ratios for CV and CP heat addition with increasing freestream Mach number. Because of this the first two processes encounter a decreasing increase of entropy, while for detonation waves, throug a one- or quasi-one-dimensional analysis an increasing entropy increase is encountered. The specific impulse actually increases and has the peak faster when the CR increases. The peak is associated with a CJ detonation wave and occurs at the lowest detonation Mach number, when $F \approx 1$. This is faster reached when M_n remains high after inlet compression, according to eq.(4.43). Still, looking at the total pressure loss and the entropy increase, a high inlet compression results in a higher performance. The specific impulse will then be reached at higher freestream Mach numbers. Though detonation waves occur at very high freestream Mach numbers, the post-combustion Mach number for normal detonation waves is lower than one, since the maximum normal detonation wave has a post Mach number of one, and decreases when the detonation wave takes on the form of strong detonation waves ($1 < F < 2$). And thus the velocity behind normal detonation waves is subsonic. Oblique detonation waves should therefore have supersonic velocities behind the combustion front. For normal detonation waves it can be concluded that the highest performance occurs at CJ conditions.

Oblique Detonation Waves

Oblique detonation waves differ from normal detonation waves by being two-dimensional. Now the velocity V can be divided into two components, one normal to the wave u and one tangential to the wave v. For the following calculations the tangential pre and post velocity component are equal, the same as for shock waves. From shock wave theory it is known that for an oblique shock wave generated over a wedge, that the shock angle δ is dependend on the Mach number and the turning or wedge angle θ.

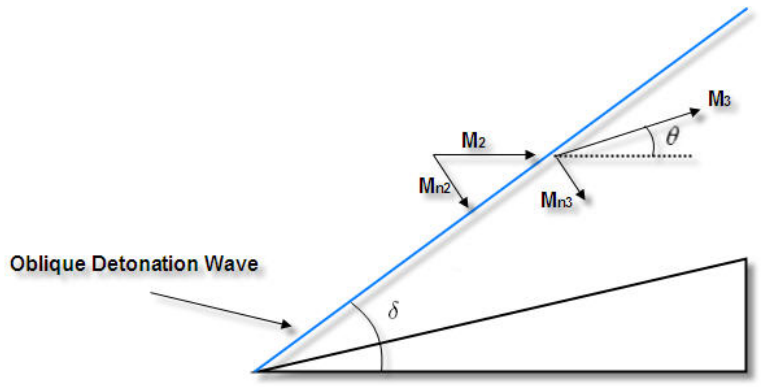

Figure 4.23: Schematic for an oblique detonation wave

It is very laboursome to derive the shock angle since it can be found using a third order polynomial. And without giving the full derivation of this polynomial, the shock angle for a weak shock wave, since these are more practical to occur, is found with (Subbarao)

$$tan\delta = \frac{(M_2^2 - 1) + 2\lambda cos\left(\frac{4\pi\beta + cos^{-1}(\xi)}{3}\right)}{3\left(1 + \frac{\gamma-1}{2}M_2^2\right)tan\theta} \tag{4.48}$$

with

$$\xi = \frac{(M_2^2 - 1)^3 - 9\left(1 + \frac{\gamma-1}{2}M_2^2\right)\left(1 + \frac{\gamma-1}{2}M_2^2 + \frac{\gamma+1}{2}M_2^4\right)tan^2(\theta)}{\lambda^3}$$

$$\lambda = \sqrt{(M_2^2 - 1)^2 - 3\left(1 + \frac{\gamma-1}{2}M_2^2\right)\left(1 + \frac{\gamma+1}{2}M_2^2\right)tan^2(\theta)}$$

For weak shock waves $\beta = 1$ and for strong shock waves $\beta = 0$. With the shock angle the normal Mach number M_{n_2} can be found and then the flow properties behind the oblique detonation wave. The results for the performance characteristics for oblique detonation waves with different CR's and different wedge angles θ and with increasing freestream Mach number are shown in figures 4.24, 4.25, and 4.26.

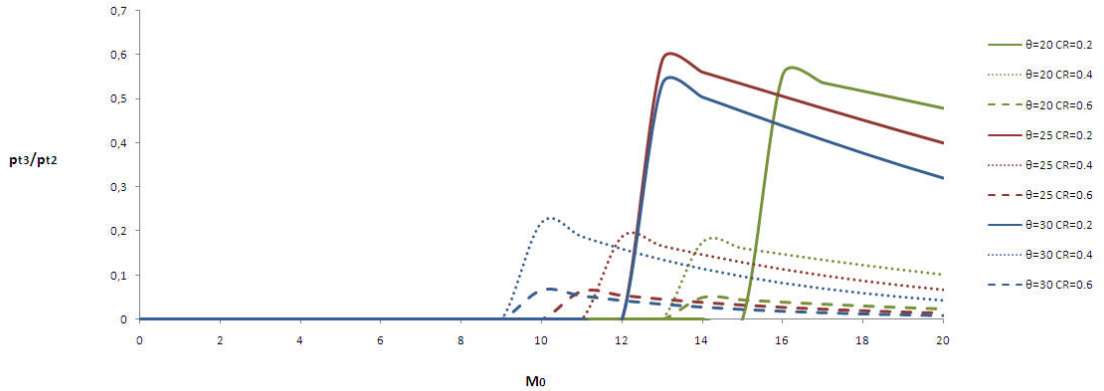

Figure 4.24: Total pressure loss for oblique detonation waves

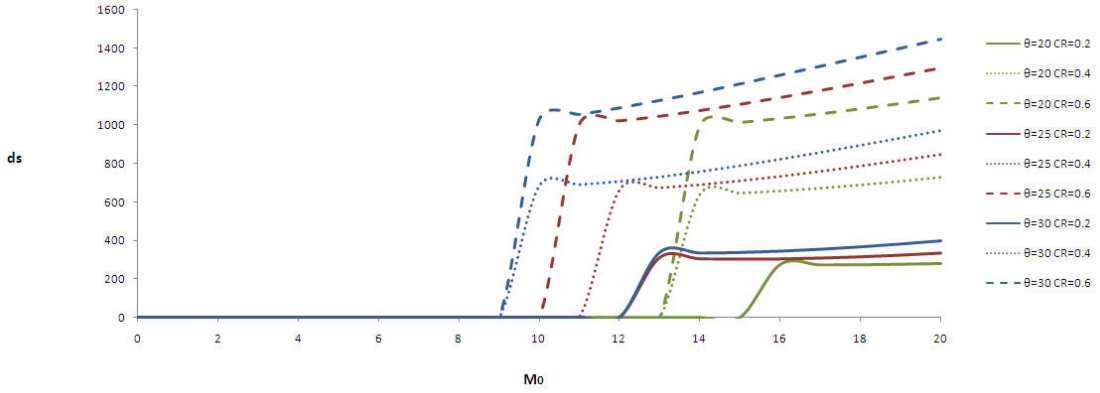

Figure 4.25: Entropy increase for oblique detonation waves

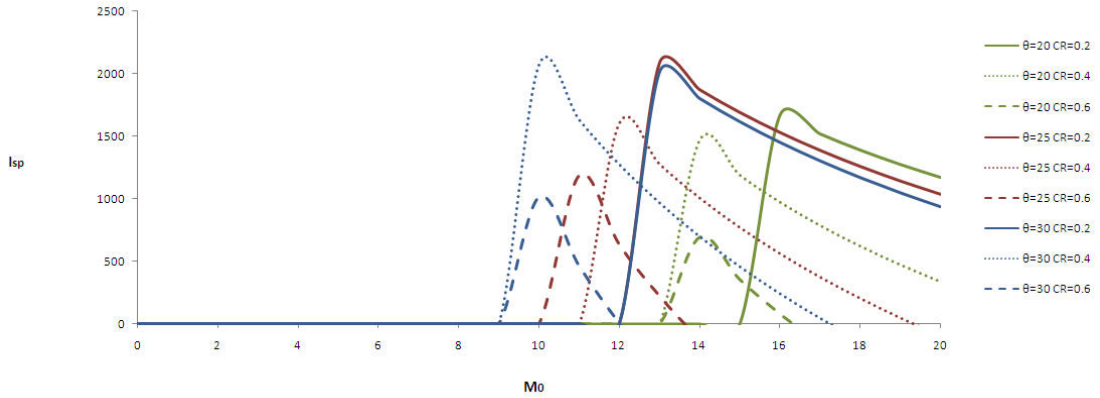

Figure 4.26: Specific impulse for oblique detonation waves

The figures show that when the CR increases the performance decreases rapidly. When the wedge angle increases it can be seen that the performance peak is reached faster than with lower wedge angles, but it can be seen that the height of the performance first increases than decreases. This shows that the performance of oblique detonation waves is dependend on the wedge angle and thus indicates that there is a wedge angle where a maximum performance occurs. As with normal detonation waves, the peaks are associated with CJ detonation waves and show the highest performance.

Figures 4.27, 4.28, and 4.29 show both the results for normal and oblique detonation waves.

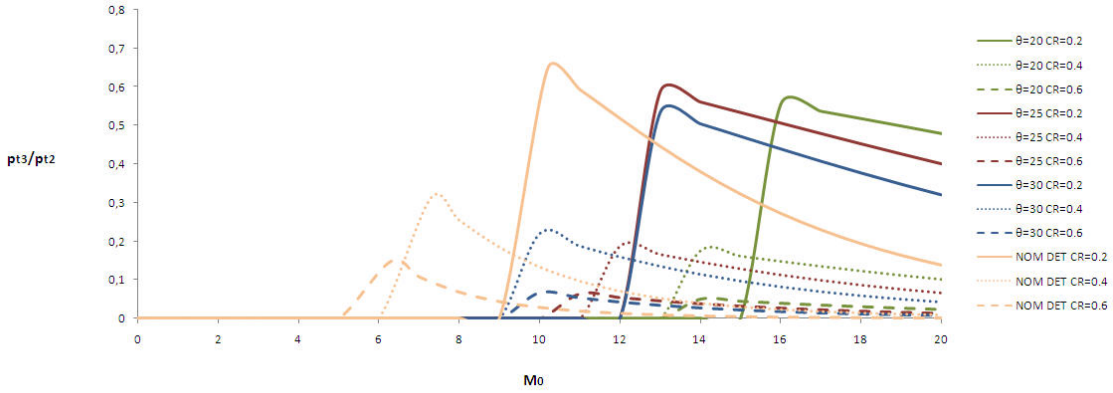

Figure 4.27: Total pressure loss for detonation waves

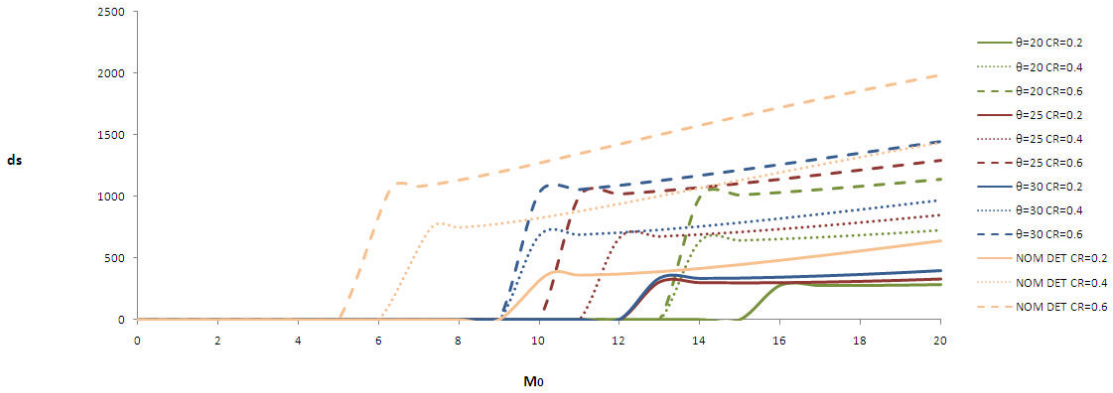

Figure 4.28: Entropy increase for detonation waves

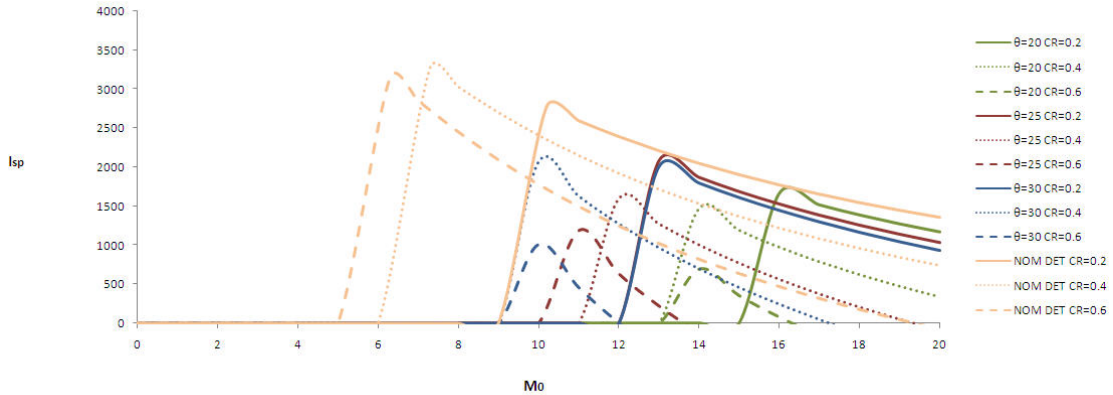

Figure 4.29: Specific impulse for detonation waves

The combined results for detonation waves show that the overall performance of oblique detonation waves is higher than for normal detonation waves in a higher flight regime. The peak of the performance for normal detonation waves occurs sooner than for oblique detonation waves, and has better results in specific impulse, but less in entropy increase and total pressure loss. This suggests that normal detonation waves could perform less than oblique detonation waves. Also, normal detonation waves are the result of normal shock waves igniting a air-fuel mixture, resulting in subsonic post-flows and even higher pressure and temperature jumps than oblique shock waves, depending on their wedge angle. When the wedge angle increases for oblique detonation waves, so does also the temperature and pressure jump. Eventually the temperature jump will be larger for oblique detonation waves, but the pressure jump remains lower compared to the pressure jump of normal detonation waves, following normal shock wave theory (see also figures 4.32 and 4.33).

4.2.4 Performance Analysis Results

Combining the one- or -quasi-one-dimensional results from the previous sections gives a clear view of the differences in performance of the three models. Starting with the total pressure loss in figure 4.30, it can be seen that CV heat addition has the lowest increase in total pressure loss, followed by CP heat addition, and then the detonation waves. The reason of the difference between CV and CP heat addition is that the total pressure loss for CP heat addition is only dependent on the Mach number. And since $M_3 < M_2$ the total pressure ratio starts to drop immediately. The total pressure loss for CV heat addition is dependent on both the static pressure jump and Mach number, and is therefore shifted and lower in increase. The shift is dependent on M_3 becoming supersonic, a subsonic M_3 shows a total pressure ratio > 1 and a supersonic M_3 shows a total pressure ratio < 1. The decrease in ratio is dependent on both the static pressure ratio and the jump in Mach number. The total pressure loss for detonation waves is dependent also on F and starts increasing when $F > 1$. Depending on CR and the CJ condition, the total pressure ratio starts when these conditions are reached first, the decrease in ratio is then dependent on the pressure jump, the jump in Mach number, and F. The decrease in ratio is stronger for normal detonation waves than for oblique detonation waves. But both have a higher total pressure loss compared to CV heat addition. Compared to CP heat addition, for a short range involving the CJ conditions, the total pressure loss is less than for CP heat addition. With higher freestream Mach numbers, the ratio decreases further below that of CP heat addition.

Figure 4.31 shows all the results for the entropy increase. The lowest increase of entropy is with CV heat addition, followed by CP heat addition and then detonation waves. It also clearly shows that the entropy increase with CV and CP heat addition decreases with increasing freestream Mach number, differing from the detonation wave entropy increase, which in fact increases with increasing freestream Mach number. This difference can be partially explained due to the fact that the model for detonation waves takes shock waves into account, which increases the entropy. Looking at the increase through the equation of entropy increase and the steep jumps in temperature and pressure for detonations, seen in figures 4.32 and 4.33, it can easily be seen why the increase occurs this way. It can be stated then that mathematically spoken, strong detonation waves are not an attractive combustion method, compared to CJ detonation waves, CV heat addition and CP heat addition in terms of entropy increase.

Figure 4.34 shows the specific impulse for the three combustion processes. It can be clearly seen that CV heat addition has the highest performance, followed by CP heat addition, and then detonation waves. It can also be seen that detonation waves with CJ-conditions have the highest performance and coincide roughly with CP heat addition. For all three processes the specific impulse is dependent on CR and decreases when CR increases. Indicating an optimal specific impulse performance when a high compression occurs within the inlet.

When combining figures 4.34 with the jump in static temperature and Mach number after heat addition (T_3, M_3) and implementing certain design and load constraints in figure 4.35, the maximum range can be shown for the three combustion processes. Since it was stated that only complete supersonic flow is investigated, normal detonation waves are disregarded. So the first design constraint is a minimal supersonic condition for M_3. Another design constraint is a maximum M_3 for CP heat addition, since both mixing and combustion have to occur within the combustion chamber for this kind of combustion process, too high Mach numbers will result in undesirable longer combustion chamber lengths. The maximum Mach number for CP heat addition is taken as $M_3 = 3$ corresponding with a velocity of approximately 1000m/s. With these two constraints a maximum range can be found for CP heat addition, and ranging from $2.5 < M_0 < 17$. When using the constraint of a maximum combustion chamber temperature T_3, which is taken as 4000K, the maximum range for CP heat addition decreases when the inlet compression increases. The maximum range for CV heat addition has only the first Mach number constraint, that of being supersonic, since mixing occurs outside of the combustion chamber and has a longer length. If a second velocity constraint is placed, it will shorten the maximum range. Otherwise the range is from $3 < M_0 < +20$ for CV heat addition. Looking at the maximum combustion chamber temperature constraint, the range would decrease only if the inlet compression ratio increases. Only oblique detonation waves have supersonic velocities after combustion and have a maximum range from $9 < M_0 < 15.5$, because of the maximum combustion chamber temperature. This range can only be extended by means of lowering the combustion chamber temperature (wall cooling for instance). The range will only shorten when the inlet compression ratio is increased.

Looking at all the performance characteristics and taking into account the maximum operating range, CV heat addition corresponding with shock-induced combustion shows the best overall performance. Section 4.1 performed an analysis on the thermodynamic efficiency and showed that Chapman-Jouguet detonation waves offered a higher efficiency than both CV and CP heat addition, and thus indicating an also possible better performance in the form of a lower increase in entropy. This gave reason to believe that detonation wave engines would be very sufficient (hypersonic) propulsion engines. But investigating an one-dimensional and quasi-one-dimensional flow analysis with heat addition, the results showed a lesser performance for DET processes compared to CP and CV heat addition processes. Now the question arises why.

One way of explaining this contradiction is looking more specific at the entropy generation and irreverisble processes within the combustion chamber. Thermodynamics shows that the work obtained by combustion is maximized when the irreversibility is minimized. Irreversible generated entropy reduces the efficiency and thus the performance in specific impulse.The entropy rise during combustion has minimum component due to the energy release and the chemical reactions s_{min} and an additional irreversible component due to finite velocity, and for detonation waves the leading shock wave s_{irr}

$$ds = \Delta s_{min} + \Delta s_{irr}$$

Rewriting the equation for the entropy increase in terms of stagnation or total states

$$ds = c_p ln\left(\frac{T_{t_3}}{T_{t_2}}\right) - Rln\left(\frac{p_{t_3}}{p_{t_2}}\right) \tag{4.49}$$

The minimum entropy rise is then associated with the total temperature decrease

$$\Delta s_{min} = c_p ln\left(\frac{T_{t_3}}{T_{t_2}}\right) \tag{4.50}$$

and the irreversible component by the total pressure loss

$$\Delta s_{irr} = -Rln\left(\frac{p_{t_3}}{p_{t_2}}\right) \tag{4.51}$$

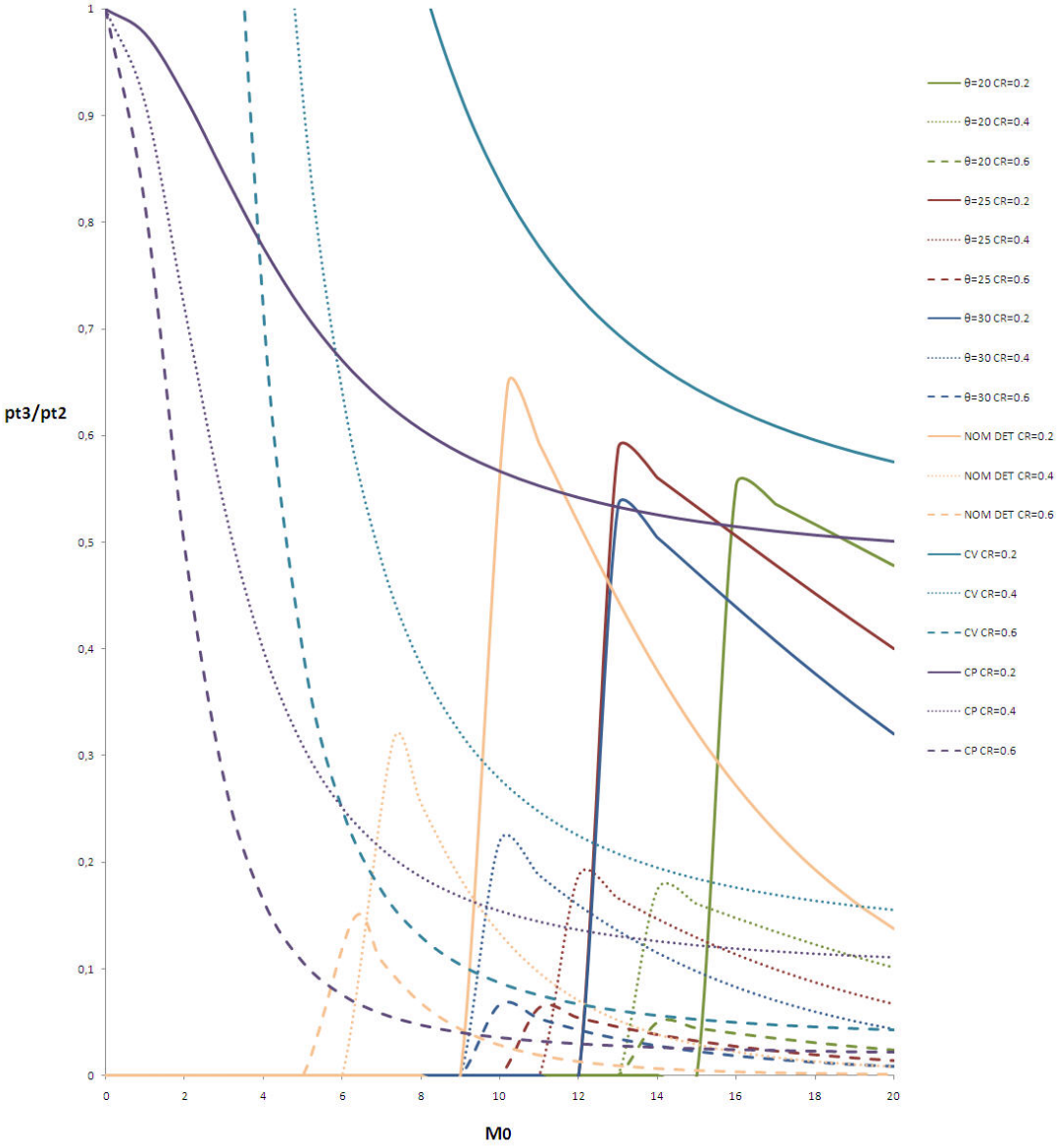

Figure 4.30: Comparison of total pressure loss

Figure 4.36 shows the generation of irreversible entropy for the three combustion processes. It shows that for detonations the irreversible entropy increase from the CJ-point increases higher than CV or CP heat addition. This corresponds with the total pressure loss of each combustion process.

Concluding, using a one- or quesi-one-dimensional analysis to indicate the performance, not the absolute performance (since no losses were taken into account), shows that CV heat addition has the best overall performance. Figure 4.37 shows the performance difference in % between CV and CP heat addition. The detonation wave as being considered an upper limit of CV heat addition remains, as far as the previous analysis shows, a theoretical upper limit, and is thus not shown in

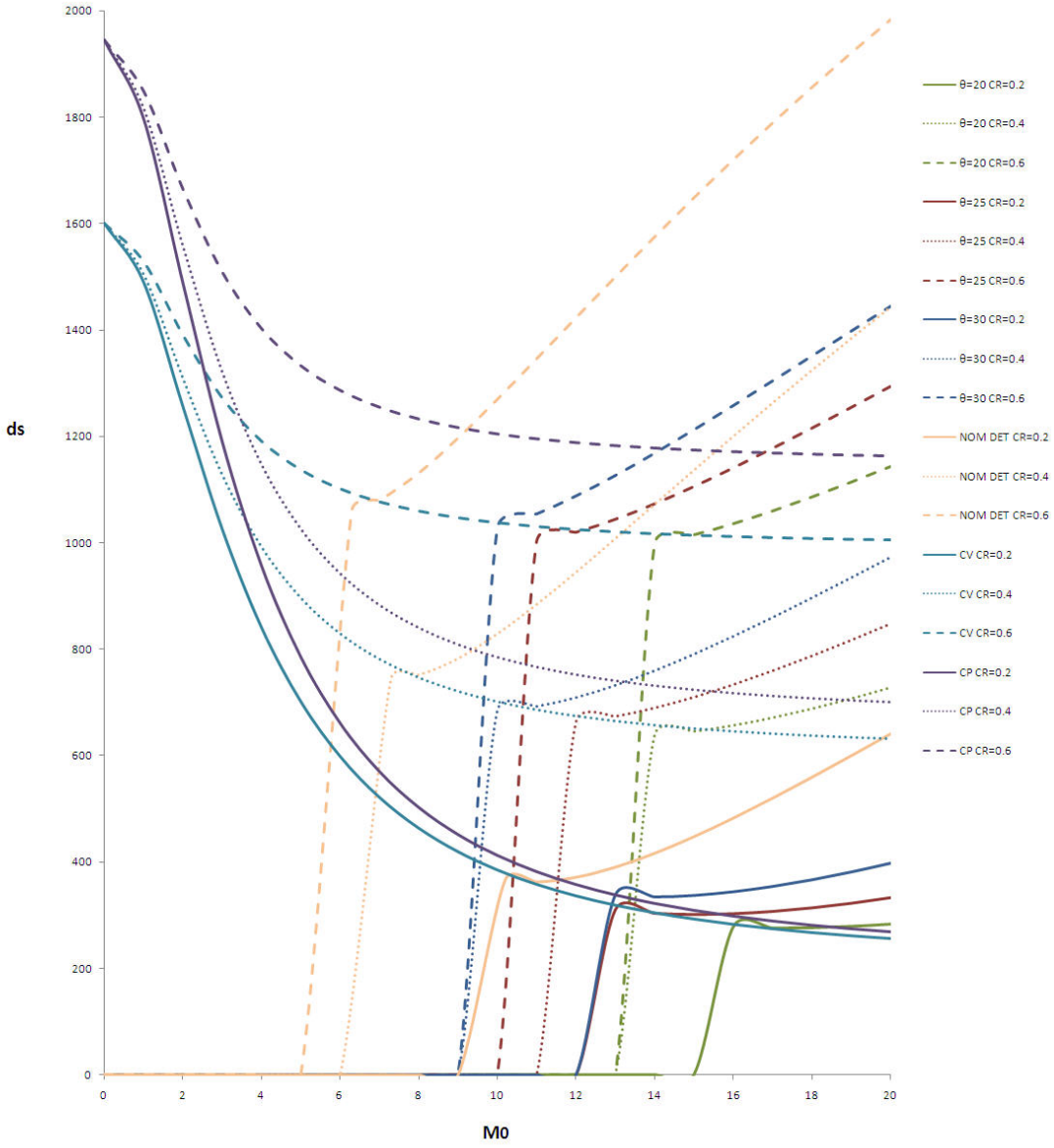

Figure 4.31: Comparison of entropy increase

figure 4.37. It can be seen that with increasing CR the absolute difference decreases, as expected (the difference in entropy increase thus has a minus sign, since CV heat addition has a lower increase in entropy than CP heat addition). Overall the absolute difference is significant with an difference of 40-75% in specific impulse, 5-15% in entropy increase, and an average of 55% in total pressure loss.

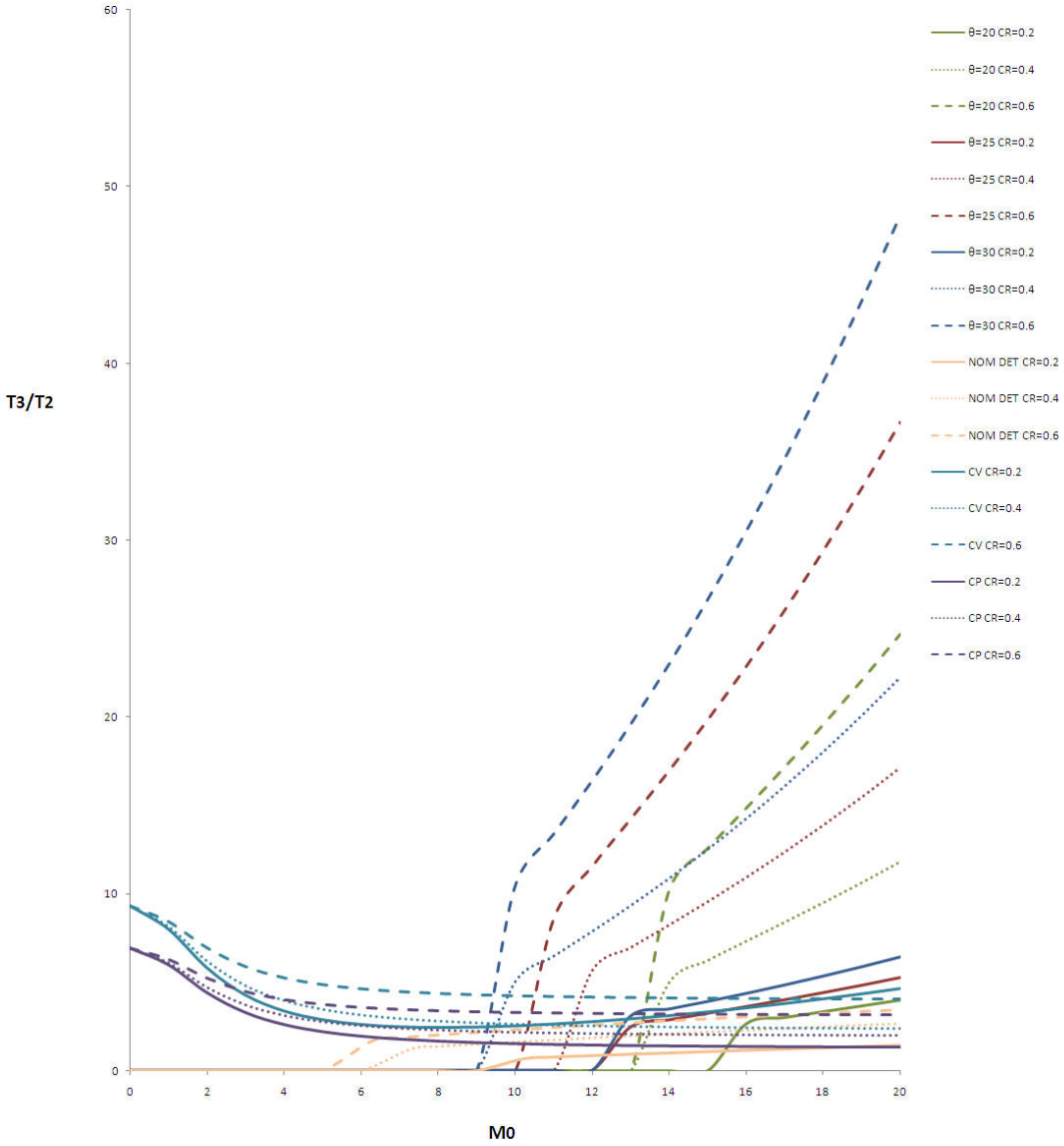

Figure 4.32: Jump in static temperature

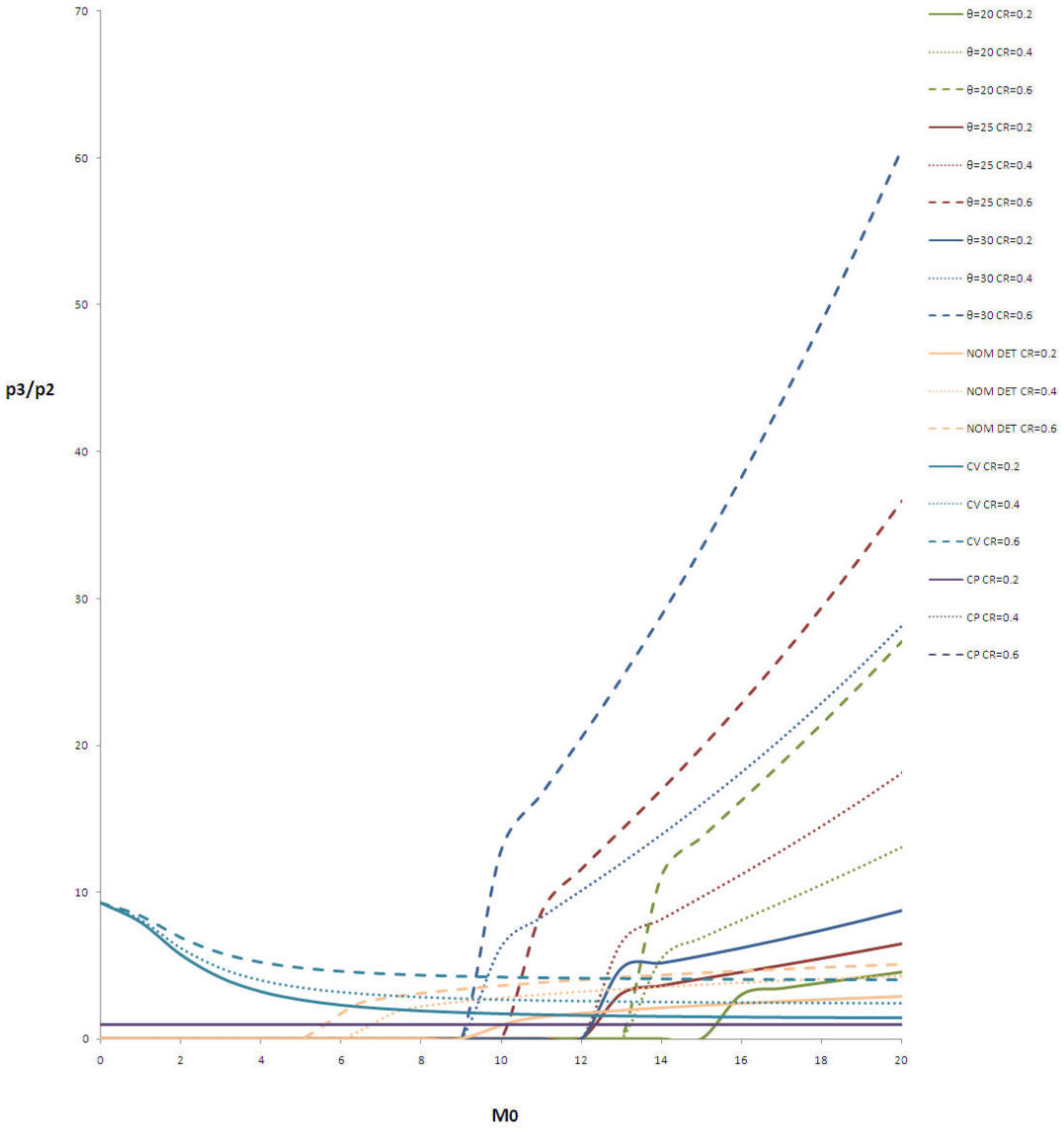

Figure 4.33: Jump in static pressure

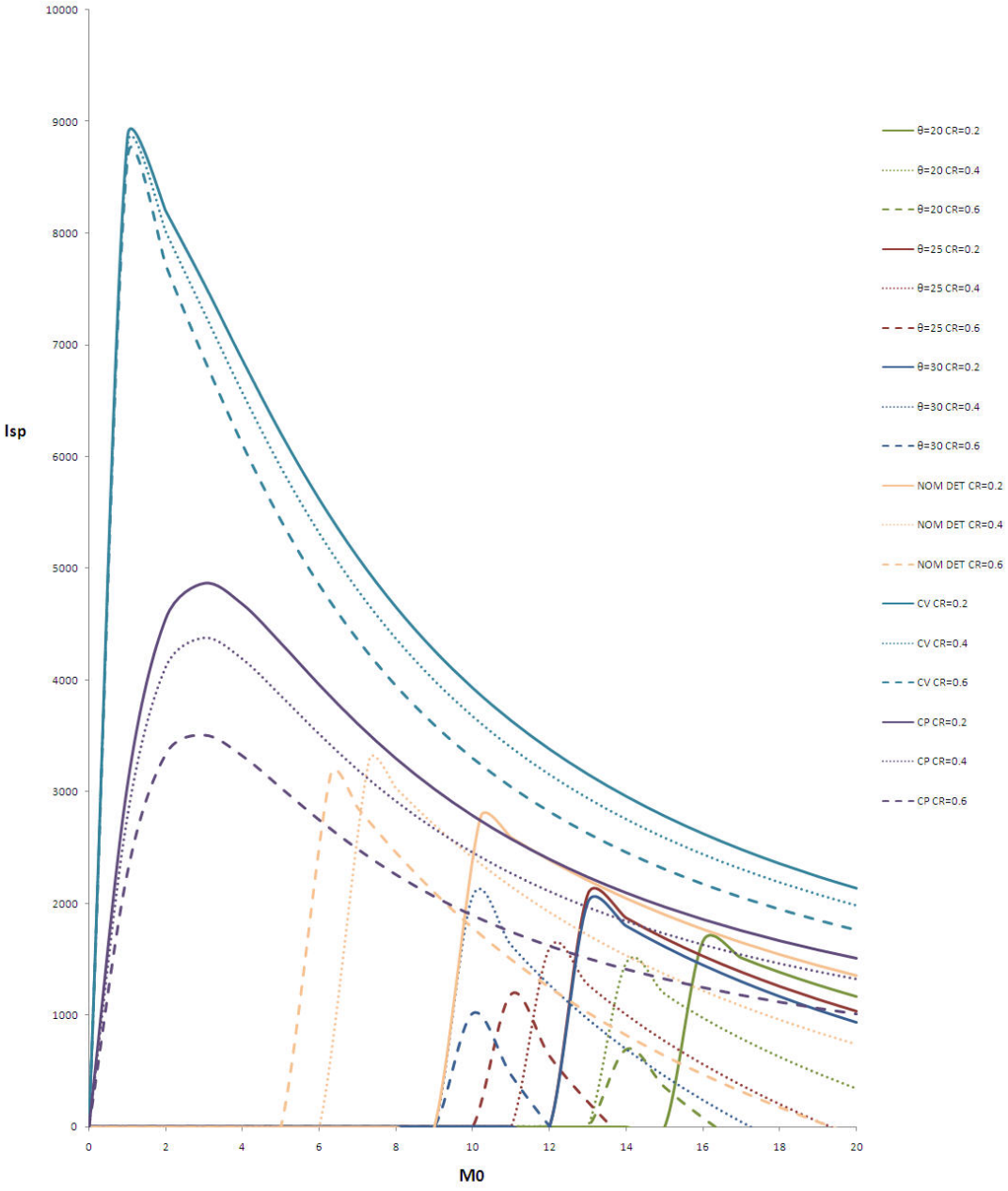

Figure 4.34: Comparison of specific impulse

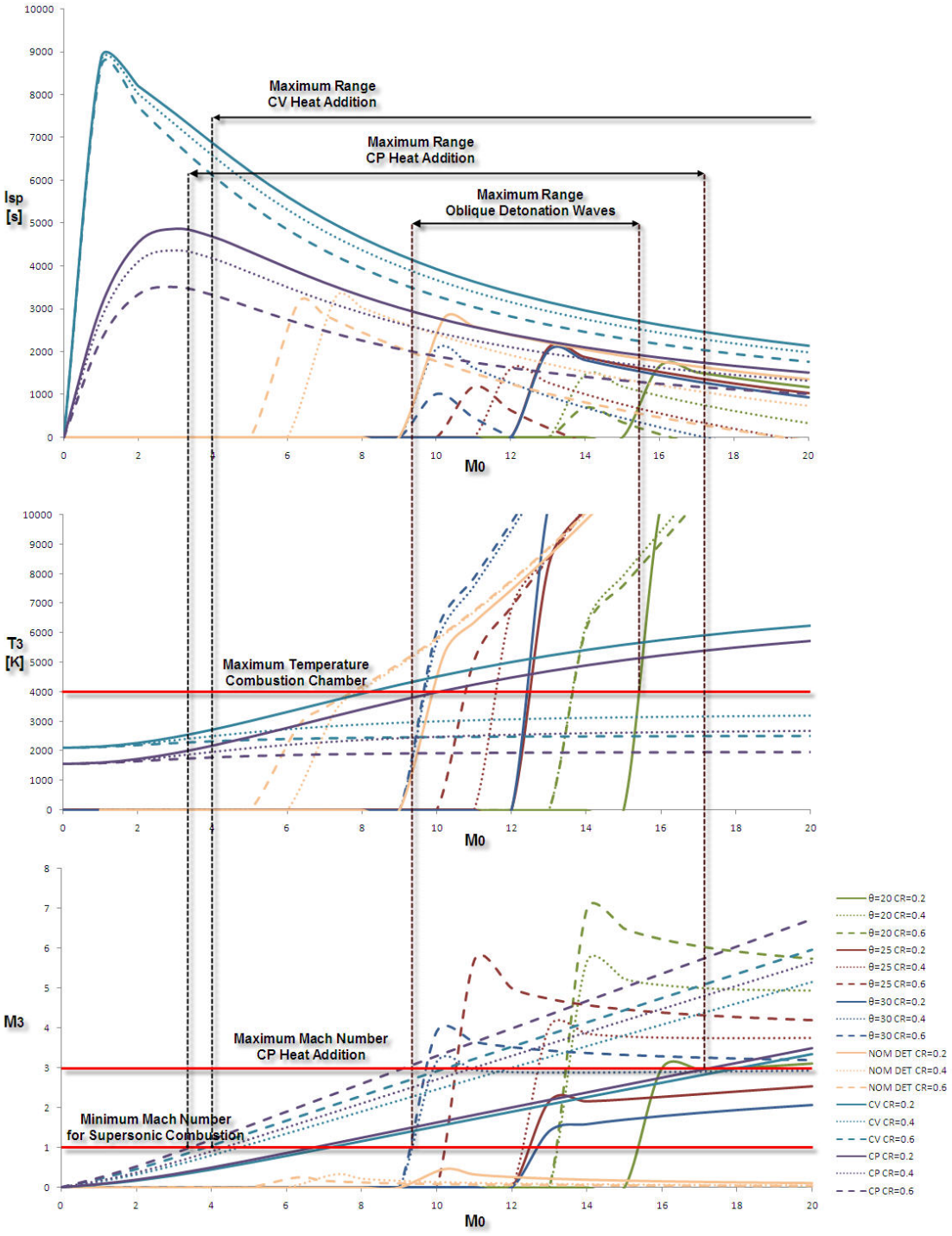

Figure 4.35: Comparison of performance range

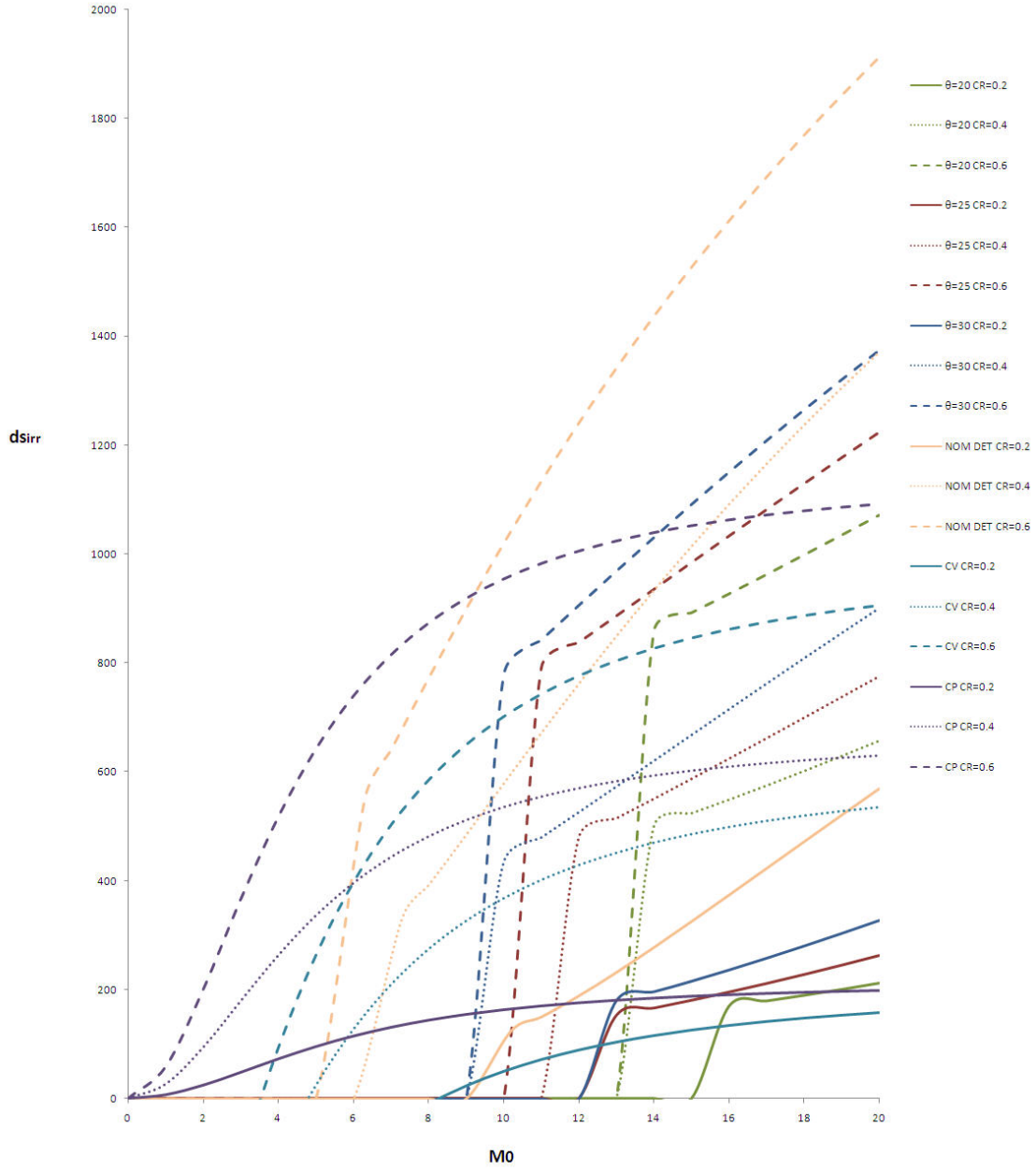

Figure 4.36: Comparison of irreversible entropy increase

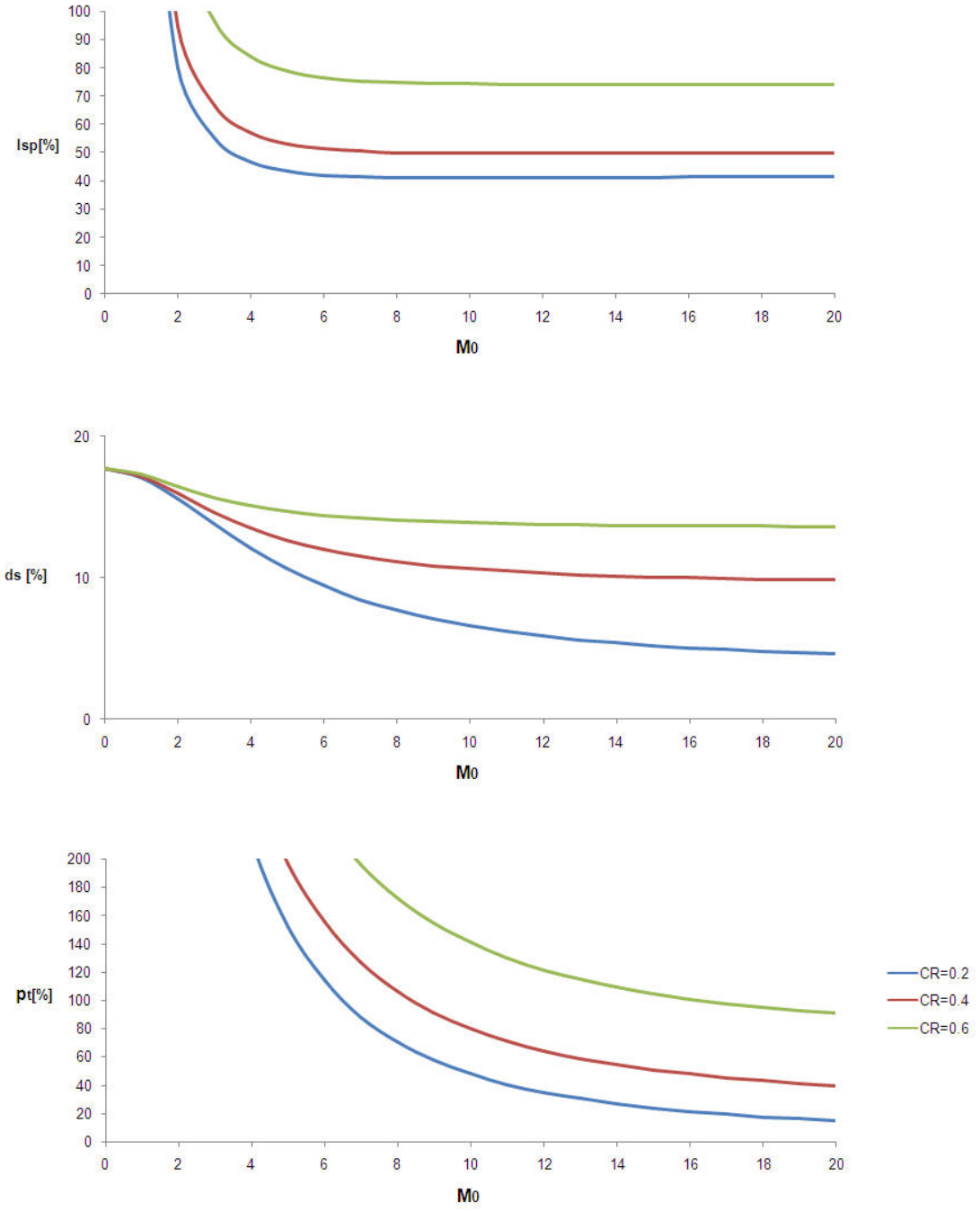

Figure 4.37: Difference in performance characteristics in percentage between CV and CP heat addition

4.3 Proof-of-Concept Test Setup Pre-Design

As is common for new engine designs, analytical and numerical models are made to simulate and investigate the behaviour of that specific engine concept. Since the engine concepts discussed in this thesis are meant to operate within the hypersonic regime, and thus with extreme high temperatures, pressures and energy flows, it is vital to explore every way of these simulations before testing it experimentally. With experimental tests, the engine concept can be divided in its key components: the inlet, the combustion chamber, and the nozzle. When testing a whole new engine concept, in this particular case a specific combustion process, a *proof-of-concept* is necessary. A proof-of-concept of an engine is in fact only that part of an engine that needs to be demonstrated for its feasibility, and is in a way a crude prototype of that engine concept. In this case the interest lies in demonstrating shock-induced combustion wave, with a detonation wave as the upper limit. Since the interest lies in supersonic flow conditions, only oblique shock-induced combustion and oblique detonation waves are considered.

Within a combustion chamber normally fuel injection, mixing and combustion occurs. For shock-induced combustion the injection and mixing of fuel is done outside the combustion chamber, so to study shock-induced combustion these two processes can be investigated separately. Assuming that injection and mixing can be done and controlled, a section needs to be designed which can facilitate one or a series of oblique shock waves and a combustion zone. This proof-of-concept test setup needs to be able to determine if indeed a combustion process is shock initiated and stabilized, indicate the levels of thrust generated, how the used material within the section reacts, and other hypersonic combustion flow characteristics.

In open literature so far two methods have been shown to produce experimental data on shock-induced combustion phenomena and detonation waves by using projectiles or wedges (Morris, 2001). The first method is by flow visualization by firing projectiles at high velocity into a test section filled with fuel-oxidizer, as seen in chapter 3 done by Lehr. This approach has the advantage of enabling a wide range of velocities to be studied with a variety of gas mixtures safely, when the projectile launching system is powerfull enough. It was primarily done to investigate the range of combustion phenomena and stability for shock-induced combustion waves and detonation waves, steady and oscillatory, around spherical, hemispherical blunted and conical projectiles.

The second method is by fixing a model in the laboratory reference frame and use a hypersonic test facility to generate a high-speed flow of combustible mixture around that model. This model can be large or small in diameter, since now a variety of geometries can be studied. Some are shown in figures 4.38 and 4.39. It is also possible to model the test section which induces shock-induced combustion waves, as shown in figure 4.40. The main dificulty with this method lies with assuring a fully pre-mixed high-speed uniform flow just before entering the test section with model. Supersonic wind tunnels can be used to produce flow Mach numbers around 3, for even higher Mach numbers one can think of expansion tubes, offering the advantage of directly accelerating a pre-mixed combustible gas mixture, so that fuel-air mixing issues are avoided.

Since it is desired to validate a shock-induced combustion wave in a supersonic/hypersonic flow, the second method is chosen here to elaborate on. A proof-of-concept can be done either simplistic or in a complex manner, and it is best to start in a simple manner. By this, it is meant the uniformity of the flow field created within the test section, either by the test section walls or by the model used. An example is shown in figure 4.41 where the complexity of the flow field increases when more oblique shock waves are introduced within the test section. The problem then is that a complex temperature field is created with different Mach numbers and shock-induced ignition of the fuel-air mixture might not occur there were it is wanted. Also for simplicity reasons, the model placed in the flow is recommended to be axi-symmetric and with a blunted noise with a small radios, to avoid excessive heating.

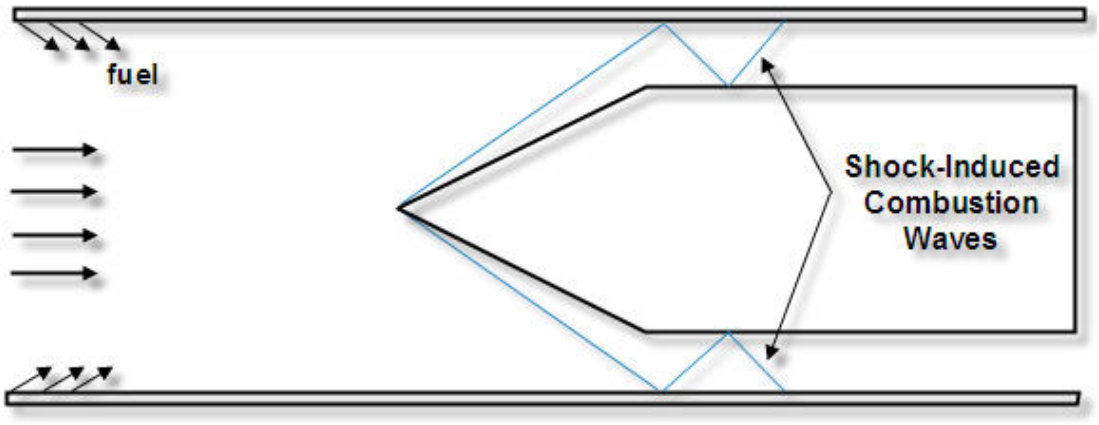

Figure 4.38: Test section with fixed model generating shock waves

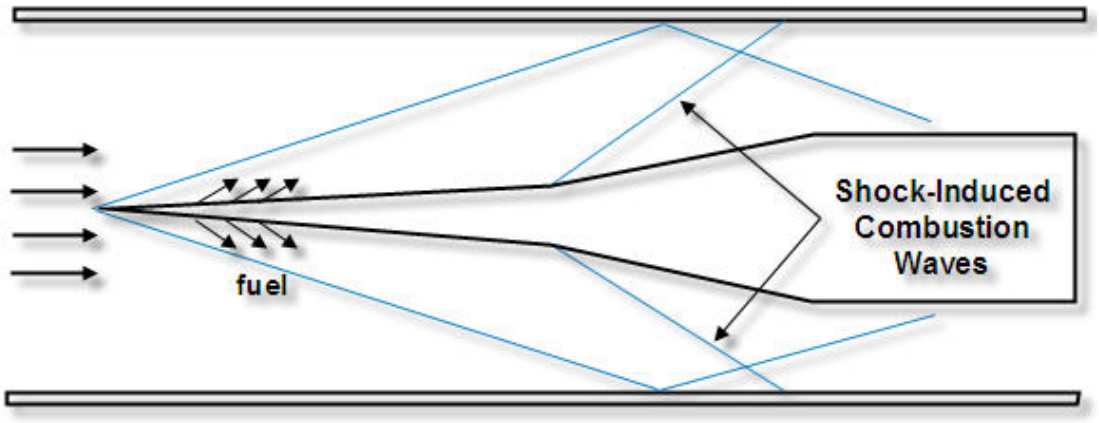

Figure 4.39: Test section with fixed model with fuel injectors and generating shock waves

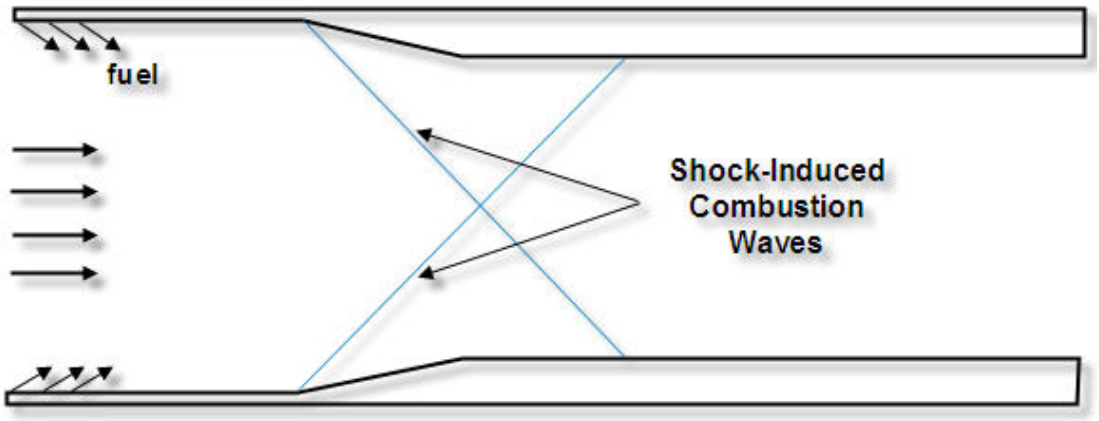

Figure 4.40: Test section with compression corners in the inner wall inducing shock-induced combustion waves

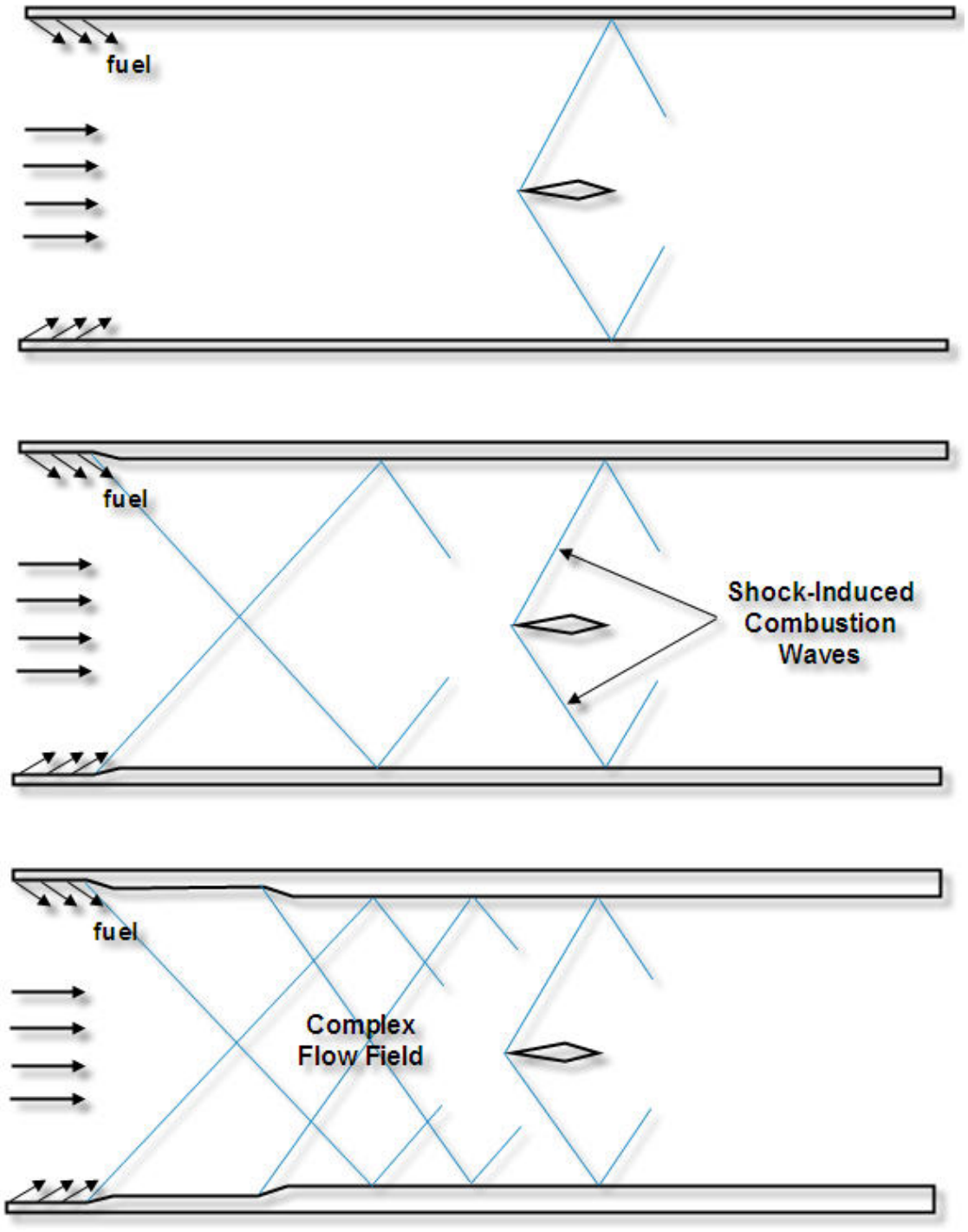

Figure 4.41: Test section with model and increasing flow complexity

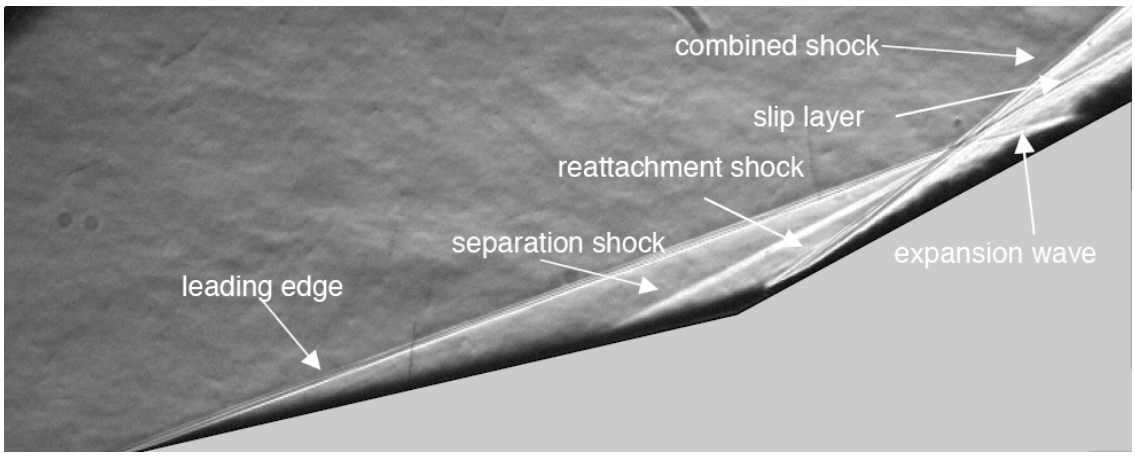

Figure 4.42: Schlieren image of the 15^0-30^0 wedge in a Mach 7 flow, adjusted from source: [Schrijer, 2005]

Region	Mach
0	7
1	4.40
2	4.07
3	3.26
4	2.25
5	3.40

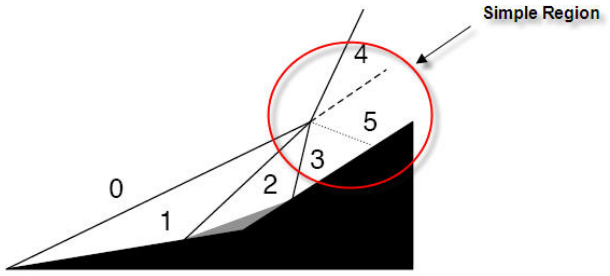

Figure 4.43: Schematic of the 15^0-30^0 wedge shock pattern, source: [Schrijer, 2005]

When the model also has fuel injectors as shown in figure 4.39 , the test section with that model becomes more realistic in appearance compared to the ramjet engine concept shown in section 3.3.1. Although fuel can be injected and mixed with the flow before entering the test section, it is more realistic to do this from the model. A major concern would then be pre-mature ignition within the boundary layer near the body, as seen in section 3.3.1. There have been experimental tests done for viscid flow analysis over axi-symmetrical cones with one or two compression corners comparable with the model shown in figure 4.39 without fuel injection or combustion (Schrijer, 2003/2005). The tests show a viscid flow analysis over a cone, which disregards the effects of the entropy layer, a characteristic of hypersonic flow, for simplicity (Anderson, 1989). The boundary layer present can be divided into two regions, being a subsonic region and a supersonic region due to a no-slip condition at the wall (section 2.1.1). In this subsonic region it was already mentioned that downstream disturbances can send information upstream *warning* the flow in advance. Compression corners can thus be felt by the flow and the subsonic region has a continuous pressure rise depending on the compression corner angle, resulting in a system of compression waves which merge into one shock wave. The increasing adverse pressure rise causes the boundary layer at some point to separate, enlarging the upstream influence of the compression corner resulting in a complex shock structure. The resulting separation region, which can be seen as a recirculation bubble, is enclosed by two compression systems, one resulting in the separation shock and the other into the reattachment shock. Both compression systems will thus merge into one single stronger shock. An experimental test of a compression corner in a Mach 7 flow is shown in figure 4.42, with the characteristics in the flow mentioned above. The Mach distribution due to the shock

waves, or shock pattern is given in figure 4.43. The result shows a simple shock region structure with region 4 having the lowest Mach number.

Another experimental test was done in a Mach 7 flow with the same type of cone, but now with the design angle of the second compression corner increased and exceeding the maximum flow deflection for an attached shock, resulting in a curved shock wave. Figure 4.44 shows a double-compression ramp with angles 15^0 and 45^0 and the curved separation shock wave interacting with the leading edge shock wave in a Mach 7 flow. For curved shock waves, normal shock wave theory is not applicable anymmore and is replaced with curved shock wave theory, which introduces the characteristic of rotational flow behind the curved shock wave (Sobieczky, 1990). Rotational flow increases instabillity of the combustion wave and must therefore be avoided in order to gain a (more) stable shock wave. The Mach distrubtion in figure 4.45 also reveals subsonic regions and thus will coincide with high temperature regions, making pre-mature shock-induced combustion possible. This example thus shows that carefull design is necessary for testing, since stable shock-induced combustion can only be achieved with a stable shock wave system. A simple proof-of-concept can thus be generated with an example of the test section model shown in figure 4.39.

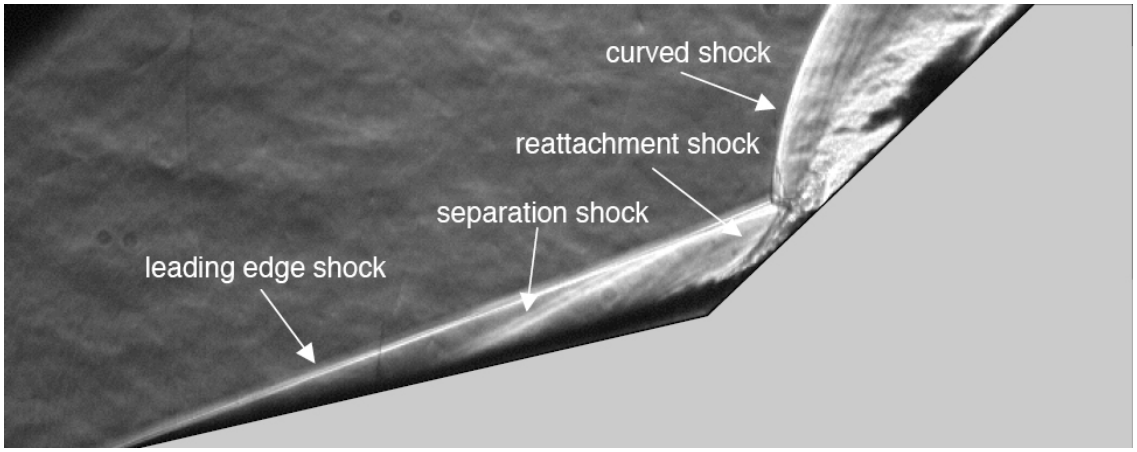

Figure 4.44: Schlieren image of the 15^0-45^0 wedge in a Mach 7 flow, adjusted from source: [Schrijer, 2005]

Region	Mach
0	7
1	4.40
2	4.07
3	2.16
4	1.59
5	0.40
6	2.69
7	2.07
8	3.67
9	3.27

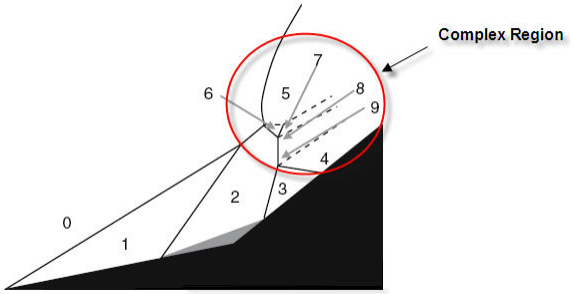

Figure 4.45: Schematic of the 15^0-45^0 wedge shock pattern, source: [Schrijer, 2005]

Chapter 5

Conclusion and Recommendations

5.1 Conclusion

Due to recent interest in ramjets operating in the hypersonic regime, this thesis investigated several ramjet engine concepts capable of operating within that velocity regime in order to determine their overall performance. Using the results from this investigation, the overall best performing ramjet engine concept was chosen to test its feasibility by means of a proof-of-concept test setup pre-design. In a simple analysis it was shown that a ramjet operating with subsonic combustion has higher structural load penalties than when it operates with supersonic combustion in the hypersonic velocity regime. The structural load penalties here are high thermal loads and high internal pressures, which are lower when the velocity is compressed to supersonic velocities. Because of these load penalties supersonic combustion ramjet engine types were investigated and divided into two types of combustion: diffusion combustion and pre-mixed combustion. The difference between them lies in the placing of the injection and mixing process within the engine flow path. Diffusion combustion makes use of a combustion chamber where fuel is injected, mixed followed by combustion, while pre-mixed combustion places fuel injection and mixing outside of the combustion chamber. For diffusion combustion there is also a complex, and sometimes turbulent, temperature and pressure flow field within the combustion chamber which causes self-ignition of the mixed fuel-air flow. Pre-mixed combustion makes use of shock waves entering the combustion chamber, and uses one of those shock waves to self-ignite the fuel-air mixture. In theory, this can be a less complex flow field compared to the one present with diffusion combustion.

In chapter 2 two ramjet engine concepts were discussed using diffusion combustion: the supersonic combustion ramjet (scramjet) and the dual-mode combustor. It was found that for both concepts a divergent combustion chamber cross-section has higher performance results than a constant cross-section and that it can modelled in such a way that the static pressure was the same before

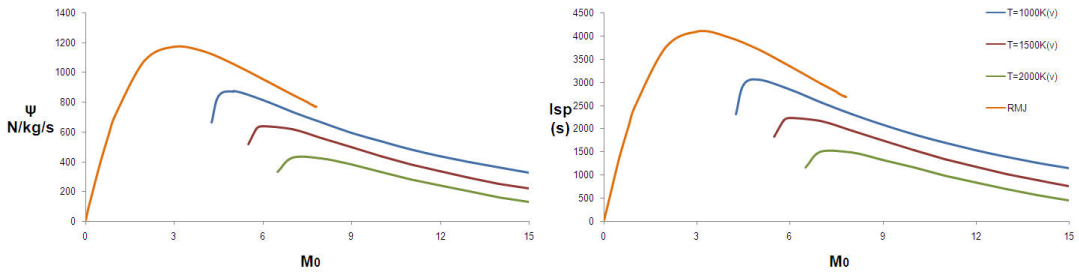

Figure 5.1: Comparison of specific thrust and specific impulse between the scramjet and ramjet

and after the combustion process. Because of this, the combustion process was modelled as a constant-pressure heat addition model. A comparison between the scramjet and the ramjet showed that for supersonic freestream Mach numbers ($1 < M_0 < 5$) the subsonic ramjet shows a higher performance, but when the freestream Mach numbers increase into the hypersonic regime ($M_0 > 6$) the subsonic ramjet loses its advantage due to the too high structural and thermal loads. The scramjet then shows a higher specific thrust and specific impulse, summarized again in figure 5.1, since it has lower structural loads. This method also clearly points out that scramjets can be used only for higher freestream Mach numbers in order to produce thrust.

In chapter 3 pre-mixed combustion was investigated and was compared to a relative new combustion concept: shock-induced combustion and detonation waves. It was stated that a detonation wave is a limit for a shock-induced combustion wave when the reaction zone following a preceding shock wave is minimalized and the combustion wave starts to interact with the preceding shock wave. The limit of detonation waves is the so-called Chapman-Jouguet detonation wave and this limit has the condition that the Mach number normal to the preceding shock wave is 1. Both combustion waves can be modelled as a discontinuity decelerating the flow velocity to subsonic velocities followed by a region where heat release occurs and thus accelerating the flow again to almost choking conditions. Normal shock-induced combustion waves or detonation waves thus have subsonic velocities behind the combustion front. Oblique shock-induced combustion and detonation waves thus have supersonic velocities behind the combustion front and were then of interest in this thesis. Two engine concepts using either shock-induced combustion or detonation waves were discussed, being the shock-induced combustion ramjet (shcramjet) and the oblique detonation wave engine (ODWE). It was stated that both combustion processes occurred with high enough velocities that it could be modelled as a constant-volume heat addition process. Compared to a constant-pressure heat addition process, constant-volume heat addition showed a higher thermal efficiency, again shown in figure 5.2. This results led to believe shock-induced combustion and detonation waves are capable of producing more mechanical work than constant-pressure combustion cycles.

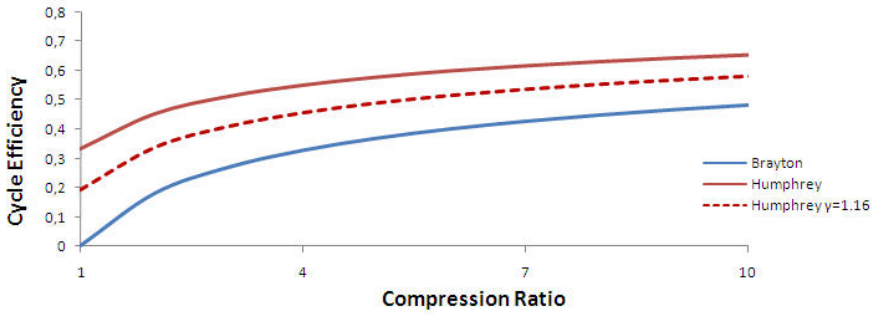

Figure 5.2: Comparison of thermal efficiency between CV and CP heat addition

Chapter 4 than gave an overall performance analysis consisting of an thermal efficiency comparison and an one-, or quasi-one-dimensional analytical analysis. To determine the difference between shock-induced combustion and detonation waves, another model was used to represent the detonation wave, the one-γ model or Fickett-Jacob model. The thermal efficiency again showed that both constant-volume heat addition and detonation waves have a higher efficiency than constant-pressure heat addition. The detonation wave, modelled as a CJ-detonation wave showed a just higher efficiency than CV-heat addition, as seen again in figure 5.3. This adds to the theory of a detonation wave being a limit of a shock-induced combustion wave.

In the analytical one-, and quasi-one-dimensional analysis done for CP heat addition it became clear that a higher inlet compression resulted in a higher overall performance. It also showed that for higher Mach numbers ($M_0 > 8$) the combustion chamber cross-sectional area ratio remained constant. For moving into the hypersonic regime this can be very advantageous, since then a fixed geometry can be used.

The one-, and quasi-one-dimensional analysis for CV heat addition showed that the assumption of a constant combustion chamber cross-sectional area ratio is justified since an increasing ratio shows poor results. It also showed that both the total pressure loss and entropy increase are dependent on the inlet compression ratio. When the inlet compression ratio decreases (stronger inlet compression) the two performance characteristics also decrease, the specific impulse however shows almost no

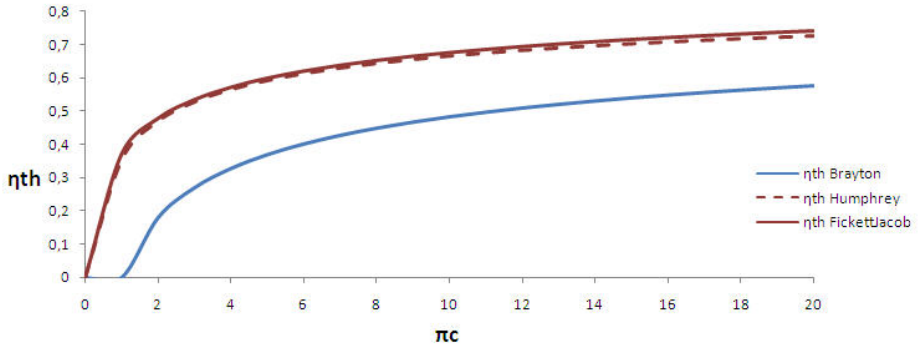

Figure 5.3: Comparison of thermal efficiency between CJ-detonation, CV and CP heat addition

change when the compression ratio is varied. Though it is assumed that constant-volume heat addition can represent shock-induced combustion, the model says nothing about the occurrence or nature of the phenomena. Therefore modelling the combustion phenomena in this way, it can be seen as an absolute model, with no indication of the nature of the shock wave.

Though only oblique detonation waves are considered, performance results for normal detonation waves were also shown. It could be seen from the one-, and quasi-one-dimensional analysis that the maximum performance of both types of detonation waves occur at CJ conditions, but differ by presence in velocity region and too some extent in value. Normal detonation waves are accomplished with lower freestream Mach numbers than oblique detonation waves, due to the normal component of the velocity being lower for oblique waves. When the shock angle decreases for oblique detonation waves, the velocity region, where the performance is measured, increases. The overall performance shows that the normal detonation wave has an average of 5-10% lower total pressure loss, a higher increase in entropy increase, and a higher specific impulse with an average of 10-15% ,with the lowest oblique detonation wave angle. The overall performance of the oblique detonation wave is shown to have a maximum with an occurring shock wave angle between 20 and 30 degrees. For both detonation waves a higher inlet compression results in a higher overall performance, adding to result that the performance is related to the height of the freestream Mach number and initial temperature both needing to be high. When the combustion process keeps occurring at CJ conditions, the combustion process becomes more attractive within this type of analysis.

Comparing the three heat addition models, CV heat addition has the best overall performance. This result shows the first conclusion that CV heat addition is the best overall heat addition process, and that when the cross-sectional area ratio remains constant it has the best perfor-

mance results. Surprisingly, detonation waves, either normal or oblique, show poor performance results compared to CV and CP heat addition. The reason of this result lies in the generation of irreversible entropy, which is shown to be the highest for the detonation wave model. This contradiction results in another important conclusion that a detonation wave can be modelled as a discontinuity with heat release, but that it cannot be shown to be a maximum of CV heat addition, since a detonation wave is considered as a limit of a shock-induced combustion wave. From these results, it is concluded that CV heat addition or shock-induced combustion is best suited for a proof-of-concept design for operating in the hypersonic regime. The design could also make it possible to show experimentally if the detonation wave is a real limit or again a theoretical limit of a shock-induced combustion wave.

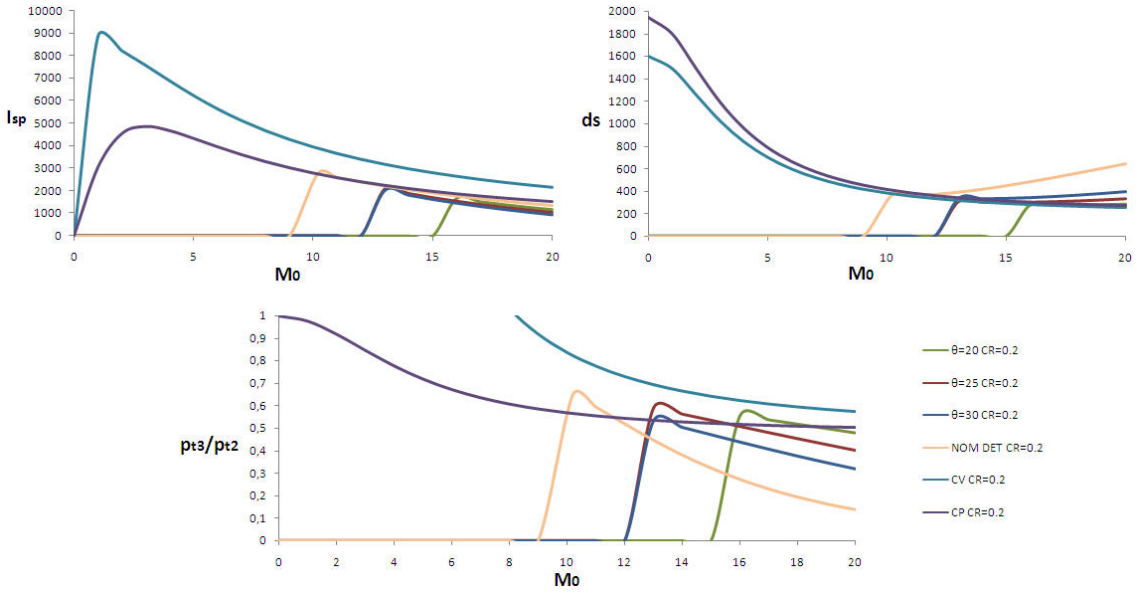

Figure 5.4: Comparison of overall performance between detonation waves, CV and CP heat addition with CR=0.2

5.2 Recommendations

Within this thesis, many topics on ramjet technology have been discussed and investigated. Entire papers and thesises were read which only discussed small portions, for instance just the inlet, or combustion phenomena within the ramjet. To see or investigate the entire scope of ramjet technology topics, a large area of knowledge and expertise needs to be used. One of the first recommendations is to specify what needs to be researched first before researching the ramjet entirely. One can start with investigating more thoroughly the three important components of the ramjet concept; the inlet/isolator, the combustion chamber, and the nozzle. From thereon, one can zoom in further into specifics, like the injection system, or the cooling system. Or zooming out, looking at the interaction between components or even at the whole engine concept. The following recommendations will give insight as to how to proceed when wanting to investigate shock-induced combustion waves as a propulsion system.

To determine the overall performance of specific ramjet engine concepts, they were modelled through analytical heat addition processes to determine the overall best performing ramjet engine concept, or heat addition process. Three performance characteristics (total pressure loss, entropy increase, and specific impulse) were chosen to represent the overall performance. One could also

use other ways to indicate the overall performance, say for instance by drag or thrust, specific fuel consumption, structural loads, etc. The point is that it is subjective to what is important to know, when making an overall performance comparison. Ultimately, one can make an absolute performance comparison, with specific tailored models for each ramjet engine concept with non-ideal conditions, as these are present in real flows.

One can now speculate if the previous found performance results will change if the analysis is done two-, or even three-dimensional and with or without certain losses. Performing an ideal one-dimensional analysis is a good start to indicate some sort of ideal result, and then to proceed with investigating it even better in a numerical way, before experimental testing. The proof-of-concept design given in section 4.3 can also be used as a design for numerical model calculation with a combustion model. Numerical models can predict even more in detail how the internal flow path will behave. Especially how the flow behaves around fuel injectors and the body inducing shock waves. And also how this affects the overall or absolute performance of the concept. It is therefore recommended that before proceeding to actual experimental testing, to investigate numerically.

There are specific areas which are useful to investigate for shock-induced combustion. The most important one is the stability and structure of the combustion zone. Gaining more insight into this gives a more realistic view of the feasibility to use it as a propulsion system. As was discussed in chapter 3, the heat release within the reaction zone influences the preceding shock wave due to pressure waves travelling or bouncing within the induction zone, which is subsonic. How this affects the overall stability of the combustion wave is a point of interest. Another point of interest is the nature of the preceding shock wave, what is the maximum or minimum angle, and which angle has the highest performance? This can be to some extent be investigated numerically, but to really see how the combustion zone reacts to different shock angles one must investigate it experimentally. Simple test section designs are then necessary to investigate that particular point of interest, like the designs suggested in section 4.3. The example given of hypersonic flow testing is one that could be modified to have a combustible mixture moving over the cone. Though different materials need to be used for the cone and the test section, since very high temperatures are present after combustion. Active cooling is then also a point of interest. Pre-mature ignition within the boundary layer is also a point of interest, since this can be representative for the proposed inlet/fuel injection system for the shcramjet, as seen in section 3.3.1.

Zooming out on shock-induced combustion, and looking more closely at the design of an engine using that kind of combustion, a point of interest will then be one of the suggested advantages of shock-induced combustion, being a reduced combustion chamber length. So far, as to the knowledge of the author, no experimental or numerical investigation has been done to validate this assumption. One can investigate how long the reaction zone is and look into the length needed for combustion products to recombine. The entire design of a combustion chamber can then also be investigated, the cross-sectional area being either rectangular or elliptical, or even divergent in length. And of course the body inducing shock waves. What is an efficient design, and what kind of material? And how the total design affects the shock waves within.

Then of course the inlet/fuel injection system, currently being investigated (see also section 3.3.1.), is of high interest, since this is vital to the success of the shcramjets functionality. The length and shape of the inlet, cooling systems, materials to be used, injection scheme designs, are but a few areas of interest and need to be investigated thoroughly. Most of the work done now is done numerically, and plans exist to test experimentally. These test should give more insight into the feasibility of a shcramjet inlet and overall working. Since fuel injection systems are being developed, one could also look into the design of the inlet, for instance the use of side-walls, or the minimal length needed for optimal mixing of the flow with the fuel, before entering the combustion chamber. Also the modelling of the compression corners, since multiple shock waves are needed, but not at the cost of excessive boundary layer development, since they can produce hot spots and cause pre-mature ignition. This can be done either through numerical or experimental testing,

but preferably in that order to avoid safety concerns and excessive costs.

If possible and within the test section the flow velocity can be increased during actual combustion, one can try to experimentally produce a detonation wave. This however is tricky, since tailored conditions are necessary, for instance at certain pre-combustion static temperatures certain flow Mach numbers need to be reached first. With low static temperatures higher Mach numbers are needed, thus high static temperatures require a lower flow Mach number but increase the risk of pre-mature ignition. Also the materials used have to be strong enough to cope with the extreme pressures and temperatures for some period of time. If, however, this is possible, the field of investigation can be extended from shock-induced combustion waves to detonation waves, and even back. This would show experimentally the feasibility of both combustion processes being used in actual flight and how the performance would react, since both are an extension of each other. Detonation waves being a maximum for shock-induced combustion waves, and vice versa shock-induced combustion waves a minimum for detonation waves. The behaviour of the combustion zone, the thickness of the induction zone, the stability change of the wave and structure, these characteristics could then be viewed and investigated when the flow Mach number keeps increasing over a fixed model within the test section. This would give a clear and total view of both combustion processes.

Bibliography

Chapter 1: Introduction

Anderson, J. D., "Hypersonic and High Temperature Gas Dynamics", Series in Aeronautical and Aerospace Engineering, McGraw-Hill, 1989.

Curran, E. T., and Murthy, S. N. B., "Scramjet Propulsion", Progress in Astronautics and Aeronautics, Volume 189, 2000.

Kerrebrock, J. L., "Aircraft Engines and Gas Turbines", The MIT Press, The Alpine Press Inc., 1977.

Mattingly, J. D., "Elements of Gas Turbine Propulsion", Department of mechanical and Manufacturing Engineering, Seattle University, McGraw-Hill Inc., 1996.

Wolf de, W. B., "Vliegtuigvoortstuwing", reader lr13B, part I, Faculty of Aerospace Engineering, University of Delft, 1993.

Wolf de, W. B., "De stuwstraalmotor (ramjet)", annex for reader lr13B: vliegtuigvoortstuwing, Faculty of Aerospace Engineering, University of Delft, 1995.

Wolf de, W. B., "Vliegtuigvoortstuwing", reader lr13B, part II, Faculty of Aerospace Engineering, University of Delft, 1996.

Chapter 2: Supersonic Combustion Ramjets

AMES Research Staff, "Equations, Tables, and Charts for Compressible Flow", NACA Report 1135, National Advisory Committee for Aeronautics, 1953.

Bakker, P.G., "Compressibele Aerodynamica", reader 2-54, Faculty of Aerospace Engineering, Technical University Delft, 1997.

Ben-Yakar, A., and Hanson R.K., "Cavity Flameholders for Ignition and Flame Stabilization in Scramjets: Review and Experimental Study", AIAA-98-3122, 1998.

Bormotova, T.A., Volodin, V.V., Golub, V.V., and Laskin, I.N., "The Thermal Correction of the Inlet Diffuser of a Hypersonic Scramjet Engine", High Temperature, Vol. 41, No. 3, 2003, pp. 415416. Translated from Teplofizika Vysokikh Temperatur, Vol. 41, No. 3, 2003, pp. 472474.

Chen, F., Chen, L., and Chang X., "Three-Dimensional Sidewall-Compression Scramjet Inlet CFD Simulation and Experimental Comparison", 39th AIAA/ASME/SAE/ASEE Joint Propulsion Conference and Exhibit, AIAA 2003-4741, 2003.

Chun, J., Scheuermann, T., von Wolfersdorf, J., and Weigand, B., "Experimental Study on Combustion Mode Transition in a Scramjet wih Parallel Injection", 14th AIAA/AHI Space Planes and Hypersonic Systems and Technologies Conference, AIAA-paper 2006-8063, AIAA, 2006.

Curran, E.T., and Murthy, S.N.B., "Scramjet Propulsion", Progress in Astronautics and Aeronautics, Volume 189, AIAA Reston, 2000.

Delale, C.F., Schnerr, G.H., and Zierep, J., "The Mathematical Theory of Thermal Choking in Nozzle Flows", ZAMP, Birkhäuser Verlag, Basel, 1993.

Donohue, J., Haj-Hariri, M., "Vorticity Generation Mechanisms in Parallel Ijection Schemes for Supersonic Mixing", AIAA-1992-3286, SAE, ASME, and ASEE, Joint Propulsion Conference and Exhibit, 28th, Nashville, TN, July 6-8, 1992.

Glawe, D.D., and Samimy, M., "Effects of Nozzle Geometry on Parallel Injection into a Supersonic Flow", *Journal of Propulsion and Power*, Vol. 12, No. 6, November and December, 1996.

Gruber, M.R., and Nejad, A.S., "Transverse Injection from Circular and Elliptic Nozzles into a Supersonic Crossflow", *Journal of Propulsion and Power*, Vol. 16, No. 3, May-June, 2000.

Heiser, W. H., and Pratt, D. T., "Hypersonic Airbreathing Propulsion", AIAA Education Series, AIAA, Washington, DC, 1994.

Kanda, T., Chinzei, N., Kudo, K., and Murakami, A., "Dual-Mode Operation in a Scramjet Combustor", AIAA paper 2001-1816, 2001.

Kato, K., Kanda, T., Kobayashi, K., Kudo, K., and Murakami, A., "Experimental Study of Downstream Combustion Ramjet-Mode", 43rd AIAA Aerospace Sciences Meeting and Exhibit, AIAA 2005-617, January, 2005.

Kuo, K.K., "Principles of Combustion", 2nd edition, John Wiley & Sons, USA, 2005.

Lee, S., and Mitani, T., "Mixing Augmentation of Transverse Injection in Scramjet Combustor", *Journal of Propulsion and Power*, Vol. 19, No. 1, January-February, 2003.

Li, J., Ma, F., and Yang, V., "A Comprehensive Study of Combustion Oscillations in a Hydrocarbon-Fueled Scramjet Engine", AIAA 2007-836, january, 2007.

Ma, F. H., Li, J., Yang, V., Lin, K. C., and Jackson, T. A., "Thermoacoustic Flow Instability in a Scramjet Combustor", AIAA Paper 2005-3824, July, 2005.

Matsuo, K., Miyazato, Y., and Kim, H., "Shock Train and Pseudo-Shock Phenomena in Internal Gas Flows", Progress in Aerospace Sciences 35, 33-100, Pergamon, 1999.

Mingbo, S., Hui, G., Jianhan, L., Zhenguo, W., "Investigation of Supersonic Combustion of Hydrogen Injection Upstream of Cavity flameholders in SCRAMJET", AIAA 2007-5383, July, 2007.

Mölder, S., Timofeev, E.V., and Tahir, R.B., "Flow Starting in High Compression Hypersonic Air Inlets by Mass Spillage", *AIAA Paper* 2004-4130, AIAA, 2004.

Oswatitsch, K., "Pressure Recovery for Missiles with Reaction Propulsion at High Supersonic Speeds (the Efficiency of Shock Diffusers)," NACATM 1140 (translation), 1947.

Ran, H., and Mavris, D., "Preliminary Design of a 2D Supersonic Inlet to Maximize Total Pressure Recovery", AIAA 5th Aviation, Technology, Integration, and Operations Conference, AIAA 2005-7357, September, 2005.

Smart, M.K., and Ruf, E.G., "Free-jet Testing of a REST Scramjet at Off-Design Conditions", AIAA Paper 2006-2955, 25th AIAA Aerodynamic Measurement Technology and Ground Testing Conference, California, June, 2006.

Tam, C., Eklund, D., Behdadnia, R., and Jackson, T., "Investigation of Boundary Layer Bleed for Improving Scramjet Isolator Performance", AIAA/CIRA 13th International Space Planes and Hypersonics Systems and Technologies, AIAA 2005-3286, 2005.

Timnat, Y.M., "Advanced Airbreathing Propulsion", Orbit Foundation Series. Malabar: Krieger, 1996.

Van Wie, D.M., Kwok, F.T, and Walsh, R.F., "Starting Characteristics of Supersonic Inlets", *AIAA Paper* 96-2914, AIAA, 1996(a).

Van Wie, D.M., and Rice, T., "Quantification of Data Uncertainties and Validation of CFD Results in the Development of Hypersonic Airbreathing Engines", *AIAA Paper* 96-2028, AIAA, 1996(b).

Van Wie, D.M., "Scramjet Propulsion", (Chapter 7), *Scramjet Propulsion, Progress in Aeronautics and Astronautics*, edited by E. T. Curran and S.N.B.Murthy, AIAA, Vol. 189, 2000, pp. 447-511.

Wang, C.P., Zhang, K., and Yang, J., "Analysis of Flows in Scramjet Isolator Combined with Hypersonic Inlet", AIAA 2005-24, 2005.

Wittenberg, H., "Some Fundamentals on the Performance of Ramjets with Subsonic and Supersonic Combustion", Delft University Press, Delft, Netherlands, 2000.

Wolf de, W. B., "Vliegtuigvoortstuwing", reader lr13B, part I, Faculty of Aerospace Engineering, University of Delft, 1993.

Wolf de, W. B., "De stuwstraalmotor (ramjet)", annex for reader lr13B: vliegtuigvoortstuwing, Faculty of Aerospace Engineering, University of Delft, 1995.

Wolf de, W. B., "Vliegtuigvoortstuwing", reader lr13B, part II, Faculty of Aerospace Engineering, University of Delft, 1996.

Xu Xu, X., and Guobiao, C., "Optimization Design for Scramjet and Analysis of its Operation Performance", *Acta Astronautica*, Acta Astronautica 57 390-403, 2005.

Zierep, J., "Theory of Flows in Compressible Media with Heat Addition", AGARD-AG-191, 1974.

Zimont, V.L., Levin, V.M., Meshcheryakov, E.A., and Sabel'nikov, V.A., "Characteristics of supersonic combustion of unmixed gases in channels", translated from Fizika Goreniya i Vzryva, Vol. 19, No. 4, pp. 7578, Moscow, JulyAugust, 1983.

Chapter 3: Shock-Induced Combustion Ramjets

Ahuja, J., K., and Tiwari, S., N.,Parametric Study of Shock-Induced Combustion in a Hydrogen-Air System, NASA-CR-197134, 1994.

Ahuja, J., K., and Tiwari, S., N.,Investigation of Shock-Induced Combustion Past Blunt Projectiles, NASACR- 4724, 1996.

Bengherbia, T., Yao, Y., and Bauer, P., Computational Investigation of Transitional Viscous Flow over a Ram Accelerator Projectile in Sub-Detonative Propulsion Mode, AIAA 2006-558, 2006, England.

Bratkovich, T.E., Aarnio, M.J., Williams, J.T., and Bussing, T.R.A., "An Introduction to Pulse Detonation Rocket Engines (PDREs)", AIAA-1997-2742, AIAA/ASME/SAE/ASEE Joint Propulsion Conference and Exhibit, 1997.

Bundy, C., Knowlen, C., and Bruckner, A.P., Unsteady Effects on Ram Accelerator Operation at Elevated Fill Pressures, Journal of Propulsion and Power, Vol. 20, No. 2, 2004, pp. 801-810.

Bussing, T. and Pappas, G., "Pulse Detonation Engine Theory and Concepts", in *Developments in High-Speed-Vehicle Propulsion Systems*, ed. S.N.B. Murthy and E.T. Curran, AIAA, 1996, pp. 421472.

Clutter, K., Krishnamurty, V., and Shyy, W.,Combustion and Turbulence Effects in Hypersonic Projectile Flows, AIAA, Aerospace Sciences Meeting Exhibit, 35th, Reno, NV, Jan. 6-9, 1997.

Deiterding, R., Numerical Structure Analysis of Regular Hydrogen-Oxygen Detonations, SSCI Fall 2003 Meeting, Session 03F-28.

Dudebout, R., Sislian, J. P., and Oppitz, R., Numerical Simulation of Hypersonic Shock-Induced Combustion Ramjets, Journal of Propulsion and Power, Vol. 14, No. 6, Nov-Dec 1998.

Eckett, A.C., Numerical and Analytical Studies of the Dynamics of Gaseous Detonations,Ph.D. Thesis, California Institute of Technology, Pasadena, California, September 2000.

Fickett, W., and Davis, W.C., Detonation, Theory and Experiment, University of California Press, Berkely, California, 1979.

Fusina, G., Sislian, J.P., and Parent, B., Formation and Stability of Near Chapman-Jouguet Standing Oblique Detonation Waves, AIAA Journal, Vol. 43, No. 7, July, 2005.

He, L., and Lee, J.H.S., The Dynamical Limit of One-Dimensional Detonations, Physics of Fluids, May, 1995.

Hertzberg, A., Bruckner, A.P., and Bogdanoff, D.W., Ram Accelerator: A New Chemical

Method for Accelerating Projectiles to Ultrahigh Velocities, AIAA Journal, Vol. 26, No. 2, 1988, pp. 195-203.

Kailasanath, K., "Review of Propulsion Applications of Detonation Waves", *AIAA* Journal Vol. 38, No. 9, September, 2000.

Lee, J.H.S., Dynamic Parameters of Gaseous Detonations, Annual Review of Fluid Mechanics 16, pp. 311- 336, 1984.

Lee, J.J., Dupre, G., Knystautas, R., and Lee, J.H., Doppler Interferometry Study of Unstable Detonations, Shock Waves, Volume 5, Number 3, October, 1995.

Lehr, H. F., "Experiments on Shock-Induced Combustion"' Astronautica Acta, Vol. 17, No. 10, pp. 589597, 1972.

McVey, J. B., and Toong, T. Y., Mechanism of Instabilities of Exothermic Hypersonic Blunt-Body Flow, Combustion Science and Technology, Vol. 3, pp.63-76, 1971.

Naughton, J. W., Cattafesta, L. N., and Settles, G. S., An Experimental Study of the Effect of Streamwise Vorticity on Supersonic Mixing Enhancement, AIAA Paper 89-2456, July 1989.

Nicholls, J. A., Standing DetonationWaves, Ninth Symposium of Combustion, Academic press, NewYork/London, p.488-496, 1963.

Parent, B., and Sislian, J. P., Turbulent Hypervelocity Fuel/Air Mixing by Cantilevered Ramp Injectors, AIAA Paper 2001-1888, April 2001.

Rueg, F. W., and Dorsey, W. W., A Missile Technique for the Study of Detonation Waves, J. res. Nat. Bur. stand, 66C, p.51-58, 1962.

Sanchez, A.L., Clavin, P., andWilliams, F.A., One-Dimensional Overdriven Detonations with Branched-Chain Kinetics, Physics of Fluids, March, 2001.

Schultz, Knowlen, C., and Bruckner, A.P., "Starting Envelope of the Subdetonative Ram Accelerator ", Journal of Propulsion and Power 2000 0748-4658 vol.16 no.6 (1040-1052), 2000.

Seiner, J. M., Dash, S. M., and Kenzakowski, D. C., Historical Survey on Enhanced Mixing in Scramjet Engines, Journal of Propulsion and Power, Vol. 17, No. 6, 2001, pp. 1273-1286.

Shchelkin, K. I., and Troshin, Y.K., Gasdynamics of Combustion, Mono Book Corp., Baltimore, MD, 1965.

Shepherd, J., Chemical Kinetics of Hydrogen-Air-Diluent Detonations, In Progress in Aeronautics and Astronautics, Volume 106, pp. 263-293, 1986.

Sislian, J. P. and Schumacher, J., A Comparative Study of Hypersonic Fuel/Air Mixing Enhancement by Ramp and Cantilevered Ramp Injectors, AIAA paper 99-4873, Nov. 1999.

Sislian, J.P., Dudebout, R., Schumacher, J., Islam, M., and Redford, T., Incomplete Mixing and Off-Design Effects on Shock-Induced Combustion Ramjet Performance, Journal of Propulsion and Power, Vol. 16, No. 1, January-February, 2000.

Sislian, J.P., Dudebout, R., Schumacher, J., and Schirmer, H., Propulsive Performance of

Hypersonic Oblique Detonation Wave and Shock-Induced Combustion Ramjets, Journal of Propulsion and Power, Vol. 17, No. 3, May-June, 2001.
Sislian, J. P., Martens, R.P., and Schwartzentruber, T.E., Numerical Simulation of a Real Shcramjet Flowfield, Journal of Propulsion and Power, Vol. 22, No. 5, September-October, 2006.

Soloukhin, R. I., shock waves and detonations in gases, Mono Book Corp. Baltimore, 1966.

Strehlow, R.A., Fundamentals of Combustion, Scranton: International Textbook, McGraw-Hill Series in Energy, Combustion and Environment, 1968.

Thompson, P. A., Compressible Fluid Dynamics, Advanced Engineering Series, Rensselaer Polytechnic Institute, pp. 347359, 1988.

Wagner, H. Gg., Reaction Zone and Stability of Gaseous Detonation, Ninth Symposium of Combustion. Academic Press, New York/London, p.454-460, 1963.

Westbrook, C. K., and Urtiew, P.A., Chemical kinetic prediction of critical parameters in gaseous detonations, In Proceedings of the 19th Symposium on Combustion, pp. 615-623, 1982.

Wintenberger, E., Application of Steady and Unsteady Detonation Waves to Propulsion, Thesis, 2004.

Wisman, W.H., "Inleiding Thermodynamica", Delftse Uitgevers Maatschappij, Delft, 1994.

Yungster, S., and Radhakrishnan, K.,A Fully Implicit Time Accurate Method for Hypersonic Combustion: Application to Shock-Induced Combustion Instability, Shock Waves, nr.5, p.293-303, 1996.

Yungster, S., and Radhakrishnan, K.,Computational Study of near-Limit Propagation of Detonation in Hydrogen- Air Mixtures, NASA Paper CR-2002-211889, October, 2002.

Zeldovich, B., and Kompaneets, A.S., Theory of Detonation, Academic Press, New York, 1960.

Chapter 4: Performance Analysis

Anderson, J. D., "Hypersonic and High Temperature Gas Dynamics", Series in Aeronautical and Aerospace Engineering, McGraw-Hill, 1989.

Hozumi, K., Yamamoto, Y., and Fujii, K., "Investigation of Hypersonic Compression Ramp Heating at High Angles of Attack", *Journal of Spacecraft and Rockets*, Vol. 38, No. 4, JulyAugust, 2001.

Lehr, H. F., "Experiments on Shock-Induced Combustion"' Astronautica Acta, Vol. 17, No. 10, pp. 589597, 1972.

Morris, C., I., "Shock-Induced Combustion in High-Speed Wedge Flows", dissertation, University of Stanford, 2001.

Morrison, R. B., "Oblique Detonation Wave Ramjet", NASA Contractor Report, NASA

CR-159192, January, 1980.

Schrijer, F.F.J., "Transient heat Transfer Measurements in a Short Duration Hypersonic Facility on a Blunted Cone-Flare using QIRT", Master thesis, Technical University of Delft, department of Aerodynamics, March, 2003.

Schrijer, F.F.J., Scarano, F., and van Oudheusden, B., W., "Application of PIV in a Mach 7 double-ramp flow", Experiments in Fluids, Springer, Volume 41, number 2, August, 2006.

Sislian, J. P. and Schumacher, J., A Comparative Study of Hypersonic Fuel/Air Mixing Enhancement by Ramp and Cantilevered Ramp Injectors, AIAA paper 99-4873, Nov. 1999.

Sislian, J.P., Dudebout, R., Schumacher, J., Islam, M., and Redford, T., Incomplete Mixing and Off-Design Effects on Shock-Induced Combustion Ramjet Performance, Journal of Propulsion and Power, Vol. 16, No. 1, January-February, 2000.

Sislian, J.P., Dudebout, R., Schumacher, J., and Schirmer, H., Propulsive Performance of Hypersonic Oblique Detonation Wave and Shock-Induced Combustion Ramjets, Journal of Propulsion and Power, Vol. 17, No. 3, May-June, 2001.

Sislian, J. P., Martens, R.P., and Schwartzentruber, T.E., Numerical Simulation of a Real Shcramjet Flowfield, Journal of Propulsion and Power, Vol. 22, No. 5, September-October, 2006.

Sobieczky, H., Dougherty, F.C., and Jones, K., "Hypersonic Waverider Design from Given Shock Waves", First International Waverider Symposium, University of Maryland, 1990.

Takeno, T., Uno, T., and Kotani, Y., "An experimental study on shock-induced combustion of hydrogen", *Acta Astronautica*, Vol. 6, pp. 891-915, Pergamon Press Ltd., 1979.

Thompson, P. A., "Compressible Fluid Dynamics", Advanced Engineering Series, Rensselaer Polytechnic Institute, pp. 347359, 1988.

Townend, L., H., "An Analysis of Oblique and Normal Detonation Waves", Aerodynamics Dept., R.A.E. Farnborough, Reports and Memoranda, No. 3638, 1970.

Wintenberger, E., Application of Steady and Unsteady Detonation Waves to Propulsion, Thesis, 2004.

Wisman, W.H., "Inleiding Thermodynamica", Delftse Uitgevers Maatschappij, Delft, 1994.

Wittenberg, H., "Some Fundamentals on the Performance of Ramjets with Subsonic and Supersonic Combustion", Delft University Press, Delft, Netherlands, 2000.